Advances in Clinical and Experimental Medicine

MONTHLY ISSN 1899-5276 (PRINT) ISSN 2451-2680 (ONLINE) www.advances.umed.wroc.pl

2021, Vol. 30, No. 3 (March)

Impact Factor (IF) – 1.514
Ministry of Science and Higher Education – 40 pts.
Index Copernicus (ICV) – 152.95 pts

Wroclaw Medical University

Advances
in Clinical and Experimental
Medicine

Advances
in Clinical and Experimental Medicine

ISSN 1899-5276 (PRINT) ISSN 2451-2680 (ONLINE) www.advances.umed.wroc.pl

MONTHLY 2021
Vol. 30, No. 3
(March)

Advances in Clinical and Experimental Medicine (*Adv Clin Exp Med*) publishes high quality original articles, research in progress and reviews of recognized scientists that deal with all clinical and experimental medicine.

Editorial Office
ul. Marcinkowskiego 2–6
50-368 Wrocław, Poland
Tel.: +48 71 784 11 36
E-mail: redakcja@umed.wroc.pl

Publisher
Wroclaw Medical University
Wybrzeże L. Pasteura 1
50-367 Wrocław, Poland

Online edition is the original version of the journal

Editorial Policy

Advances in Clinical and Experimental Medicine (Adv Clin Exp Med) is an independent multidisciplinary forum for exchange of scientific and clinical information, publishing original research and news encompassing all aspects of medicine, including molecular biology, biochemistry, genetics, biotechnology and other areas. During the review process, the Editorial Board conforms to the "Uniform Requirements for Manuscripts Submitted to Biomedical Journals: Writing and Editing for Biomedical Publication" approved by the International Committee of Medical Journal Editors (www.ICMJE.org/). The journal publishes (in English only) original papers and reviews. Short works considered original, novel and significant are given priority. Experimental studies must include a statement that the experimental protocol and informed consent procedure were in compliance with the Helsinki Convention and were approved by an ethics committee.

For all subscription-related queries please contact our Editorial Office:
redakcja@umed.wroc.pl

For more information visit the journal's website:
www.advances.umed.wroc.pl

Pursuant to the ordinance No. 134/XV R/2017 of the Rector of Wroclaw Medical University (as of December 28, 2017) from January 1, 2018 authors are required to pay a fee amounting to 700 euros for each manuscript accepted for publication in the journal Advances in Clinical and Experimental Medicine.

Indexed in: MEDLINE, Science Citation Index Expanded, Journal Citation Reports/Science Edition, Scopus, EMBASE/Excerpta Medica, Ulrich's™ International Periodicals Directory, Index Copernicus

Typographic design: Monika Kolęda, Piotr Gil
DTP: Wydawnictwo UMW
Cover: Monika Kolęda
Printing and binding: ARGI SC

Advances
in Clinical and Experimental Medicine

MONTHLY 2021, Vol. 30, No. 3 (March)

ISSN 1899-5276 (PRINT)
ISSN 2451-2680 (ONLINE)
www.advances.umed.wroc.pl

Contents

Original papers

Reviews

Laparoscopic histological mapping for the determination of the length of aganglionic segment in children with Hirschsprung disease

Bartosz Bogusz[1,A–D], Małgorzata Smolec-Zamora[1,B,C,E], Andrzej Zając[1,B,E], Adam Mol[2,B,E], Wojciech Górecki[1,E,F]

[1] Department of Pediatric Surgery, University Children's Hospital, Jagiellonian University Medical College, Kraków, Poland
[2] Department of Pediatric Surgery, University Children's Hospital, Kraków, Poland

A – research concept and design; B – collection and/or assembly of data; C – data analysis and interpretation;
D – writing the article; E – critical revision of the article; F – final approval of the article

Advances in Clinical and Experimental Medicine, ISSN 1899–5276 (print), ISSN 2451–2680 (online) *Adv Clin Exp Med*. 2021;30(3):233–237

Address for correspondence
Bartosz Bogusz
E-mail: bjbart@poczta.onet.pl

Funding sources
None declared

Conflict of interest
None declared

Received on June 24, 2020
Reviewed on July 7, 2020
Accepted on October 29, 2020

Published online on March 23, 2021

Abstract

Background. Modern approach to the surgical treatment of Hirschsprung's disease (HD) consists in the earliest possible repair and reduction of the number of surgical interventions. Primary one-stage transanal endorectal pull-through (TEPT) technique requires preoperative determination of the length of aganglionic segment. The efficacy of the standard method – contrast enema – is questionable in patients with a poorly defined transitional zone.

Objectives. To present the proposed laparoscopic method for the management pathway in patients with HD, in whom the determination of the length of aganglionic segment with contrast enema was not possible.

Materials and methods. A retrospective analysis of the diagnostic and therapeutic management employed in 14 patients, from 2 weeks to 55 months of age, with diagnosed HD, treated between January 2013 and May 2020. Laparoscopic histological mapping was performed with the use of 3 laparoscopic ports of 3–5 mm diameter.

Results. In all patients, laparoscopic mapping allowed for the determination of the length of aganglionic segment and the mode of surgical treatment. Four children with determined short-segment disease underwent TEPT, while 2 underwent temporary colostomy formation using the Duhamel–Martin–Ikeda method. Five patients with long-segment HD underwent laparoscopic-assisted TEPT. One patient with long-segment disease was treated with a temporary double-barrel colostomy and definitive surgery was performed 3 months later using the Duhamel–Martin–Ikeda method. In 2 patients with an initial diagnosis of HD established using current diagnostic pathway, HD pathology was later excluded based on the results of laparoscopic mapping and repeat rectal suction biopsy. No complications related to the laparoscopic procedure were identified.

Conclusions. The method of laparoscopic mapping is effective in the determination of the length of aganglionic segment in children with diagnosed HD. In doubtful cases, it can be the preferred option in establishing the final mode of surgical treatment.

Key words: laparoscopy, biopsy, Hirschsprung

Cite as
Bogusz B, Smolec-Zamora M, Zając A, Mol A, Górecki W. Laparoscopic histological mapping for the determination of the length of aganglionic segment in children with Hirschsprung disease. *Adv Clin Exp Med*. 2021;30(3):233–237. doi:10.17219/acem/129575

DOI
10.17219/acem/129575

Background

The modern approach to the definite surgical treatment of Hirschsprung's disease (HD) focuses on the earliest possible repair, and reducing the number of surgical interventions. Total transanal surgery for HD – transanal endorectal pull-through (TEPT) – represents the latest development in the concept of minimally invasive surgery for HD.[1,2] The feasibility, safety and efficacy of this approach has been established.[3–5] Nevertheless, it depends on the length of the aganglionic segment, as well as the general condition of the patient. The success of surgical correction of HD using the TEPT technique requires precise determination of the length of aganglionic segment before the operation. The efficacy and sensitivity of the standard method used for this purpose – contrast enema – is questionable, especially in the group of patients in whom, because of an early presentation of the disease, bowel distension above the transitional zone is not well demarcated. On the other hand, the lack of visible transitional zone in older children with confirmed HD does not necessarily represent long-segment disease.[6,7] The lack of precise determination of the length of aganglionic segment before operation using the TEPT technique can result in an unwanted intraoperative change of therapeutic strategy.

Objectives

Following the idea of laparoscopic-assisted TEPT, presented by Georgeson,[8–10] the aim of this study was to present the current procedure employed in our institution for the determination of the length of aganglionic segment, as well as surgical treatment mode in patients with diagnosed HD, in whom the determination of the length of aganglionic segment was not possible with the use of contrast enema.

Materials and methods

Between January 2013 and May 2020, HD was diagnosed in 56 patients treated in the Department of Pediatric Surgery of the University Children's Hospital in Kraków, Poland. The diagnostic scheme routinely employed in patients admitted with suspected HD included: plain abdominal X-ray, anorectal manometry and rectal suction biopsy for acetylcholinesterase (AChE) histochemical staining and hematoxylin & eosin (H&E) staining. In cases of uncertain results from the abovementioned studies, calretinin immunostaining of rectal biopsy was performed. Barium contrast enema was employed in order to determine the length of aganglionic segment (Fig. 1). In the studied group, contrast enema failed to show the length of aganglionic segment in 14 children with HD diagnosed using the aforementioned diagnostic pathway. These patients were qualified for laparoscopic mapping. The mode of further treatment including, if possible, consecutive one-stage surgical treatment during the same procedure, depended on the results of histopathological evaluation of seromuscular intestinal biopsies. The age of patients on admission ranged from 2 weeks to 55 months.

Technique of laparoscopic mapping

Patients were placed in supine position. The surgeon stood on the right side of the patient, near the head. Pneumoperitoneum was established using the Hasson technique. The applied intraabdominal pressure was 6–10 mm Hg. A 5-mm, 30° scope was introduced through the umbilical port. Two 3-mm or 5-mm working ports were introduced bilaterally at the level of the umbilicus, lateral to the mid-clavicular lines, or in the right epigastric region and right hypogastric area. Seromuscular intestinal biopsies were obtained using 3-mm or 5-mm instruments. If the transitional zone was visualized, biopsies were taken with endoshears distally and proximally to the suspected level of normal innervation of the intestine in order to confirm the diagnosis and length of aganglionic segment. In cases where the visualization of the transitional zone was not possible, biopsies were taken as follows:

a) middle part of the sigmoid colon – normal innervation – confirmation of short-segment HD and possible TEPT;

b) splenic flexure – normal innervation, with aganglionosis in biopsy taken from site a);

c) proximal section of the transverse colon – normal innervation with aganglionosis in biopsies at sites a) and b) – possible laparoscopic-assisted TEPT with the mobilization of descending colon, splenic and hepatic flexures as well as the whole transverse colon;

d) cecum – differentiation between long-segment HD if normal innervation; and total colonic aganglionosis if aganglionosis found in biopsy – in our experience requiring multistage treatment with temporary colostomy or ileostomy;

e) ileum about 5–10 cm proximal to the ileocecal valve; and higher biopsies – determination of the level for ileostomy.

Biopsy sites were closed with absorbable, braided 4.0 or 5.0 sutures in the case of suspected perforation, or in order to mark the level of normal innervations (Fig. 2). All biopsy samples were evaluated intraoperatively for the decision-making results as described above, except for the first patient in the series – in this case, the decision concerning further procedures was made after receiving the results of histopathological examination. The waiting time for the intraoperative evaluation of each frozen specimen was less than 15 min for a single biopsy.

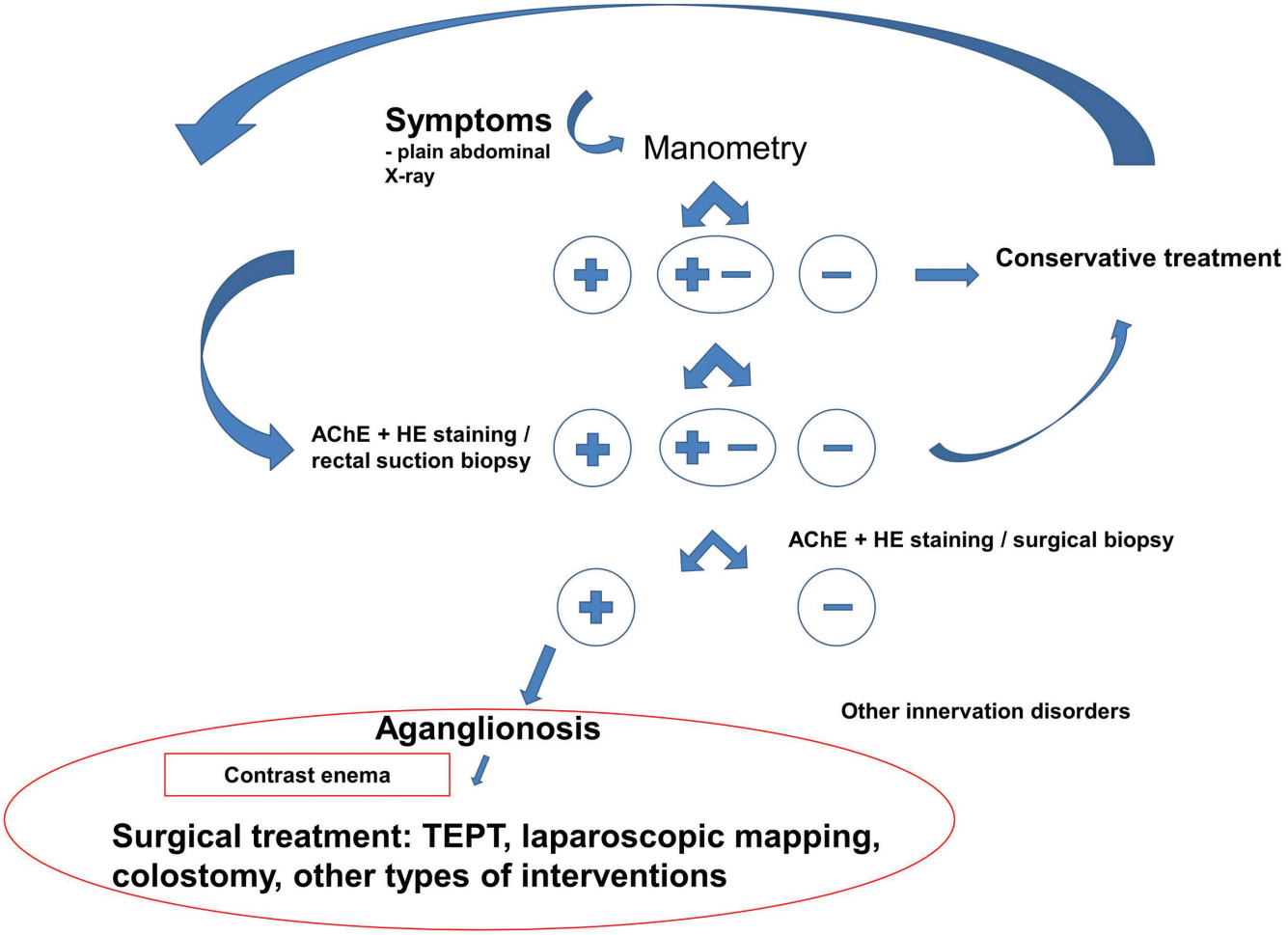

Fig. 1. Diagnostic/decision-making scheme for patients with suspected HD

Results

Forty-nine biopsy samples were collected from 14 children. In 7 patients, it was necessary to collect 5 samples (including 1 case of unavailable intraoperative sample assessment, 5 cases with long-segment HD and 1 case finally diagnosed with immature ganglion cells). In 7 other patients, 2 biopsies were sufficient to establish the length of aganglionic segment (including 4 children with short-segment HD and 2 with long-segment HD). The last patient in this group was finally diagnosed with immature ganglion cells.

Out of 49 biopsy samples, 4 were intraoperatively assessed as unsuitable for histopathological analysis. Eighteen biopsy sites required intracorporeal suturing because of suspected perforation of the mucous membrane. Sites with normal innervation determined during intraoperative histological evaluation were marked with sutures to facilitate their identification during further procedures (transanal dissection or colostomy), without the need for additional biopsies.

In 12 patients, laparoscopic histological mapping allowed for the determination of final diagnosis and establishment of the mode of surgical treatment. Short-segment aganglionosis (transitional zone determined in the medial or distal part of the sigmoid colon) was diagnosed in 6 cases, and long-segment aganglionosis in 6 cases (in 1 case, normal innervation determined in the descending colon biopsy and in 2 cases, within the samples from the middle section of transverse colon). In 2 patients, despite initial diagnosis of HD, this pathology was excluded on the basis of the results of laparoscopic mapping and repeat rectal biopsy. The results of preoperative contrast enema did not correspond with the histopathological picture in any of the presented patients.

Three children with determined short-segment disease underwent TEPT during the same procedure. Two children with determined short-segment disease underwent temporary colostomy and definite surgical treatment using the Duhamel–Martin–Ikeda method due being over the age of 12 months at diagnosis. One patient with short-segment HD underwent TEPT in a consecutive procedure (intraoperative evaluation of samples was unavailable at the time of laparoscopic mapping). Five patients with long-segment HD (innervation level between the descending colon and middle section of transverse colon) underwent laparoscopic-assisted TEPT. One patient

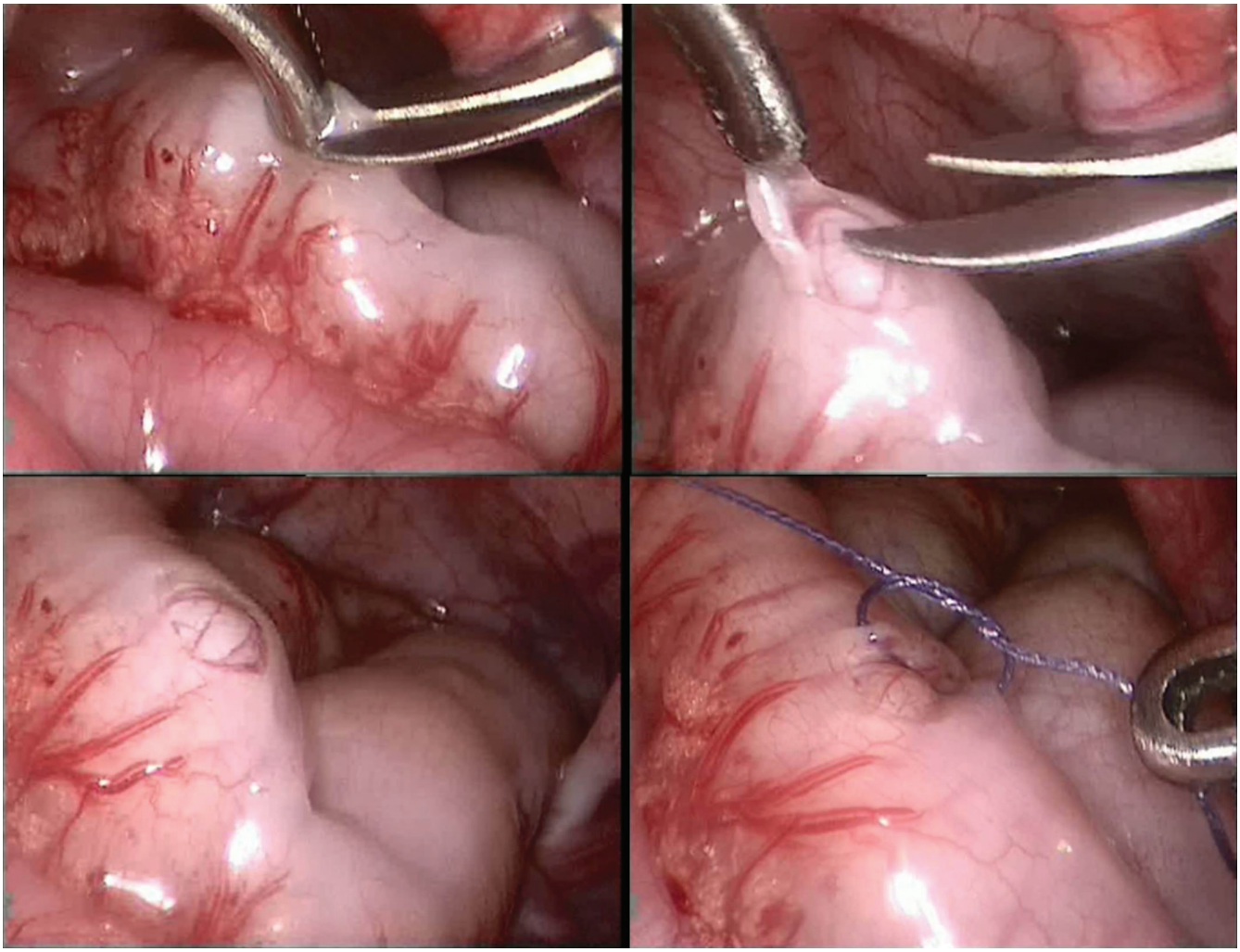

Fig. 2. Technique of seromuscular biopsy of the intestine (3-mm instruments)

with long-segment disease (with aganglionosis extending to the right section of the transverse colon) underwent a temporary double-barrel colostomy (directly after laparoscopic mapping, during the same procedure). The definite operation in this patient was performed 3 months later using the Duhamel–Martin–Ikeda method. There were no identified complications related to the laparoscopic mapping procedures.

Discussion

The implementation of TEPT in the treatment of HD is connected with the problem of its application in children with long-segment HD or uncertain diagnosis concerning the length of aganglionic segment. A solely transanal approach technique in misdiagnosed long-segment HD disease can result in an unplanned open or laparoscopic intra-abdominal intervention. Thus, a sensitive method for the detection of the length of aganglionic segment seems necessary, particularly concerning the risk associated with attempts of transanal dissection of retroperitoneal colon sections.

A method we considered helpful to avoid the above-mentioned problem was developed by Georgeson et al.[8,9] The author emphasized the benefits of his method – laparoscopic-assisted transanal endorectal pull-through – such as the ability to verify the level of aganglionosis before endorectal dissection. We believe this is the most vital benefit of the method, and our observations have been confirmed by the reports of other authors.[10,11] Before the introduction of laparoscopic mapping, we encountered problems with the identification of the transitional zone on the basis of contrast enema, which resulted in the need for an unplanned laparotomy in 2 children operated with TEPT for misdiagnosed long-segment HD.

Numerous authors underline the benefits of laparoscopic intra-abdominal mobilization of the aganglionic segment, such as avoiding overdilation of the internal anal sphincter during TEPT (which may lead to possible weakening of the patient's fecal continence), a more definitive endpoint for endorectal dissection, and greater versatility in fashioning the ganglionated pedicle, allowing for pull-through operations in patients with longer aganglionic segments.[9,12–14] On the other hand, some researchers currently

question the deliberate use of laparoscopic assistance in diagnosed short-segment HD, because of longer operation time and additional incisions.[15] A meta-analysis published by Thomson et al. (405 patients), comparing short and long-term outcomes following total transanal endorectal pull-through with laparoscopic-assisted pull-through procedures, failed to show any advantages of either of these approaches.[16] This conclusion has been confirmed, particularly for rectosigmoid HD, in the European Reference Network for rare and inherited and congenital digestive disorders (ERNICA) guidelines.[7]

Limitations

In our experience, consistent with the observations of other authors, the use of TEPT is connected with a postoperative tendency to constipation rather than incontinence.[17] Following the use of the De la Torre technique for almost 10 years in our department, we also did not find any additional benefit of laparoscopic assistance in children with diagnosed short-segment HD. However, marking the precise level of innervation with seromuscular sutures in doubtful cases appears helpful in the determination of the level of resection of the aganglionic segment during transanal dissection. Laparoscopic assistance not only shows the level of innervation, but also allows for the dissection of the aganglionic segment during the same surgical procedure. This makes possible to perform TEPT even in patients with aganglionosis involving the descending and transverse colon.

Conclusions

The laparoscopic histological mapping of the colon and ileum is safe and effective in the determination of the length of aganglionic segment in neonates and infants with diagnosed HD, and in doubtful cases, it can be helpful in establishing the final mode of surgical treatment. Laparoscopic assistance makes one-stage treatment possible in selected patients with long-segment HD.

ORCID iDs

Bartosz Bogusz https://orcid.org/ 0000-0002-8763-0990
Małgorzata Smolec-Zamora https://orcid.org/ 0000-0001-8993-3867
Andrzej Zając https://orcid.org/ 0000-0003-4676-0446
Adam Mol https://orcid.org/ 0000-0001-9378-549X
Wojciech Górecki https://orcid.org/ 0000-0003-4907-0520

References

1. De La Torre-Mondragon L, Ortega-Salgado JA. Transanal endorectal pull-through for Hirschsprung's disease. *J Pediatr Surg.* 1998;33(8):1283–1286. doi:0.1016/s0022-3468(98)90169-5
2. Langer JC, Durrant AC, de la Torre L, et al. One-stage transanal Soave pullthrough for Hirschsprung's disease: A multicenter experience with 141 children. *Ann Surg.* 2003;238(4):569–583, discussion 583–585. doi:10.1097/01.sla.0000089854.00436.cd
3. Albanese CT, Jennings RW, Smith B, Bratton B, Harrison MR. Perineal one-stage pull-through for Hirschsprung's disease. *J Pediatr Surg.* 1999;34(3):377–380. doi:10.1016/s0022-3468(99)90480-3
4. Gao Y, Li G, Zhang X, et al. Primary transanal rectosigmoidectomy for Hirschsprung's disease: Preliminary results in the initial 33 cases. *J Pediatr Surg.* 2001;36(12):1816–1819. doi:10.1053/jpsu.2001.28847
5. Höllwarth ME, Rivosecchi M, Schleef J, et al. The role of transanal endorectal pull-through in the treatment of Hirschsprung's disease: A multicenter experience. *Pediar Surg Int.* 2002;18(5–6):344–348. doi:10.1007/s00383-002-0747-x
6. Smith GHH, Cass D. Infantile Hirschsprung's disease: Is barium enema useful? *Pediatr Surg Int.* 1991;6:318–321.
7. Kyrklund K, Sloots CEJ, de Blaauw I, et al. ERNICA guidelines for the management of rectosigmoid Hirschsprung's disease. *Orphanet J Rare Dis.* 2020;15:164. doi:10.1186/s13023-020-01362-3
8. Georgeson KE, Fuefner MM, Hardin WD. Primary laparoscopic pull-through for Hirschsprung's disease in infants and children. *J Pediatr Surg.* 1995;30(7):1017–1021, discussion 1021–1022. doi:10.1016/0022-3468(95)90333-x
9. Georgeson KE, Cohen RD, Hebra A, et al. Primary laparoscopic endorectal colon pull-through for Hirschsprung's disease: A new gold standard. *Ann Surg.* 1999;229(5):678–682. doi:10.1097/00000658-199905000-00010
10. Li X, Li X, Cheng J, et al. Laparoscopic-assisted endorectal pull-through for Hirschsprung's disease: A retrospective study. *Saudi Med J.* 2017;38(12):1255–1258. doi:10.15537/smj.2017.12.20859
11. Fang Y, Bai J, Zhang B, Wu D, Lin Y, Liu M. Laparoscopic Soave procedure for long-segment Hirschsprung's disease: Single-center experience. *Videosurgery Miniinv.* 2020;15(1):234–238. doi:10.5114/wiitm.2019.86807
12. Wulkan ML, Georgeson KE. Primary laparoscopic endorectal pull-through for Hirschsprung's disease in infants and children. *Semin Laparosc Surg.* 1999;5(1):9–13. doi:10.1177/155335069800500103
13. El Sadat AM. Laparoscopic-assisted transanal endorectal pull-through for Hirschsprung's disease: Experience with 15 cases. *Ann Ped Surg.* 2009;5(3):181–186.
14. El-Elah Ali KA. Transanal endorectal pull-through for Hirschsprung's disease during the first month of life. *Ann Ped Surg.* 2010;6(2):81–88.
15. van de Ven TJ, Sloots CE, Wijnen MH, et al. Transanal endorectal pull-through for classic segment Hirschsprung's disease: With or without laparoscopic mobilization of the rectosigmoid? *J Pediatr Surg.* 2013;48(9):1914–1918. doi:10.1016/j.jpedsurg.2013.04.025.
16. Thomson D, Allin B, Long AM, Bradnock T, Walker G, Knight M. Laparospic assistance for primary transanal pull-through in Hirschsprung's disease: A systemic review and meta-analysis. *BMJ Open.* 2015;5(3):e006063. doi:10.1136/bmjopen-2014-006063
17. De La Torre L, Langer JC. Transanal endorectal pull-through for Hirschsprung's disease: Technique, controversies, pearls, pitfalls, and an organized approach to the management of postoperative obstructive symptoms. *Semin Pediatr Surg.* 2010;19:96–106. doi:10.1053/j.sempedsurg.2009.11.016

Short-term trajectories of exercise-induced plasma lipid changes in overweight females, with a focus on HDL-cholesterol

Pavel Suchánek[A–C,E,F], Věra Lánská[A,C,E,F], Petr Stávek[B,C,E,F], Jaroslav Alois Hubáček[A,C–F]

Institute for Clinical and Experimental Medicine (IKEM), Prague, Czech Republic

A – research concept and design; B – collection and/or assembly of data; C – data analysis and interpretation; D – writing the article; E – critical revision of the article; F – final approval of the article

Advances in Clinical and Experimental Medicine, ISSN 1899–5276 (print), ISSN 2451–2680 (online) *Adv Clin Exp Med*. 2021;30(3):239–243

Address for correspondence
Pavel Suchánek
E-mail: pasu@ikem.cz

Funding sources
This study was supported within the project (Ministry of Health of Czech Republic) for development of research – organization 00023001 (IKEM, Prague, Czech Republic) – institutional support.

Conflict of interest
None declared

Acknowledgements
We wish to thank all the patients for their participation in the study.

Received on July 14, 2020
Reviewed on September 10, 2020
Accepted on October 29, 2020

Published online on March 23, 2021

Abstract

Background. Increased levels of plasma lipoproteins are among some of the modifiable risk factors for cardiovascular disease (CVD). Dietary changes and increased physical activity are the most powerful non-pharmacological interventions for achieving optimal plasma lipid levels.

Objectives. To investigate the effect of an intensive short-term lifestyle intervention on plasma lipid trajectories in overweight non-diabetic females.

Materials and methods. A total of 202 healthy overweight (body mass index (BMI) >27.5 kg/m^2) females underwent an intensive short-term (ten-week) intervention (at least 4 units of one-hour exercise activity weekly at optimal energy intake) aimed at lowering body weight. Plasma lipid (total cholesterol (TC), low-density-lipoprotein cholesterol (LDL-C), high-density-lipoprotein cholesterol (HDL-C), and triglycerides (TG)) levels were examined at baseline and every 2 weeks over the course of the ten-week intervention.

Results. There was a significant decrease in BMI (Δ –4.7%, $p < 0.001$) and body weight (Δ –4.9%, $p < 0.001$) after the intervention. Positive changes (decreases) in TC (Δ –8%, $p < 0.001$), TG (Δ –9%, $p < 0.001$) and LDL-C (Δ –11%, $p < 0.001$) were observed immediately after 2 weeks, but levels did not decrease further thereafter. In contrast, HDL-C did not increase as expected: after 2 weeks of intervention, we observed a significant decrease of about 6% ($p < 0.001$) followed by a slow return to baseline values. But even after 10 weeks of intervention, HDL-C values had not reached the values detected at baseline.

Conclusions. In overweight females, HDL-C decreased after short-term intensive lifestyle intervention. To confirm the protective effect of increased physical activity, plasma lipids need to be examined over a longer time period.

Key words: physical activity, overweight, HDL-cholesterol, short-term intervention

Cite as
Suchánek P, Lánská V, Stávek P, Hubáček JA. Short-term trajectories of exercise-induced plasma lipid changes in overweight females, with a focus on HDL-cholesterol. *Adv Clin Exp Med*. 2021;30(3):239–243. doi:10.17219/acem/129574

DOI
10.17219/acem/129574

Background

Despite progress in diagnostics and treatment, cardiovascular diseases (CVD) are still the major cause of mortality and morbidity in developed countries.[1] The major CVD risk factors are age, male sex, genetic predisposition, smoking, obesity, hypertension, diabetes, and dyslipidemia.[2]

Plasma lipids – especially the build-up of plasma cholesterol – play an important role in atherosclerotic plaque development.[3] The current recommended values are <5.0 mmol/L for total cholesterol (TC), <3.0 mmol/L for low-density-lipoprotein cholesterol (LDL-C), and <1.7 mmol/L for triglycerides (TG); these values should be even lower in individuals at high risk for CVD. High-density-lipoprotein cholesterol (HDL-C) values should be >1.0 mmol/L in males and >1.2 mmol/L in females.[4]

Both genetic and environmental factors affect plasma lipid values.[5–8] Among the environmental risk factors that lead to dyslipidemia, obesity seems to be the most important. The energy imbalance resulting in increased body weight and body mass index (BMI) values is influenced not only by insufficient physical activity and excess energy intake, but also (in addition to unfavorable genetic backgrounds) by other less discussed factors, such as side effects of commonly prescribed drugs, non-exercise activity thermogenesis and air-conditioning.[9,10]

As one of the main factors associated with CVD, obesity correlates with plasma lipid levels. Obese individuals typically exhibit increased levels of plasma LDL-C and TG, and decreased levels of plasma HDL-C.[11]

Increased physical activity (any kind of exercise) is a common lifestyle intervention widely used in treating obesity. Such regimens can lead to positive changes in lipid profiles, reductions in plasma LDL-C and TG and increases in plasma HDL-C.[12,13] However, studies on short-term lipid trajectories during lifestyle interventions are scarce, limited by very low numbers of examined subjects (between 10 and 25) and focus almost exclusively on males.[14–17]

Objectives

The aim of our study was to assess the impact of exercise on short-term trajectories (10 weeks) of plasma lipid fractions in a large sample of overweight adult females.

Materials and methods

Examined subjects

In total, 202 overweight (BMI at least 27.5 kg/m^2) adult females within the age range of 19–71 years (with quintiles interface 34/43/50 and 58 years, respectively), recruited through an advertisement on a lifestyle website and a women's magazine, were enrolled in the study. Individuals with diabetes, endocrine/autoimmune disease or any chronic inflammatory or neoplastic disease were excluded from the study. Detailed characteristics of the subjects and a summary of the data are presented in Table 1.

Six examinations were performed: (i) before intervention (baseline); (ii) after every two-week period (4 examinations); (iii) after the 10th week of intervention.

The study protocol was approved by the ethics committees at the Institute for Clinical and Experimental Medicine (Prague, Czech Republic) and Thomayer Hospital (Prague, Czech Republic) in agreement with the Helsinki Declaration of 1975. All subjects provided voluntary informed consent to participate in the study.

Anthropometrical parameters

Body weight was measured using an electronic weight scale (scaled to the nearest 0.1 kg). Height was measured with a stadiometer to the nearest 0.5 cm. Waist and hip circumferences were measured to an accuracy of 0.5 cm. The waist-to-hip ratio (WHR) and BMI were also calculated. To avoid potential inter-individual inaccuracies

Table 1. Characteristics of the subjects

Parameter	Time point							
	baseline	week 2	week 4	week 6	week 8	week 10	p-value*	p-value#
Age [years]	46.7 ±11.4	n.a.	n.a.	n.a.	n.a.	n.a.	–	–
Body weight [kg]	89.9 ±13.8	88.5 ±13.6	87.5 ±13.6	86.8 ±13.2	86.3 ±13.0	85.7 ±13.0	0.0001	0.0001
Waist [cm]	113.4 ±11.6	111.9 ±10.8	110.6 ±10.6	109.6 ±10.4	108.6 ±9.9	107.7 ±10.1	0.0001	0.0001
Hip [cm]	102.4 ±8.7	100.0 ±10.9	98.5 ±8.1	97.0 ±8.4	95.9 ±8.0	94.8 ±10.7	0.0001	0.0001
BMI [kg/m^2]	32.1 ±4.4	31.6 ±4.3	31.2 ±4.3	31.0 ±4.2	30.8 ±4.1	30.6 ±4.0	0.0001	0.0001
TC [mmol/L]	5.3 ±0.94	4.8 ±0.94	4.9 ±0.92	4.9 ±0.91	4.9 ±0.89	4.9 ±0.89	0.0001	0.0001
LDL-C [mmol/L]	3.23 ±0.83	2.88 ±0.84	2.94 ±0.78	2.96 ±0.78	2.98 ±0.79	3.01 ±0.80	0.0001	0.0005
HDL-C [mmol/L]	1.46 ±0.33	1.37 ±0.30	1.38 ±0.30	1.38 ±0.30	1.40 ±0.30	1.44 ±0.31	0.0001	n.s.
TG [mmol/L]	1.44 ±0.71	1.31 ±0.78	1.33 ±0.67	1.27 ±0.68	1.27 ±0.55	1.32 ±0.63	0.0001	0.0001

Data are presented as mean ± standard deviation (SD); p-values denote differences between baseline and week 2 (p-value*) and between baseline and week 10 (p-value#); n.a. – not applicable; n.s. – not significant.

in measurements, 1 trained nurse performed all of the anthropometrical examinations.

Intervention

The program was based on supervised ten-week lifestyle modification interventions.[18–20] Dietary intervention involved adjusting energy intake to the age-related optimum (max. 7500 kJ/day). Three times per week, the subjects participated in a sixty-minute-long supervised training session at a fitness center. Participants were advised to carry out 2 additional sessions per week (jogging, brisk walking or cycling), with at least 1 self-reported session performed per subject. All activities included aerobic exercise.

Participants were examined every 2 weeks. Subjects completed a one-day dietary report before each examination to assess compliance with the recommended dietary changes. Dietary recommendations were optimized after each control visit.

Lipid parameters

Blood samples were collected after twelve-hour overnight fasting at the beginning, and after every 2 weeks, of intervention. The final samples were taken after 10 weeks of intervention. Serum from blood was obtained through separation by centrifugation at 3500 rpm (10 min) and stored at –80°C. In all cases, aliquots of samples were analyzed on the same day as the entire experiment was completed. Concentrations of plasma TG and TC and LDL-C were analyzed using Roche Diagnostics kits (Basel, Switzerland; Ref. No. for kits: TG – 11730711, TC – 11491458, LDL-C – 27714423). The HDL-C level was determined after separation of apolipoprotein B-containing particles using a phosphotungstate-based method. The Hitachi 920 autoanalyzer (Hitachi, Tokyo, Japan) was used for all measurements. The laboratory was under the External Quality Assurance program of the Centers for Disease Prevention and Control (CDC; Atlanta, USA).

Statistical analysis

Multivariate analysis of variance (MANOVA) was used for statistical analysis. Parameter changes were adjusted for age, smoking and BMI (for plasma lipids only) at baseline. The TG values were logarithmically transformed before analysis. Results are presented as a percentage decrease, with values given as mean ± standard deviation (SD). A p-value <0.05 was considered significant.

Results

The characteristics of the individuals in the study examined before and after each intervention period are summarized in Table 1. The mean BMI at baseline was

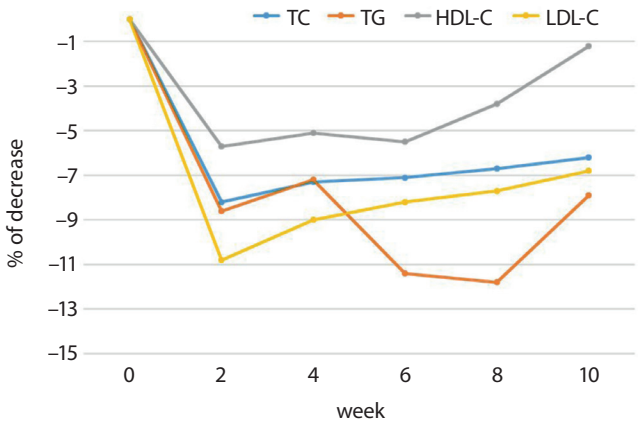

Fig. 1. Overview of short-term trajectories of plasma lipids over the ten-week intervention period

32.3 ±4.3 kg/m^2 with a minimum of 27.7 kg/m^2 and a maximum of 50.6 kg/m^2. Of the total participants, 30% were overweight while 43% had grade I obesity, 20% grade II obesity, and 7% grade III obesity.

As expected, there were significant continuous decreases in body weight ($p < 0.0001$), BMI ($p < 0.0001$) and waist ($p < 0.0001$) and hip ($p < 0.0001$) measurements after intervention (Table 1). Individual anthropometrical changes differed widely between baseline and final examinations. For example, the smallest decrease in body weight was only 0.2 kg (–0.3%), while the largest achieved was 15.0 kg (–11.3%). For mean values, all anthropometrical parameters examined revealed continuous decreases across all 5 measurements (Fig. 1).

Positive changes in anthropometrical parameters were accompanied by immediate and significant changes across all lipid parameters examined.

In the cases of both TC ($p < 0.0001$) and LDL-C ($p < 0.0001$), we observed a steep reduction in values (of about 8% for TC and as much as 11% for LDL-C) as early as after the first two-week intervention period (Table 1, Fig. 1). Values were relatively stable across the following measurements, with no further significant decreases observed. In fact, we observed a slight trend for a return to baseline values.

In the case of TG values, we observed a quick and highly significant ($p < 0.0001$) decrease in plasma values as early as after the first 2 weeks of intervention (Table 1, Fig. 1). In contrast to plasma total- and LDL-C values, TG values did not reach the minimum after the first 2 weeks, and there was a trend (albeit nonlinear) toward a further slight lowering of values.

Finally, the most interesting results pertained to HDL-C. In contrast to other plasma lipids, where changes in expected positive directions were observed almost immediately after the start of the intervention (at the first examination), HDL-C values did not follow this trend. In contrast, there was a significant drop in plasma HDL-C of 5.7% ($p < 0.0001$). For all subsequent measurements,

HDL-C values remained lower than those recorded at baseline. We did, however, note a slight increase beginning in week 8, with HDL-C almost reaching baseline levels after 10 weeks (but still 1.3% lower).

Discussion

In this study, we found that a short-term intensive lifestyle modification regime involving an increase in physical activity and optimization of energy intake in metabolically healthy overweight females led to a rapid decrease (within 2 weeks) in all plasma lipid parameters, including HDL-C levels.

The results of our study highlight the different trajectories of plasma lipids when analyzed over short intensive periods of intervention. We observed rapid and dramatic changes in plasma TC, LDL-C and TG concentrations in desirable directions. However, subsequent weeks of increased physical activity did not result in further decreases in these values.

Unexpectedly, plasma HDL-C concentrations decreased in the same manner (albeit not as dramatically) as other plasma counterparts. Even after 10 weeks of intervention, no HDL-C increases, in comparison to baseline values, were detected.

Our findings are in contrast to similar studies on the topic. In a study examining the short-term (20 min of physical exercise for 4 days) effect of physical activity among males (n = 10), Sabaka et al.[16] observed no effect on plasma HDL-C concentrations but a significant decrease in small dense HDL particles, with the effects disappearing after 2 days of rest. In a study using a similar protocol to ours (physical activity 3 times per week for 16 weeks), no effect on HDL-C was observed in patients with chronic kidney disease (n = 25, both males and females).[17] Similarly, the authors of another study involving 20 subjects (10 males and 10 females) with metabolic syndrome found that 3 months of moderately intensive exercise training (on cycle ergometers) did not lead to changes in HDL-C levels.[15] In their study of 14 young healthy men, Bounds et al.[14] reported a significant increase in HDL-C concentrations and a decrease in TG after only 2 weeks of aerobic exercise. Finally, the authors of the large interethnic HERITAGE study, which involved more than 600 adult males and females, documented a 3% increase in HDL-C with huge inter-individual variability in response to 20 weeks of supervised cycle ergometer exercise.[21] It is important to note that most of these studies were performed among males and recruited significantly lower numbers of participants (max. 25) in comparison to our study (n = 202).

Our study is also in contrast with results from a meta-analysis performed by Dattilo and Kris-Etherton.[22] They suggest that HDL-C decreases are linearly associated with the amount of body weight lost. However, the trajectories we observed show that maximal HDL-C decrease is achieved very quickly – specifically, just after 2 weeks of intervention. At this time point, the mean body weight loss was only 1.5 kg. Importantly, further body weight reduction was not accompanied by HDL-C decrease, but rather with slight return to baseline. Thus, there was no linear decrease in HDL-C concentrations in subjects that were actively losing weight.

Interestingly, it has been reported (in a review by März et al.[23]) that pharmacological treatment used to increase HDL-C concentrations is not accompanied by adequate reductions in cardiovascular outcomes. However, increasing HDL-C through lifestyle changes (not only increased physical activity, but also smoking cessation, for example) has positive effects on CVD outcomes.

Generally, it is recommended that physical activity be increased to improve plasma concentrations of HDL-C.[12] Our short-term study involving overweight, but otherwise healthy, female subjects shows that within about the first 2 months of starting exercise, plasma concentrations of HDL-C decreased in line with the same trajectories as other plasma lipids. Even after 10 weeks of intervention, plasma HDL-C values remained slightly below the baseline values found before the start of the intervention.

Limitations

Besides the strengths of our study – namely it being the first study of its kind to focus exclusively on females, and involving a well-controlled intensive lifestyle intervention boasting of a large number of highly motivated subjects, as well as ethnic homogeneity – our study also had some limitations. Unfortunately, the protocol of our study did not allow us to detect the time point at which HDL-C levels may have achieved significant improvement (i.e., a significant increase). And as our study only involved relatively healthy females, short-term lipid trajectories may be different in males and in individuals suffering from metabolic disease.

Conclusions

In conclusion, our short-term intervention involving physical activity and dietary intake optimization in overweight females led to reductions in HDL-C levels.

ORCID iDs

Pavel Suchánek https://orcid.org/ 0000-0001-7030-9992
Věra Lánská https://orcid.org/ 0000-0002-2832-5689
Petr Stávek https://orcid.org/ 0000-0002-5203-6537
Jaroslav Alois Hubáček https://orcid.org/ 0000-0001-6537-1353

References

1. Roth GA, Huffman MD, Moran AE, et al. Global and regional patterns in cardiovascular mortality from 1990 to 2013. *Circulation*. 2015; 132(17):1667–1678. doi:10.1161/CIRCULATIONAHA.114.008720
2. Tzoulaki I, Elliott P, Kontis V, Ezzati M. Worldwide exposures to cardiovascular risk factors and associated health effects: Current knowledge and data gaps. *Circulation*. 2016;133(23):2314–2333. doi:10.1161/CIRCULATIONAHA.115.008718
3. Goldstein JL, Brown MS. A century of cholesterol and coronaries: From plaques to genes to statins. *Cell*. 2015;161(1):161–172. doi:10.1016/j.cell.2015.01.036

4. Graham IM, Catapano AL, Wong ND. Current guidelines on prevention with a focus on dyslipidemias. *Cardiovasc Diagn Ther*. 2017; 7(Suppl 1):S4–S10. doi:10.21037/cdt.2017.04.04
5. Hegele RA. Plasma lipoproteins: Genetic influences and clinical implications. *Nat Rev Genet*. 2009;10(2):109–121. doi:10.1038/nrg2481
6. Durstine JL, Grandjean PW, Cox CA, Thompson PD. Lipids, lipoproteins, and exercise. *J Cardiopulm Rehabil*. 2002;22(6):385–398. doi:10.1097/00008483-200211000-00002
7. Schwarzova L, Hubacek JA, Vrablik M. Genetic predisposition of human plasma triglyceride concentrations. *Physiol Res*. 2015;64(Suppl 3): S341–S354. doi:10.33549/physiolres.933197
8. Siri-Tarino PW, Krauss RM. Diet, lipids, and cardiovascular disease. *Curr Opin Lipidol*. 2016;27(4):323–328. doi:10.1097/MOL.0000000000000310
9. Hubácek JA. Eat less and exercise more: Is it really enough to knock down the obesity pandemia? *Physiol Res*. 2009;58(Suppl 1):S1–S6. doi:10.33549/physiolres.931855
10. McAllister EJ, Dhurandhar NV, Keith SW, et al. Ten putative contributors to the obesity epidemic. *Crit Rev Food Sci Nutr*. 2009;49(10):868–913. doi:10.1080/10408390903372599
11. Klop B, Elte JW, Cabezas MC. Dyslipidemia in obesity: Mechanisms and potential targets. *Nutrients*. 2013;5(4):1218–1240. doi:10.3390/nu5041218
12. Gordon B, Chen S, Durstine JL. The effects of exercise training on the traditional lipid profile and beyond. *Curr Sports Med Rep*. 2014; 13(4):253–259. doi:10.1249/JSR.0000000000000073
13. Escolà-Gil JC, Julve J, Griffin BA, Freeman D, Blanco-Vaca F. HDL and lifestyle interventions. *Handb Exp Pharmacol*. 2015;224:569–592. doi:10.1007/978-3-319-09665-0_18
14. Bounds RG, Grandjean PW, O'Brien BC, Inman C, Crouse SF. Diet and short term plasma lipoprotein-lipid changes after exercise in trained men. *Int J Sport Nutr Exerc Metab*. 2000;10(2):114–127. doi:10.1123/ijsnem.10.2.114
15. Casella-Filho A, Chagas AC, Maranhão RC, et al. Effect of exercise training on plasma levels and functional properties of high-density lipoprotein cholesterol in the metabolic syndrome. *Am J Cardiol*. 2011;107(8):1168–1172. doi:10.1016/j.amjcard.2010.12.014
16. Sabaka P, Kruzliak P, Balaz D, et al. Effect of short term aerobic exercise on fasting and postprandial lipoprotein subfractions in healthy sedentary men. *Lipids Health Dis*. 2015;14:151. doi:10.1186/s12944-015-0148-5
17. Miele EM, Headley SAE, Germain M, et al. High-density lipoprotein particle pattern and overall lipid responses to a short-term moderate-intensity aerobic exercise training intervention in patients with chronic kidney disease. *Clin Kidney J*. 2017;10(4):524–531. doi:10.1093/ckj/sfx006
18. Dlouhá D, Suchánek P, Lánská V, Hubáček JA. Body mass index change in females after short-time life style intervention is not dependent on the FTO polymorphisms. *Physiol Res*. 2011;60(1):199–202. doi:10.33549/physiolres.932065
19. Suchanek P, Lorenzova A, Poledne R, Hubacek JA. Changes of plasma lipids during weight reduction in females depends on APOA5 variants. *Ann Nutr Metab*. 2008;53(2):104–108. doi:10.1159/000165358
20. Suchánek P, Lánská V, Hubáček JA. Body composition changes in adult females after lifestyle intervention are influenced by the NYD-SP18 variant. *Cent Eur J Public Health*. 2015;23(Suppl):S19–S22. doi:10.21101/cejph.a4105
21. Leon AS, Gaskill SE, Rice T, et al. Variability in the response of HDL cholesterol to exercise training in the HERITAGE Family Study. *Int J Sports Med*. 2002;23(1):1–9. doi:10.1055/s-2002-19270
22. Dattilo AM, Kris-Etherton PM. Effects of weight reduction on blood lipids and lipoproteins: A meta-analysis. *Am J Clin Nutr*. 1992;56(2): 320–328. doi:10.1093/ajcn/56.2.320
23. März W, Kleber ME, Scharnagl H, et al. HDL cholesterol: Reappraisal of its clinical relevance. *Clin Res Cardiol*. 2017;106(9):663–675. doi:10.1007/s00392-017-1106-1

Relationships between circulating galectin-3, extracellular matrix fibrosis and outcomes in dilated cardiomyopathy

Paweł Rubiś[1,A–F], Katarzyna Holcman[1,B,C,E,F], Ewa Dziewięcka[1,B,C,E,F], Sylwia Wiśniowska-Śmiałek[1,B,C,F], Aleksandra Karabinowska[1,B,C,F], Maria Szymonowicz[1,B,C,F], Lusine Khachatryan[1,B,C,F], Ewa Wypasek[1,A,C,E,F], Ann Garlitski[2,C,D,F], Andrzej Gackowski[1,C–F], Piotr Podolec[1,C,E,F]

[1] Department of Cardiac and Vascular Disease, John Paul II Hospital, Jagiellonian University Medical College, Kraków, Poland
[2] Tufts Medical Center, Boston, USA

A – research concept and design; B – collection and/or assembly of data; C – data analysis and interpretation; D – writing the article; E – critical revision of the article; F – final approval of the article

Advances in Clinical and Experimental Medicine, ISSN 1899–5276 (print), ISSN 2451–2680 (online) *Adv Clin Exp Med*. 2021;30(3):245–253

Address for correspondence
Paweł Rubiś
E-mail: pawelrub@poczta.onet.pl

Funding sources
This work was founded through the National Science Centre, Poland (grant No. 2013/09/D/NZ5/00252) and the Department of Scientific Research and Structural Funds of the Jagiellonian University Medical College, Kraków, Poland (grant No. K/ZDS/007192).

Conflict of interest
None declared

Received on December 15, 2018
Reviewed on March 17, 2019
Accepted on December 5, 2019

Published online on March 23, 2021

Cite as
Rubiś P, Holcman K, Dziewięcka E, et al. Relationships between circulating galectin-3, extracellular matrix fibrosis and outcomes in dilated cardiomyopathy. *Adv Clin Exp Med*. 2021;30(3):245–253. doi:10.17219/acem/115081

DOI
10.17219/acem/115081

Abstract

Background. Galectin-3 is an emerging biomarker in cardiovascular disease. Myocardial galectin-3 is involved in the pathology of cardiac fibrosis; however, the role of circulating galectin-3 is not yet established.

Objectives. To assess the relationships between circulating galectin-3, fibrosis and outcomes in dilated cardiomyopathy (DCM).

Materials and methods. We included 70 patients (age: 48 ±12.1 years, ejection fraction (EF) 24.4 ±7.4%) with new-onset DCM (n = 35, ≤6 months). Galectin-3 and procollagen type I and III (PICP, PINP, PIIICP, and PIIINP), transforming growth factor β (TGF-β), connective tissue growth factor (CTGF), osteopontin (OPN), matrix metalloproteinases (MMP-2 and -9), and tissue inhibitor (TIMP-1) were determined in serum at baseline and after 3 and 12 months. Patients underwent endomyocardial biopsy. The endpoint was a combination of death and urgent hospitalization at 12 months.

Results. Galectin-3 did not correlate with biopsy-determined fibrosis. Baseline galectin-3 correlated with OPN,, TIMP-1, PIIICP, and MMP-2. In new-onset DCM, galectin-3 levels at baseline were higher than at 3 and 12 months, whereas in chronic DCM there was no difference. Galectin-3 was a predictor of the endpoint (hazard ratio (HR) = 1.115; 95% confidence interval (95% CI) = 1.009–1.231; $p < 0.05$). The best cut-off value was 14.54 ng/mL (area under the curve (AUC) = 0.67). Patients with galectin-3 ≥14.54 ng/mL had an increased risk of events (HR = 2.569; 95% CI = 1.098–6.009; $p < 0.05$).

Conclusions. Circulating galectin-3 is unrelated to fibrosis. Serial measurements of galectin-3 correlated with markers of fibrosis, including markers of collagen synthesis and OPN. Circulating galectin-3 was independently associated with cardiovascular (CV) outcomes in DCM.

Key words: fibrosis, kinetics, galectin-3, dilated cardiomyopathy

Background

Fibrosis of the extracellular matrix (ECM) is a common pathway in many cardiac diseases leading ultimately to the development of heart failure (HF).[1] Patients with dilated cardiomyopathy (DCM) are particularly predisposed to extensive ECM fibrosis, specifically reactive fibrosis, which contributes to functional impairment and subsequent ventricular arrhythmias.[2] The mechanisms responsible for ECM fibrosis are incompletely described.

Galectin-3 belongs to the β-galactoside-binding lectin family and serves as a matricellular protein which binds basic components of ECM, such as collagens, elastin and fibronectin.[3] In vitro studies have revealed that galectin-3 is a pivotal protein involved in the development of ECM fibrosis, as it stimulates transdifferentiation of fibroblasts into highly active myofibroblasts that produce ECM compounds, e.g., collagens and elastin, in excess.[4] Additionally, galectin-3 is an important component of the renin–angiotensin–aldosterone pathway that enhances ECM fibrosis.[5] Thus, the significance of myocardial (in situ) galectin-3 in ECM fibrosis has been unequivocally proven. However, the role of circulating galectin-3 is unclear.

Numerous claims were published that circulating galectin-3 is a marker of cardiac fibrosis.[6–8] Upon our review of the medical literature, it seems that these assertions are premature. In fact, very few studies performed an in-depth evaluation of the associations between circulating galectin-3 and ECM fibrosis in HF.[9–11] In those studies, cardiac fibrosis was assessed, either invasively (by means of endomyocardial biopsy (EMB) followed by a detailed laboratory assessment of samples) or non-invasively (with magnetic resonance imaging (MRI)). The determination of late gadolinium enhancement (LGE) or post-LGE T1 relaxation time served as surrogates of ECM fibrosis. However, even in those studies, an association between circulating galectin-3 and ECM fibrosis (assessed with either method) was not clearly confirmed.

Objectives

Although a considerable amount of work has been published on the subject of galectin-3 in cardiomyopathy and HF, we have identified knowledge gaps that warrant further exploration. The relationship between circulating galectin-3 and cardiac fibrosis is inconclusive. Thus, our study rigorously explores the associations between galectin-3 and invasively determined ECM fibrosis (expressed qualitatively and quantitatively) in a homogenous group of DCM patients. Furthermore, the relationship between galectin-3 and other serum markers of fibrosis (such as markers of collagen synthesis, fibrosis controlling factors or metalloproteinases (MMPs)) is generally unknown. The kinetics of serum galectin-3 in DCM patients stratified according to disease duration and fibrosis status have not been well described. Finally, we aim to explore the association between galectin-3 and survival in HF in DCM patients, as few studies have reported on this relationship.

Materials and methods

Study population

Between July 2014 and October 2015, we enrolled 70 consecutive DCM patients who fulfilled pre-specified criteria and were willing to participate in the study. Dilated cardiomyopathy was diagnosed according to the definition of the European Society of Cardiology 2007 guidelines, after an exclusion of significant coronary artery disease (CAD), primary heart valve disease, congenital heart disease, and arterial hypertension.[12] Based on the duration of symptoms, patients were divided into equal groups consisting of 35 subjects with new-onset (group 1, ≤6 months) and chronic (group 2, >6 months) DCM. The duration of HF symptoms was defined as the time from the onset of subjective symptoms (dyspnea on exertion or at rest, paroxysmal nocturnal dyspnea, orthopnea, palpitations) and/or edema to the index hospitalization or ambulatory visit in cardiology clinic. Patients with the presence of concomitant non-cardiac diseases, such as bone and joint diseases, chronic liver insufficiency, peripheral atherosclerosis, and neoplasms affecting collagen metabolism and circulating levels of procollagens, were excluded. Each patient's clinical status was re-evaluated, with echocardiography and blood sampling repeated at 3 and 12 months (patients' flowchart is presented in Fig. 1). We also evaluated 20 healthy volunteers as a control group who underwent blood sampling and echocardiography. The study protocol was approved by the John Paul II Institutional Review Board and the Kraków Medical Chamber Ethics Committee (reference No. 134/KBL/OIL/2013). All patients gave a written informed consent prior to inclusion in the study.

Endomyocardial biopsy

Endomyocardial biopsy (EMB) procedures were performed by experienced operators via a femoral or jugular vein approach. Long (104 cm), flexible, disposable 7 French biopsy forceps with small jaws (Cordis®; Johnson & Johnson Co Inc., Miami Lakes, USA) were used.[13] Up to 5 myocardial samples were obtained, which were immediately stored in formalin for light microscopic examination. The presence of fibrosis was determined qualitatively and quantitatively by an experienced pathologist blinded to the clinical data. Specimens for fibrosis assessment were stained with Masson's trichrome; fibrotic areas stained blue, and normal muscle fibers stained red. Collagen volume fraction (CVF) was assessed with quantitative morphometry as previously described.[14]

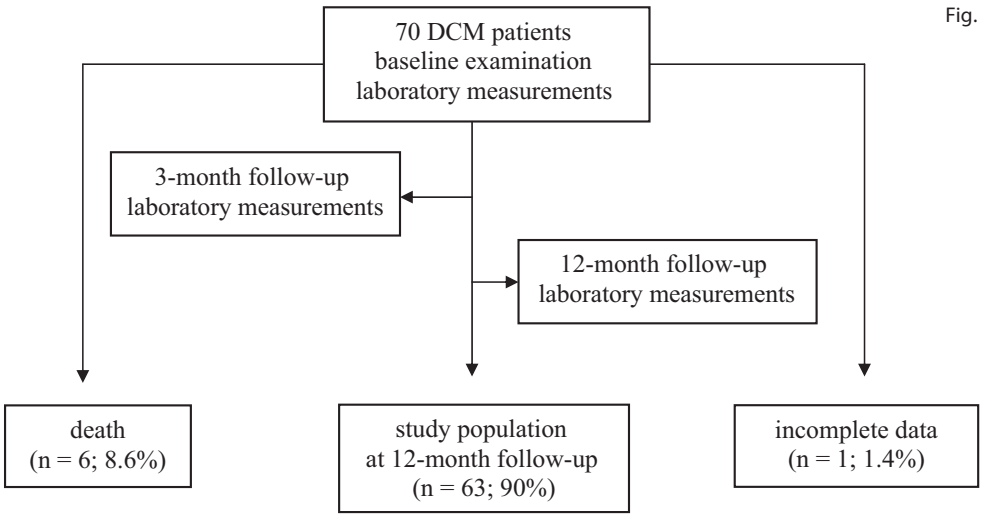

Fig. 1. Study flowchart

Laboratory measurements

Venous blood samples for biomarkers measurements were drawn after an overnight fast, typically between 8 a.m. and 9 a.m. After centrifugation, the supernatant was stored at –20°C. The concentration of collagen synthesis markers (carboxy- and amino-terminal propeptides of procollagen type I and III (PICP, PINP, PIIICP, and PIIINP)) and fibrosis controlling factors (transforming growth factor β (TGF-β) and connective tissue growth factor (CTGF), osteopontin (OPN), as well as matrix metalloproteinases (MMP-2 and -9) and tissue inhibitor (TIMP-1)) were determined in plasma using a commercially available enzyme-linked immunosorbent assay (ELISA), as previously described.[15] The levels of galectin-3 were measured with ELISA using a commercially available kit (Human Galectin-3 ELISA, RAF015R; BioVendor, Brno, Czech Republic). The serum samples and galectin-3 standard dilutions were added to microwells that were coated with anti-galectin-3 antibody. Galectin-3 present in the sample or standard was bound to antibodies adsorbed to the microwells. Following incubation, a wash step was performed and the horseradish peroxidase (HRP)-conjugated anti-galectin-3 antibodies were added binding to galectin-3 captured by the first antibody. Again following incubation, unbound HRP-conjugated anti-galectin-3 antibodies were removed during a wash step, and a substrate solution reactive with HRP was added to the wells. A colored product was formed in proportion to the amount of galectin-3 present in the sample or standard. The reaction was terminated by the addition of acid and absorbance was measured at 450 nm. The galectin-3 sample concentration was determined based on the standard curve. Baseline, 3- and 12-month measurements of galectin-3, PICP, PINP, PIIICP, PIIINP, TGF-β, CTGF, and OPN were obtained; however, for MMP-2, MMP-9 and TIMP-1, only baseline measurements were available. Intra-assay and inter-assay coefficients of variation were <7%.

Statistical analysis

The data are presented either as mean ± standard deviation (SD), median and interquartile range (IQR), or count and percentages. The normality of the distribution of variables was assessed with a Shapiro–Wilk test. Comparisons of clinical parameters between 2 groups were conducted with a Mann–Whitney U test, as a lack of normality was found. Univariate relationships between galectin-3 and serum markers of fibrosis were determined with Spearman correlation analysis. Two endpoints were analyzed: cardiovascular (CV) death and the combined endpoint that was composed of CV death and urgent HF hospitalization at 12 months. Survival data were analyzed using the Kaplan–Meier method, and compared with the log-rank test. To examine the associations of galectin-3 with endpoints of interest (unadjusted analyses and analyses adjusted for age, duration of disease, CVF, ejection fraction (EF), and N-terminal pro-B-type natriuretic peptide (NT-proBNP)) Cox proportional hazard analyses were performed. Calculations for the optimal cut-off values of galectin-3 (in order to determine the cut-off values for adverse outcomes) were carried out using a receiver operating characteristic (ROC) curve. Patients were compared according to a galectin-3 optimal cut-off value, derived from ROC analysis, with the use of a log-rank test. All results were considered statistically significant when the p-value was <0.05. All the analyses were conducted in R software v. 3.3.2 (The R Foundation for Statistical Computing, Vienna, Austria).

Results

Baseline characteristics

Table 1 shows the baseline characteristics of the study population. The majority of patients were male (63; 90%) with symptomatic HF (New York Heart Association (NYHA)

Table 1. Baseline characteristics of the study population

Parameter	DCM (n = 70)
Age [years]	48 ±12.1
Sex [male/female]	63 (90%)/7 (10%)
BMI [kg/m^2]	26.8 ±5.4
NYHA class	2.49 ±0.7
Duration [months]	24.3 ±35.6
LBBB [n, %]	18 (25.7%)
LVESd/BSA [mm/m^2]	30.1 ±7.1
LVEDd/BSA [mm/m^2]	35.6 ±7.0
LVESvol/BSA [mL/m^2]	96.1 ±49.0
LVEDvol/BSA [mL/m^2]	126.8 ±59.8
EF [%]	24.4 ±7.4
E/E'(average sep+years)	20.8 ±11.4
ECM fibrosis [n, %]	24 (34.3%)
PA mean [mm Hg]	23.1 ±10.9
PH [n, %]	27 (39.7%)
VO_2 peak [mL/kg/min]	16.5 ±6.1
Hb [g/dL]	14 ±1.6
hs-troponin T [ng/mL]	0.022 ±0.018
hs-CRP [mg/dL]	9.52 ±23.6
NT-proBNP [pg/mL]	3373 ±5428
β-blocker [n, %]	69 (98.6%)
ACE-I or ARB [n, %]	68 (97.1%)
MRA [n, %]	66 (94%)
Furosemide [n, %]	42 (60%)
CRT-D [n, %]	20 (28.6%)

Data are presented as mean ±SD or n (%); DCM – dilated cardiomyopathy; BMI – body mass index; NYHA – New York Heart Association; LBBB – left bundle branch block; LVESd – left ventricle end-systolic diameter indexed to body surface area; LVEDd – left ventricle end-diastolic diameter indexed to body surface area; LVEDd/BSA; EF – ejection fraction; E/E' – ratio of early mitral inflow velocity to early mitral myocardial velocity; ECM – extracellular matrix; PA mean – mean pulmonary pressure; VO_2 peak – peak oxygen uptake; Hb – hemoglobin; hs-CRP – high-sensitivity C-reactive protein; NT-proBNP – N-terminal pro-B-type natriuretic peptide; ACE-I – angiotensin-converting enzyme inhibitors; ARB – angiotensin II receptor blockers; MRA – mineralocorticoid receptor antagonists; CRT-D – cardiac resynchronization therapy with cardioverter/defibrillator.

class 2.49 ±0.7). All patients had severely remodeled left ventricle (LV; indexed to BSA left ventricle end-systolic (LVES) volume 96.1 ±49 mL/m^2 and left ventricle end-diastolic (LVED) volume 126.8 ±59.8 mL/m^2) with significantly depressed LV systolic (EF 24.4 ±7.4%) and diastolic (E/E' 20.8 ±11.4) function. Approximately 1/3 (24 (34.3%)) of patients had ECM fibrosis diagnosed with EMB. Patients had significantly increased serum NT-proBNP level (3373 ±5428 pg/mL). All patients were on optimal medical therapy: β-blockers in 69 (98.6%), angiotensin-converting enzyme inhibitors/angiotensin II receptor blockers (ACE-I/ARB) in 68 (97.1%), mineralocorticoid receptor antagonists (MRA) in 66 (94%), and implantable cardiac device with or without cardiac resynchronization therapy (ICD ±CRT) in 20 (28.6%).

Comparison of baseline, 3- and 12-month galectin-3 between DCM patients and control group

The control group consisted of 20 healthy subjects that were previously characterized.[15] Comparison of the baseline, 3- and 12-month serum galectin-3 values of DCM patients with baseline values of 20 control subjects is presented in Table 2. All measurements were significantly higher in DCM patients compared to controls.

Relationships between galectin-3, invasively determined ECM fibrosis and serum markers of fibrosis

Baseline galectin-3 did not correlate with either qualitative ECM fibrosis assessment ($r = -0.13$, $p = 0.29$) or quantitative measurement, expressed as CVF ($r = -0.12$, $p = 0.58$). Baseline galectin-3 correlated with the following baseline markers of fibrosis: OPN (0.27; $p < 0.02$), TIMP-1 (0.23; $p < 0.03$), PIIICP (0.27; $p < 0.03$), and MMP-2 (0.27; $p < 0.03$). Galectin-3 at 3-month follow-up correlated with the following 3-month markers: OPN (0.37; $p < 0.004$), PINP (0.27; $p < 0.03$) and PIIINP (0.34; $p < 0.006$). Galectin-3 at 12-month follow-up correlated only with 12-month OPN (0.35; $p < 0.005$) and PIIICP (0.29; $p < 0.04$).

Kinetics of galectin-3 in new-onset and chronic DCM

In patients with new-onset DCM, serum levels of galectin-3 at baseline were significantly higher than galectin-3 levels at 3-and 12-month follow-up (14.01 ng/mL (11.17–17.8 ng/mL) compared to 12.42 ng/mL (10.34–14.59 ng/mL) compared to 12.32 ng/mL (10.22–15.26 ng/mL), respectively;

Table 2. Comparison of serum galectin-3 between DCM patients and control group at baseline, 3 and 12-month follow-up

Parameter	DCM (n = 70)	Control (n = 20)	p-value
Baseline galectin-3 [ng/mL]	14.26 (11.03–17.47)	9.84 (8.6–10.9)	<0.001
3-month galectin-3 [ng/mL]	12.5 (10.22–15.07)	9.84 (8.6–10.9)	0.002
12-month galectin-3 [ng/mL]	13.23 (10.43–16.06)	9.84 (8.6–10.9)	<0.001

Data are presented as median and interquartile range; DCM – dilated cardiomyopathy.

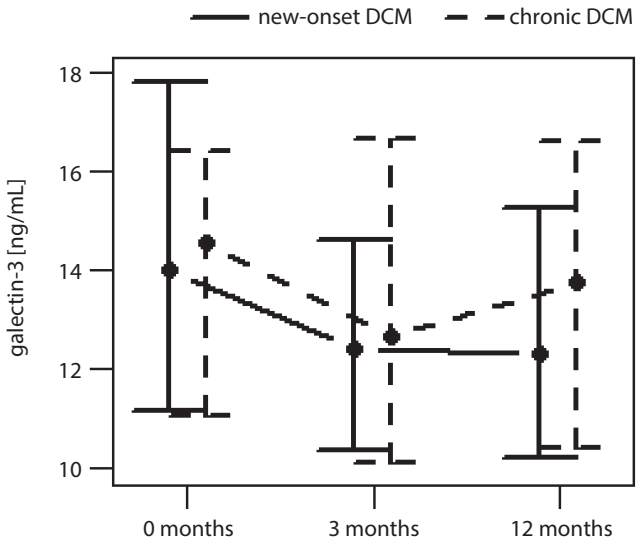

Fig. 2. 12-month patterns of serum galectin-3 in new-onset and chronic DCM

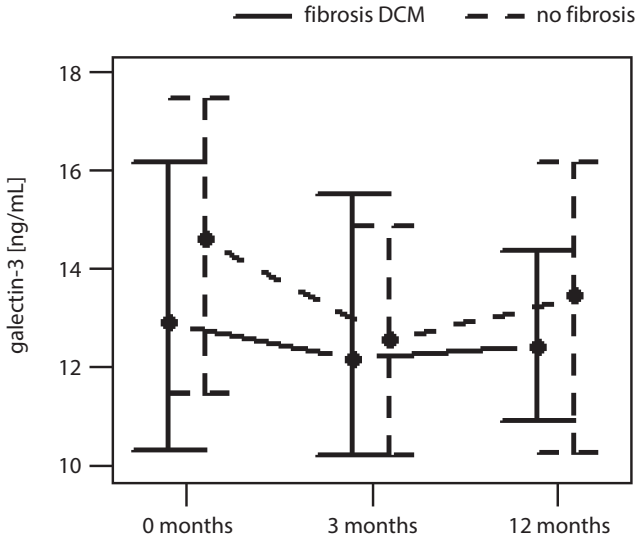

Fig. 3. 12-month patterns of serum galectin-3 in DCM with and without fibrosis

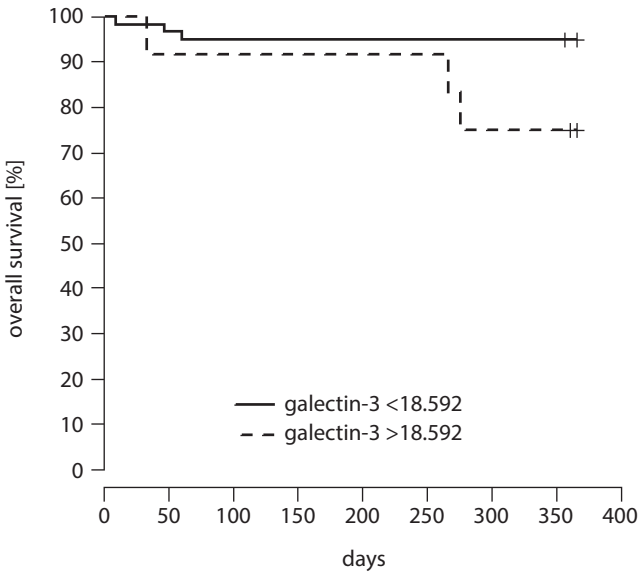

Fig. 4. Kaplan–Meier 12-month survival curves for galectin-3 cut-off value of 18.592 ng/mL

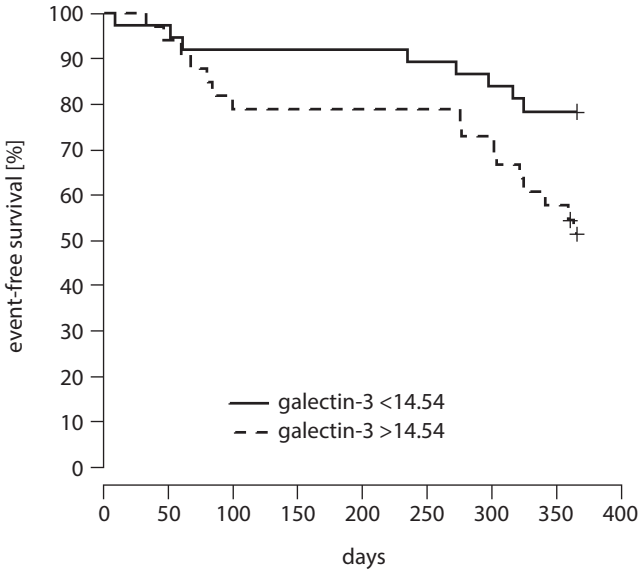

Fig. 5. Kaplan–Meier 12-month event-free curves for galectin-3 cut-off value of 14.54 ng/mL

$p < 0.001$). Of note, there was no difference between values at 3- and 12-month follow-up. In contrast, galectin-3 levels in patients with chronic DCM were similar at baseline and at 3 and 12 months (14.54 ng/mL (11.04–16.39 ng/mL) compared to 12.66 ng/mL (10.12–16.65 ng/mL) compared to 13.74 ng/mL (10.43–16.59 ng/mL), respectively; $p = 0.18$ and $p = 0.58$, respectively). Similarly, there were no differences between 3- and 12-month follow-up ($p = 0.27$). The kinetics of galectin-3 over the 12-month follow-up are presented separately for new-onset and chronic DCM groups in Fig. 2 and Fig. 3. The kinetics of galectin-3 in new-onset DCM are characterized by a decreasing pattern (Fig. 2); in chronic DCM, the kinetics of galectin-3 are flat. Comparisons of baseline, 3- and 12-month galectin-3 values between new-onset and chronic DCM revealed that there were no differences between the 2 groups (Table 3, Fig. 4).

Kinetics of galectin-3 in DCM patients with and without fibrosis

Galectin-3 serum levels were similar at the index visit, 3- and 12-month follow-up in patients with ECM fibrosis (12.9 ng/mL (10.33–16.18 ng/mL) compared to 12.18 ng/mL (10.23–15.49 ng/mL) compared to 12.43 ng/mL (10.89–14.38 ng/mL); $p = 0.64$ and $p = 0.99$, respectively). No differences were observed between 3- and 12-month measurements ($p = 0.54$). However, in patients without ECM fibrosis, galectin-3 levels significantly decreased between baseline and 3-month follow-up (14.61 ng/mL (11.46–17.47 ng/mL) compared to 12.58 ng/mL (10.23–14.87 ng/mL); $p < 0.001$). Although galectin-3 levels

Table 3. Correlations between galectin-3 and serum markers of fibrosis, measured at baseline and at 3- and 12-months follow-up

Parameter	Baseline measurements r-; p-value	3-month measurements r-; p-value	12-month measurements r-; p-value
PICP [ng/mL]	–0.08; 0.52	0.01; 0.92	0.07; 0.63
PINP [pg/mL]	–0.06; 0.64	0.27; 0.03	0.17; 0.25
PIIICP [ng/mL]	0.27; 0.03	0.19; 0.13	0.29; 0.05
PIIINP [ng/mL]	0.12; 0.34	0.35; 0.006	0.13; 0.37
OPN [ng/mL]	0.27; 0.02	0.37; 0.004	0.35; 0.005
TGF-β1 [pg/mL]	0.17; 0.17	–0.08; 0.51	0.05; 0.97
CTGF [ng/mL]	–0.09; 0.45	–0.04; 0.75	0.09; 0.53
MMP-2 [ng/mL]	0.27; 0.03	–	–
MMP-9 [pg/mL]	0.05; 0.68	–	–
TIMP-1 [pg/mL]	0.27; 0.03	–	–

r – Spearman rho correlation coefficient; PICP – carboxy-terminal propeptide of procollagen type I; PINP – amino-terminal propeptide of procollagen type I; PIIICP – carboxy-terminal propeptide of procollagen type III; PIIINP – amino-terminal propeptide of procollagen type III; OPN – osteopontin; TGF-β1 – transforming growth factor β1; CTGF – connective tissue growth factor; MMP-2 – matrix metalloproteinase-2; MMP-9 – matrix metalloproteinase-9; TIMP-1 – tissue inhibitor-1.

Table 4. Levels of galectin-3 at baseline and at 3- and 12-month follow-up in patients with new-onset and chronic DCM

Parameter	New-onset DCM (n = 35)	Chronic DCM (n = 35)	p-value
Baseline galectin-3 [ng/mL]	14.01 (11.17–17.8)	14.54 (11.04–16.39)	0.79
3-month galectin-3 [ng/mL]	12.42 (10.34–14.59)	12.66 (10.12–16.65)	0.53
12-month galectin-3 [ng/mL]	12.32 (10.22–15.26)	13.74 (10.43–16.59)	0.29

Data are presented as median and interquartile range; DCM – dilated cardiomyopathy.

Table 5. Levels of galectin-3 at baseline and at 3- and 12-month follow-up in DCM patients with and without ECM fibrosis

Parameter	Fibrosis negative DCM (n = 46)	Fibrosis positive (n = 24)	p-value
Baseline galectin-3 [ng/mL]	14.61 (11.46–17.47)	12.9 (10.33–16.18)	0.29
3-month galectin-3 [ng/mL]	12.58 (10.23–14.87)	12.18 (10.23–15.49)	0.94
12-month galectin-3 [ng/mL]	13.44 (10.28–16.17)	12.43 (10.89–14.38)	0.53

Data are presented as median and interquartile range.

had a tendency to increase between 3- and 12-months, at 12-months the levels still remained significantly lower in comparison to baseline values (14.61 ng/mL (11.46–17.47 ng/mL) compared to 13.44 ng/mL (10.28–16.17 ng/mL); $p < 0.05$). The comparison of galectin-3 levels between 3- and 12-months showed similar results ($p = 0.15$). Those patterns reveal that circulating galectin-3 decreases in DCM patients without fibrosis; in patients with fibrosis, galectin-3 levels are unchanged.

Galectin-3 and CV outcomes in DCM

During the 12-month follow-up, CV death occurred in 6 (8.6%) patients and urgent HF hospitalization in 19 (27.1%) patients. Thus, the combined endpoint occurred in 25 patients. Cox proportional hazard analyses revealed that baseline galectin-3 was a predictor of CV death in unadjusted (hazard ratio (HR) = 1.204; 95% confidence interval (95% CI) = 1.024–1.415; $p < 0.05$) and adjusted (HR = 1.246; 95% CI = 1.02–1.523; $p < 0.05$) models. In addition, galectin-3 was also a significant predictor of the combined endpoint in unadjusted (HR = 1.105; 95% CI = 1.012–1.207; $p < 0.05$) and adjusted (HR = 1.115; 95% CI = 1.009–1.231; $p < 0.05$) models. The ROC analysis was conducted to identify the optimal galectin-3 level for the prediction of CV death and the combined endpoint. The optimal galectin-3 cut-off value for the prediction of CV death was 18.592 ng/mL, with a sensitivity of 66.7% and specificity of 84.4% (area under curve (AUC) = 0.74). Event rates were calculated using a Kaplan–Meier analysis according to the galectin-3 cut-off value determined with the ROC curve (Fig. 4). Patients with galectin-3 ≥18.592 ng/mL had a significantly increased risk of CV death (HR = 5.053; 95% CI = 1.02–25.049; $p < 0.05$) compared to those with galectin-3 <18.592 ng/mL. The event curves are initially superimposed but begin to diverge after approx. 250 days. In terms of galectin-3 and the combined endpoint, the optimal cut-off value for galectin-3 was 14.54 ng/mL, with a sensitivity of 70.3% and specificity of 63% (AUC = 0.67). In addition, event rates were calculated according

to the galectin-3 cut-off of 14.54 ng/mL (Fig. 5). Patients with galectin-3 ≥14.54 ng/mL had a significantly increased risk of the combined endpoint (HR = 2.569; 95% CI = 1.098–6.009; p < 0.05) compare to those with galectin-3 <14.54 ng/mL. The event curves diverge quickly at approx. 50 days and continue to diverge with time.

Discussion

Relationships between galectin-3 and ECM fibrosis and serum markers of fibrosis

Based on numerous in vitro experiments, galectin-3 has been established as an important pro-fibrotic protein.[4,5,16] However, the question remains whether serum galectin-3 level is associated with cardiac fibrosis and consequently can be used as a reliable biomarker. To date, investigators have reported contradictory findings. Following long-term LV assist device (LVAD) therapy, Lok et al. observed an increase in myocardial fibrosis that paralleled an increase in the concentration of galectin-3. Although the authors did not perform robust statistical calculations on the associations between fibrosis and galectin-3, these findings highlight their potential link.[10] In contrast, Besler et al. observed relatively strong correlations (r = 0.63) between myocardial galectin-3 and biopsy-proven ECM fibrosis in inflammatory DCM. Importantly, the authors did not observe any relationship between serum galectin-3 and fibrosis.[17] Our study extends this negative finding on the lack of association between ECM fibrosis and serum galectin-3 to non-inflammatory DCM (as no acute or chronic myocardial inflammation was observed in myocardial samples).

The ECM fibrosis can also be assessed non-invasively by means of magnetic resonance imaging. Vergaro et al. observed that serum galectin-3 was an independent predictor of LV fibrosis as assessed by LGE in DCM patients.[11] In a similar fashion, Lepojärvi et al. found that patients with stable coronary artery disease who had the highest values of plasma galectin-3 had the lowest post-LGE T1 relaxation time, which was used as a non-invasive marker of cardiac fibrosis.[18] There are both advantages and disadvantages to determining fibrosis via biopsy or resonance. Nevertheless, our study clearly demonstrated the absence of a relationship between biopsy-proven fibrosis and circulating galectin-3.

Another approach used to estimate cardiac fibrosis is the measurement of circulating markers of fibrosis. However, this strategy should be interpreted with caution, as numerous studies have demonstrated the absence of associations between various markers of fibrosis and invasively determined fibrosis.[15,19–21] We report weak to moderate correlations between baseline galectin-3 and markers of collagen synthesis such as PIIICP, OPN, MMP-2, and TIMP-1. Uniquely, we investigated associations between galectin-3 and markers of collagen synthesis, OPN, TGF, and CTGF at 3 and 12 months. In terms of markers of collagen synthesis, the observed pattern is not consistent as we observed changing correlations between markers of collagen type I and III synthesis. On the other hand, for fibrosis controlling factors, the pattern is clear, as galectin-3 repeatedly correlated with OPN.

Kinetics of galectin-3 in dilated cardiomyopathy

Despite extensive exploration of galectin-3 in various cardiac conditions, the kinetics of galectin-3 have not been well-defined in patients with and without ECM fibrosis. As suggested in a recent American Heart Association (AHA) document, galectin-3 is a promising marker, but knowledge gaps – such as kinetic patterns – need to be addressed.[22]

Before any attempt is made to analyze the kinetics of any circulating marker, it is of paramount importance to understand its reference intervals, variability and biologic determinants. Krintus et al. have recently established galectin-3 reference intervals based on a study of 180 healthy individuals. They reported the lack of impact of known biological determinants, including age, on galectin-3 blood measurements.[23] In terms of HF and galectin-3, it was reported that galectin-3 short-term biologic variability, defined as 5 measurements within a three-week period, was 7.1%, and long-term (3 measurements within a three-month period) was 7.7%.[24] Similar observations were made by Meijers et al.; there were low levels of biologic variability of galectin-3 in HF, in comparison to much higher variability of NT-proBNP, over a six-week period.[25] In addition, we have previously reported the 12-month kinetics of serum markers of collagen synthesis, TGF and CTGF, which differ between patients with and without ECM fibrosis.[26] In the present study, the kinetics of galectin-3 were analyzed over a longer 3- and 12-month follow-up, and the observed values significantly exceeded previously reported biological variability. In terms of galectin-3 in patients with ECM fibrosis, repeated measurements are within expected biologic variability. We identified 2 distinct patterns of galectin-3 over a 12-month period. The 1st pattern was characterized by a gradual decrease and was observed in patients with a recent diagnosis of DCM and without ECM fibrosis. The 2nd pattern was characterized by stable measurements and was observed in patients with chronic DCM and with ECM fibrosis.

Galectin-3 and outcomes in dilated cardiomyopathy

Despite numerous studies, the relationship between circulating galectin-3 and CV outcomes has not been definitively defined. Recently, professional cardiac societies

have suggested that galectin-3 is a potential new biomarker in the field of HF. However, the scientific evidence supporting the prognostic role of galectin-3 is weak and requires further evaluation. We identified studies with contradictory conclusions on the prognostic role of galectin-3 in HF.[27–36] Imran et al. have recently published a meta-analysis of 13 studies that evaluated the prognostic role of galectin-3 in the context of NT-proBNP and parameters of renal function.[37] The authors concluded that galectin-3 was independently associated with CV mortality, both in HF and in the general population. In our study, we do not attempt to conclusively define the relationship of galectin-3 role in HF given study limitations such as a small sample size and a short observational period. However, we studied a homogenous mid-sized DCM cohort and used well-defined, clinical endpoints of CV mortality and the combined endpoint of CV mortality and urgent HF hospitalization. We observed that galectin-3 was clearly associated with predefined endpoints. Based on ROC analyses, we were able to identify patients with a worse prognosis. Larger, well-designed studies are required to ultimately verify the prognostic role of galectin-3 before it can be included in diagnostic pathways.

Limitations

We would like to acknowledge several limitations of the study. The proper assessment of fibrosis may be influenced by sampling error, patchy distribution of fibrosis, and harvesting from right ventricle (RV) compared to LV. The MMP-2, MMP-9 and TIMP-1 were measured only at baseline. Our study population of 70 patients may seem small, and the observation period of 1 year may be relatively short. On the other hand, all of our patients underwent biopsy, making the cohort at least a moderate-size population in the field of DCM and biopsy studies. During the 12-month follow-up, we observed the occurrence of the primary endpoint in 25 patients (6 deaths and 19 urgent hospital admissions), which constitutes a large number of events for analysis.

Conclusions

Circulating galectin-3 is unrelated to invasively-determined ECM fibrosis in DCM. Serial measurements of galectin-3 correlated with markers of fibrosis, including markers of collagen synthesis and OPN. However, there were no correlations between galectin-3 and TGF or CTGF. Galectin-3 kinetics vary at 12 months in patients stratified according to disease duration and fibrosis status. Circulating galectin-3 was independently associated with CV outcomes in DCM.

ORCID iDs

Paweł Rubiś https://orcid.org/ 0000-0002-6979-3411
Katarzyna Holcman https://orcid.org/ 0000-0002-6895-4076
Ewa Dziewięcka https://orcid.org/ 0000-0002-7921-5447
Sylwia Wiśniowska-Śmiałek https://orcid.org/ 0000-0002-7563-6586
Aleksandra Karabinowska https://orcid.org/ 0000-0003-2126-8236
Maria Szymonowicz https://orcid.org/ 0000-0003-0653-5156
Lusine Khachatryan https://orcid.org/ 0000-0002-0218-9092
Ewa Wypasek https://orcid.org/ 0000-0002-4225-6405
Ann Garlitski https://orcid.org/ 0000-0003-2793-7816
Andrzej Gackowski https://orcid.org/ 0000-0003-4545-6514
Piotr Podolec https://orcid.org/ 0000-0001-6101-2935

References

1. Weber KT. Cardiac interstitium in health and disease: The fibrillar collagen network. *J Am Coll Cardiol*. 1989;13(7):1637–1652. doi:10.1016/0735-1097(89)90360-4
2. Japp AG, Gulati A, Cook SA, Cowie MR, Prasad SK. The diagnosis and evaluation of dilated cardiomyopathy. *J Am Coll Cardiol*. 2016;67(25):2996–3010. doi:10.1016/j.jacc.2016.03.590
3. Gil CD, Cooper D, Rosignoli G, Perretti M, Oliani SM. Inflammation-induced modulation of cellular galectin-1 and -3 expression in a model of rat peritonitis. *Inflamm Res*. 2006;55(3):99–107.
4. Sharma UC, Pokharel S, van Brakel TJ, et al. Galectin-3 marks activated macrophages in failure-prone hypertrophied hearts and contributes to cardiac dysfunction. *Circulation*. 2004;110(19):3121–3131. doi:10.1161/01.CIR.0000147181.65298.4D
5. Calvier L, Martinez-Martinez E, Miana M, et al. The impact of galectin-3 inhibition on aldosterone-induced cardiac and renal injuries. *JACC Heart Fail*. 2015;3(1):59–67. doi:10.1016/j.jchf.2014.08.002
6. Ho JE, Liu C, Lyass A, et al. Galectin-3, a marker of cardiac fibrosis, predicts incident heart failure in the community. *J Am Coll Cardiol*. 2012;60(14):1249–1256. doi:10.1016/j.jacc.2012.04.053
7. De Boer RA, Voors AA, Muntendam P, Van Gilst WH, Van Veldhuisen DJ. Galectin-3: A novel mediator of heart failure development and progression. *Eur J Heart Fail*. 2009;11(9):811–817. doi:10.1093/eurjhf/hfp097
8. Lok DJ, Van Der Meer P, de la Porte PW, et al. Prognostic value of galectin-3, a novel marker of fibrosis, in patients with chronic heart failure: Data from the DEAL-HF study. *Clin Res Cardiol*. 2010;99(5):323–328. doi:10.1007/s00392-010-0125-y
9. López B, González A, Querejeta R, Zubillaga E, Larman M, Díez J. Galectin-3 and histological, molecular and biochemical aspects of myocardial fibrosis in heart failure of hypertensive origin. *Eur J Heart Fail*. 2015;17(4):385–392. doi:10.1002/ejhf.246
10. Lok SI, Nous FM, van Kuik J, et al. Myocardial fibrosis and pro-fibrotic markers in end-stage heart failure patients during continuous-flow left ventricular assist device support. *Eur J Cardiothorac Surg*. 2015;48(3):407–415. doi:10.1093/ejcts/ezu539
11. Vergaro G, Del Franco A, Giannoni A, et al. Galectin-3 and myocardial fibrosis in nonischemic dilated cardiomyopathy. *Int J Cardiol*. 2015;184:96–100. doi:10.1016/j.ijcard.2015.02.008
12. Elliott P, Andersson B, Arbustini E, et al. Classification of the cardiomyopathies: A position statement from the European Society of Cardiology Working Group on Myocardial and Pericardial Diseases. *Eur Heart J*. 2007;29(2):270–277. doi:10.1093/eurheartj/ehm342
13. Cooper LT, Baughman KL, Feldman AM, et al; American Heart Association; American College of Cardiology; European Society of Cardiology; Heart Failure Society of America; Heart Failure Association of the European Society of Cardiology. The role of endomyocardial biopsy in the management of cardiovascular disease: A scientific statement from the American Heart Association, the American College of Cardiology, and the European Society of Cardiology. *Circulation*. 2007;50(19):1914–1931. doi:10.1016/j.jacc.2007.09.008
14. Rubiś P, Totoń-Żurańska J, Wiśniowska-Śmiałek S, et al. Relations between circulating microRNAs (miR-21, miR-26, miR-29, miR-30 and miR-133a), extracellular matrix fibrosis and serum markers of fibrosis in dilated cardiomyopathy. *Int J Cardiol*. 2017;231:201–206. doi:10.1016/j.ijcard.2016.11.279

15. Rubiś P, Wiśniowska-Śmiałek S, Wypasek E, et al. Fibrosis of extracellular matrix is related to the duration of the disease but is unrelated to the dynamics of collagen metabolism in dilated cardiomyopathy. *Inflamm Res*. 2016;65(12):941–949. doi:10.1007/s00011-016-0977-3
16. Yu L, Ruifrok WP, Meissner M, et al. Genetic and pharmacological inhibition of galectin-3 prevents cardiac remodeling by interfering with myocardial fibrogenesis. *Circ Heart Fail*. 2013;6(1):107–117. doi:10.1161/CIRCHEARTFAILURE.112.971168
17. Besler C, Lang D, Urban D, et al. Plasma and cardiac galectin-3 in patients with heart failure reflects both inflammation and fibrosis: Implications for its use as a biomarker. *Circ Heart Fail*. 2017;10(3):e003804. doi:10.1161/CIRCHEARTFAILURE.116.003804
18. Lepojärvi ES, Piira OP, Pääkkö E, et al. Serum PINP, PIIINP, galectin-3, and ST2 as surrogates of myocardial fibrosis and echocardiographic left venticular diastolic filling properties. *Front Physiol*. 2015;6:200. doi:10.3389/fphys.2015.00200
19. Lopez B, Gonzalez A, Ravassa S, et al. Circulating biomarkers of myocardial fibrosis: The need for a reappraisal. *J Am Coll Cardiol*. 2015;65(22):2449–2456. doi:10.1016/j.jacc.2015.04.026
20. López-Andrés N, Rossignol P, Iraqi W, et al. Association of galectin-3 and fibrosis markers with long-term cardiovascular outcomes in patients with heart failure, left ventricular dysfunction, and dyssynchrony: Insights from the CARE-HF (Cardiac Resynchronization in Heart Failure) trial. *Eur J Heart Fail*. 2012;14(1):74–81. doi:10.1093/eurjhf/hfr151
21. Lin YH, Lin LY, Wu YW, et al. The relationship between serum galectin-3 and serum markers of cardiac extracellular matrix turnover in heart failure patients. *Clin Chim Acta*. 2009;409(1–2):96–99. doi:10.1016/j.cca.2009.09.001
22. Chow SL, Maisel AS, Anand I, et al; American Heart Association Clinical Pharmacology Committee of the Council on Clinical Cardiology; Council on Basic Cardiovascular Sciences; Council on Cardiovascular Disease in the Young; Council on Cardiovascular and Stroke Nursing; Council on Cardiopulmonary, Critical Care, Perioperative and Resuscitation; Council on Epidemiology and Prevention; Council on Functional Genomics and Translational Biology; and Council on Quality of Care and Outcomes Research. Role of biomarkers for the prevention, assessment, and management of heart failure: A scientific statement from the American Heart Association. *Circulation*. 2017;135(22):e1054–e1091. doi:10.1161/CIR.0000000000000490
23. Krintus M, Kozinski M, Fabiszak T, et al. Establishing reference intervals for galectin-3 concentrations in serum requires careful consideration of its biological determinants. *Clin Biochem*. 2017;50(10–11):599–604. doi:10.1016/j.clinbiochem.2017.03.015
24. Schindler EI, Szymanski JJ, Hock KG, Geltman EM, Scott MG. Short- and long-term biologic variability of galectin-3 and other cardiac biomarkers in patients with stable heart failure and healthy adults. *Clin Chem*. 2016;62(2):360–366. doi:10.1373/clinchem.2015.246553
25. Meijers WC, van der Velde AR, Muller Kobold AC, et al. Variability of biomarkers in patients with chronic heart failure and healthy controls. *Eur J Heart Fail*. 2017;19(3):357–365. doi:10.1002/ejhf.669
26. Rubiś P, Wiśniowska-Śmiałek S, Wypasek E, et al. 12-month patterns of serum markers of collagen synthesis, transforming growth factor and connective tissue growth factor are similar in new-onset and chronic dilated cardiomyopathy in patients both with and without cardiac fibrosis. *Cytokine*. 2017;96:217–227. doi:10.1016/j.cyto.2017.04.021
27. Wojciechowska C, Romuk E, Nowalany-Kozielska E, Jacheć W. Serum galectin-3 and ST2 as predictors of unfavorable outcome in stable dilated cardiomyopathy patients. *Hellenic J Cardiol*. 2017;58(5):350–359. doi:10.1016/j.hjc.2017.03.006
28. Hu DJ, Xu J, Du W, Zhang JX, Zhong M, Zhou YN. Cardiac magnetic resonance and galectin-3 level as predictors of prognostic outcomes for non-ischemic cardiomyopathy patients. *Int J Cardiovasc Imaging*. 2016;32(12):1725–1733. doi:10.1007/s10554-016-0958-1
29. Demissei BG, Cotter G, Prescott MF, et al. A multimarker multi-time point-based risk stratification strategy in acute heart failure: Results from the RELAX-AHF trial. *Eur J Heart Fail*. 2017;19(8):1001–1010. doi:10.1002/ejhf.749
30. Sygitowicz G, Tomaniak M, Filipiak KJ, Kołtowski Ł, Sitkiewicz D. Galectin-3 in patients with acute heart failure: Preliminary report on first Polish experience. *Adv Clin Exp Med*. 2016;25(4):617–623. doi:10.17219/acem/60527
31. Nymo SH, Aukrust P, Kjekshus J, et al; CORONA Study Group. Limited added value of circulating inflammatory biomarkers in chronic heart failure. *JACC Heart Fail*. 2017;5(4):256–264. doi:10.1016/j.jchf.2017.01.008
32. Wang CH, Cheng ML, Liu MH, Kuo LT, Shiao MS. Metabolic profile provides prognostic value better than galectin-3 in patients with heart failure. *J Cardiol*. 2017;70(1):92–98. doi:10.1016/j.jjcc.2016.10.005
33. Wang H, Chen Q, Li Y, Jing X, Liang T, Yang J. Prognostic value of galectin-3 on admission in Chinese patients with heart failure: A prospective observational study. *Acta Cardiol*. 2017;72(2):188–195. doi:10.1080/00015385.2017.1291187
34. McEvoy JW, Chen Y, Halushka MK, et al. Galectin-3 and risk of heart failure and death in Blacks and Whites. *J Am Heart Assoc*. 2016;5(5):e003079.
35. Sudharshan S, Novak E, Hock K, Scott MG, Geltman EM. Use of biomarkers to predict readmission for congestive heart failure. *Am J Cardiol*. 2017;119(3):445–451. doi:10.1016/j.amjcard.2016.10.022
36. Mueller T, Gegenhuber A, Leitner I, Poelz W, Haltmayer M, Dieplinger B. Diagnostic and prognostic accuracy of galectin-3 and soluble ST2 for acute heart failure. *Clin Chim Acta*. 2016;463:158–164. doi:10.1016/j.cca.2016.10.034
37. Imran TF, Shin HJ, Mathenge N, et al. Meta-analysis of the usefulness of plasma galectin-3 to predict the risk of mortality in patients with heart failure and in the general population. *Am J Cardiol*. 2017;119(1):57–64. doi:10.1016/j.amjcard.2016.09.019

Puerarin pretreatment inhibits myocardial apoptosis and improves cardiac function in rats after acute myocardial infarction through the PI3K/Akt signaling pathway

Feng Chen[1,A,C,D,F], Zhi-Qing Chen[2,B,C,F], He Wang[1,B,F], Ji-jin Zhu[3,A,E,F]

[1] Department of Emergency, The First Affiliated Hospital of Guangxi Medical University, Nanning, China
[2] Department of Cardiology, The First Affiliated Hospital of Guangxi Medical University, Nanning, China
[3] Department of Emergency & Cardiology, The First Affiliated Hospital of Guangxi Medical University, Nanning, China

A – research concept and design; B – collection and/or assembly of data; C – data analysis and interpretation;
D – writing the article; E – critical revision of the article; F – final approval of the article

Advances in Clinical and Experimental Medicine, ISSN 1899–5276 (print), ISSN 2451–2680 (online) *Adv Clin Exp Med*. 2021;30(3):255–261

Address for correspondence
Ji-jin Zhu
E-mail: Zhujijin63@163.com

Funding sources
Natural Science Foundation of Guangxi, China (grant No. 2015GXNSFAA139156).

Conflict of interest
None declared

Received on May 5, 2020
Reviewed on November 11, 2020
Accepted on December 17, 2020

Published online on March 25, 2021

Abstract

Background. Puerarin demonstrates a protective effect in many cardiovascular diseases. However, the role of puerarin in acute myocardial infarction (AMI)-induced injury and the exact molecular mechanisms are not fully understood.

Objectives. To investigate whether puerarin pretreatment improves cardiac function and to study the mechanism of action of puerarin.

Materials and methods. Thirty rats were grouped into sham group, AMI group and AMI+puerarin (PUE) group at random (n = 10 per group). Except for the sham group, a model of AMI was established via left anterior descending artery ligation. The PUE group received puerarin 120 mg/(kg × day) for 7 days before the operation. Echocardiography was used for evaluation of cardiac function in rats and TUNEL staining for measuring myocardial apoptosis. The expression levels of p-PI3K, t-Akt, p-Akt, Bax, Bcl-2, and cleaved caspase-3 proteins were measured with western blot.

Results. Compared to the sham group, the AMI group demonstrated poor cardiac function and decreased p-PI3K, p-Akt and Bcl-2 proteins levels, while Bax, cleaved caspase-3, and myocardial apoptosis levels increased. Compared with the AMI group, the PUE group showed significant improvement in cardiac function and increased protein expression of p-PI3K, p-Akt and Bcl-2, while Bax and cleaved caspase-3 levels decreased and myocardial apoptosis was attenuated.

Conclusions. Puerarin pretreatment in AMI can effectively improve cardiac function by inhibiting myocardial apoptosis. The molecular mechanism of this protective effect may be mediated by activating the PI3K/Akt pathway in cardiomyocytes.

Key words: puerarin, cardiac function, PI3K/Akt signaling pathway, acute myocardial infarction, myocardial apoptosis

Cite as
Chen F, Chen ZQ, Wang H, Zhu JJ. Puerarin pretreatment inhibits myocardial apoptosis and improves cardiac function in rats after acute myocardial infarction through the PI3K/Akt signaling pathway. *Adv Clin Exp Med*. 2021;30(3):255–261. doi:10.17219/acem/131754

DOI
10.17219/acem/131754

Background

As a myocardial perfusion obstructing disease, acute myocardial infarction (AMI) remains the leading cause of morbidity and mortality worldwide.[1] Myocardial apoptosis is a form of cellular death in cardiomyocytes, which leads to the loss of cardiomyocytes and participates in myocardial injury during myocardial infarction (MI).[2] At present, many articles have shown that myocardial apoptosis is the chief cell injury in AMI and plays an important role in reducing cardiac function, while the inhibition of myocardial apoptosis is beneficial in preventing and treating myocardial injury caused by ischemia and hypoxia.[3–5] Nevertheless, the molecular mechanisms of cardiomyocyte apoptosis in AMI are complex and diverse. A previous study found that AMI-mediated myocardial apoptosis via inhibition of PI3K/Akt signaling is one of the main causes of progressive cardiac dysfunction.[6] Therefore, it is reasonable to propose that intervention measures to reduce myocardial apoptosis by activating this signaling pathway can protect the heart from AMI-related dysfunction and improve heart function.

Puerarin is the major isoflavone extracted from *Radix puerariae*, which can dilate blood vessels, improve microcirculation, increase blood flow, reduce blood pressure, and prevent coronary artery disease.[7] Studies have found that puerarin has a positive preventive and therapeutic effect on diabetes, hypertension, arteriosclerosis, and cerebral ischemia.[8] However, effects of puerarin on cardiomyocyte apoptosis and cardiac function in AMI rat models and its exact molecular mechanisms are not clear, and no relevant research currently exists. Thus, facilitating the realization of the relationship between puerarin and myocardial apoptosis will be helpful for the prevention and therapy of AMI.

Objectives

Therefore, we investigated the effects of puerarin pretreatment on cardiomyocyte apoptosis and the PI3K/Akt pathway in an AMI rat model to elucidate the underlying protective mechanism of puerarin.

Materials and methods

Animal preparation

Animal experiments were conducted based on the guidelines for the Care and Use of Experimental Animals and were approved by the Animal Use Ethics Committee of Guangxi Medical University, Nanning, China. Our study was conducted in accordance with the National Institutes of Health Guide for the Care and Use of Laboratory Animals. Thirty Sprague Dawley (SD) rats (male, weight 250–300 g) were purchased from the experimental animal center of Guangxi Medical University. The rats were kept in a room with temperature of 23 ±2°C and humidity of 50–60%, and sufficient food and water were guaranteed for a 12 h/12 h light-dark cycle.

Grouping and modeling

Thirty SD rats were randomly divided into 3 groups: sham operation group, AMI group and AMI+puerarin (PUE) group, with 10 rats in each group. With reference to the method described by Zhang et al., in the PUE group, 120 mg/(kg × day) puerarin was injected intraperitoneally for 7 days before the AMI model was established.[9] This dose has been shown to improve cardiac function in rats with AMI. The AMI model was established by ligating the left anterior descending (LAD) coronary artery following the method described by Curaj et al.[10] In brief, 1% pentobarbital sodium (40 mg/kg) was intraperitoneally injected into rats for anesthesia. Endotracheal intubation was then performed and breathing was assisted by a ventilator, followed by left thoracotomy at the 3rd and 4th ribs to expose the heart. Next, a 5-0 polypropylene monofilament suture was placed around the LAD, which was 1–2 mm away from the left auricular tip. After ligation, pale staining of the left ventricular anterior wall and apex, transient weakening of heartbeat, and ST-segment elevation of related ECG leads were seen, which verified a successful performance of LAD occlusion. The chest layers were closed, and the rats were put on a thermostatic blanket until they woke up from anesthesia. For control, the rats in the sham group underwent a similar thoracotomy without coronary artery ligation.

Echocardiography

Three days after the operation, we evaluated cardiac function in the 3 groups of rats. The transthoracic echocardiographic study was conducted by an ultrasound physician blind to this research. The left ventricular ejection fraction (LVEF), left ventricular fractional shortening (LVFS), left ventricular end-systolic diameter (LVESD), and left ventricular end-diastolic dimension (LVEDD) were measured using a Hewlett-Packard Sonos 7500 ultrasonic instrument with a 12.0 MHz probe (Philips Technologies, Andover, USA). The measurements were averaged over 3 cardiac cycles.

Sample collection and processing

After echocardiography, 2 mL 10% KCl was injected via the tail vein into rats to arrest the heart in diastole and to enable immediate harvesting. Rat death was determined by respiration and cardiac arrest, loss of nerve reflexes, pupil dilation, and muscle relaxation. Then, the ventricles were infused with cold saline until the rinsing solution was

not stained. The atria and large vessels were separated, followed by separation of the left and right ventricles (including the ventricular septum). Next, parallel to the atrioventricular sulcus, the left ventricle was laterally divided from the midpoint of the long axis into apical and basal parts. The apical part was immediately frozen in liquid nitrogen and then transferred to –80°C storage for subsequent western blot detection. Furthermore, the basal part was fixed in 4% paraformaldehyde for 24 h and cut into 4-μm slices after paraffin embedding for terminal deoxynucleotidyl transferase dUTP nick end labeling (TUNEL) staining.

Determination of cardiomyocyte apoptosis

Cardiomyocyte apoptosis was detected using the TUNEL apoptosis detection kit (Roche, Indianapolis, USA) manufacturer instructions. As observed by light microscopy, the normal nucleus was light blue, while the apoptotic nucleus was yellowish brown (TUNEL-positive). In each slice specimen, 20 non-overlapping regions (magnified ×400) were randomly selected to calculate the total number of cardiomyocytes and the number of apoptotic cardiomyocytes in the infarcted and marginal regions. The apoptotic index (AI) was calculated as:

$$\text{number of apoptotic cardiomyocytes} / \text{total number of cardiomyocytes} \times 100\%.$$

Western blot detection

Total myocardial proteins were extracted from the apex portion with protein lysis buffer, and the bicinchoninic acid (BCA) assay was used to determine the protein concentration. Next, equivalent protein samples were separated using SDS-PAGE assay and then electrically transferred to polyvinylidene fluoride (PVDF) membrane (Merck Millipore, Burlington, USA). The membrane was blocked with 5% bovine serum albumin (BSA) or skim milk for 1 h at room temperature and then incubated overnight at 4°C with primary antibodies against p-PI3K, p-Akt, t-Akt, Bax, cleaved caspase-3, Bcl-2, or GAPDH. The cleaved caspase-3, p-Akt and t-Akt antibodies were acquired from Cell Signaling Technology (Beverly, USA), while p-PI3K, Bax, Bcl-2, and GAPDH were obtained from Abcam (Cambridge, USA). Then, the membrane was washed 5 times with tris-buffered saline with Tween 20 (TBST) and incubated at room temperature for 1 h with secondary antibody conjugated with horseradish peroxidase (HRP; Abcam). Finally, the signals on the membrane were detected using the chemiluminescence detection equipment (Pierce, Holmdel, USA). The protein bands were evaluated and quantified using the ImageJ software (National Institutes of Health, Bethesda, USA).

Statistical analysis

In the present study, statistical analysis was conducted using SPSS software v. 17 (IBM Corp., Armonk, USA). The data was expressed as mean ± standard deviation (SD), and the number of repetitions for each group of data was at minimum n = 3. The Student's t-test was used for comparisons of 2 groups, and one-way analysis of variance (ANOVA) was used for comparing 3 groups. A p-value of <0.05 was considered statistically significant. GraphPad Prism software v. 8.0 (GraphPad Software, San Diego, USA) was used for statistical mapping.

Results

Puerarin ameliorated cardiac function following AMI

Table 1 and Fig. 1 present the results of the echocardiography. Briefly, systolic function decreased in the AMI group compared to the sham group, which manifested as decreased LVFS and LVEF and increased LVESD and LVEDD ($p < 0.05$). However, compared with the AMI group, in the PUE group, the cardiac function index significantly improved after AMI; this was reflected in the increase of LVFS and LVEF and the decrease of LVESD and LVEDD. These results suggest that puerarin pretreatment could improve cardiac function in AMI rats.

Effects of puerarin on cardiomyocytes apoptosis after AMI

Cardiomyocyte apoptosis was detected usingTUNEL staining (Fig. 2). A small amount of myocardial apoptosis was observed in the sham group. However, apoptosis was notably higher in the AMI group than in the sham group ($p < 0.05$), and most of the apoptotic cells were concentrated

Table 1. Changes in cardiac function (mean ±SD)

Group	n	LVEF (%)	LVFS (%)	LVEDD [mm]	LVESD [mm]
Sham	10	85.20 ±3.85	48.90 ±4.07	4.87 ±0.14	2.47 ±0.25
AMI	10	63.90 ±5.67[a]	30.00 ±4.22[a]	5.28 ±0.18[a]	3.67 ±0.15[a]
AMI+Pue	10	78.10 ±2.69[ab]	41.20 ±2.66[ab]	5.06 ±0.19[ab]	2.98 ±0.20[ab]

[a]$p < 0.05$, compared with the sham group; [b]$p < 0.05$, compared with the AMI group. AMI – acute myocardial infarction; LVEF – left ventricle ejection fraction; LVFS – left ventricle fractional shortening; LVEDD – left ventricular end-diastolic diameter; LVESD – left ventricular end-systolic diameter; Pue – puerarin.

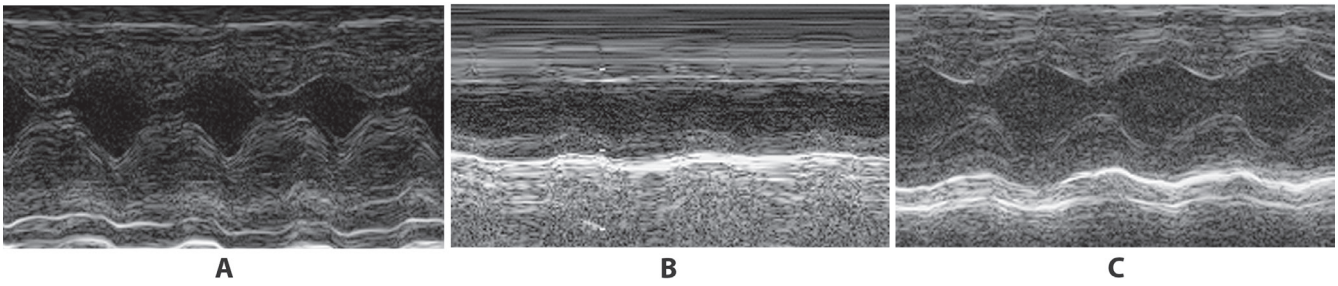

Fig. 1. Echocardiographic analysis of rats in 3 groups

A. Sham group; B. AMI group; C. AMI+Pue group; AMI – acute myocardial infarction; Pue – puerarin.

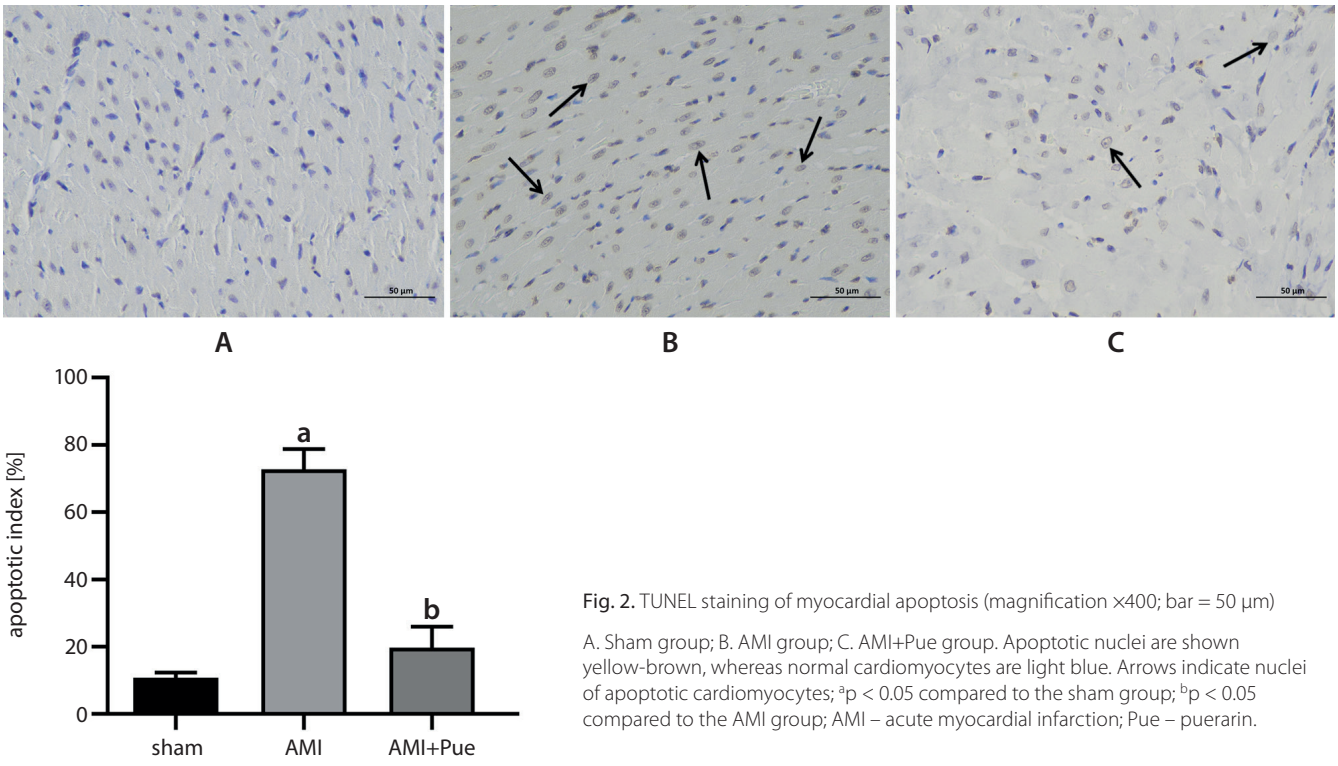

Fig. 2. TUNEL staining of myocardial apoptosis (magnification ×400; bar = 50 μm)

A. Sham group; B. AMI group; C. AMI+Pue group. Apoptotic nuclei are shown yellow-brown, whereas normal cardiomyocytes are light blue. Arrows indicate nuclei of apoptotic cardiomyocytes; [a]p < 0.05 compared to the sham group; [b]p < 0.05 compared to the AMI group; AMI – acute myocardial infarction; Pue – puerarin.

in and around the infarcted area. Meaningfully, compared with the AMI group, the number of apoptotic cardiomyocytes were reduced significantly in the PUE group ($p < 0.05$). The rates of myocardial apoptosis in the sham, AMI, and PUE groups were 10.33 ±1.35%, 72.70 ±6.10% and 19.77 ±6.21%, respectively. Overall, these data indicate that puerarin pretreatment could reduce the apoptosis rate.

Effects of puerarin on cleaved caspase-3, Bcl-2 and Bax protein expression

Cleaved caspase-3, Bcl-2 and Bax protein expression was detected to confirm myocardial apoptosis after AMI. Compared to the sham group, the cleaved caspase-3 and Bax protein expression increased in the AMI group, while Bcl-2 protein levels decreased distinctly and caused a significant decrease in the Bcl-2/Bax ratio ($p < 0.05$) (Fig. 3). After pretreatment with puerarin, Bcl-2 protein expression increased, while cleaved caspase-3 and Bax decreased, resulting in a significant increase in the Bcl-2/Bax ratio. This indicates that puerarin has an anti-apoptotic effect on myocardial injury caused by AMI.

Effect of puerarin on protein expression in the PI3K/Akt signaling pathway

Notably, there was no difference in total Akt expression among the 3 groups (Fig. 4). Myocardial level of p-Akt and p-PI3K in the AMI group and PUE group was lower compared to the sham group ($p < 0.05$). Nevertheless, after puerarin pretreatment, myocardial level of p-PI3K as well as p-Akt was increased significantly ($p < 0.05$), which suggests that puerarin improved rat cardiac function after AMI, possibly by activating PI3K/Akt pathway.

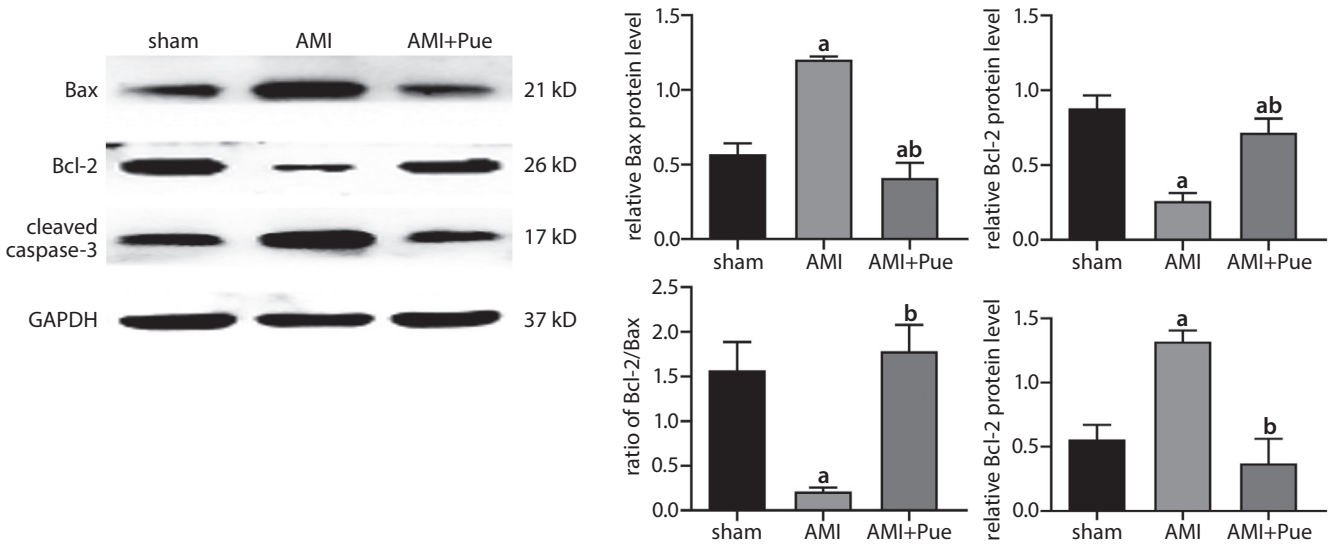

Fig. 3. Effect of puerarin on protein expression of Bax, Bcl-2 and cleaved caspase-3. Values are presented as mean ±SD. Data from at least 3 independent experiments

[a]p < 0.05 compared with the sham group; [b]p < 0.05 compared with the AMI group; SD – standard deviation; AMI – acute myocardial infarction.

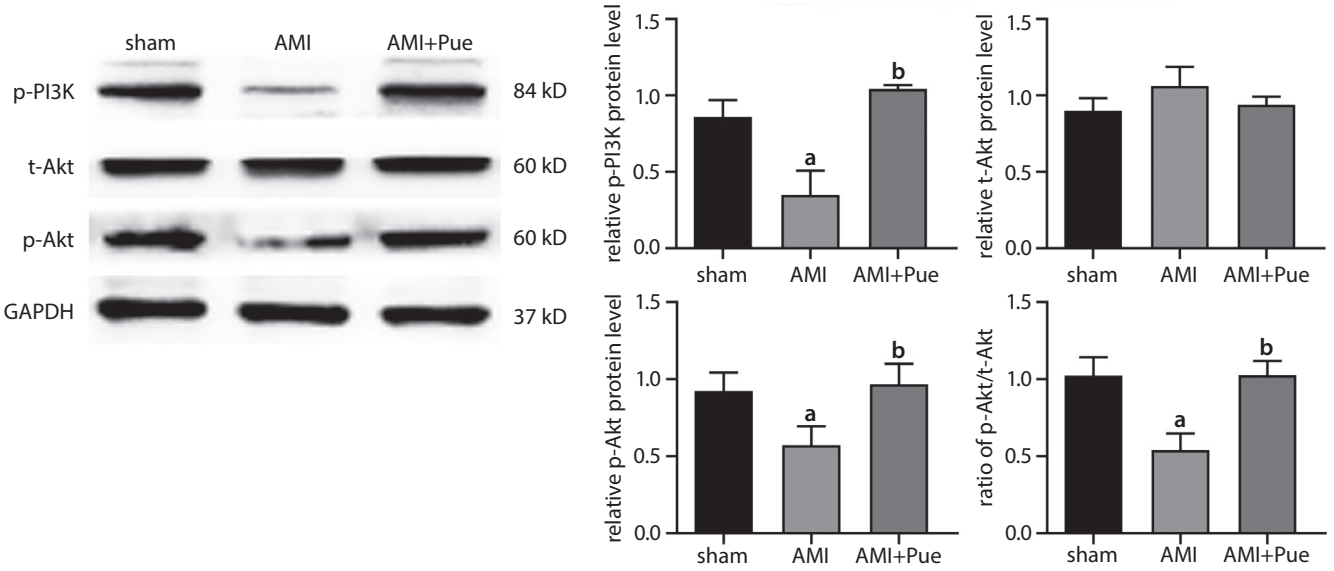

Fig. 4. Effect of puerarin on protein expression of the PI3K/Akt signaling pathway. Values are presented as mean ±SD. Data from at least 3 independent experiments

[a]p < 0.05 compared with the sham group; [b]p < 0.05 compared with the AMI group; SD – standard deviation; AMI – acute myocardial infarction.

Discussion

The data provided in this work demonstrate the following 3 points. First, myocardial apoptosis plays a considerable role in myocardial injury after AMI, which may be caused by inhibition of the PI3K/Akt signaling pathway. Second, puerarin pretreatment can significantly reduce myocardial apoptosis and improve myocardial dysfunction induced by AMI. Third, the potential protective mechanism of puerarin may be activation of the PI3K/Akt signaling pathway, thus reducing myocardial apoptosis.

In this study, rats developed left ventricular systolic dysfunction and cardiomyocyte apoptosis increased in them after AMI modeling. These results, like previous studies, indicate that cardiomyocyte apoptosis plays an important role in the irreversible injury of cardiomyocytes caused by AMI. However, after puerarin pretreatment, cardiac function was improved and cardiomyocyte apoptosis was reduced in AMI rats. These results, confirmed in regard to several different aspects, validate the conclusion that puerarin improves cardiac function by inhibiting cardiomyocyte apoptosis induced by AMI. In addition, when exploring the molecular mechanism of action of puerarin, it was found to act at least partially through the activation of the PI3K/Akt signaling pathway. At present, although reperfusion therapy reduces the mortality of AMI, it also increases the risk of heart

failure caused by the loss of cardiomyocytes in secondary injury. Therefore, in combination with reperfusion therapy, exploring and developing multiple adjuvant drugs to reduce cardiomyocyte loss will provide important support for the prevention and treatment of MI. To some extent, our research provides new evidence that puerarin exerts an inhibitory effect on myocardial apoptosis induced by AMI through PI3K/Akt pathway. However, in order to translate this into clinical application, there are still many problems that need to be further studied and resolved.

Although percutaneous coronary intervention can significantly improve patient survival, it is undeniable that AMI survivors still face a high risk of death within a few years of an AMI incident.[11] Data showed that the three-year all-cause mortality of AMI survivors tends to be greater than 50%.[12] As an important form of cell death after injury, apoptosis plays a very important and key role in AMI-induced myocardial injury, which occurs early in AMI.[3,13] Importantly, several studies demonstrated that anti-apoptotic therapies could decrease myocardial apoptosis and significantly ameliorate cardiac dysfunction caused by AMI.[1,14,15] Therefore, a therapeutic strategy to limit cardiomyocyte loss by inhibiting apoptosis may be a feasible method to prevent and treat AMI.

Puerarin is the main monomer component in *Radix puerariae*, used in traditional Chinese medicine (Kudzu root), which has anti-oxidative, anti-inflammatory and anti-apoptotic effects.[16,17] As mentioned previously, puerarin can dilate blood vessels, improve coronary circulation, increase blood flow, and reduce blood pressure and heart rate.[7,8] Because of its rich sources and high relative safety, as well as multiple mechanisms of action, puerarin possesses broad application potential in cardiovascular disease.[18] In addition to these benefits, previous studies have demonstrated that puerarin alleviates cadmium-induced hepatocyte injury by inhibiting apoptosis and restoring autophagy.[19] Similarly, in lead-induced rat kidney injury models, puerarin reduces renal apoptosis by regulating the PI3K/Akt/eNOS pathway.[17] Moreover, puerarin protects the brain from ischemic injury by inhibiting apoptosis of astrocytes, which may be connected with activation of the PI3K/Akt and MAPK/ERK pathways.[20] Deng et al. demonstrated that puerarin can inhibit the expression of tissue factor induced through oxidative low-density lipoprotein by inhibiting the activation of NF-κB and ERK1/2 and activating the PI3K/Akt/eNOS pathway.[21] In the present work, the results indicate that puerarin distinctly reduced myocardial apoptosis in an AMI rat model, thereby alleviating myocardial injury induced by AMI.

As myocardium is a terminally differentiated tissue, damaged cardiomyocytes cannot be regenerated and repaired. Therefore, protecting the activity of cardiomyocytes against ischemic diseases is essential. Myocardial apoptosis is widespread during AMI, leading to the loss of a large number of cardiomyocytes and severe cardiac dysfunction. In this situation, the activation of anti-apoptotic pathways, as well as the expression of specific anti-apoptotic proteins, are particularly important for the protection of cardiac function.[6] Interestingly, PI3K/Akt is not only an important signaling pathway that mediates apoptosis, growth and survival, but also a common pathway for a variety of cardiovascular drugs to achieve myocardial protection.[6,22–24]

In cells, a vital function of activated PI3K is to inhibit programmed cell death, and Akt – as a direct downstream target mediating PI3K-dependent cell-survival response – is also closely related to anti-apoptosis.[25] The PI3K/Akt pathway can regulate the levels of apoptosis-related proteins, such as caspase-3, Bax and Bcl-2. Bcl-2 is a significant and indispensable anti-apoptotic protein, while Bax is an important pro-apoptotic protein, so the Bcl-2/Bax ratio is a crucial factor in determining the apoptosis threshold.[26] Moreover, the aspartic acid-specific protease family, caspases, are also considered to be a key factor in inducing apoptosis.[27] Caspase-3 is a well-known family member that catalyzes apoptosis, and its activation is the most critical and important executor of apoptosis.[28,29] One of the mechanisms through which the PI3K/Akt signaling pathway reduces apoptosis is via phosphorylated PI3K activating Akt, which then phosphorylates Bad, thus freeing Bcl-2 to inhibit Bax.[30] In this study, the decrease in Bcl-2 and p-Akt after AMI injury means decreased anti-apoptotic activity in the heart. However, puerarin pretreatment upregulated the expression of p-Akt and p-PI3K, as well as Bcl-2. The increased expression of phosphorylated proteins in the PI3K/Akt pathway means that this pathway was activated. Therefore, the protective effect of puerarin on myocardial injury may be closely related to the PI3K/Akt signaling pathway.

Limitations

The limitations of this study need to be discussed. First, puerarin was administered through intraperitoneal injection, while the most common and appropriate route of drug application clinically is oral. We will explore the effect of oral administration and the best therapeutic dose of puerarin in the future. Second, in this study, there is a lack of strong evidence proving a direct causal relationship between the expression of PI3K and Akt and cleaved caspase-3, Bax and Bcl-2. Third, PI3K inhibitors were not used in this study to confirm that puerarin indeed exerts cardioprotective effects by activating the PI3K/Akt signaling pathway. In future research, we will strive to improve these shortcomings.

Conclusions

The PI3K/Akt pathway is inhibited after AMI and exerts a key effect on myocardial apoptosis induced by AMI. Pretreatment with puerarin can distinctly activate the PI3K/Akt signaling pathway, inhibit cardiomyocyte apoptosis induced by AMI and ameliorate cardiac function.

ORCID iDs

Feng Chen https://orcid.org/0000-0003-1051-2053
Zhi-Qing Chen https://orcid.org/0000-0002-6451-9317
He Wang https://orcid.org/0000-0002-4278-5892
Ji-jin Zhu https://orcid.org/0000-0001-6419-1350

References

1. Huang W, Zhang Q, Qi H, et al. Deletion of neuropeptide Y attenuates cardiac dysfunction and apoptosis during acute myocardial infarction. *Front Pharmacol*. 2019;10:1268. doi:10.3389/fphar.2019.01268
2. Saaby L, Poulsen TS, Hosbond S, et al. Classification of myocardial infarction: Frequency and features of type 2 myocardial infarction. *Am J Med*. 2013;126(9):789–797. doi:10.1016/j.amjmed.2013.02.029
3. Abbate A, Bussani R, Amin MS, Vetrovec GW, Baldi A. Acute myocardial infarction and heart failure: Role of apoptosis. *Int J Biochem Cell Biol*. 2006;38(11):1834–1840. doi:10.1016/j.biocel.2006.04.010
4. Yang J, Huang X, Hu F, Fu X, Jiang Z, Chen K. LncRNA ANRIL knockdown relieves myocardial cell apoptosis in acute myocardial infarction by regulating IL-33/ST2. *Cell Cycle*. 2019;18(23):3393–3403. doi:10.1080/15384101.2019.1678965
5. Xiaochuan B, Qianfeng J, Min X, Xiao L. RASSF1 promotes cardiomyocyte apoptosis after acute myocardial infarction and is regulated by miR-125b. *J Cell Biochem*. 2020;121(1):489–496. doi:10.1002/jcb.29236
6. Xu L, Jiang X, Wei F, Zhu H. Leonurine protects cardiac function following acute myocardial infarction through anti apoptosis by the PI3K/AKT/GSK3β signaling pathway. *Mol Med Rep*. 2018;18(2):1582–1590. doi:10.3892/mmr.2018.9084
7. Zhang Z, Lam TN, Zuo Z. *Radix puerariae*: An overview of its chemistry, pharmacology, pharmacokinetics, and clinical use. *J Clin Pharmacol*. 2013;53(8):787–811. doi:10.1002/jcph.96
8. Luo CF, Cai B, Hou N, et al. UDP-glucuronosyltransferase 1A1 is the principal enzyme responsible for puerarin metabolism in human liver microsomes [published correction appears in *Arch Toxicol*. 2012;86(11):1691]. *Arch Toxicol*. 2012;86(11):1681–1690. doi:10.1007/s00204-012-0874-7
9. Zhang S, Chen S, Shen Y, et al. Puerarin induces angiogenesis in myocardium of rat with myocardial infarction. *Biol Pharm Bull*. 2006;29(5):945–950. doi:10.1248/bpb.29.945
10. Curaj A, Simsekyilmaz S, Staudt M, Liehn E. Minimal invasive surgical procedure of inducing myocardial infarction in mice. *J Vis Exp*. 2015;(99):e52197. doi:10.3791/52197
11. Abbate A, Salloum FN, Vecile E, et al. Anakinra, a recombinant human interleukin-1 receptor antagonist, inhibits apoptosis in experimental acute myocardial infarction. *Circulation*. 2008;117(20):2670–2683. doi:10.1161/CIRCULATIONAHA.107.740233
12. Kochanek KD, Murphy SL, Anderson RN, Scott C. Deaths: Final data for 2002. *Natl Vital Stat Rep*. 2004;53(5):1–115. PMID:15587328
13. Zhang Y, Köhler K, Xu J, et al. Inhibition of p53 after acute myocardial infarction: Reduction of apoptosis is counteracted by disturbed scar formation and cardiac rupture. *J Mol Cell Cardiol*. 2011;50(3):471–478. doi:10.1016/j.yjmcc.2010.11.006
14. Huang W, Tian SS, Hang PZ, Sun C, Guo J, Du ZM. Combination of microRNA-21 and microRNA-146a attenuates cardiac dysfunction and apoptosis during acute myocardial infarction in mice. *Mol Ther Nucleic Acids*. 2016;5(3):e296. doi:10.1038/mtna.2016.12
15. Zhang Y, Li C, Meng H, et al. BYD ameliorates oxidative stress-induced myocardial apoptosis in heart failure post-acute myocardial infarction via the P38 MAPK-CRYAB signaling pathway. *Front Physiol*. 2018;9:505. doi:10.3389/fphys.2018.00505
16. Chang Y, Hsieh CY, Peng ZA, et al. Neuroprotective mechanisms of puerarin in middle cerebral artery occlusion-induced brain infarction in rats. *J Biomed Sci*. 2009;16(1):9. doi:10.1186/1423-0127-16-9
17. Liu CM, Ma JQ, Sun YZ. Puerarin protects rat kidney from lead-induced apoptosis by modulating the PI3K/Akt/eNOS pathway. *Toxicol Appl Pharmacol*. 2012;258(3):330–342. doi:10.1016/j.taap.2011.11.015
18. Sun XH, Ding JP, Li H, et al. Activation of large-conductance calcium-activated potassium channels by puerarin: The underlying mechanism of puerarin-mediated vasodilation. *J Pharmacol Exp Ther*. 2007;323(1):391–397. doi:10.1124/jpet.107.125567
19. Zhou XL, Wan XM, Fu XX, Xie CG. Puerarin prevents cadmium-induced hepatic cell damage by suppressing apoptosis and restoring autophagic flux. *Biomed Pharmacother*. 2019;115:108929. doi:10.1016/j.biopha.2019.108929
20. Wang N, Zhang Y, Wu L, et al. Puerarin protected the brain from cerebral ischemia injury via astrocyte apoptosis inhibition. *Neuropharmacology*. 2014;79:282–289. doi:10.1016/j.neuropharm.2013.12.004
21. Deng HF, Wang XL, Sun H, Xiao XZ. Puerarin inhibits expression of tissue factor induced by oxidative low-density lipoprotein through activating the PI3K/Akt/eNOS pathway and inhibiting activation of ERK1/2 and NF-κB. *Life Sci*. 2017;191:115–121. doi:10.1016/j.lfs.2017.10.018
22. Fresno Vara JA, Casado E, de Castro J, Cejas P, Belda-Iniesta C, González-Barón M. PI3K/Akt signalling pathway and cancer. *Cancer Treat Rev*. 2004;30(2):193–204. doi:10.1016/j.ctrv.2003.07.007
23. Cheng S, Zhang X, Feng Q, et al. Astragaloside IV exerts angiogenesis and cardioprotection after myocardial infarction via regulating PTEN/PI3K/Akt signaling pathway. *Life Sci*. 2019;227:82–93. doi:10.1016/j.lfs.2019.04.040
24. Zhang X, Huang LF, Hua L, Feng HK, Shen B. Resveratrol protects myocardial apoptosis induced by ischemia-reperfusion in rats with acute myocardial infarction via blocking P13K/Akt/e-NOS pathway. *Eur Rev Med Pharmacol Sci*. 2019;23(4):1789–1796. doi:10.26355/eurrev_201902_17142
25. Franke TF, Hornik CP, Segev L, Shostak GA, Sugimoto C. PI3K/Akt and apoptosis: Size matters. *Oncogene*. 2003;22(56):8983–8998. doi:10.1038/sj.onc.1207115
26. Murphy KM, Streips UN, Lock RB. Bax membrane insertion during Fas(CD95)-induced apoptosis precedes cytochrome c release and is inhibited by Bcl-2. *Oncogene*. 1999;18(44):5991–5999. doi:10.1038/sj.onc.1203001
27. Gravely AA, Cutting A, Nugent S, Grill J, Carlson K, Spoont M. Validity of PTSD diagnoses in VA administrative data: Comparison of VA administrative PTSD diagnoses to self-reported PTSD Checklist scores. *J Rehabil Res Dev*. 2011;48(1):21–30. doi:10.1682/jrrd.2009.08.0116
28. Li XM, Yu LJ, Wang C, et al. The effect of aerobic exercise training on growth performance, digestive enzyme activities and postprandial metabolic response in juvenile qingbo (*Spinibarbus sinensis*). *Comp Biochem Physiol A Mol Integr Physiol*. 2013;166(1):8–16. doi:10.1016/j.cbpa.2013.04.021
29. Wu L, Xi Z, Guo R, et al. Exogenous ARC down-regulates caspase-3 expression and inhibits apoptosis of broiler chicken cardiomyocytes exposed to hydrogen peroxide. *Avian Pathol*. 2013;42(1):32–37. doi:10.1080/03079457.2012.757289
30. White BC, Sullivan JM, DeGracia DJ, et al. Brain ischemia and reperfusion: Molecular mechanisms of neuronal injury. *J Neurol Sci*. 2000;179(S1–2):1–33. doi:10.1016/s0022-510x(00)00386-5

miR-124-3p targeting of TGF-β1 inhibits the proliferation of hypertrophic scar fibroblasts

Suwen Zhang[B–D,F], Simeng Pan[A,C,E,F]

Department of Plastic Surgery, Tongde Hospital of Zhejiang Province, Hangzhou, China

A – research concept and design; B – collection and/or assembly of data; C – data analysis and interpretation;
D – writing the article; E – critical revision of the article; F – final approval of the article

Advances in Clinical and Experimental Medicine, ISSN 1899–5276 (print), ISSN 2451–2680 (online) *Adv Clin Exp Med*. 2021;30(3):263–271

Address for correspondence
Simeng Pan
E-mail: simeng_pan@163.com

Funding sources
None declared

Conflict of interest
None declared

Received on May 21, 2020
Reviewed on October 24, 2020
Accepted on December 17, 2020

Published online on March 30, 2021

Abstract

Background. microRNAs are involved in a variety of physiological and pathophysiological processes, but their role in the pathogenesis of hypertrophic scars (HS) is not fully understood. Transforming growth factor β1 (TGF-β1) plays an important role in the genesis and development of HS.

Objectives. In this study, we hypothesized that a post-translational miRNA mechanism regulates the expression of TGF-β1 in HS fibroblasts (HSFBs) and participates in the development of HS.

Materials and methods. Predictions from EBCORI, PicTar and miRBase databases showed that miR-124-3p can target and regulate the expression of TGF-β1. We collected HS tissue and corresponding normal tissue from 25 patients with HS who had been operated on for the first time.

Results. The expression level of miR-124-3p in HS tissue was significantly lower than in normal tissue, while the expression level of TGF-β1 mRNA was significantly higher than in normal tissue ($p < 0.05$), showing a negative correlation between them. Results from a luciferase reporter assay showed that miR-124-3p targets the 3'-UTR of TGF-β1 and inhibits its expression. After miR-124-3p mimics were transfected into HSFBs, the expression of TGF-β1, α-smooth muscle actin (α-SMA), collagen I, survivin, and Bcl-2 were reduced and the expression of Bax was increased, with significant decreases in DNA synthesis, proliferation and survival. However, after a miR-124-3p inhibitor was transfected into HSFBs, these effects were reversed as the expression of TGF-β1, α-SMA, collagen I, survivin, and Bcl-2 increased, expression of Bax decreased, and DNA synthesis, proliferation and survival cells increased significantly.

Conclusions. miR-124-3p can inhibit the proliferation of HSFBs by targeting TGF-β1, and miR-124-3p may thus be a potential therapeutic target in HS.

Key words: TGF-β1, proliferation, fibroblasts, hypertrophic scarring, miR-124-3p

Cite as
Zhang S, Pan S. miR-124-3p targeting of TGF-β1 inhibits the proliferation of hypertrophic scar fibroblasts. *Adv Clin Exp Med*. 2021;30(3):263–271. doi:10.17219/acem/131753

DOI
10.17219/acem/131753

Background

Hypertrophic scar (HS) is a type of pathological scar, which is the result of local over-healing after dermal injury of human skin. The main pathological characteristics are excessive proliferation and differentiation of fibroblasts and enhanced deposition of collagen-based extracellular matrix (ECM) components.[1] Histologically, HS contains myofibroblasts, which participate in the contraction of scars.[2] These cells cause contraction of the surrounding ECM, resulting in an increase in the density of scar tissue, which not only affects the appearance and function of patients' skin, but may also cause psychological trauma. Hypertrophic scar is one of the most difficult problems to solve in burn, plastic surgery and in the general field of wound repair. Because of the lack of effective treatment methods, HS treatment is very difficult and often requires repair surgery, which leads to the formation of HS again.[3] At present, the mechanism of HS formation is not fully understood. Elucidating the molecular mechanism of HS will help contribute to the discovery of new therapeutic targets.

Hypertrophic scar is characterized by excessive proliferation of fibroblasts and aberrant ECM formation. It consists of collagen, fibronectin (FN) and aminoglycan. In normal fibroblasts, the synthesis and decomposition of ECM are in a dynamic equilibrium, which maintains the relative stability of ECM. In HS, this balance is impaired due to increased ECM synthesis, and deficiencies in its degradation and turnover. It has been shown that the amount of FN synthesized by HS fibroblasts in vitro is 4 times that of normal fibroblasts, and the amount of collagen synthesized is 3 times that of normal fibroblasts.[4] The expression level and activity of collagenase in HS fibroblasts were significantly lower than that in normal fibroblasts.[5]

Scar formation can be divided into 3 different stages: inflammation, hyperplasia and remodeling.[6] In the inflammatory stage, a large number of chemokines and inflammatory factors are produced, which can induce angiogenesis, re-epithelialization, fibroblast recruitment, proliferation, and ECM deposition. The balance between the recruitment and proliferation of fibroblasts and the production and degradation of ECM is mainly regulated by fibroblast growth factors, including insulin-like growth factor, platelet-derived growth factor and transforming growth factor β (TGF-β). Among these growth factors, TGF-β1 is widely reported to be related to the formation of HS, and mediates fibroblast proliferation, collagen production, ECM deposition, and myofibroblast differentiation during wound healing.[6–10] In HS fibroblasts, TGF-β1 has been shown to increase the phosphorylation of Smad2/3 and Smad4 and decrease Smad7 phosphorylation, resulting in the over-accumulation of Collagen-1 (Col-1).[11] In addition, TGF-β1 can induce collagen production and contraction of human skin fibroblasts (HSFBs) derived from HS.[12] This suggests that TGF-β1 may be a key target for the development of new strategies for HS treatment. The TGF-β 1 can induce macrophage M2 polarization in the process of damage repair, making M2 macrophages a "double-edged sword." On the one hand, they are essential for tissue repair, but on the other hand, they are also potential mediators of fibrosis and scar formation.[13] Studies show that inhibition of macrophage M2 polarization can inhibit fibroblast activation and the formation of scars.[14,15]

MicroRNAs (miRNA) are endogenous non-coding RNAs with regulatory function found in eukaryotes. They are involved in the regulation of cellular processes such as cell proliferation, differentiation and apoptosis. They can also aggravate or inhibit the onset and development of various diseases, including inflammation, cancer and fibrosis.[16–18] Through bioinformatic approach, we predicted that miR-124-3p may target the 3'-UTR of TGF-β1 to inhibit its expression. Recent reports show that miR-124-3p is considered to be a tumor suppressor in some cancers, including hepatocellular carcinoma,[19] cervical cancer[20] and gastric cancer.[21] Therefore, it is speculated that miRNAs may post-transcriptionally regulate the expression of TGF-β1 in HS.

Objectives

In this study, we evaluated the expression levels of miR-124-3p in HS and normal skin tissues and found that miR-124-3p was downregulated in HS and was negatively correlated with TGF-β1 expression. We found that modulating expression of miR-124-3p in HSFBs could affect cell proliferation.

Materials and methods

Samples

From January 2018 to January 2020, tissue samples from HS patients and corresponding normal tissues (NC) were collected from the plastic surgery department. Fresh tissue was stored directly in liquid nitrogen. Written informed consent was obtained from all patients. This study was approved by the ethics committee of Zhejiang Tongde Hospital (Hangzhou, China).

Cell culture and transfection

Human skin fibroblasts were prepared according to a previously reported method.[22] The human skin fibroblast cell line HSF2 was purchased from National Biomedical Experimental Cell Resource Bank (Beijing, China). They were cultured with high sugar Dulbecco's modified Eagle's medium DMEM (Gibco, Carlsbad, USA) containing 10% fetal bovine serum (FBS; Gibco), 100 U/mL penicillin G, and 100 U/mL streptomycin sulfate at 37°C and 5% CO_2.

The TGF-β1 expression vector pEX-3-TGF-β1, pGPU6-TGF-β1, miR-124-3p mimic, and miR-124-3p inhibitor were purchased from Gene Pharma (Shanghai, China).

They were transfected into HSFBs and HSF2 cells. All transfections were performed with Lipofectamine 3000 Reagent (Life Technologies, Carlsbad, USA) according to the manufacturer's protocol. pEX3 and pGPU6 empty vectors were used as negative controls.

EdU incorporation assay

EdU (5-ethynyl-2'-deoxyuridine) is a thymidine analogue, which can get incorporated into synthetic DNA molecules instead of thymine (T) during DNA replication. The ethynyl on EdU can covalently react with fluorescently labeled small molecule azide probes (such as Azide Alexa Fluor 488, Azide Alexa Fluor 555, Azide Alexa Fluor 594, and Azide Alexa Fluor 647) through the catalysis of a univalent copper ion, forming a stable triazole ring so that the newly synthesized DNA can be labeled by the corresponding fluorescent probe, allowing for the detection of proliferating cells using appropriate fluorescence detection equipment.

In order to detect DNA synthesis in different groups of cells, 2×10^4 cells were added into each well of a 24-well plate to which EdU was added at a final concentration of 20 μm; the cells were cultured for 24 h. The cells were washed twice with pre-chilled PBS and fixed for 20 min with pre-chilled 4% paraformaldehyde. They were treated with 0.5% Triton X-100 and stained with Cell-LightTM EdU In Vitro Imaging kit (Shanghai Beyotime Biotechnology Co., Ltd., Shanghai, China) according to the manufacturer's protocol. Nuclei of cells were stained with DAPI (Shanghai Beyotime Biotechnology), and EdU-positive cells were observed with an inverted immunofluorescence microscope.

Cell viability assay

Cells were harvested (from tissue), suspended in serum-free medium and plated into 96-well plates (1×10^4/well, 5 wells in each group). The cells were cultured in an incubator at 37°C and 5% CO_2 for 12 h. The MTT (10 μL, 5 mg/mL; Sigma-Aldrich, St. Louis, USA) was added into each well at 0 h, 24 h, 48 h, and 72 h respectively, and cultured for 4 h. After incubation, the culture media was discarded and dimethyl sulfoxide (DMSO; 200 μL/well) was added to the wells. The plates were placed on a shaker for 5–10 min at room temperature in the dark. Absorbance values at 570 nm were measured with a Microplate Reader (Multiskan MK3; Thermo Fisher Scientific, Waltham, USA). The experiment was repeated 3 times.

Cell apoptosis detection by flow cytometry

Apoptosis analysis was performed using the Annexin V-FITC Analysis Kit (Shanghai Beyotime Biotechnology) according to the manufacturer's protocol. Cells were collected, digested with trypsin without EDTA and washed 3 times with ice-cold phosphate-buffered saline (PBS) and centrifugation. Cells (1×10^6) were collected and resuspended in 300 μL of 1X binding buffer (Thermo Fisher Scientific). Annexin V-FITC (195 μL) and PI-PE (5 μL) were added to the cells according to the manufacturer's protocol. After 10 min of incubation at 4°C in the dark, pre-chilled 1X binding buffer (200 μL) was added. Apoptosis was detected using flow cytometry. The results were analyzed using CELLQUEST software (BD Biosciences, Franklin Lakes, USA). The experiment was repeated 3 times.

Double luciferase reporter gene analysis

In order to examine the potential interaction between miR-124-3p and the 3'-UTR of TGF-β1, we constructed wild-type (wt-pGL3-TGF-β1) and mutant (mut-pGL3-TGF-β1) luciferase reporter genes based on the predicted binding site. The constructs were co-transfected with miR-124-3p and Renilla luciferase into HEK293 cells. The cells were lysed using the Dual-Luciferase Reporter Assay System (Promega, Madison, USA) according to the instructions after culture for 48 h. The results were detected using Panomics Luminometer (Affymetrix, Santa Clara, USA) after the luminescence was added. The sea renin fluorescence was used as an internal reference.

RNA extraction and qRT-PCR

Total RNA was extracted using Trizol reagent (Invitrogen, Carlsbad, USA) according to the manufacturer's protocol. RNA concentration and purity were determined using a NanoDrop™ 1000 spectrophotometer (Thermo Fisher Scientific). Total RNA (1 μg) was subjected to reverse transcription using miScript II RT Kit (Qiagen, Hilden, Germany). Real-time polymerase chain reaction (RT-PCR) was performed using Taqman Universal Mix II No UNG (Thermo Fisher Scientific), PCR primers, miScript SYBR® Green PCR Kit (Qiagen), and the ABI StepOne Plus system (Applied Biosystems, Waltham, USA). At the end of each reaction, a melting curve analysis was performed to confirm the absence of primer dimers. The glyceraldehyde 3-phosphate dehydrogenase (*GAPDH*) gene was used as an internal control for normalization of RNA quantity and quality differences in the samples. Quantification of target gene expression was performed using the $2^{-\Delta\Delta}$Ct method. Primer sequences are listed in Table 1.

Table 1. Primers used

Primer name	Sequence (5'-3')
TGF-β1 F	GGCCAGATCCTGTCCAAGC
TGF-β1 R	GTGGGTTTCCACCATTAGCAC
GAPDH F	TGGGTGTGAACCACGAGAA
GAPDH R	GGCATGGACTGTGGTCATGA

Western blotting detection

Cells were harvested and lysed with Cell Lysis Solution (Sigma-Aldrich). The supernatant was collected after centrifugation at 4°C (10,000 rpm) for 5 min. Total proteins were extracted and protein concentration was determined using the bicinchoninic acid assay (BCA) assay. Proteins (50 μg per lane) were separated using 12% SDS-PAGE. Proteins were then electrotransferred to a polyvinylidene fluoride (PVDF) membrane (Amersham Biosciences, Piscataway, USA). The PVDF membrane was rinsed with TBS for 10–15 min and placed in TBS/T blocking buffer containing 5% (w/v) skimmed milk powder. Then, it was incubated at 4°C overnight following the addition of an appropriate dilution of primary antibodies (1:2000 α-smooth muscle actin (α-SMA); 1:1000 collagen I; 1:2000 survivin; 1:2000 Bcl-2; 1:2000 Bax; 1:5000 GAPDH; all from Abcam, Cambridge, UK). The membrane was then rinsed with TBS-Tween 20 (TBST) 3 times and incubated with a horseradish peroxidase (HRP)-labeled goat anti-mouse IgG secondary antibody (1:50,000; Abcam) at room temperature for 1 h. After incubation, the membrane was rinsed 3 times with TBST. Protein bands were detected using an enhanced chemiluminescence kit (Perkin-Elmer, Waltham, USA) and quantified as a ratio to GAPDH. Quantification was performed using Imagequant LAS4000 (GE Healthcare, Tokyo, Japan).

Statistical analysis

Statistical analysis was performed using SPSS v. 17.0 software (SPSS Inc., Chicago, USA). The data are expressed as mean ± standard deviation (SD). The 2 groups of variables, which were comparable with F-test, were compared with unpaired Student's t-test. The mean values of multiple groups were compared using one-way analysis of variance (ANOVA). The correlation of the 2 genes was examined with Spearman correlation test. A p-value <0.05 was considered to be statistically significant.

Results

miR-124-3p expression was downregulated and negatively correlated with TGF-β1 mRNA expression in HS

The RT-PCR results showed that the expression levels of miR-124-3p in HS tissues were significantly lower than that in NC tissue (Fig. 1A), while the expression levels of TGF-β1 mRNA in HS tissues were significantly higher than in NC tissue (Fig. 1B), and there was a negative correlation between them (Fig. 1C). The miR-124-3p expression in HSFBs was significantly lower than in HSF2 cells (Fig. 1D), while TGF-β1 mRNA expression in HSFBs was significantly higher than in HSF2 (Fig. 1E).

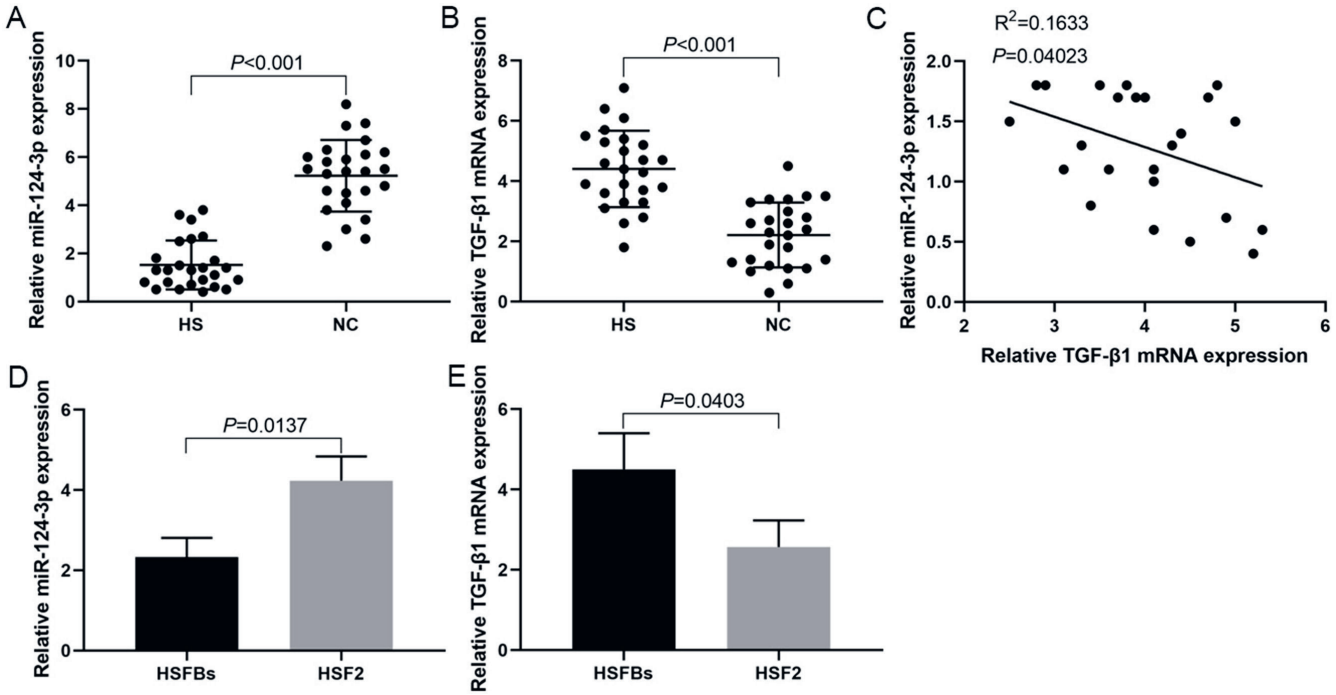

Fig. 1. miR-124-3p expression was downregulated, and is negatively correlated with TGF-β1 expression in HS. A. miR-124-3p expression levels in HS tissues and NC tissues; B. TGF-β1 expression in HS tissues and NC tissues; C. Correlation analysis of miR-124-3p and TGF-β1 mRNA expression in HS tissue; D. miR-124-3p expression in HSFBs and HSF2; E: TGF-β1 mRNA expression in HSFBs and HSF2

miR-124-3p inhibits HSFB cell proliferation

In HSFBs with low expression of miR-124-3p, DNA synthesis, cell proliferation and cell survival significantly decreased after being transfected with miR-124-3p mimics (Fig. 2A,C,E). However, in HSF2 cells with high expression of miR-124-3p, DNA synthesis, cell proliferation and cell survival significantly increased after transfection transfected with a miR-124-3p inhibitor (Fig. 2B,D,F).

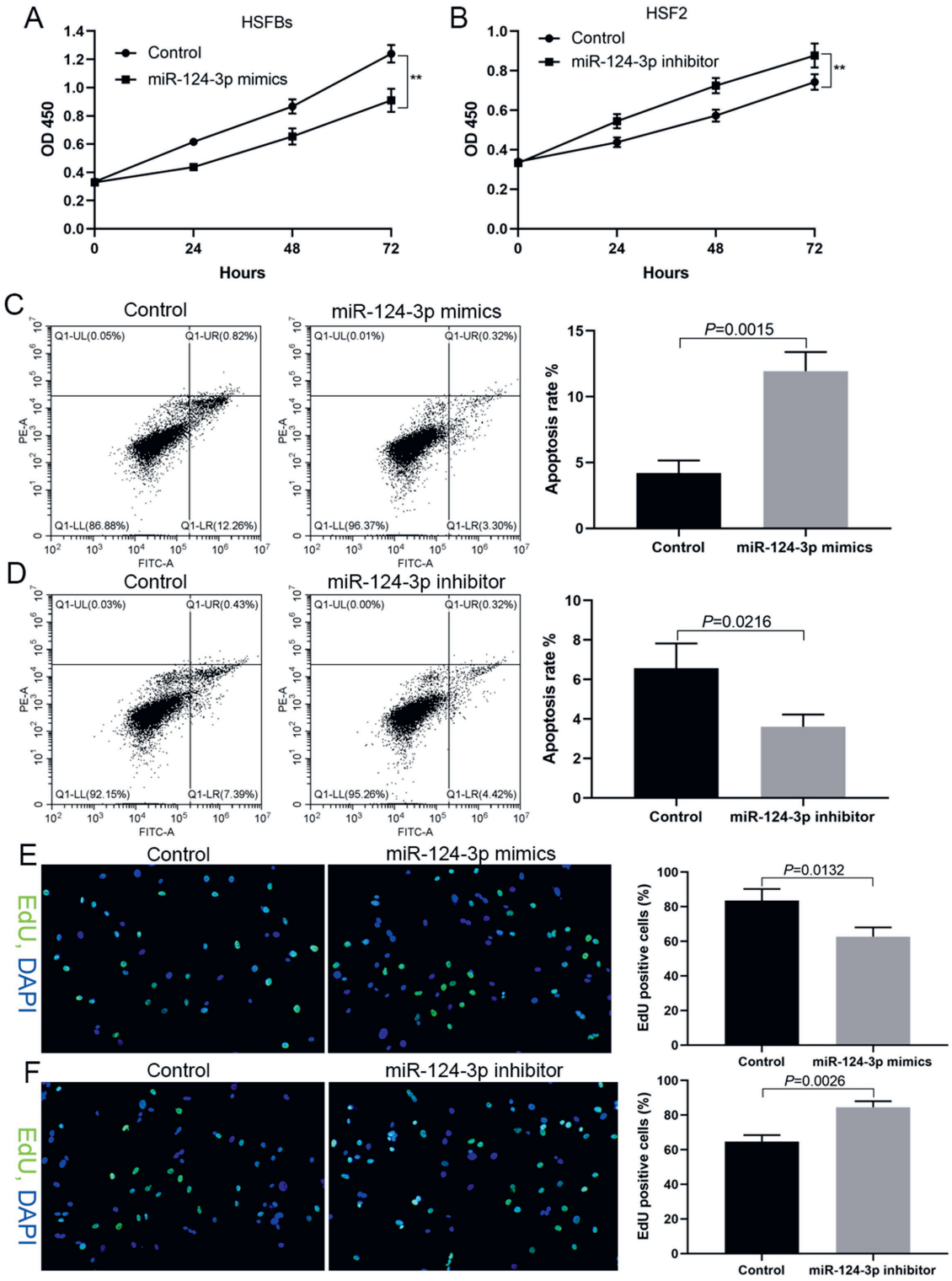

Fig. 2. miR-124-3p inhibits HSFB proliferation. A. Evaluation of cell proliferation after miR-124-3p mimics were transfected into HSFBs cells using the CCK-8 assay; B. Cell proliferation after miR-124-3p inhibitor was transfected into HSF2 cells using the CCK-8 assay; C. Detection of apoptosis using flow cytometry after miR-124-3p mimics were transfected into HSFBs cells; D. Detection of apoptosis using flow cytometry after miR-124-3p inhibitor was transfected into HSF2 cells; E. Measurement of DNA synthesis after miR-124-3p mimics were transfected into HSFBs cells; F. Measurement of DNA synthesis after miR-124-3p inhibitor was transfected into HSF2 cells

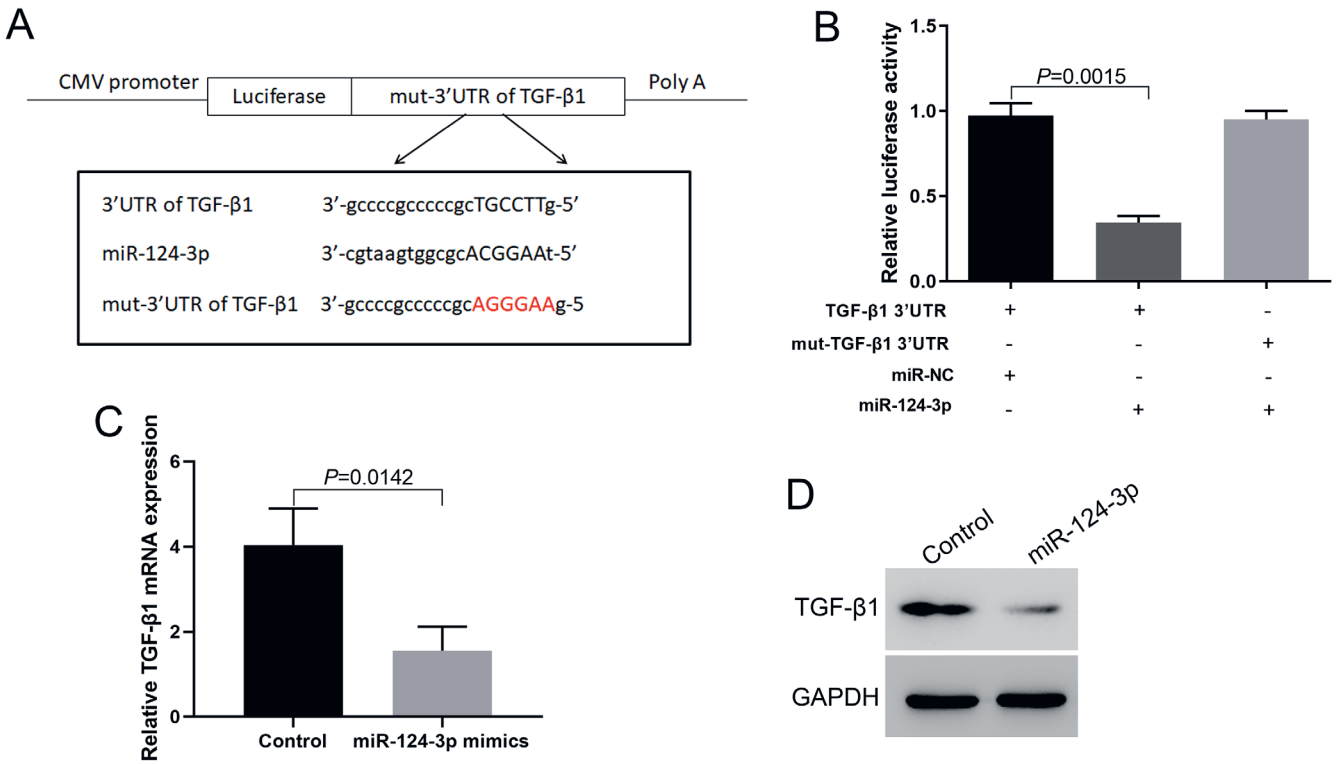

Fig. 3. miR-124-3p targets the 3'-UTR of TGF-β1 and inhibit TGF-β1 expression. A. Bioinformatics prediction shows that there is a binding site for miR-124-3p in the 3'-UTR of TGF-β1; B. Double-luciferase reporter gene analysis showed that miR-124-3p targets the 3'-UTR of TGF-β1 to inhibit the expression of luciferase; C. The effect of miR-124-3p on TGF-β 1 mRNA expression was detected with RT-PCR; D. The effect of miR-124-3p on TGF-β 1 protein expression was detected with western blot

miR-124-3p can target the 3'-UTR of TGF-β1 and inhibit TGF-β1 expression

Bioinformatics prediction showed that miR-124-3p can target the 3'-UTR of TGF-β1 (Fig. 3A). The double-luciferase reporter gene assay showed that miR-124-3p could target the 3'-UTR of TGF-β1 to inhibit the expression of luciferase. When the 3'-UTR of TGF-β1 was mutated, the inhibition of miR-124-3p was eliminated (Fig. 3B). RT-PCR and western blotting results showed that miR-124-3p can directly downregulate TGF-β1 expression (Fig. 3C,D).

miR-124-3p affected the proliferation of HSFBs by regulating TGF-β1 expression

In HSFBs transfected with miR-124-3p mimics or shRNA against TGF-β1, cell proliferation was inhibited, while in HSFBs co-transfected with miR-124-3p mimics and TGF-β1, cell proliferation was restored (Fig. 4A,C,E). In HSF2 transfected with miR-124-3p inhibitor or TGF-β1, cell proliferation was promoted, while in HSF2 co-transfected with miR-124-3p inhibitor and TGF-β1 shRNA, cell proliferation was inhibited (Fig. 4B,D,F).

miR-124-3p affects the expression of downstream effectors related to HS formation

The expression of α-SMA, collagen I, survivin, and Bcl-2 was inhibited, and Bax expression increased after transfection of miR-124-3p mimics into HSFBs (Fig. 5A). However, the expression of α-SMA, collagen I, survivin, and Bcl-2 was promoted, and Bax expression was inhibited with a miR-124-3p inhibitor (Fig. 5B).

Discussion

miRNA is a type of endogenous, non-coding, small molecule RNA that has generally 19–22 nucleotides in length and is involved in the regulation of gene expression at the post-transcriptional level. It has been shown that miRNA can regulate the development of HS in many ways, including through the TGF-β/Smad signaling pathway,[23] ECM synthesis and degradation,[24] proliferation and differentiation of HSFBs, and epithelial–mesenchymal transition (EMT).[25] miR-140-5p, miR-23b, miR-let-7b, and miR-153 can all regulate the TGF-β/Smad signaling pathway including TGF-β type I and type II receptors (RI and RII, respectively): miR-140-5p can negatively regulate the expression of TGF-βRII, while

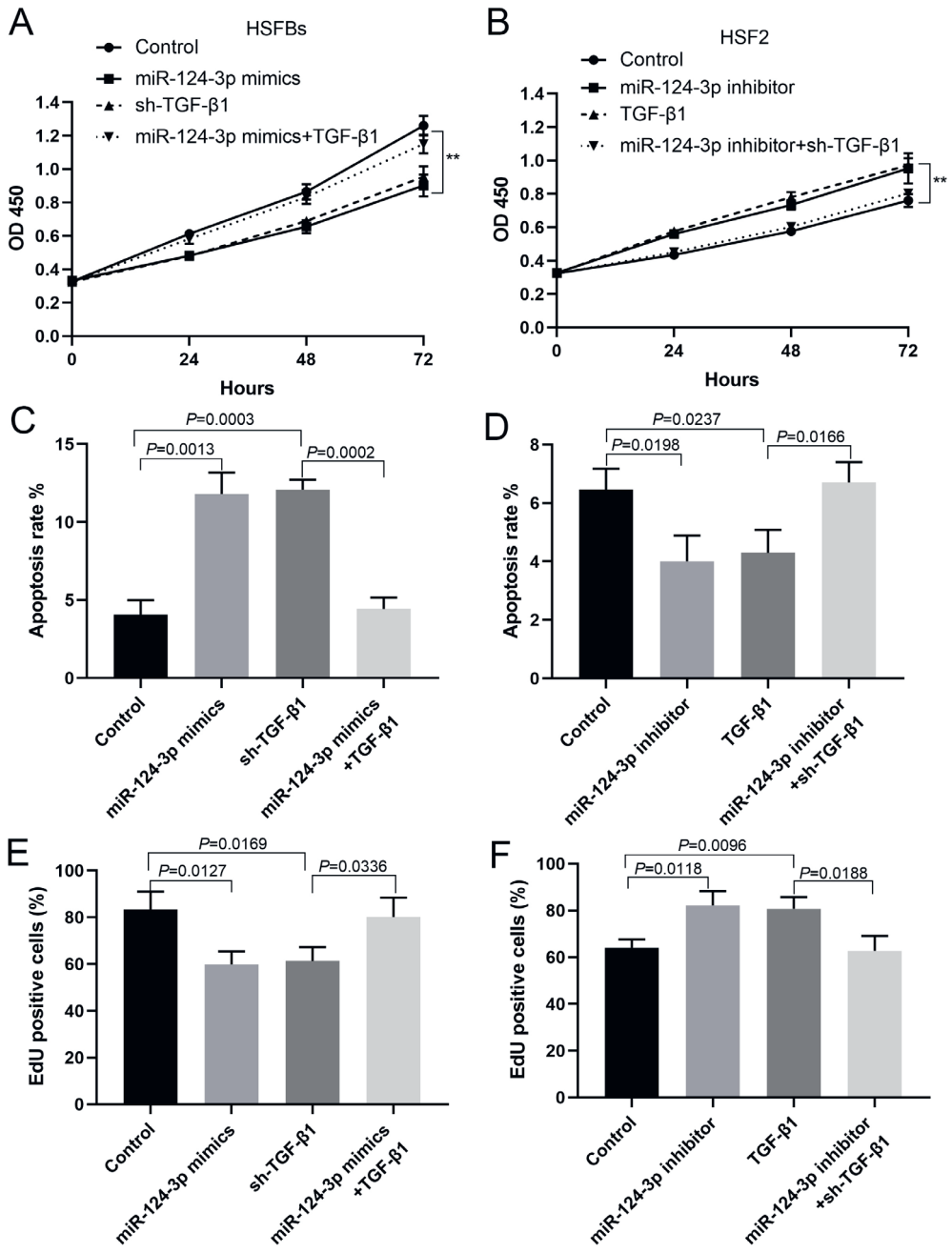

Fig. 4. miR-124-3p affects the proliferation of HSFBs by regulating TGF-β1 expression. A. Detection of HSFBs proliferation with CCK-8 assay; B. Detection of HSF2 proliferation using CCK-8 assay; C. Detection of HSFBs apoptosis using flow cytometry; D. Detection of HSF2 apoptosis using flow cytometry. E. Detection of apoptosis in HSFBs using the EdU assay; F. Detection of apoptosis in HSF2 cells using the EdU assay

miR-23b and miR-let-7b can upregulate TGF-βRII expression. miR-17-5p and miR-20 are also closely related to HS through their regulation of TGF-βRII expression.[26] miR-21 and miR-503 can also act on Smad7, a negative regulator of TGF-β/Smad signaling.[26] miR-29b can also act on the 3'-UTR of collagen I and inhibit its expression directly.[27] miR-10a and miR-181 can target PAI-1 and UPA to regulate the expression of collagen I in HS.[28] In HSFBs, the expression of miR-196a is significantly decreased, resulting in increased expression of collagen I and III and promotion of scar formation.[29] miR-146a inhibits the differentiation of HSFBs by acting on Smad4.[30] The miR-200 family can affect EMT in HSFBs by regulating the expression of ZEB1 and ZEB2.[31]

The miR-124 family of miRNAs is highly expressed in differentiated and mature neurons. They were first found in large numbers in the mouse brain, accounting for 5–48% of total miRNAs in the organ.[32] It was found that miR-124-3p belonged to the miR-124 family, members of which not only participate in brain development and nerve function, but also as tumor suppressors in some cancers. For example, miR-124-3p can target BCL2L11 to inhibit cell proliferation in angiomyolipoma cells,[33] and in gastric cancer, miR-124-3p can target Rac1 and SP1 to inhibit cell proliferation and could be used as an independent indicator of survival and treatment strategies.[20] In hepatocellular carcinoma, the long non-coding RNA (lncRNA) lncRNA MALAT1 can act as a molecular sponge

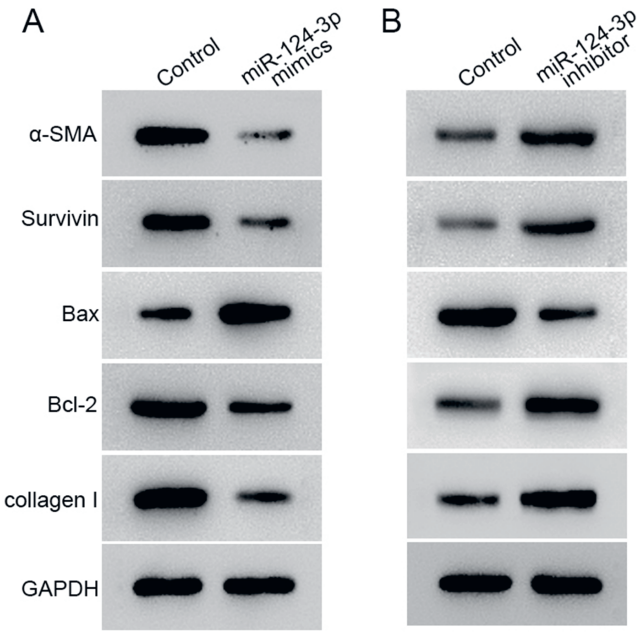

Fig. 5. miR-124-3p can affect the expression of downstream effectors associated with HS formation. A. The expression of α-SMA, collagen I, survivin, Bcl-2, and Bax after transfection of miR-124-3p mimics into HSFBs; B: The expression of α-SMA, collagen I, survivin, Bcl-2, and Bax after transfection of miR-124-3p mimics into HSF2

to absorb miR-124-3p to inhibit its effects and upregulate expression of the EMT marker Slug to promote tumor metastasis.[34] Aberrant cell proliferation similar to tumors is observed in HS. Whether miR-124-3p is involved in regulating HSFB cell proliferation, has not yet been reported.

In this study, we found that expression levels of miR-124-3p in HS tissue was significantly lower than that in corresponding normal skin tissue, and miR-124-3p in HSFBs was also significantly lower than that in HSF2 cells. miR-124-3p targeted the 3'-UTR of TGF-β1 to inhibit its expression. The expression of TGF-β1 in HS tissue was significantly higher than that in corresponding normal skin tissue, and the expression levels of miR-124-3p was negatively correlated with TGF-β1 expression.

The TGF-β1 has a variety of biological functions. After skin injury, high amounts of TGF-β1 are released to increase collagen and ECM deposition.[35] The TGF-β1 can induce collagen production and contraction of fibroblasts in HS. It can also upregulate the expression of α-SMA and promote the differentiation of normal fibroblasts into myofibroblasts.[36] In a study by Shah et al., it was found that neutralization of TGF-β1 could reduce scar formation in rats, which provided direct evidence of a role for TGF-β1 in the formation of scars.[37] Loiselle et al. found that regulation of the TGF-β signaling pathway prevents scar formation during flexor tendon repair.[38] Fibroblasts are the main participants in wound repair, being involved in the formation of granulation tissue, collagen synthesis and interaction with the ECM to promote scar hyperplasia. In the process of HS formation, the proliferation of fibroblasts promotes the secretion of collagen, resulting in a large amount of collagen deposition. At the same time, fibroblasts also release a lot of growth factors to promote scar hyperplasia. Therefore, the uncontrolled proliferation of fibroblasts is the basis of scar formation.

Limitations

The main limitation of this study is the small sample size. More clinical samples need to be analyzed to clarify the clinical significance of miR-124-3p in hypertrophic scarring.

Conclusions

In this study, we found that transfection of miR-124-3p mimics in HSFBs inhibit the expression of TGF-β1, α-SMA, collagen I, survivin, and Bcl-2, while promoting Bax expression. However, inhibition of miR-124-3p in normal human skin fibroblast cells (HSF2) promotes the expression of TGF-β1, α-SMA, collagen I, survivin, and Bcl-2, and inhibits Bax expression. These results suggested that in HS, miR-124-3p may target TGF-β1 to inhibit the expression of anti-apoptotic proteins such as survivin and Bcl-2, and promote the expression of the pro-apoptotic protein Bax. The transformation of fibroblasts into myofibroblasts is one of the important mechanisms of scar formation. There are a large number of myofibroblasts in HS tissue; α-SMA is a myofibroblast marker.[39] Myofibroblasts increase the deposition of ECM. The number and function of myofibroblasts determine the speed and degree of scar formation. Inhibition of fibroblast to myofibroblast transformation is an important strategy in preventing scar tissue development. This study showed that miR-124-3p inhibits the expression of α-SMA and collagen I, suggesting that miR-124-3p plays an important role in TGF-β1-induced differentiation of HS fibroblasts. In summary, we found that miR-124-3p inhibited the proliferation of HSFBs by inhibiting TGF-β1 expression, which suggests that miR-124-3p may be a potential therapeutic target in HS.

ORCID iDs

Suwen Zhang https://orcid.org/0000-0002-1862-436X
Simeng Pan https://orcid.org/0000-0003-2717-5049

References

1. Zhang J, Li Y, Bai X, Li Y, Shi J, Hu D. Recent advances in hypertrophic scar. *Histol Histopathol*. 2018;33(1):27–39. doi:10.14670/HH-11-908
2. Hinz B. The role of myofibroblasts in wound healing. *Curr Res Transl Med*. 2016;64(4):171–177. doi:10.1016/j.retram.2016.09.003
3. Lee HJ, Jang YJ. Recent understandings of biology, prophylaxis and treatment strategies for hypertrophic scars and keloids. *Int J Mol Sci*. 2018;19(3):711. doi:10.3390/ijms19030711
4. Ishise H, Larson B, Hirata Y, et al. Hypertrophic scar contracture is mediated by the TRPC3 mechanical force transducer via NFkB activation. *Sci Rep*. 2015;5(1):11620. doi:10.1038/srep11620

5. Trisliana Perdanasari A, Torresetti M, Grassetti L, et al. Intralesional injection treatment of hypertrophic scars and keloids: A systematic review regarding outcomes. *Burns Trauma*. 2015;3:14. doi:10.1186/s41038-015-0015-7
6. Kwan PO, Tredget EE. Biological principles of scar and contracture. *Hand Clin*. 2017;33(2):277–292. doi:10.1016/j.hcl.2016.12.004
7. Wei G, Xu Q, Liu L, et al. LY2109761 reduces TGF-beta1-induced collagen production and contraction in hypertrophic scar fibroblasts. *Arch Dermatol Res*. 2018;310(8):615–623. doi:10.1007/s00403-018-1849-1
8. Nong X, Rajbanshi G, Chen L, et al. Effect of artesunate and relation with TGF-beta1 and SMAD3 signaling on experimental hypertrophic scar model in rabbit ear. *Arch Dermatol Res*. 2019;311(10):761–772. doi:10.1007/s00403-019-01960-7
9. Yang JH, Yoon JY, Moon J, Min S, Kwon HH, Suh DH. Expression of inflammatory and fibrogenetic markers in acne hypertrophic scar formation: Focusing on role of TGF-beta and IGF-1R. *Arch Dermatol Res*. 2018;310(8):665–673. doi:10.1007/s00403-018-1856-2
10. Sun Q, Guo S, Wang CC, et al. Cross-talk between TGF-beta/Smad pathway and Wnt/beta-catenin pathway in pathological scar formation. *Int J Clin Exp Pathol*. 2015;8(6):7631–7639. PMID:26261683
11. Zhang YF, Zhou SZ, Cheng XY, et al. Baicalein attenuates hypertrophic scar formation via inhibition of the transforming growth factor-beta/Smad2/3 signaling pathway. *Br J Dermatol*. 2016;174(1):120–130. doi:10.1111/bjd.14108
12. Fang X, Hu X, Zheng Z, et al. Smad interacting protein 1 influences transforming growth factor-beta1/Smad signaling in extracellular matrix protein production and hypertrophic scar formation. *J Mol Histol*. 2019;50(6):503–514. doi:10.1007/s10735-019-09844-w
13. Eming SA, Wynn TA, Martin P. Inflammation and metabolism in tissue repair and regeneration. *Science*. 2017;356(6342):1026–1030. doi:10.1126/science.aam7928
14. Chen J, Zhou R, Liang Y, Fu X, Wang D, Wang C. Blockade of lncRNA-ASLNCS5088-enriched exosome generation in M2 macrophages by GW4869 dampens the effect of M2 macrophages on orchestrating fibroblast activation. *FASEB J*. 2019;33(11):12200–12212. doi:10.1096/fj.201901610
15. Sun X, Phan TN, Jung SH, et al. LCB 03-0110, a novel pan-discoidin domain receptor/c-Src family tyrosine kinase inhibitor, suppresses scar formation by inhibiting fibroblast and macrophage activation. *J Pharmacol Exp Ther*. 2012;340(3):510–519. doi:10.1124/jpet.111.187328
16. Nejad C, Stunden HJ, Gantier MP. A guide to miRNAs in inflammation and innate immune responses. *FEBS J*. 2018;285(20):3695–3716. doi:10.1111/febs.14482
17. Liu B, Shyr Y, Cai J, Liu Q. Interplay between miRNAs and host genes and their role in cancer. *Brief Funct Genomics*. 2018;18(4):255–266. doi:10.1093/bfgp/elz002
18. O'Reilly S. MicroRNAs in fibrosis: Opportunities and challenges. *Arthritis Res Ther*. 2016;18:11. doi:10.1186/s13075-016-0929-x
19. Long HD, Ma YS, Yang HQ, et al. Reduced hsa-miR-124-3p levels are associated with the poor survival of patients with hepatocellular carcinoma. *Mol Biol Rep*. 2018;45(6):2615–2623. doi:10.1007/s11033-018-4431-1
20. Liu F, Hu H, Zhao J, et al. miR-124-3p acts as a potential marker and suppresses tumor growth in gastric cancer. *Biomed Rep*. 2018;9(2):147–155. doi:10.3892/br.2018.1113
21. Salazar-Ruales C, Arguello JV, Lopez-Cortes A, et al. Salivary MicroRNAs for early detection of head and neck squamous cell carcinoma: A case-control study in the high altitude Mestizo Ecuadorian population. *Biomed Res Int*. 2018;2018:9792730. doi:10.1155/2018/9792730
22. Kashiyama K, Mitsutake N, Matsuse M, et al. miR-196a downregulation increases the expression of type I and III collagens in keloid fibroblasts. *J Invest Dermatol*. 2012;132(6):1597–1604. https://doi.org/10.1038/jid.2012.22
23. Guo J, Lin Q, Shao Y, Rong L, Zhang D. miR-29b promotes skin wound healing and reduces excessive scar formation by inhibition of the TGF-beta1/Smad/CTGF signaling pathway. *Can J Physiol Pharmacol*. 2017;95(4):437–442. doi:10.1139/cjpp-2016-0248
24. Bi S, Cao C, Chai LL, Li SR, Yang DY. Regulatory mechanism of miR-29 over TGF-beta1 and COL1 in scar cells. *Eur Rev Med Pharmacol Sci*. 2017;21(10):2512–2517. PMID:28617563
25. Guo B, Hui Q, Xu Z, Chang P, Tao K. miR-495 inhibits the growth of fibroblasts in hypertrophic scars. *Aging (Albany NY)*. 2019;11(9):2898–2910. doi:10.18632/aging.101965
26. Li H, Yang R, Fan X, et al. MicroRNA array analysis of microRNAs related to systemic scleroderma. *Rheumatol Int*. 2012;32(2):307–313. doi:10.1007/s00296-010-1615-y
27. Tsitoura E, Wells AU, Karagiannis K, et al. MiR-185/AKT and miR-29a/collagen 1a pathways are activated in IPF BAL cells. *Oncotarget*. 2016;7(46):74569–74581. doi:10.18632/oncotarget.12740
28. Li C, Zhu HY, Bai WD, et al. MiR-10a and miR-181c regulate collagen type I generation in hypertrophic scars by targeting PAI-1 and uPA. *FEBS Lett*. 2015;589(3):380–389. doi:10.1016/j.febslet.2014.12.024
29. Lu Q, Guo Z, Xie W, et al. The lncRNA H19 mediates pulmonary fibrosis by regulating the miR-196a/COL1A1 axis. *Inflammation*. 2018;41:896–903. doi:10.1016/j.febslet.2014.12.024
30. Qiu M, Li T, Wang B, Gong H, Huang T. miR-146a-5p Regulated cell proliferation and apoptosis by targeting SMAD3 and SMAD4. *Protein Pept Lett*. 2020;27(5):411–418. doi:10.2174/0929866526666190911142926
31. Xiong M, Jiang L, Zhou Y, et al. The miR-200 family regulates TGF-beta1-induced renal tubular epithelial to mesenchymal transition through Smad pathway by targeting ZEB1 and ZEB2 expression. *Am J Physiol Renal Physiol*. 2012;302(3):F369–F379. doi:10.1152/ajprenal.00268.2011
32. Krichevsky AM, Sonntag KC, Isacson O, Kosik KS. Specific microRNAs modulate embryonic stem cell-derived neurogenesis. *Stem Cells*. 2006;24(4):857–864. doi:10.1634/stemcells.2005-0441
33. Cai Y, Wang W, Guo H, Li H, Xiao Y, Zhang Y. Correction: miR-9-5p, miR-124-3p, and miR-132-3p regulate BCL2L11 in tuberous sclerosis complex angiomyolipoma. *Lab Invest*. 2019;99(3):443–444. doi:10.1038/s41374-018-0131-7
34. Cui RJ, Fan JL, Lin YC, et al. miR-124-3p availability is antagonized by LncRNA-MALAT1 for Slug-induced tumor metastasis in hepatocellular carcinoma. *Cancer Med*. 2019;8(14):6358–6369. doi:10.1002/cam4.2482
35. Pan SC, Lee CH, Chen CL, Fang WY, Wu LW. Angiogenin attenuates scar formation in burn patients by reducing fibroblast proliferation and transforming growth factor beta1 secretion. *Ann Plast Surg*. 2018;80(2S Suppl 1):S79–S83. doi:10.1097/SAP.0000000000001306
36. Goldberg MT, Han YP, Yan C, Shaw MC, Garner WL. TNF-alpha suppresses alpha-smooth muscle actin expression in human dermal fibroblasts: An implication for abnormal wound healing. *J Invest Dermatol*. 2007;127(11):2645–2655. doi:10.1038/sj.jid.5700890
37. Shah M, Foreman DM, Ferguson MW. Neutralisation of TGF-beta 1 and TGF-beta 2 or exogenous addition of TGF-beta 3 to cutaneous rat wounds reduces scarring. *J Cell Sci*. 1995;108(Pt 3):985–1002. PMID:7542672
38. Loiselle AE, Yukata K, Geary MB, et al. Development of antisense oligonucleotide (ASO) technology against Tgf-beta signaling to prevent scarring during flexor tendon repair. *J Orthop Res*. 2015;33(6):859–866. doi:10.1002/jor.22890
39. Muchaneta-Kubara EC, el Nahas AM. Myofibroblast phenotypes expression in experimental renal scarring. *Nephrol Dial Transplant*. 1997;12(5):904–915. doi:10.1093/ndt/12.5.904

Identification of a localization wire tip in an occult breast lesion using a handheld magnetometer

Bartłomiej Szynglarewicz[1,2,A,D], Bartosz Dołęga-Kozierowski[3,B,C], Rafał Szulc[1,B,C], Piotr Kasprzak[3,A,F], Rafał Matkowski[1,2,A,E,F]

[1] Breast Unit, Division of Breast Surgery, Lower Silesian Oncology Center, Wrocław, Poland
[2] Department of Oncology, Wroclaw Medical University, Poland
[3] Breast Unit, Division of Breast Imaging, Lower Silesian Oncology Center, Wrocław, Poland

A – research concept and design; B – collection and/or assembly of data; C – data analysis and interpretation; D – writing the article; E – critical revision of the article; F – final approval of the article

Advances in Clinical and Experimental Medicine, ISSN 1899–5276 (print), ISSN 2451–2680 (online) *Adv Clin Exp Med*. 2021;30(3):273–278

Address for correspondence
Bartłomiej Szynglarewicz
E-mail: breastunit@dco.com.pl

Funding sources
This research was financed through a statutory subsidies by the Minister of Science and Higher Education as part of the Wroclaw Medical University Department of Oncology research grant SUB.C280.21.023 (record number in the Simple System).

Conflict of interest
None declared

Acknowledgements
Authors would like to thank Dr. Jacob Bronowicki for his kind assistance in linguistic revision of this manuscript.

Received on August 13, 2020
Reviewed on October 24, 2020
Accepted on December 17, 2020

Published online on March 23, 2021

Cite as
Szynglarewicz B, Dołęga-Kozierowski B, Szulc R, Kasprzak P, Matkowski R. Identification of a localization wire tip in an occult breast lesion using a handheld magnetometer. *Adv Clin Exp Med*. 2021;30(3):273–278. doi:10.17219/acem/131751

DOI
10.17219/acem/131751

Abstract

Background. The Sentimag hand-held probe detects the magnetic response from iron oxide particles trapped in a sentinel node.

Objectives. To investigate if an electromagnetic probe can be helpful in the identification of a hook wire tip located in an occult breast lesion.

Materials and methods. Forty-two patients undergoing lumpectomy without axillary procedure were enrolled. In all cases, suspicious non-palpable microcalcifications without mass were found, and a vacuum-assisted stereotactic biopsy was performed. On the day of surgery, a traditional localization wire (LW) was placed under imaging guidance. The Sentimag magnetometer was used to precisely detect the wire tip through the skin. Then, the skin incision was made and Sentimag was used again to guide the surgeon to the lumpectomy bed. The accuracy of excision was assessed with intra-operative specimen 3D tomosynthesis.

Results. Median lesion size was 16 mm (range: 4–38 mm) and median depth was 33 mm (range: 14–78 mm). In all cases, the wire tip was successfully identified. Neither wire displacement nor transection occurred. Intraoperative radiography demonstrated doubtful margin requiring selective cavity shaving in 6 patients (14%). The need for cavity shaving was significantly influenced by the lesion size and histology: median size 30 mm (range: 24–38 mm) compared to 15 mm (range: 4–28 mm) and histology of ductal carcinoma in situ (DCIS) compared to atypical ductal hyperplasia (ADH) and lobular neoplasia (LN). Tumors requiring cavity shaving tended to be deeper – they had a median depth of 43 mm (range: 17–78 mm) compared to 32 mm (range: 14–76 mm) in patients who did not need cavity shaving, but this parameter was statistically significant.

Conclusions. Intraoperative identification of the wire tip using Sentimag is a simple technique facilitating targeted excision without excessive removal of breast tissue. Since it is not associated with additional costs, it may be worth considering, particularly in developing countries.

Key words: breast cancer, minimally invasive biopsy, biopsy site indicator, magnetic tracer, occult lesion localization

Background

The Sentimag system is one of the recent promising alternatives to traditional sentinel node mapping using a ^{99m}Tc-radiolabelled nanocolloid.[1] In this technique, a hand-held magnetometer detects a magnetic response from superparamagnetic iron oxide (SPIO) nanoparticles trapped in a sentinel node.[2] Non-inferiority for Sentimag and SPIO over traditional isotope and blue dye has been demonstrated.[3–8] As a radiotracer-independent method, it simplifies logistics, eliminates possible hazards to the patient and staff, provides a very comfortable timeframe, and offers benefits where nuclear medicine units are not available. Because of these advantages, paramagnetic mapping and SPIO-guided sentinel node biopsy have been introduced in our institution as a standard technique since 2017. However, since the magnetometer detects a magnetic response, it could also potentially allow for precise targeting of a localization wire (LW) placed into a non-palpable breast lesion.

Objectives

The aim of this study was to investigate if the Sentimag probe can be helpful in the identification of a LW tip and, therefore, to facilitate a targeted lumpectomy without excessive breast tissue excision.

Materials and methods

Patients

We retrospectively reviewed patients who underwent minimally invasive percutaneous biopsy of a non-palpable breast lesion, followed by LW-guided surgical excision, in our institution in the years 2018–2019. In 42 cases, a Sentimag probe was used to help the surgeon to identify the LW tip. All procedures were performed in accordance with institutional and national recommendations. The study was conducted according to the Declaration of Helsinki. In each case, informed consent was obtained for all diagnostic and surgical procedures, as well as for the collection and publication of their medical data. Since the study was a retrospective analysis and did not involve any experimental interventions, an independent ethics committee approval was not required. The Institutional Review Board reviewed and approved the study (approval No. NDBI/5/2019/KP).

Biopsy

All studied patients underwent a vacuum-assisted stereotactic biopsy of the non-palpable suspicious breast microcalcifications. Biopsies were performed by 1 breast-dedicated radiologist (P.K.) at the same breast care unit. Procedures were performed under local anesthetic with 1% lidocaine using a two-step approach (superficially and deeply), and were completed under digital mammography guidance using a designated prone table unit (Mammotest Plus/S; Fisher Imaging, Denver, USA) with a 10-G needle (EnCore Enspire Breast Biopsy System; C.R. Bard Inc., Tempe, USA). Biopsy specimens were radiographed to confirm the presence of microcalcifications. In cases where there were no residual microcalcifications, a single biopsy clip (non-magnetic), visible on mammogram, was placed (Gel Mark Ultra, Breast Tissue Marker GMUEC10GSS; SenoRx Inc., Tempe, USA). Baseline characteristics are presented in Table 1.

Table 1. Baseline characteristics

Characteristics	n (%)
Patients age [years]	
median, mean ±SD, range	52, 52.3 ±9.9, 32–75
Side	
right	20 (48)
left	22 (52)
Lesion histology	
ductal carcinoma in situ	22 (52)
atypical ductal hyperplasia	14 (33)
lobular neoplasia	6 (19)
Lesion size [mm]	
median, mean ±SD, range	16, 17.6 ±8.3, 4–38
Localization wire target	
post-biopsy clip	10 (24)
residual microcalcifications	32 (76)

Targeted surgery

On the day of surgery, a single hooked LW (Accura BLN 20G; Argon Medical Devices Inc., Frisco, USA) was inserted under stereotactic guidance to target the biopsy clip or residual microcalcifications. A bracketing technique with multiple wires was not used. Due to the absence of a concomitant mass neither preoperative nor intraoperative localization ultrasound were used. The procedure was performed by 3 board-certified breast-dedicated radiologists experienced in localization techniques of non-palpable breast lesions. To confirm successful localization, a two-view mammography (cranio-caudal and medio-lateral) was conducted (Fig. 1). Intraoperative LW tip localization was performed by the surgeon using the hand-held Sentimag magnetometer (Endomagnetics Ltd., Cambridge, UK). Prior to skin incision, the probe was used to scan the area from the entry point, along the LW, detecting the transcutaneous magnetic signal with real-time audible and visual numeric feedback from the detector. As both numeric count and audio tone are related to the strength of the magnetic field, a continuous decrease of signal was observed along the LW, as its distance from the skin increased. A sharp discontinuation of the signal indicated

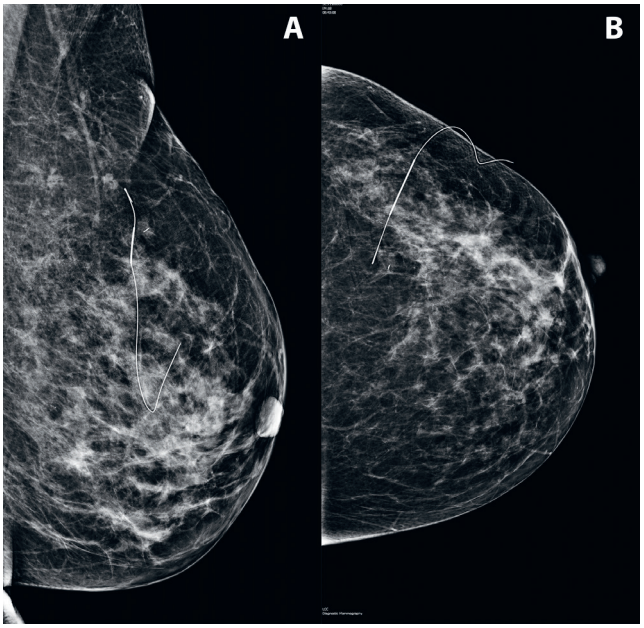

Fig. 1. Localization wire on mammography

A. medio-lateral view; B. cranio-caudal view.

the probable location of the LW tip (Fig. 2A). The skin incision was then made, and Sentimag was used again to guide the surgeon to the lumpectomy bed (Fig. 2B). After the excision was complete, the surgical specimen was properly aligned by placing stitches to mark the sides (Fig. 3A). A 3D tomosynthesis radiogram was performed using the MOZART System (Kubtec Medical Imaging; KUB Technologies Inc., Stratford, USA) to confirm the LW had not been dislocated and to confirm that all the residual microcalcifications, or the biopsy clip, were excised (Fig. 3B). Excision was performed by 4 board-certified breast-dedicated surgical oncologists. The specimen was inked in the operating room and then sent to pathology. Cavity shaving was not routinely performed, only being utilized to remove doubtful margins shown on imaging. Due to possible bias caused by breast compression, the depth of lesion was not evaluated on a mammogram. Instead, the actual surgical depth was assessed intraoperatively using a disposable straightedge, taking measurements of the distance between the skin and the posterior margin of the cavity. All the procedures (biopsy, localization and surgery) were completed at the Division of Breast Imaging and the Division of Breast Surgery of the same Breast Unit, Wroclaw Comprehensive Cancer Center, Poland).

Statistical analysis

All clinical and pathological data was entered into a computer database. The median, range and mean with standard deviation (SD) values were calculated where appropriate. The correlation between categorical variables was

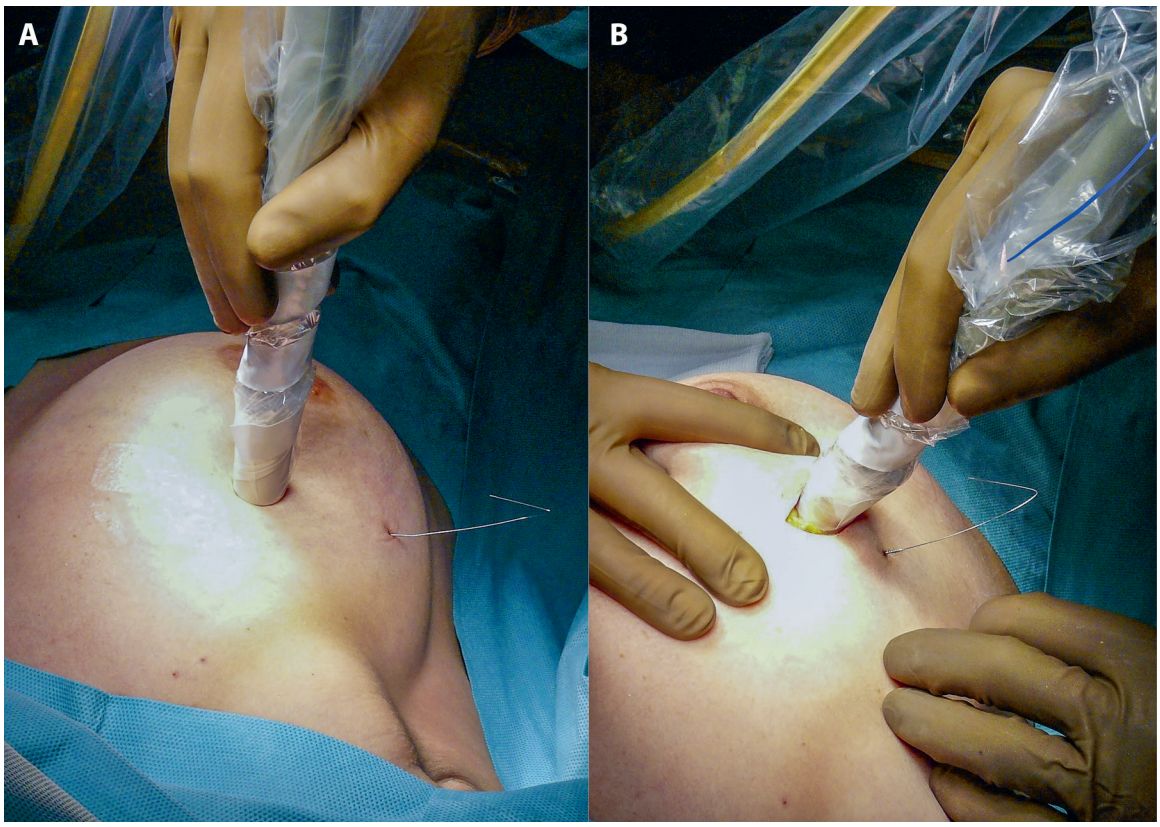

Fig. 2. Identification of the localization wire tip

A. transcutaneous scanning to find the tip; B. targeting the tip during lumpectomy.

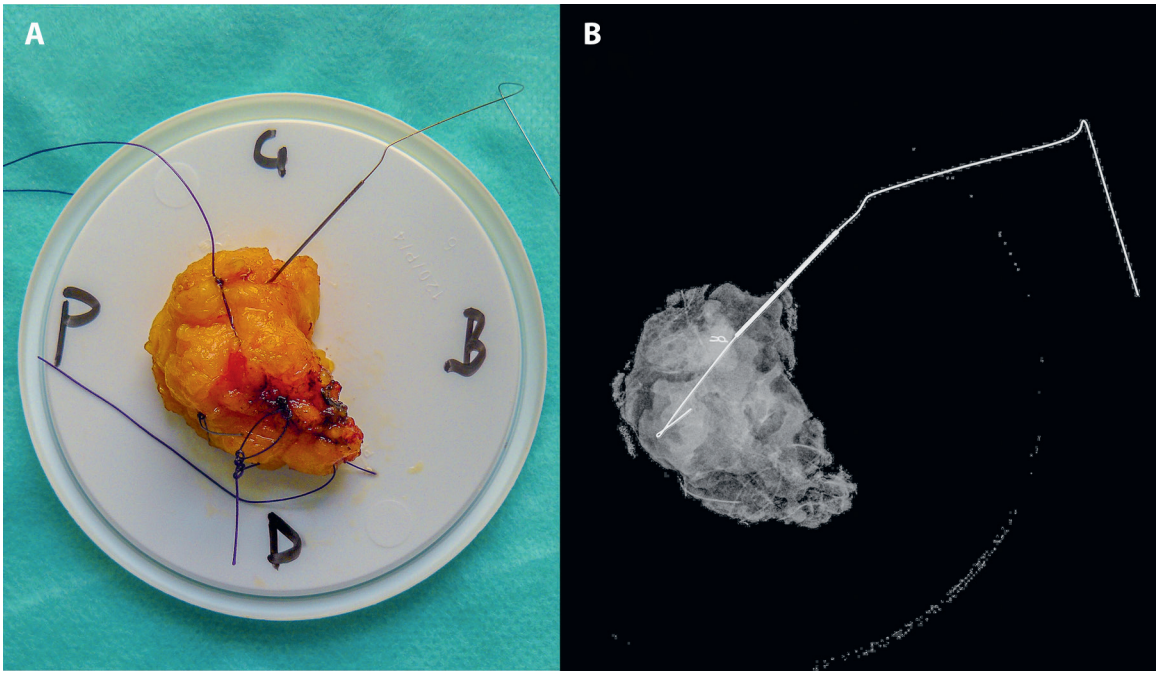

Fig. 3. Surgical specimen

A. specimen oriented with stitches, before inking; B. specimen radiography.

assessed using the χ^2 test with a Yates's correction, and correlation between continuous variables was assessed using the Mann–Whitney U test. Statistical significance was assumed at a p-value of less than 0.05.

Results

In all cases, the operation was completed without any difficulties. The LW tip was successfully identified, and the lesion with surrounding tissues was excised. Neither wire displacement nor transection occurred. Intraoperative specimen radiography demonstrated a doubtful margin in 6 cases (14%). Those patients underwent additional cavity shaving at the questionable margins. The postoperative pathologic report showed R0 resection in 40 cases (no ink on tumor), including primary margins in the 4 re-excised patients. In the remaining 2, the margin of the primary excision was microscopically positive; however, following cavity shaving, it was diagnosed as negative.

Lesions requiring cavity shaving were significantly larger than these not required such procedure (median; range; mean ±SD): 30 mm; 24–38 mm; 30 ±4.9 mm compared to 15 mm; 4–28 mm; 15.6 ±6.9 mm (z-score = –3.52254; p = 0.0004). Lesion histology also significantly influenced the need for cavity shaving; all cases requiring cavity shaving were ductal carcinoma in situ (DCIS): 27% (6/22) compared to 0% (0/20) (χ^2 = 4.331; p = 0.037), which did not require cavity shaving. Patients' age was similar (median; range; mean ±SD): 53 years; 38–68 years; 52.5 ±9.8 years in patients who required cavity shaving compared to 52 years; 32–75 years; 52.3 ±10.1 years in patients who did not require it (z-score = –0.08986; p = 0.928). Cavity shaving was not needed in any of the cases where the LW target was the biopsy clip: 0% (0/10) patients requiring cavity shaving compared to 19% (6/32) in the other group. Probably, due to the small sample size, the difference was not significant (χ^2 = 0.924; p = 0.336). The posterior margin of the tumor cavity tended to be deeper in those requiring cavity shaving (median; range; mean ±SD): 43 mm; 17–78 mm; 44.2 ±23.1 mm compared to 32 mm; 14–76 mm; 34.8 ±14.2 mm in those who did not need such procedure. However, the impact of lesion depth was not statistically

Table 2. Surgical findings

Feature	n (%)
Cavity depth [mm]	
median, mean ±SD, range	33, 36.1 ±15.8, 14–78
Radiological margin	
negative	36 (86)
doubtful	6 (14)
Cavity shaving	
required	6 (14)
not required	36 (86)
Microscopic margin before shaving	
negative	40 (95)
positive	2 (5)
Microscopic margin after shaving	
negative	42 (100)
positive	0 (0)
Risk factors for cavity shaving	
lesion size	p < 0.001
lesion histology	p < 0.050
cavity depth	not significant
patients age	not significant
localization wire target	not significant

significant (z-score = –0.95252; p = 0.342). Due to the small volume of the removed glandular tissue, advanced oncoplastic techniques for breast reshaping were not required. In all patients, the surgical defect was closed with simple tissue undermining and re-approximation (level I oncoplasty). Surgical findings are presented in Table 2.

Discussion

Needle localization for non-palpable breast lesions was first described in 1965 by Dodd et al.[9] A key modification of a LW, a self-retaining hooked tip at its distal end to anchor the wire at the intended target, was presented by Frank et al. in 1976.[10] For decades, it remained the method of choice for non-palpable breast tumors requiring surgical excision. The LW has several drawbacks, most notably the necessity of performing its implantation the same day as the surgery, which complicates scheduling and can lead to delays in the operating theater as well as possible displacement of the wire.[11,12] Other important disadvantages include: possibility of wire transection, an additional procedure adding to patient stress, a possibility that placement of surgical incision can be limited by the wire entry point, and common vasovagal episodes.[13,14] In addition, pneumothorax, site-specific pain, retention of wire fragments, hematoma, bleeding, infection, adjacent tissue injury, hemoptysis, hemothorax, non–target tissue excision, and breast implant puncture can occur.[15] However, because of its low cost, simplicity and effectiveness, as well as the important limitations of other methods, use of a LW remains the most widely adopted approach to non-palpable breast lesions. Moreover, it is the only localization technique that can be performed under imaging guidance using all modalities. Thus, some claim that a LW should be considered the gold standard, with new localization techniques randomized against it.[16]

Among the new alternatives, radio-guided occult lesion localization with injection of 99 Technetium (ROLL), seed of radioactive 125 Iodine (RIS), radiofrequency identification with microprocessor tag (RFID), SCOUT Radar using infrared light, and paramagnetic-based seeds have been investigated most extensively.[12–17] Magnetic systems in particular are believed to be very promising because they overcome the disadvantages of both LW and radioactive techniques and potentially offer logistical benefits (easy deploying, comfortable scheduling, no operating theater delays). Magnetic-based localization has been demonstrated as a safe, accurate, efficient, and effective method, and supposedly demonstrates potential to replace the conventional approach.[18–21]

During LW-guided excision, one of the common difficulties is the possible interference with the surgical approach.[16] Moreover, to accurately discern the position of the wire tip intraoperatively may be a challenge.[22] The entry point of the LW may be at some distance from the wire tip, making optimal incision placement a challenge, and may lead to extensive dissection to remove the target lesion.[20] We have demonstrated that the Sentimag probe can detect the magnetic response of the LW in a similar way to the signature generated by Magseed. As the magnetic signal is weak, the LW tip can be precisely targeted. In Poland, it makes for a much less expensive alternative to the dedicated magnetic seeds.

The paramagnetic-based localization systems have some disadvantages. The hand-held magnetometer requires regular calibration during usage which extends the duration of surgery. Electrocautery can also interfere with the signal.[17] Stainless steel surgical instruments, such as metal surgical retractors, are not compatible with Magseed. When it is in use, non-magnetic tools (titanium or polymer) must be used. This may add separate per-use fees in addition to the dedicated console and probe.[15] However, none of our cases required the use of non-magnetic instruments as the Sentimag LW tip targeting and the step-by-step breast tissue dissection were performed in an alternating fashion. In cases of cancer, another possible limitation may be the potential overlapping of the magnetic signals of the sentinel node (SPIO) and the tumor located close to the axilla (Magseed). However, in the study of this entirely magnetic technique, that complication was not observed.[23] The Magseed manufacturer reports the sensing depth to be 3 cm, but notes that it is greater with palpation.[14] Harvey et al. detected Magseed clips with a Sentimag probe at depths ranging from 3.5 mm to 30 mm as measured on ultrasound.[20] In a series by Hersi et al., the distance from the skin to the tumor reached up to 65 mm, but the magnetic signal was not detected before the skin incision in 6% of patients.[23] In such extremely deep lesions, some Magseed investigators used a traditional LW instead of a magnetic clip.[21] Some others postulate that Magseed and Sentimag are effective at all depths, especially for posterior lesions in very large breasts.[20] This topic warrants further research.

The reported re-excision rate due to positive margins for non-palpable cancer following a LW-guided lumpectomy varies from 13–14% up to 47%.[14,15] In contrast, we obtained clear margins in all patients in our series. This was probably due to both accurate LW placement and accurate excision bolstered by tip detection. On the other hand, it was also influenced by the availability of intraoperative imaging with 3D tomosynthesis and subsequent cavity shaving in patients with doubtful local control, identified by a radiologically close margin. In case of a higher budget, a bracketing technique employing multiple LW is worth considering, as it can significantly reduce the risk of positive margins and the need for re-excision, as well as reduce the volume of normal breast tissue removed.[24,25]

Limitations

Our study has some important limitations. Firstly, it is just a preliminary observational report based on a case series. Secondly, it is not a multi-institutional study. Thus,

we cannot be sure that our findings will be repeatable by other radiological and surgical teams or in a different patient setting. Thirdly, due to the small sample size, the statistical power of comparison is low. No comparison with other localization methods was conducted. Moreover, the ratio of resected tumor tissue to healthy breast tissue was not calculated. Therefore, no definitive conclusions can be drawn. However, our findings demonstrate that the accessory application of the paramagnetic-based Sentimag hand-held probe is safe, effective and not associated with additional costs.

Conclusions

Our initial findings suggest that the simple technique of targeting the LW tip using the Sentimag detector is safe and promising. It should be considered for further investigations if it facilitates more selective and targeted excision, helps to avoid excessive removal of breast tissue and, consequently, improves surgical intervention and benefits the patient. We believe that it may be particularly worth considering in developing countries with a public health service functioning on a tight budget.

ORCID iDs

Bartłomiej Szynglarewicz https://orcid.org/ 0000-0002-1153-5647
Bartosz Dołęga-Kozierowski https://orcid.org/ 0000-0001-8495-2794
Rafał Szulc https://orcid.org/ 0000-0002-0321-419X
Piotr Kasprzak https://orcid.org/ 0000-0001-6651-4459
Rafał Matkowski https://orcid.org/ 0000-0002-1705-5097

References

1. Qiu SQ, Zhang GJ, Jansen L, et al. Evolution in sentinel lymph node biopsy in breast cancer. *Crit Rev Oncol Hematol.* 2018;123:83–94. doi:10.1016/j.critrevonc.2017.09.010
2. Johnson L, Pinder SE, Douek M. Deposition of superparamagnetic iron-oxide nanoparticles in axillary sentinel lymph nodes following subcutaneous injection. *Histopathology.* 2013;62(3):481–486. doi:10.1111/his.12019
3. Karakatsanis A, Christiansen PM, Fischer L, et al. The Nordic SentiMag trial: A comparison of super paramagnetic iron oxide (SPIO) nanoparticles versus Tc(99) and patent blue in the detection of sentinel node (SN) in patients with breast cancer and a meta-analysis of earlier studies. *Breast Cancer Res Treat.* 2016;157(2):281–294. doi:10.1007/s10549-016-3809-9
4. Thill M, Kurylcio A, Welter R, et al. The Central-European SentiMag study: Sentinel lymph node biopsy with superparamagnetic iron oxide (SPIO) vs radioisotope. *Breast.* 2014;23(2):175–179. doi:10.1016/j.breast.2014.01.004
5. Pineiro-Madrona A, Torro-Richart JA, de Leon-Carrillo JM, et al; Grupo de Estudios Senologicos de la Sociedad Espanola de Patologia Mamaria (SESPM). Superparamagnetic iron oxide as a tracer for sentinel node biopsy in breast cancer: A comparative non-inferiority study. *Eur J Surg Oncol.* 2015;41(8):991–997. doi:10.1016/j.ejso.2015.04.017
6. Rubio IT, Diaz-Botero S, Esgueva A, et al. The superparamagnetic iron oxide is equivalent to the Tc99 radiotracer method for identifying the sentinel lymph node in breast cancer. *Eur J Surg Oncol.* 2015;41(1):46–51. doi:10.1016/j.ejso.2014.11.006
7. Douek M, Klaase J, Monypenny I, et al; SentiMAG Trialists Group. Sentinel node biopsy using a magnetic tracer versus standard technique: The SentiMAG Multicentre Trial. *Ann Surg Oncol.* 2014;21(4):1237–1245. doi:10.1245/s10434-013-3379-6
8. Houpeau JL, Chauvet MP, Guillemin F, et al. Sentinel lymph node identification using superparamagnetic iron oxide particles versus radioisotope: The French SentiMag feasibility trial. *J Surg Oncol.* 2016;113(5):501–507. doi:10.1002/jso.24164
9. Dodd GD, Fry K, Delany W. Pre-operative localization of occult carcinoma in the breast. In: Nealon TF, ed. *Management of the Patient with Cancer.* Philadelphia, PA: Saunders; 1966:88–113.
10. Frank HA, Hall FM, Steer ML. Preoperative localization of nonpalpable breast lesions demonstrated by mammography. *N Engl J Med.* 1976;295(5):259–260. doi:10.1056/NEJM197607292950506
11. Kopans DB. Migration of breast biopsy localization wire. *AJR Am J Roentgenol.* 1988;151(3):614–615. doi:10.2214/ajr.151.3.614
12. Kapoor MM, Patel MM, Scoggins ME. The wire and beyond: Recent advances in breast imaging preoperative needle localization. *Radiographics.* 2019;39(7):1886–1906. doi:10.1148/rg.2019190041
13. Dua SM, Gray RJ, Keshtgar M. Strategies for localisation of impalpable breast lesions. *Breast.* 2011;20(3):246–253. doi:10.1016/j.breast.2011.01.007
14. Spalluto LB, DeBenedectis CM, Morrow MS, Lourenco AP. Advances in breast localization techniques: An opportunity to improve quality of care and patient satisfaction. *Semin Roentgenol.* 2018;53(4):270–279. doi:10.1053/j.ro.2018.08.004
15. Hayes MK. Update on preoperative breast localization. *Radiol Clin North Am.* 2017;55(3):591–603. doi:10.1016/j.rcl.2016.12.012
16. Chan BK, Wiseberg-Firtell JA, Jois RH, Jensen K, Audisio RA. Localization techniques for guided surgical excision of non-palpable breast lesions. *Cochrane Database Syst Rev.* 2015;12:CD009206. doi:10.1002/14651858.CD009206.pub2
17. Jeffries DO, Dossett LA, Jorns JM. Localization for breast surgery: The next generation. *Arch Pathol Lab Med.* 2017;141(10):1324–1329. doi:10.5858/arpa.2017-0214-RA
18. Lamb LR, Bahl M, Specht MC, D'Alessandro HA, Lehman CD. Evaluation of a nonradioactive magnetic marker wireless localization program. *AJR Am J Roentgenol.* 2018;211(4):940–945. doi:10.2214/AJR.18.19637
19. Nicolae A, Dillon J, Semple M, Hong NL, Ravi A. Evaluation of a ferromagnetic marker technology for intraoperative localization of nonpalpable breast lesions. *AJR Am J Roentgenol.* 2019;212(4):727–733. doi:10.2214/AJR.18.20195
20. Harvey JR, Lim Y, Murphy J, et al. Safety and feasibility of breast lesion localization using magnetic seeds (MagSeed): A multi-centre, open-label cohort study. *Breast Cancer Res Treat.* 2018;169(3):531–536. doi:10.1007/s10549-018-4709-y
21. Price ER, Khoury AL, Esserman LJ, Joe BN, Alvarado MD. Initial clinical experience with an inducible magnetic seed system for preoperative breast lesion localization. *AJR Am J Roentgenol.* 2018;210(4):913–917. doi:10.2214/AJR.17.18345
22. Rahusen FD, Bremers AJ, Fabry HF, van Amerongen AH, Boom RP, Meijer S. Ultrasound-guided lumpectomy of nonpalpable breast cancer versus wire-guided resection: A randomized clinical trial. *Ann Surg Oncol.* 2002;9(10):994–998. doi:10.1007/BF02574518
23. Hersi AF, Eriksson S, Ramos J, Abdsaleh S, Wärnberg F, Karakatsanis A. A combined, totally magnetic technique with a magnetic marker for non-palpable tumour localization and superparamagnetic iron oxide nanoparticles for sentinel lymph node detection in breast cancer surgery. *Eur J Surg Oncol.* 2019;45(4):544–549. doi:10.1016/j.ejso.2018.10.064
24. Burkholder HC, Witherspoon LE, Burns RP, Horn JS, Biderman MD. Breast surgery techniques: Preoperative bracketing wire localization by surgeons. *Am Surg.* 2007;73(6):574–578, discussion 578–579. PMID:17658094
25. Cordiner CM, Litherland JC, Young IE. Does the insertion of more than one wire allow successful excision of large clusters of malignant calcification? *Clin Radiol.* 2006;61(8):686–690. doi:10.1016/j.crad.2006.02.009

RR interval analysis based on a newly developed PC program as a predictor of interventions in implantable cardioverter-defibrillator patients

Michał Lewandowski[A–F], Ilona Kowalik[C,E,F]

National Institute of Cardiology, Warszawa, Poland

A – research concept and design; B – collection and/or assembly of data; C – data analysis and interpretation; D – writing the article; E – critical revision of the article; F – final approval of the article

Advances in Clinical and Experimental Medicine, ISSN 1899–5276 (print), ISSN 2451–2680 (online) *Adv Clin Exp Med*. 2021;30(3):279–288

Address for correspondence
Michał Lewandowski
E-mail: mlewandowski@ikard.pl

Funding sources
Polish Ministry of Science and Higher Education
Grant No. 3P05C00923.

Conflict of interest
None declared

Received on September 14, 2020
Reviewed on December 2, 2020
Accepted on December 17, 2020

Published online on March 23, 2021

Abstract

Background. Prediction of sudden cardiac death remains a significant challenge. There is some evidence that ventricular ectopic activity could be regarded as a predictive marker.

Objectives. We carried out an analysis to explore whether premature ventricular complexes (PVCs) are a risk factor in implantable cardioverter-defibrillator (ICD) interventions.

Materials and methods. The study method was a RR interval series analysis (n = 184) of arrhythmic events and controls from the ICD. Study group consisted of patients with a mean age of 55 ±27 years; 74% of them were male, 85% were secondary prevention patients, 62% had coronary artery disease (CAD), 15% hypertropic cardiomyopathy (HCM), 15% dilated cardiomyopathy (DCM), and 8% diseases of other etiology. The mean follow-up time was 64 months (range: 3–126 months). The study population was divide into patients with at least 1 appropriate intervention ventricular tachycardia/ventricular fibrillation (VT/VF) (group A, n = 101) and controls without interventions (group B, n = 83). The number of PVC/4000 RR cycles, the shortest coupling intervals between a PVC and preceding R as well as the number of PVCs of very short (180–220 ms), short (220–280 ms) and different cycle lengths (CL) as well as the incidence of short-long-short (SLS) sequences were compared.

Results. The number of PVCs/4000 RR cycles was significantly higher in group A (263 ±32 compared to 43 ±17, $p < 0.0001$). The mean shortest PVC CL was significantly shorter in group A (320 ±13 compared to 400 ±38, $p = 0.029$). The number of PVCs with a very short CL was 1 ±0.4 compared to 0.1 ±0.1 ($p = 0.028$). The number of PVCs with a short CL was 5 ±1.2 compared to 0.6 ±0.4 ($p = 0.0007$) in groups A and B, respectively. The incidence of SLS sequences was significantly higher in group A than in group B (67 (94% of patients) and 4 (33% of patients) respectively ($p < 0.0001$)).

Conclusions. Significant differences were found in the characteristics of PVCs and SLS sequences between patients with appropriate ICD interventions and controls. A newly developed basic computer program called PCRR was applied for RR interval analysis. This simple method could be a predictor of PVC burden and life-threatening arrhythmias in different populations.

Key words: implantable cardioverter-defibrillator, initiation of ventricular fibrillation and ventricular tachycardia, sudden cardiac death prevention, premature ventricular complexes, RR interval

Cite as
Lewandowski M, Kowalik I. RR interval analysis based on a newly developed PC program as a predictor of interventions in implantable cardioverter-defibrillator patients. *Adv Clin Exp Med*. 2021;30(3):279–288. doi:10.17219/acem/131747

DOI
10.17219/acem/131747

Background

The implantable cardioverter-defibrillator (ICD) has been a primary therapy for the treatment of life-threatening arrhythmias for 4 decades. While having a powerful therapy for sudden cardiac death (SCD) prevention is a boon to medicine, the mechanisms leading to fatal outcomes are still not fully understood. Extensive studies concerning mechanisms of initiation of ventricular tachyarrhythmias started in the last 2 decades of the 20th century. Since the publication by de Luna, Coumel and Leclercq in 1989, this clinical problem has been better understood.[1] Recently, more studies have revealed some insight into the mechanisms of SCD.[2–4] Heart rate variability (HRV), QT dispersion, baroreflex sensitivity (BRS), and T wave alternans have been described as predictors of cardiovascular mortality. Nevertheless, prediction of SCD is still a challenge. Nowadays, ICD technology allows us to store information about the actual heart rhythm and the onset of arrhythmias, so that the electrical trigger of the event can be investigated. An experienced cardiologist can easily distinguish between various kinds of RR patterns and discriminate whether a particular episode is a benign or a lethal one by assessing the series of RR intervals presented in the form of intracardiac electrograms (IEGM). Knowledge of typical kinds of tachycardias and common electrocardiography (ECG) understanding is used to recognize arrhythmias. In the present study, we attempted a scientific assessment of various types of patterns in order to identify the one which carries the biggest "risk" on the basis of RR values, rather than relying on a subjective assessment by a physician.

Most of re-entrant arrhythmias occur due to unidirectional block and premature beats. There is some evidence that abrupt changes in cycle lengths may facilitate tachycardia initiation.[5] The Purkinje system and premature ventricular complexes (PVCs) have been shown to play an important role in the initiation of ventricular tachycardia/ventricular fibrillation (VT/VF).[6–9] The short-long-short (SLS) sequence increases the dispersion of repolarization and may also facilitate re-entry.[3] The PVC and SLS sequence examples are presented in Fig. 1A. In this IEGM, a SLS sequence (RR intervals 590 ms, 992 ms and 422 ms) initiates VT/VF. Antitachycardia pacing (ATP) was unsuccessful in terminating the arrhythmia; high-voltage therapy of 36 J which terminates the arrhythmia was required ("return to sinus", Fig. 1B).

Objectives

The aim of this study was to analyze whether PVCs remain a risk factor for appropriate ICD interventions and to categorize cardiac rhythm episodes of device

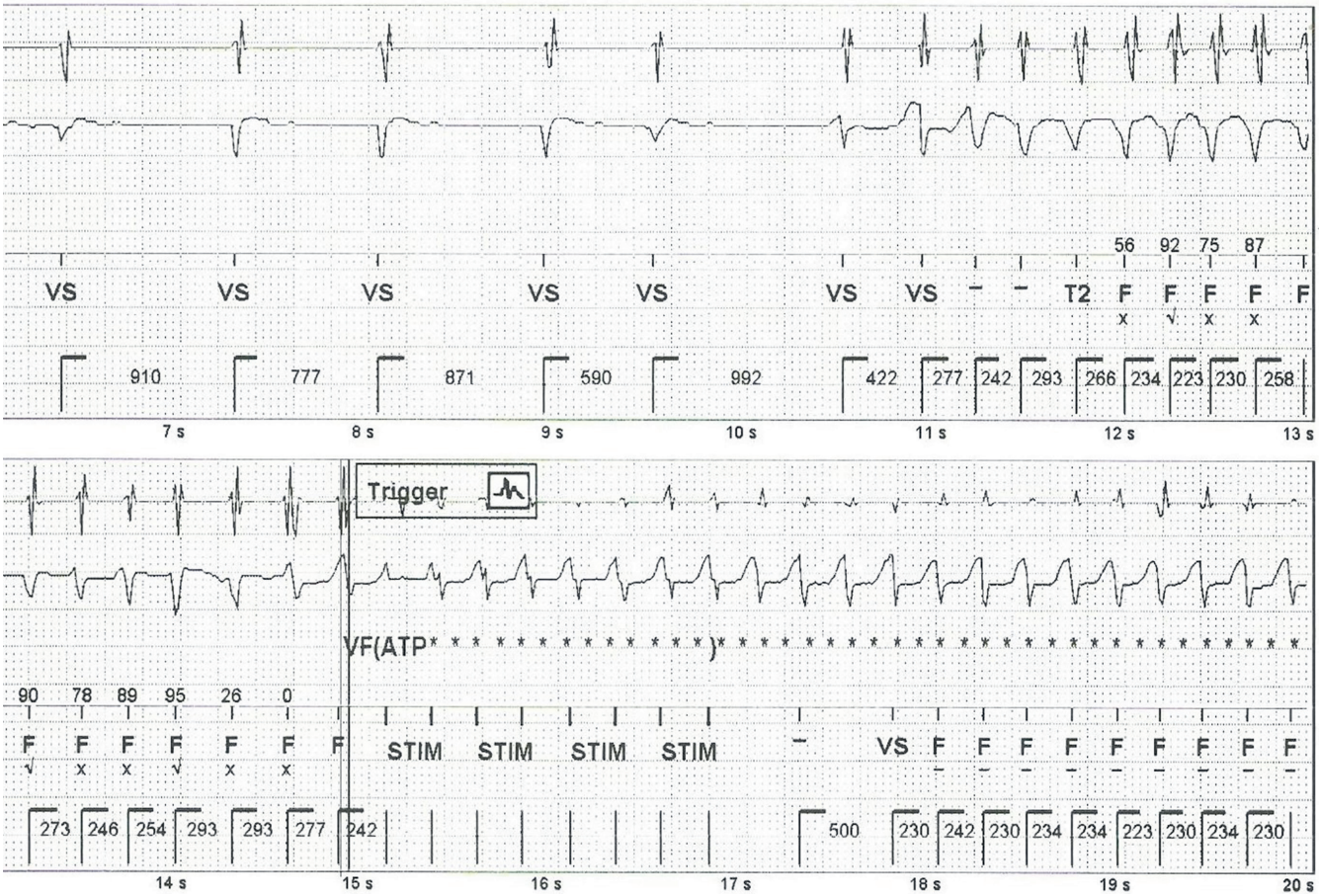

Fig. 1A. The IEGM of the PVC and short-long-short sequence

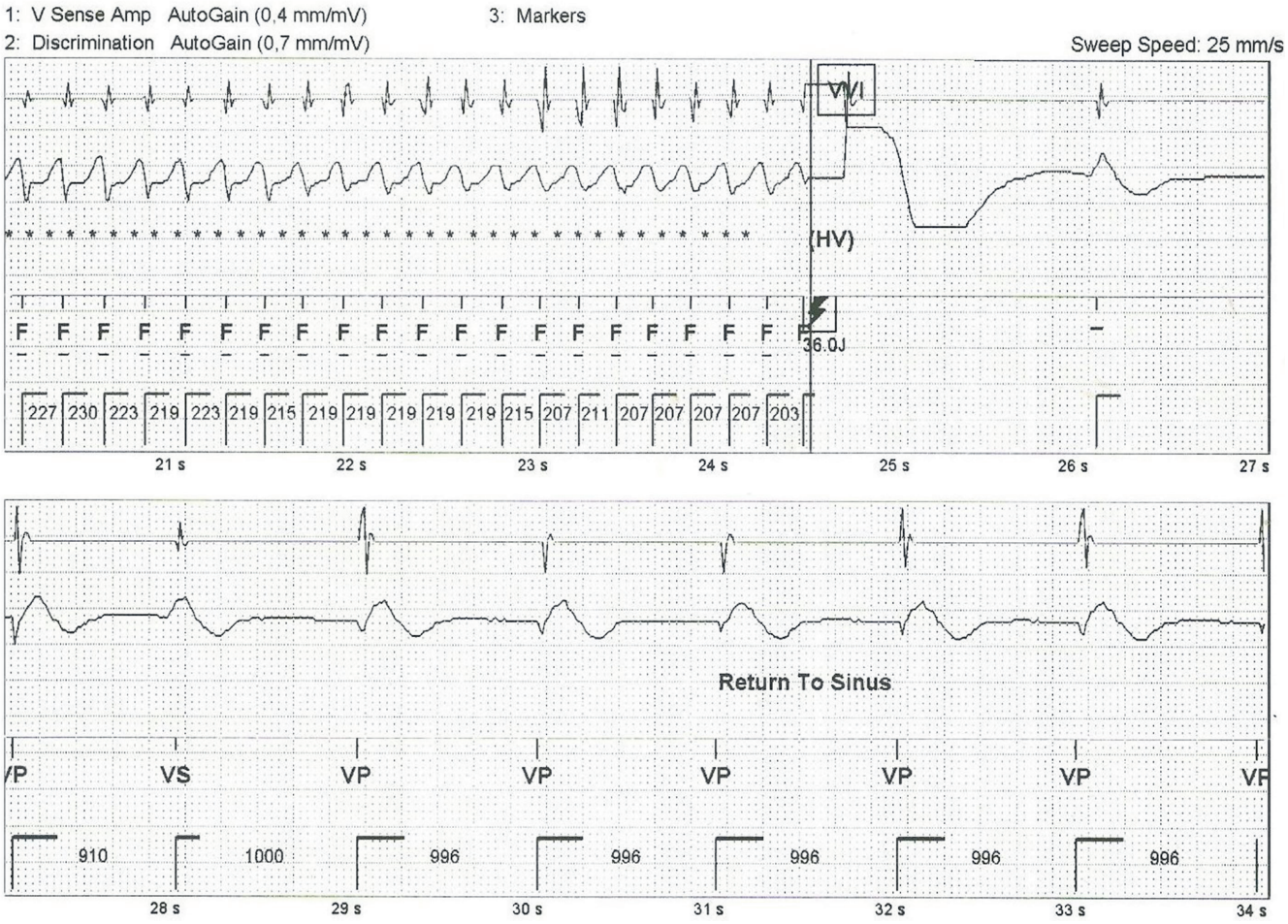

Fig. 1B. The short-long-short sequence cycle impact on ICD intervention

interrogation. If possible with the proposed methodology, it could be used as a relative simple predictor of PVC burden and life-threatening arrhythmias in patients without an ICD. The paper thus presents a new computer program for cardiac RR interval analysis and its potential application for the internet data transfer.

Materials and methods

Study group

Consecutive patients were divided into those with at least 1 appropriate intervention due to VT/VF in the form of ATP or high-energy therapy (group A, n = 101) and controls without ICD intervention revealed during device interrogations in the follow-up (group B, n = 83). Group B included RR intervals extracted during a scheduled clinical visit from device interrogations of ICDs in 2 subgroups of patients: 1) 31 patients in whom the interrogation was not preceded by any therapy, i.e., who did not experience any cardiac arrhythmias; and 2) 52 patients from group A in whom interrogations did not precede ICD therapy (comparison of the episodes was done within the same patients, i.e., episodes not only before the therapy but also remote from the therapy were included). Thus, the study group consisted of 131 patients, while 184 RR interval series were analyzed. The mean follow-up was 38 months (range: 12–64 months).

The number of PVC/4000 RR cycles, the shortest coupling intervals (CI) between PVCs and preceding R, the number of PVCs of very short cycle lengths (180–220 ms) and short CI (220–280 ms), PVC of different CI, the incidence of non-sustained ventricular tachycardia (NSVT), and the incidence of SLS sequence (defined as RR 2 < 75% of the last 4 RR intervals of the underlying rhythm, followed by RR 3 > 75% of the last 4 cycles) were examined and compared. An example of NSVT is presented in Fig. 2.

For PVC analysis, 2 models were defined: coupling interval between PVC and preceding R defined as RR interval >10% than the predecessor of the underlying rhythm (model 1) and RR > 20% than the predecessor of the underlying rhythm (model 2).

For the analysis of the RR intervals, searches for the rate and values of the phenomena defined in the protocol, a computer program was developed by an experienced

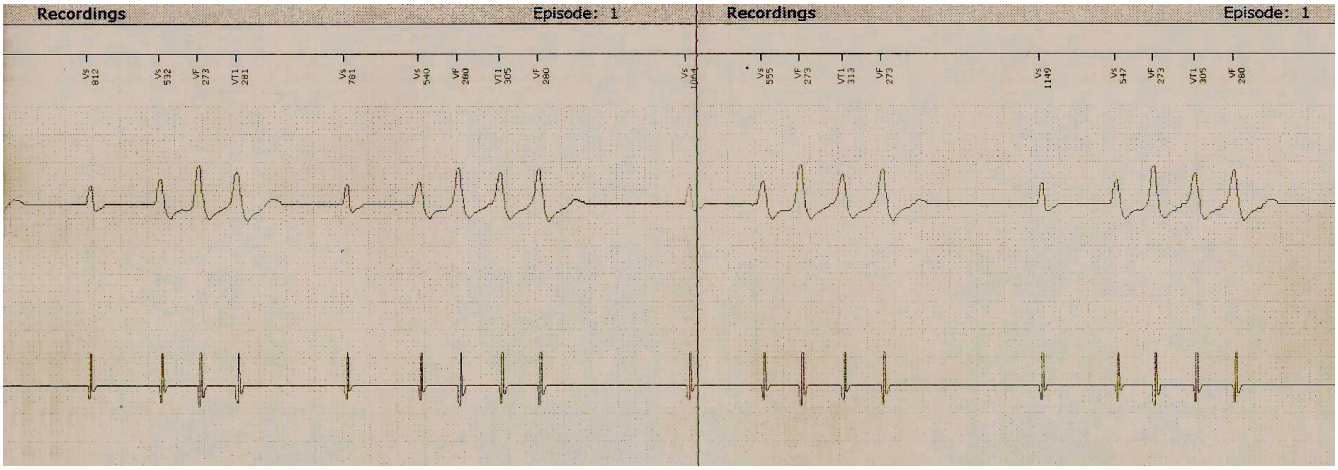

Fig. 2. The IEGM of non-sustained ventricular tachycardia (nsVT)

biostatistician (I.K.) and tested before the final implementation. The program (called PCRR) uses the same input signals as the existing ICDs with RR interval as the primary input variable. This program was created on the basis of the SAS v. 9e statistical package (SAS Institute, Cary, USA). Before the final implementation in the presented study, the use of PCRR was validated on different 36 recordings containing 4000–9890 RR intervals.

Methods

From the database containing an RR intervals series of the arrhythmia events and controls stored in ICD memory (Biotronik models Belos VR (n = 45), Phylax XM (n = 32), Lexos VR (n = 47), and Micro Phylax (n = 18)), 142 consecutive patients recordings with IEGMs were included in the analysis. The basic inclusion criterion was the presence of sinus rhythm and at least 4000 RR intervals and the corresponding IEGM, recorded 66 ±15 min before an ICD intervention or before a follow-up visit if there was no intervention. Patients with paced rhythm were not included. The 2000 PDM-Patient Data Manager software (Biotronik, Berlin, Germany) was used for data storage and graphical analysis, made independently by 2 experienced cardiologists. The RR patterns could be presented in a graphical form as a map of dots in relation to their predecessors. This method, however, is not widely used in clinical practice. All RR pattern figures presented in this paper, except the PCRR program, were produced with the 2000 PDM-Patient Data Manager. Data were collected during follow-up visits on a six-month schedule or after clinical events, whichever came first. Eleven patients were excluded due to a lack of a full dataset or due to the presence of supraventricular arrhythmias (atrial fibrillation or flutter).

This study complies with the Declaration of Helsinki and research protocol and was approved by the local ethics committee. Informed consent was obtained from all patients.

Statistics

Statistical analyses were performed using the SAS v. 9e statistical package. For descriptive purposes, all data are presented as mean ± standard deviation (SD; continuous variables) or as absolute frequencies and percentages, where indicated (discrete variables). T or χ^2 tests were used, as appropriate. All test procedures were two-sided with a p-value of less than 0.05 indicating statistical significance.

The receiver operating characteristics curve (ROC) analysis was used to determine the cut-off point value of the PVC count to predict the appropriate ICD intervention event. The optimal cut-off was defined as the value of the maximal sum of sensitivity and specificity. Comparison of the PVC ROC in the 2 models was performed on the basis of area under curve (AUC). Binary logistic regression was performed.

Results

Detailed patient characteristics (demographic data, etiology, laboratory results, major comorbidities, etc.) are presented in Table 1. The rate and the values of the phenomena defined in the study protocol are presented in Table 2.

In the overall analysis, the number of PVCs/4000 RR intervals was significantly higher in group A (263 ±32 compared to 43 ±17, $p < 0.0001$). The mean PVC coupling interval was significantly shorter in group A (320 ±13 compared to 400 ±38, $p = 0.029$). The number of PVCs of very short cycle lengths (180–220 ms) in group A and B was 1 ±0.4 compared to 0.1 ±0.1, respectively ($p = 0.028$). The number of PVCs of short cycle lengths (220–280 ms) in group A and B was 5 ±1.2 compared to 0.6 ±0.4, respectively ($p = 0.0007$). The incidence of SLS sequences was significantly higher in group A than in group B ($p < 0.0001$).

The percentage of patients demonstrating different cycle length intervals of PVC events appears in Fig. 3

Table 1. Patient characteristics (demographic data, etiology, laboratory results, major comorbidities, etc.)

Parameter	Study group A (n = 101)	Controls group B (n = 83)	p-value
Age [years], mean (SD)	65 (23)	41 (11)	p < 0.001
BMI [kg/m^2], mean (SD)	24.5 (7.0)	21 (4.0)	p < 0.0001
Male sex, n (%)	74 (73.3)	44 (53.1)	p < 0.004
Diabetes, n (%)	55 (54.5)	28 (33.7)	p < 0.005
LVEF [%], mean (SD)	31.3 (8.2)	45.2 (9.8)	p < 0.002
CAD, n (%)	60 (59.4)	30 (36.1)	p < 0.001
MI, n (%)	50 (50)	5 (6.02)	p < 0.001
Arterial hypertension, n (%)	75 (74.3)	35 (42.2)	p < 0.001
Previous cardiac arrest, n (%)	85 (84.1)	32 (38.5)	p < 0.001
HCM (%)	18 (17.8)	14 (16.9)	NS
DCM (%)	15 (14.9)	12 (14.5)	NS
Other etiology (%)	8 (7.9)	11 (13.2)	NS
Creatinine [mg/dL], mean (SD)	1.0 (0.30)	0.85 (0.14)	NS

SD – standard deviation; NS – not significant; BMI – body mass index; LVEF – left ventricular ejection fraction; CAD – coronary artery disease; MI – myocardial infarction; HCM – hypertropic cardiomyopathy; DCM – dilated cardiomyopathy.

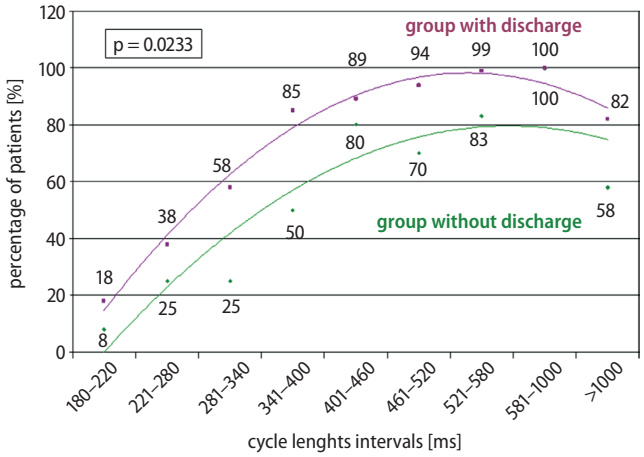

Fig. 3. Comparison of patients (%) within different cycle lengths intervals of PVC events in group A and B

(p = 0.0233). Graphical representation of RR interval patterns from PDM 2000 (comparing patients from group A and group B) are presented in Fig. 4.

The template presented in the upper panel in Fig. 4 would be regarded as a "risk pattern" for group A, with frequent PVCs of short coupling interval, and the lower panel would be typical for a normal, healthy heart. The upper recording comes from a 72-year-old patient after myocardial infarction, EF = 20%. During the observation period, many episodes of VT (145 bpm) with unsuccessful ATP occurred, terminated with cardioversion of 10 joules. The lower panel in Fig. 4 represents the case of a 52-year-old patient after acute myocarditis with VF in the acute phase. Initial EF after the episode was 30% and ICD was implanted. Later on, complete recovery with the improvement of EF to normal

Table 2. The rate and the values of the phenomena defined in the study protocol

Parameter	Group A	Group B	p-value
PVC defined as RR interval shorter >10% than the predecessor			
Mean RR of PVC (c.l.)	640 ±101	625 ±213	NS
Minimal RR of PVC (c.l.)	**314 ±112**	**400 ±132**	**0.019**
Maximal RR of PVC (c.l.)	945 ±192	896 ±190	NS
PVC number/4000 RR	**263 ±32**	**43 ±17**	**<0.0001**
PVC defined as RR interval shorter >20% than the predecessor			
Mean RR of PVC (c.l.)	**593 ±82**	**529 ±183**	**0.049**
Minimal RR of PVC (c.l.)	**320 ±112**	**400 ±132**	**0.029**
Maximal RR of PVC (c.l.)	891 ±160	828 ±146	NS
PVC number/4000 RR	**174 ±24**	**15 ±7**	**<0.0001**
Mean number of cycles			
CI: 180–220 ms	1 ±0.4	0.1 ±0.1	0.028
CI: 220–280 ms	5 ±1.2	0.6 ±0.4	0.0007
CI: 280–340 ms	18 ±11	51 ±49	NS
CI: 340–400 ms	23 ±9	16 ±15	NS
CI: 400–460 ms	88 ±46	17 ±11	NS
CI: 460–520 ms	126 ±79	189 ±129	NS
CI: 520–580 ms	315 ±9	350 ±150	NS
CI: 580–1000 ms	2870 ±134	3075 ±245	NS
CI: 1200–2000 ms (long cycles)	523 ±134	273 ±117	NS
Mean RR interval in relation to predecessor	**45 ±37**	**19 ±13**	**<0.0001**
Incidence of short-long-short (SLS) sequence, number of patients (%)	**67 (94%)**	**4 (33%)**	**<0.001**
Couplets	45 (63%)	4 (33%)	NS
Runs of nsVT	**28 (39%)**	**1 (8%)**	**0.0490**

PVC – premature ventricular complex; NS – not significant; c.l. – cycle lengths; CI – coupling intervals. Values in bold are statistically significant.

limits and no ICD therapies in the follow-up period were observed.

Graphical representation of RR interval patterns from PDM 2000 within the same patient are presented in Fig. 5. The RR interval series presented in upper panels in Fig. 4 and 5 originated from the same patient. They are presented in such a manner for better visual comparison with lower panels. The PCRR program makes RR interval analysis possible. The results are presented above, at the beginning of the Results section. However, the program also generates graphs with RR interval distributions and corresponding PVC burden in different CI. An example of RR distribution in patients from group B (left panel) and group A (right panel), generated as a print-out created from the PCRR program, is presented in the form of a graphical abstract in Fig. 6. It summarizes the differences between PVC characteristics in a graphical form in relation to RR interval cycle length.

The ROC were created as a predictor of ICD intervention for both models described in method section (Fig. 7 below; left panel: model 1, right panel: model 2). The results of ROC comparison of statistical significance for PVC in the 2 tested models on the basis of AUC are presented in Table 3.

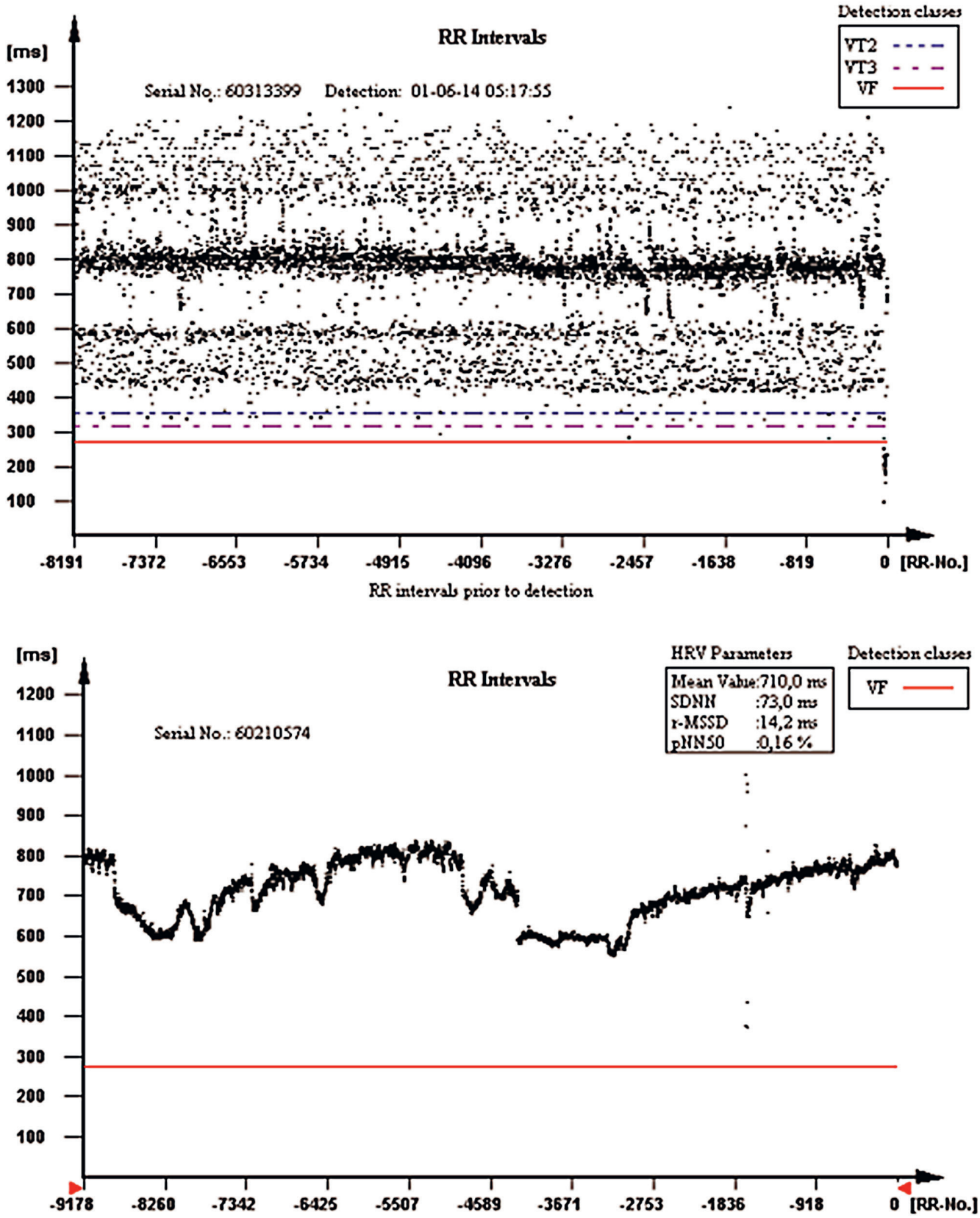

Fig. 4. Graphical differences of RR pattern from PDM 2000 (between patients from group A and group B)

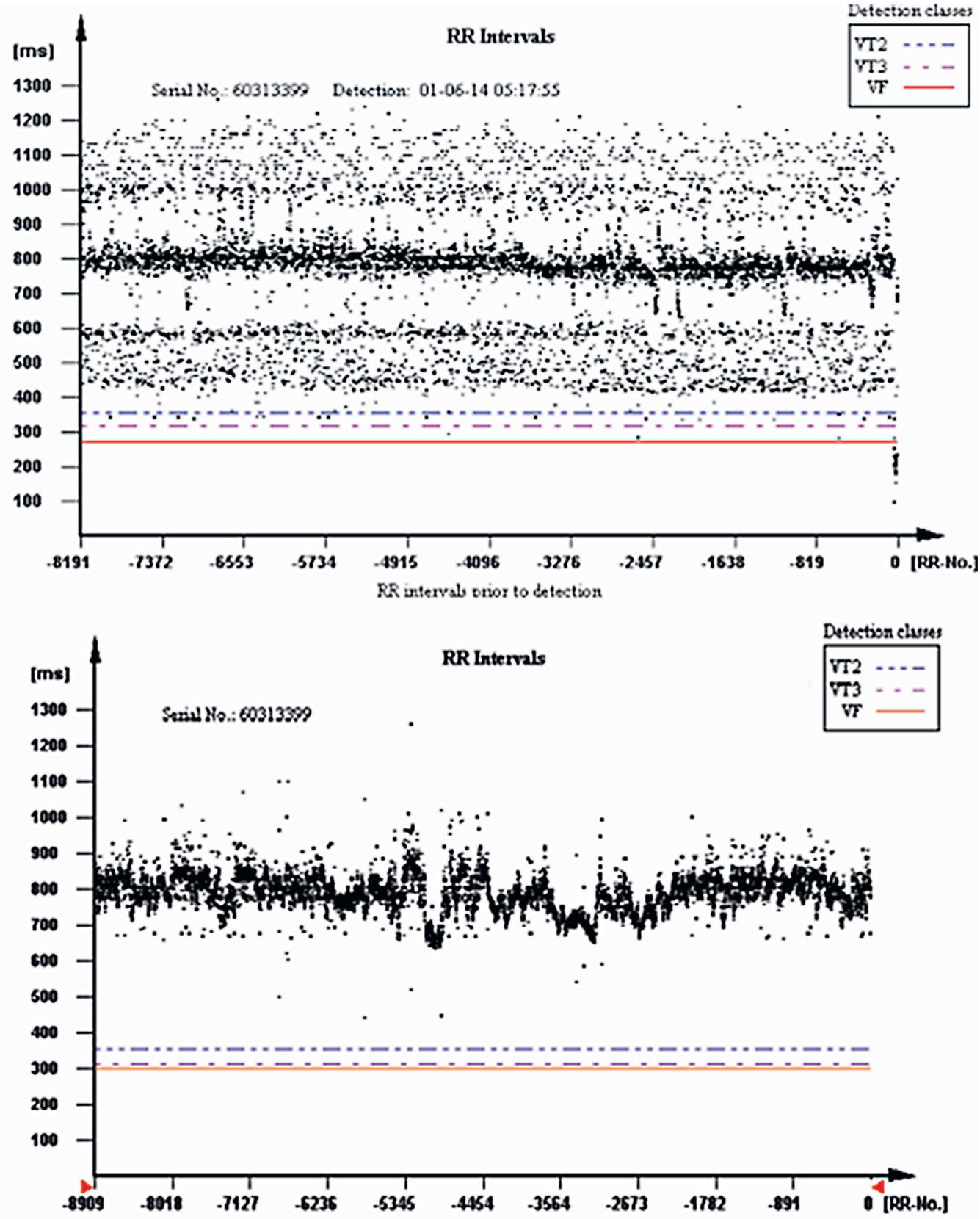

Fig. 5. Graphical differences of RR pattern from PDM 2000 within the same patient. Upper panel – RR recordings just before VF; lower panel – RR series during a routine follow-up visit without arrhythmia and no ICD intervention

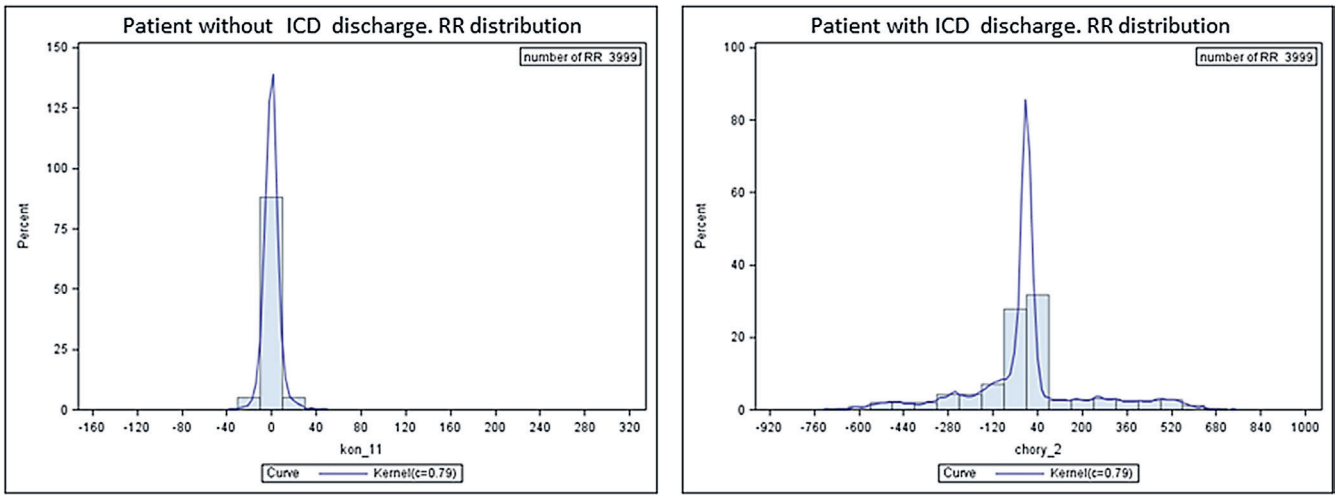

Fig. 6. Graphical differences of RR pattern from PCRR (between patients from group B and group A)

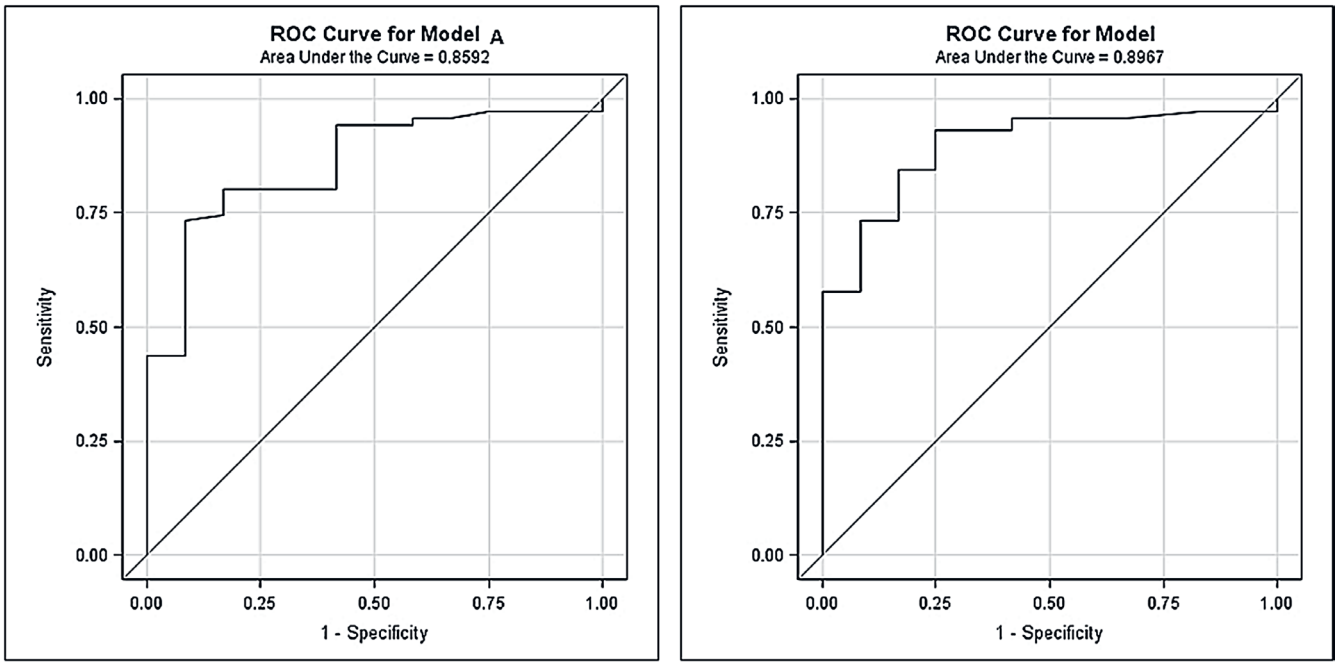

Fig. 7. ROC curves as a predictor of ICD intervention for the analyzed PVC models: 1 (left panel) and 2 (right panel)

Discussion

The mechanisms leading to VT/VF initiation are still not fully understood. In patients with CAD and heart failure (e.g., MADIT trial population), a characteristic pattern of ventricular tachyarrhythmias initiation has been recognized; namely, 77% of the episodes were initiated by PVC and 23% with an SLS sequence.[3] In this etiology, it is suggested that the Purkinje fibers are resistant to ischemia so these surviving cells surrounded by necrotic tissue demonstrate a high degree of automaticity, triggered activity and abnormal excitability.[9] It has been demonstrated that the Purkinje fibers also play a role in VF initiation in structural heart diseases such as DCM, amyloidosis and chronic myocarditis, and in hereditary syndromes without structural heart disease, such as long QT syndrome, Brugada syndrome and catecholaminergic polymorphic ventricular tachycardia.[7,10] Two mechanisms are postulated in this situation: the triggered activity from Purkinje tissue or re-entry in the Purkinje system. On the cellular level, Ca^{2+} overload is considered as a trigger for delayed afterdepolarizations; in some cases, it can be suppressed using verapamil. There is some evidence that PVCs could trigger VF, but sometimes a PVC will precede an arrhythmia event without triggering it.[8] In some reports, idiopathic VF and polymorphic ventricular tachycardia were associated with a short-coupling interval between PVCs and conducted beats.[11] Our study is concordant with this observation. PVCs with very short and short cycle lengths (180–220 ms and 220–280 ms, respectively) were more

Table 3. Results of the ROC comparison for PVCs in 2 tested models

ROC for PVC Model 1 (left panel of Fig. 7)	
Odds ratio [95% CI], p-value for PVC number/4000 RR	2.1 [1.15–3.7]; p = 0.002
Area under the curve ROC	0.859
Sensitivity	88.7%
Specificity	58.3%
Cut-off point for ROC (number of episodes)	30
ROC for PVC Model 2 (right panel of Fig. 7)	
Odds ratio [95% CI], p-value for PVC number/4000 RR	4.7 [1.34–16.3]; p = 0.003
Area under the curve ROC	0.897
Sensitivity	88.7%
Specificity	75%
Cut-off point for ROC (number of episodes)	12

PVC – premature ventricular complex; 95% CI – 95% confidence interval; ROC – receiver operating characteristic.

frequent in patients with appropriate ICD therapy. Sanchez et al. found no significant difference between PVC coupling intervals of those that did or did not trigger VF.[8,11] Also, it was shown that the origin of PVCs is important. The PVCs originating from a peripheral Purkinje network were more likely to be present during the occurrence of electrical storm than those coming from the right ventricular outflow tract (RVOT).[9] The latter PVC could still trigger VF, albeit less frequently, as there are reports of successful radiofrequency catheter ablation of unifocal PVC of RVOT origin for recurrent VF.[11] Of course, the origin of the PVC was not in our dataset, as our data came from ICD IEGM, not from the localization technique used in electrophysiology laboratory.

The PVC ablation is considered a feasible technique and could be considered as an indication for reducing ICD shock rates and even withholding the ICD implantation decision.[12] A multicenter study followed 38 patients after PVC RFA for idiopathic VF.[7] Eighteen percent had recurrent VF and 5 were treated successfully with redo procedures of triggering PVC ablation during the five-year follow-up period. A relationship between PVC burden and left ventricular function was recognized.[13] The reported percentage of daily PVC burden (determined by 24-hour Holter monitoring), which led to the deterioration of the left ventricular systolic function (PVC-mediated cardiomyopathy), varies from 10%, through 16% and 24%, to 30%.[14] Catheter ablation techniques for PVCs have recently become successful treatment in clinical practice with a success rate >80%.[15–17] Search for different mechanisms leading to VT/VF initiation and the discussion on the organization of VF in human myocardium is still of broad and current interest.[18]

Baseline PVC assessment is important as a significant burden is associated with increased risk for SCD and total cardiac death.[19] Screening for the presence of frequent PVCs should be part of the decision-making process in primary prophylaxis ICD implantation as trigger ablation is an effective therapy in scar-related or PVC-triggered arrhythmias. The ESC SCD Guidelines (2016) recommend catheter ablation (Class IIa, Level B) in patients with LV dysfunction, PVC burden >24% and short coupling PVC intervals (<300 ms).[20] Our findings strongly supports these recommendations and other recent reports.[21] On the basis of our pilot report on patients with ICD, we believe that the created program and the associated rate variability pattern could be a tool for prediction of SCD risk in different populations. The main advantage of the PCRR program is its low computational complexity. Its simplicity allows for either hardware implementation in a specific integrated circuit or implementation in software on standard microprocessors.

In addition, no pre-processing of the IEGM raw signal is necessary. In the past, we have shown that it is possible to transfer RR intervals recordings in a simple text format transfer, as shown on the dedicated website (http://defib.imio.pw.edu.pl/).[22] The PCRR implementation can easily make the transition to telemedicine-based practices, e.g., monitoring of ECG and implantable loop recorders.

The fact that there are still gaps in the basis of evidence for sudden cardiac death clinical predictors encouraged us to work in this field and create a new RR interval analysis program (PCRR) to question whether ventricular ectopic activity could be regarded as a predictive marker. Heart rate variability (HRV) and others have been proposed as SCD risk factors but they are not widely used due to their complexity and sophistication.

Limitations

This study is a single-center, retrospective analysis. The enrollment number is limited due to a lack of full data, i.e., an RR interval pattern with the corresponding IEGM. The study group is heterogeneous in terms of risk etiology and clinical characteristics, but the main aim of the study was to create the RR interval analysis program on the basis of a consecutive ICD patient group. For this reason, we performed an analysis of coupling intervals preceding VT/VF and controls only. It should be kept in mind that more complex trigger factors are involved in the induction of tachyarrhythmias, such as electrolyte imbalance or worsening of heart failure leading to myocardium electric instability. We were not able to compare the episodes within the same patients in all cases (e.g., device interrogations just before the therapy compared to remote from the therapy). Therefore, we compared interrogations after the therapy and during the scheduled clinical visit which was not preceded by any therapy. Some participants were treated with amiodarone, which could have affected the PVC pattern compared to those not receiving antiarrhythmic drugs. The RR interval sequences were

based on the coupling intervals and compensatory pauses. The IEGM does not enable verification of PVC morphologies. We merged ATP and ICD shocks recordings in one group intentionally to obtain a larger RR tachyarrhythmias database. The time between the ICD implantation and therapy varied from a few months to 3 years. Therefore, a further prospective and a more extensive study is needed to validate the value of the proposed methodology.

Conclusions

Significant differences were found in the characteristics of PVCs and SLS sequences in patients with appropriate ICD interventions and controls. A newly developed basic computer program called PCRR was used for RR interval analysis. The proposed program could be a new tool to assess PVC burden and arrhythmia risk in different populations.

ORCID iDs

Michał Lewandowski https://orcid.org/0000-0002-6829-7491
Ilona Kowalik https://orcid.org/0000-0002-8040-5109

References

1. Bayes de Luna A, Coumel P, Leclercq JF. Ambulatory sudden cardiac death: Mechanisms of production of fatal arrhythmia on the basis of data from 157 cases. *Am Heart J*. 1989;117(1):151–159. doi:10.1016/0002-8703(89)90670-4
2. Sacher F, Victor J, Hocini M, et al. Characterisation of premature ventricular contraction initiating ventricular fibrillation [in French]. *Arch Mal Coeir Vaiss*. 2005;98(9):867–873. PMID:16231572
3. Anthony R, Daubert JP, Zareba W, et al; Multicenter Automatic Defibrillator Implantation Trial-II Investigator. Mechanisms of ventricular fibrillation initiation in MADIT II patients with implantable cardioverter-defibrillators. *Pacing Clin Electrophysiol*. 2008;31(2):144–150. doi:10.1111/j.1540-8159.2007.00961.x
4. Tabereaux PB, Dosdall DJ, Ideker RE. Mechanisms of VF maintenance: Wandering wavelets, mother rotors, or foci. *Heart Rhythm*. 2009;6(3):405–415. doi:10.1016/j.hrthm.2008.11.005
5. Haissaguerre M, Hocini M, Sacher F, Shah A. Sudden cardiac death, a major scientific challenge [in French]. *Bull Acad Natl Med*. 2010;194(6):983–995. PMID:21513133
6. Nogami A. Purkinje-related arrhythmias part II: Polymorphic ventricular tachycardia and ventricular fibrillation. *Pacing Clin Electrophysiol*. 2011;34(8):1034–1049. doi:10.1111/j.1540-8159.2011.03145.x
7. Partemi S, Batlle M, Berne P. Analysis of the arrhythmogenic substrate in human heart failure. *Cardiovasc Pathol*. 2013;22(2):133–140. doi:10.1016/j.carpath.2012.07.003
8. Sanchez Munoz JJ, Garcia-Alberola A, Martinez-Sanchez J, et al. Premature ventricular complexes as a trigger for ventricular fibrillation. *Rev Esp Cardiol*. 2010;63(7):798–801. doi:10.1016/s1885-5857(10)70164-x
9. Schmidt B, Chun KR, Kuck KH, Ouyang F. Ventricular tachycardias originating in the his-purkinje system: Bundle branch reentrant ventricular tachycardias and fascicular ventricular tachycardias. *Herz*. 2009;34(7):554–560. doi:10.1016/s1885-5857(10)70164-x
10. Cho YR, Park JS. Radiofrequency catheter ablation for unifocal premature ventricular complexes triggering recurrent ventricular fibrillations in a young man without structural heart disease. *Korean Circ J*. 2012;42(8):575–579. doi:10.4070/kcj.2012.42.8.575
11. Del Carpio Munoz F, Syed FF, Noheria A, et al. Characteristics of premature ventricular complexes as correlates of reduced left ventricular systolic function: Study of the burden, duration, coupling interval, morphology, and site of origin of PVCs. *J Cardiovasc Electrophysiol*. 2011;22(7):791–798. doi:10.1111/j.1540-8167.2011.02021.x
12. Penela D, Acosta J, Aguinaga L, et al. Ablation of frequent PVC in patients meeting criteria for primary prevention ICD implant: Safety of withholding the implant. *Heart Rhythm*. 2015;12(12):2434–2442. doi:10.1016/j.hrthm.2015.09.011
13. Hasdemir C, Ulucan C, Yavuzgil O, et al. Tachycardia-induced cardiomyopathy in patients with idiopathic ventricular arrhythmias: The incidence, clinical and electrophysiologic characteristics, and the predictors. *J Cardiovasc Electrophysiol*. 2011;22(6):663–668. doi:10.1111/j.1540-8167.2010.01986.x
14. Yokokawa M, Good E, Crawford T, et al. Recovery from left ventricular dysfunction after ablation of frequent premature ventricular complexes. *Heart Rhythm*. 2012;10(2):172–175. doi:10.1016/j.hrthm.2012.10.011
15. Nault I, Knecht S, Sacher F, et al. Advances in catheter ablation of primary ventricular fibrillation 2016, Thoracic Key, Chapter 96. https://thoracickey.com. Accessed May 3, 2020.
16. Cheniti G, Vlachos K, Meo M, et al. Mapping and ablation of idiopathic ventricular fibrillation. *Front Cardiovasc Med*. 2018,5:123. doi:10.3389/fcvm.2018.00123
17. Robert D, Anderson D, Kumar S, et al. Catheter ablation of ventricular fibrillation. *Heart Lung Circ*. 2019;28(1):110–122. doi:10.1016/j.hlc.2018.09.005
18. Karaguezian HS. Ventricular fibrillation: An organized delirium or uncoordinated reason? *Heart Rhythm*. 2004;1(1):24–26. doi:10.1016/j.hrthm.2004.02.014
19. Tonchev I, Luria D, Orenstein D, Lotan C, Biton Y. For whom the bell tolls: Refining risk assessment for sudden cardiac death. *Curr Cardiol Rep*. 2019;21(9):106. doi:10.1007/s11886-019-1191-z
20. Priori S, Blomstrom-Lundqvist C, Mazzanti A, et al; ESC Scientific Document Group. 2015 ESC Guidelines for the management of patients with ventricular arrhythmias and the prevention of sudden cardiac death. The Task Force for the Management of Patients with Ventricular Arrhythmias and the Prevention of Sudden Cardiac Death of the European Society of Cardiology (ESC). *Eur Heart J*. 2015;36(41):2793–2867. doi:10.1093/eurheartj/ehv316
21. Kukla P, Sławuta A, Jastrzębski M, Gajek J, Stec S. Unusual changes in ventricular repolarization before right ventricular outflow tract arrhythmias. *Am J Med Sci*. 2017;353(3):311–312. doi:10.1016/j.amjms.2016.11.009
22. Bardossy A, Blinowska A, Kuźmicz W, Ollitrault J, Lewandowski M, Przybylski A. Fuzzy logic based diagnosis algorithm for implantable cardioverter-defibrillators. *Artif Intell Med*. 2014;60(2):113–121. doi:10.1016/j.artmed.2013.12.004

Three cases of 3β-hydroxysteroid dehydrogenase deficiency: Clinical analysis

Lanni Chen[A–B,D–F], Haihua Huang[C,D], Huijiao Zhang[C], Gaohui Zhu[B], Min Zhu[A,D]

Children's Hospital of Chongqing Medical University, China

A – research concept and design; B – collection and/or assembly of data; C – data analysis and interpretation;
D – writing the article; E – critical revision of the article; F – final approval of the article

Advances in Clinical and Experimental Medicine, ISSN 1899–5276 (print), ISSN 2451–2680 (online) *Adv Clin Exp Med*. 2021;30(3):289–299

Address for correspondence
Min Zhu
E-mail: zhumin323@aliyun.com

Funding sources
None declared

Conflict of interest
None declared

Received on March 23, 2020
Reviewed on June 21, 2020
Accepted on December 6, 2020

Published online on March 23, 2021

Abstract

Background. 3β-HSD deficiency is a rare type of congenital adrenal hyperplasia (CAH), which is caused by *HSD3B2* gene mutations.

Objectives. In order to improve the understanding and diagnosis of the disease, we analyzed and summarized the clinical characteristics, genetic variants and treatment for 3 children with 3β-HSD deficiency in this study.

Materials and methods. A summary of the clinical data, hormone levels (17-hydroxyprogesterone, adrenocorticotropic hormone, cortisol, testosterone, dehydroepiandrosterone, androstenedione, renin, and aldosterone), therapeutic drugs, and gene sequencing results from 3 3β-HSD deficiency patients was created.

Results. The 3 patients developed external genital abnormalities and adrenal insufficiency in infancy. Steroid hormone levels were consistent with 3β-hydroxysteroid dehydrogenase deficiency. Gene sequencing for the 3 patients detected complex heterozygous mutations in the *HSD3B2* gene, which confirmed the diagnosis of 3β-HSD deficiency type II. Among the mutation types, c.154_162delinsTCCTGTT and c.674T>A have not been reported in the literature. The 3 children were treated with glucocorticoid and mineralocorticoid replacement, which controlled the adrenal insufficiency satisfactorily. In 2 male patients, external genital dysplasia manifested as hypospadias and small penis. After long-acting testosterone intramuscular injection to increase the penis size, the hypospadias were repaired. Mild masculinization in the female patient resulted in skin pigmentation and clitoral hypertrophy; however, no surgical intervention was required.

Conclusions. The main clinical manifestations of 3β-HSD deficiency were adrenal insufficiency and sex hormone synthesis dysfunction. There was a strong phenotype correlation between the observed clinical manifestations in conjunction with steroid hormone levels and *HSD3B2* mutations. The novel mutations c.154_162delinsTCCTGTT and c.674T>A were classified as pathogenic variants. Adrenal cortical function control was satisfactory after hormone replacement therapy, and hypospadias and small penis were attenuated using testosterone replacement therapy during mini-puberty for optimal surgical outcome.

Key words: treatment, clinical features, 3β-hydroxysteroid dehydrogenase deficiency, *HSD3B2*

Cite as
Chen L, Huang H, Zhang H, Zhu G, Zhu M. Three cases of 3β-hydroxysteroid dehydrogenase deficiency: Clinical analysis. *Adv Clin Exp Med*. 2021;30(3):289–299. doi:10.17219/acem/131220

DOI
10.17219/acem/131220

Background

There are 2 types of human 3β-hydroxysteroid dehydrogenase (3β-HSD), type I (3β-HSD1) and type II (3β-HSD2),[1] which have 93.6% homology and are encoded by the *HSD3B1* and *HSD3B2* genes, respectively. The 3β-HSD1 enzyme is mainly expressed in organs such as the placenta, breast, skin, and prostate. It catalyzes the production of different steroids at low substrate concentrations, which are necessary for the synthesis of placental progesterone during pregnancy.[2] The 3β-HSD2 enzyme is expressed in the adrenal gland and gonadal tissues.[3] It is the rate-limiting step in the synthesis of the adrenocortical and sex hormones. Their expression is regulated by negative feedback from downstream products such as sex hormones and cortisol. It mainly catalyzes the conversion of Δ5-3β-hydroxysteroids to Δ4-3β-ketosteroid.[4]

3β-HSD deficiency is a rare type of congenital adrenal hyperplasia (CAH), which is caused by *HSD3B2* gene mutations. The neonatal incidence is less than 1/1,000,000,[5] accounting for less than 5% of all CAH cases. The *HSD3B2* gene is located on chromosome 1 at 1p12 and is composed of 4 exons and 3 introns. The protein contains 371 amino acids and has 4 functional domains that include a cofactor binding domain, a ligand binding domain and 2 transmembrane domains.[6] *HSD3B2* gene mutations cause steroid hormone synthesis disorder, which eventually leads to decreased aldosterone, cortisol and sex hormone synthesis. The main clinical manifestations are adrenal insufficiency and sex hormone synthesis disorder. The severity of the clinical manifestations depends mainly on the remaining enzyme activity. Therefore, the disorder can be divided into classical and non-classical types according to enzyme activity levels and the degree of adrenal insufficiency. Children with classic 3β-HSD deficiency frequently have adrenal insufficiency, genital abnormalities in the neonatal period or infancy, and salt loss manifested through vomiting and dehydration. Typically, male genitalia have different degrees of incomplete masculinization while women may consistently be affected with mild masculinity. Therefore, the treatment of glucocorticoid combined with mineralocorticoid replacement therapy to improve adrenal function is recommended, and if necessary, surgical treatment may also be required.

Because 3β-HSD deficiency is a rare disease, there are a number of different types of mutation across different populations. More than 110 cases have been confirmed using genetic testing[7–9] and more than 50 types of *HSD3B2* gene mutations have been detected, including frameshift, missense, nonsense, splicing pathogenic variants, and deletions, among which missense variants are the most common type, while nonsense or frameshift pathogenic variants often lead to typical clinical phenotypes.[10] In order to improve the understanding and diagnosis of the disease, we analyzed and summarized the clinical characteristics, genetic variants and treatment for 3 children with 3β-HSD deficiency in this study.

Materials and methods

Subjects

During the period from January 2011 to March 2019, 3 children diagnosed with 3β-HSD deficiency were admitted to the Department of Endocrinology, Children's Hospital of Chongqing Medical University, China. Informed consent from the parents of each child was obtained and reviewed by the ethics committee of the Children's Hospital of Chongqing Medical University. Our study on humans also complies with the Helsinki Declaration.

The gender, age of onset, clinical history, family history, phenotypic features, and medication history was collected for the 3 patients.

Determination of hormone levels

Peripheral blood was taken from the children and cortisol, testosterone (T), adrenocorticotrophin (ACTH), renin, and aldosterone levels were determined with immunoluminescence. Dehydroepiandrosterone (DHEA), androstenedione (AND) and 17-hydroxyprogesterone (17-OHP) levels were determined using a radioimmunoassay.

ACTH excitatory test

A corticotropin (ACTH39 peptide 25 U = 0.25 mg) peptide was used in the excitatory test. Approximately 10 mL of normal saline was used to dilute the vein with slow intravenous injections for 5–10 min. Post-injections blood was collected at 0 min (directly afer the injection), 30 min, and 60 min to measure progesterone, cortisol, AND, DHEA, and 17-OHP levels.

Gene sequencing analysis

Blood (treated with EDTA anticoagulation) taken from the children and their parents was collected and sent to the Beijing Jinzhun Medical Laboratory (Beijing, China), the Molecular Pathology Center of the Affiliated Hospital of the Air Force Aviation Medical Research Institute (Beijing, China) and the DeyiDongfang Conversion Medical Research Center (Beijing, China) for sequencing. After DNA extraction, polymerase chain reaction (PCR) using gene-specific primers for the 4 *HSD3B2* exons, exon intron junction and V-flanking region was performed. Amplicons were sequenced using the HiSeq2500 instrument (Illumina, San Diego, USA) and variants were confirmed with Sanger sequencing.

Results

Clinical data for Case 1

Case 1 is a male with a normal karyotype (46, XY), 5 years and 8 months old now. When he was at the age of 1 month and 13 days, his parents sought medical advice of an endocrinologist due to abnormalities in the external genitalia of their son (the penis was short with hypospadias), inability to gain body weight by 1 month of age and diarrhea for at least 3 days. Soon after birth, abnormal genitalia, low body weight and other symptoms were noted, such as poor suction and regurgitation of milk, diarrhea, irritability, convulsions, lack of sweating ability, poor response, short stature, as well as intellectual and developmental retardation. His mother has had 1 pregnancy before and that has delivered once (Tanner staging of her 1st child was G1P1). He was a full-term baby, breastfed, and his birth weight was 3.4 kg, with unknown birth length. Newborn screening showed abnormal results, namely, an elevated 17-OHP value. His parents were healthy, with no consanguinity, normal puberty development age, and negative family history of genetic metabolic disease and CAH. Physical examination at the age of 1 month and 13 days showed a body length of 52 cm, body weight of 3.5 kg, normal development, normal nourishment, no abnormal facial features, rough skin, lack of pigmentation of the lip, gum and breast, lack of hair, hemorrhoids, and normal heart, lungs and muscle tension in the limbs. The features of the external genitalia included dark-colored bilateral scrotum, palpable testis, and embedded penis of approx. 1.0 cm in length and 3.0 cm in circumference with hypospadias. The Tanner staging was G1PH1 at the age of 1 month and 13 days. Laboratory findings are shown in Table 1. Laboratory results at initial diagnosis showed elevated potassium, 17-OHP and dehydroepiandrosterone, and low levels of sodium, testosterone and cortisol.

Clinical data for Case 2

Case 2 is a male (chromosome 46, XY), 3 years and 3 months old now. He was treated with hormone therapy for abnormal genitalia, poor suck and low weight after reaching 1 month of age. Shortly after birth, external genital malformations were observed. A variety of physical issues were present, namely, short penis with hypospadias, scrotal skin pigmentation, poor suction, low weight gain, irritability, convulsions, lack of sweating, and poor response. Blood gas analysis revealed abnormal potassium (high), sodium (low) and chlorine (low), with suspected CAH and treatment with 1.25 mg hydrocortisone 3 times per day and 50 µg of fluorohydrocortisone 2 times a day at 1 month of age. After treatment, weight gain was observed along with better suction and spit responses. He was a full-term baby, delivered by cesarean section, with birth weight of 3.4 kg and unknown birth length. At 7 months

Table 1. Laboratory tests of Case 1 during follow-up

Age	ACTH [pg/mL]	17-OHP [mmol/L]	Cortisol [nmol/L]	Testosterone [nmol/L]	DHEA [µmol/L]	AND [nmol/L]	Renin [µIU/mL]	Aldosterone [ng/dL]	Electrolyte [mmol/L]
1 month and 13 days	34	>75.75	–	4.02	5.92	>35	10.63	0.49	K^+ 6.12 Na^+ 126.1
1 month and 27 days	<10	8.82	–	<0.69	0.502	3.26	–	–	normal
3 months and 2 days	131	12.78	–	2.96	<0.407	1.07	–	–	normal
5 months and 12 days	19	<0.303	–	<0.69	<0.407	<1.05	–	–	normal
27 months and 15 days	12.4	<0.303	–	<0.69	<0.407	<1.05	–	–	normal
11 months and 3 days	13.7	1.03	–	<0.69	<0.407	<1.05	–	–	normal
1 year and 1 month	12.7	3.5	–	<0.69	<0.407	<1.05	–	–	normal
1 year and 4 months	29.4	<0.303	37.8	<0.69	<0.407	<1.05	–	–	normal
1 year and 8 months	31.9	<0.303	–	<0.69	<0.407	<1.05	–	–	normal
1 year and 11 months	275	1.03	<4.41	6.31	<0.407	<1.05	19.1	7.51	normal
2 years and 4 months	<10	<0.303	147	1.98	<0.41	<1.05	30.9	8.07	normal
2 years and 11 months	339	18.7	50.3	<0.69	3.12	<1.05	26	<0.97	normal
3 years and 6 months	220	11.26	<27.6	<0.69	6.08	<1.05	14.6	<0.97	normal
4 years	101	3.79	38.4	<0.69	2.77	<1.05	94.7	<0.97	normal
4 years and 7 months	629	22.57	33.4	<0.69	23.1	2.77	258.2	1.98	normal
4 years and 11 months	93.3	1.47	–	<0.69	3.61	<1.05	4.8	<0.97	normal
5 years and 2 months	599	7.12	<27.6	<0.69	4.34	<1.05	25.5	<0.97	normal
5 years and 8 months	264	6.55	<27.6	<0.69	10	<1.05	251.1	3.88	normal

Normal values: K+: 3.5–5.5 mmol/L; Na+: 130–150 mmol/L; ACTH: <46 pg/mL; 17-OHP: <29.1 mmol/L; cortisol: 124–662 nmol/L; testosterone: <0.69 nmol/L; renin: 2.8–39.9 µIU/mL; aldosterone: <23.6 ng/dL; DHEA: <0.41 µmol/L.

of pregnancy, ultrasound examination revealed that the fetus had hypospadias and amniotic fluid chromosome karyotyping showed 46 XY. After birth, neonatal screening revealed an abnormal 17-OHP level (110 nmol/L). His parents were healthy, with normal puberty, no consanguinity and no family history of genetic metabolic disease (including CAH).

Upon physical examination at the time of initial diagnosis (2 months and 27 days of age), body length was 61 cm and body weight was 6 kg. The child showed normal development, good nutrition, no abnormal facial features, lack of pigmentation in the gums, areola and skin folds, hemorrhoids, and normal heart and lungs. The external genitalia had several features such as a short penis similar to a clitoris (about 1.2 cm long, 3.0 cm in circumference), a urethral opening in the base of the penis, scrotum hypertrophy with no skin pigmentation, and Tanner staging of G1PH1. The laboratory results are shown in Table 2. The 17-OHP and potassium levels were significantly elevated, but sodium remained low at 2 months and 27 days of age. Other laboratory findings at the time of initial diagnosis were abnormal, including high ACTH and renin levels; however, 17-OHP, dehydroepiandrosterone, aldosterone, and electrolyte levels remained normal. These laboratory results may be related to hormone treatments that were being administered to the patient. At 1 year and 8 months of age, the ACTH stimulation test was completed (Table 3). The cortisol level after the challenge was less than 500 nmol/L, suggesting a glucocorticoid deficiency. Progesterone, 17-OHP, androstenedione, and other byproducts remained low, which also suggested an adrenal cortical hormone synthesis disorder. The observed lesion was located at the adrenal gland and was consistent with 3β-HSD deficiency type II, but dehydroepiandrosterone was not elevated during the challenge, which may be explained by long-term hormone replacement therapy. During the follow-up period, 17-OHP, DHEA, ACTH, aldosterone, and electrolytes levels were normal after treatment.

Clinical data for Case 3

This is a female child (46, XX) who is now 8 years and 2 months old. At 5 months and 8 days of age, she was examined by an endocrinologist due to skin pigmentation identified shortly after birth, intermittent vomiting, diarrhea, and developmental delay. This patient has bilateral clitoral hypertrophy. There was pigmentation of the labia, intermittent vomiting, diarrhea, growth delay, irritability, convulsions, lack of sweating, poor response, hemorrhoids, but normal stature and normal intelligence development. Electrolyte test results showed a concentration range of potassium from 7.26 mmol/L to 9.2 mmol/L and sodium from 96 mmol/L to 100 mmol/L. She was born at G2P1 (Tanner staging), full-term, with birth weight of 3.1 kg and unknown birth length; she was subject to artificial feeding after birth. The parents of the child are healthy, non-consanguineous, had normal puberty development, an abortion of the first child and negative family history of genetic any metabolic diseases, including CAH.

Upon physical examination at the time of initial diagnosis (age of 5 months), the patient had a body length of 59.8 cm and weight of 4.8 kg, and presented with developmental delay, malnutrition, abnormal skin and areola

Table 2. Laboratory tests of Case 2 during follow-up

Age	ACTH [pg/mL]	17-OHP [mmol/L]	Cortisol [nmol/L]	Testosterone [nmol/L]	DHEA [μmol/L]	AND [nmol/L]	Renin [μIU/mL]	Aldosterone [ng/dL]	Electrolyte [mmol/L]
Outside the hospital	–	110	–	–	–	–	–	–	K^+ 5.67 Na^+ 114.1
2 months and 27 days	262	3.7	810	4.3	<0.41	2.13	464	<0.97	normal
3 months and 26 days	42.9	3.78	81.3	17.8	0.497	5.39	88.5	<0.97	normal
5 months and 27 days	<10	<0.303	42.8	<0.69	<0.41	<1.05	6.5	<0.97	normal
9 months and 15 days	73.6	0.45	30.3	17.8	<0.41	<1.05	<0.5	1.02	normal
1 year and 4 months	150	1.74	46.9	1.76	<0.41	<1.05	29.1	1.94	normal
1 year and 8 months	126	1.97	63.2	<0.69	<0.41	<1.05	77.3	<0.97	normal
2 years and 3 months	48.3	0.83	46.4	<0.69	<0.41	<1.05	1.3	1.83	normal
2 years and 8 months	157	2.66	67.9	<0.69	<0.41	<1.05	77.3	<0.97	normal

Table 3. ACTH stimulation test of Case 2

Items	Base value	30 min	60 min	90 min	120 min
Cortisol	370	284	284	250	170
Progesterone	<0.64	<0.64	<0.64	<0.64	<0.64
Dehydroepiandrosterone	<0.41	<0.41	<0.41	<0.41	<0.41
Androstenedione	<1.05	<1.05	<1.05	<1.05	<1.05
17-hydroxyprogesterone	1.61	1.93	2.1	1.96	1.59

pigmentation, lack of pigmentation in the oral mucosa, pigmentation in the vulva, and slightly enlarged clitoris.

The laboratory results are shown in Table 4. At the time of initial diagnosis, they showed high levels of potassium, ACTH, 17-OHP, and DHEA, but sodium levels were low and renin and aldosterone level remained normal. During the treatment period, ACTH and 17-OHP, AND, aldosterone, and electrolytes were normal. At the age of 8, her bone age is 6 years and 9 months, which is slightly behind normal.

Gene sequencing results of the 3 cases

The gene sequencing results for *HSD3B2* for the 3 children are shown in Table 5 and Fig. 1. The *HSD3B2* gene screening results in Case 1 showed 2 heterozygous sequence changes, namely, c.154_162delinsTCCTGTT/p.Arg52Serfs*10 and c.1003C>T/p.Arg335Ter. The c.154_162delinsTCCTGTT pathogenic variant was inherited from the mother, indicating that bases between 154 and 162 were deleted, creating a frameshift mutation with a premature stop codon. In addition, the c.1003C>T nonsense pathogenic variant, which was predicted to result in premature termination, was not detected in the father. The *HSD3B2* gene screening results for Case 2 showed 2 missense heterozygous pathogenic variants, c.424G>A (p.E142K) change inherited from the father and c.674T>A (p.V225D) inherited from the mother. Moreover, *HSD3B2* gene screening of Case 3 showed 2 pathogenic variants, a missense c.776CcT (p.T259M) change inherited from the mother and a nonsense c.1003C>T (p.R335X) change expected to result in premature termination inherited from the father.

Table 4. Laboratory tests of Case 2 during follow-up

Age	ACTH [pg/mL]	17-OHP [mmol/L]	Cortisol [nmol/L]	Testosterone [nmol/L]	DHEA [µmol/L]	AND [nmol/L]	Renin [µIU/mL]	Aldosterone [ng/dL]	Electrolyte [mmol/L]
5 months and 8 days	>1250	>75.5	497	2.13	>27.1	>35	10.59	0.408	K^+ 7.66 Na^+ 119.5
6 months and 18 days	<10	1.38	–	<0.069	–	–	8.27	0.059	normal
7 months and 15 days	<10	<0.303	–	<0.069	–	–	0.27	0.058	normal
10 months and 29 days	23.9	–	–	<0.069	–	–	0.41	0.078	normal
1 year and 2 months	14.5	<0.303	–	<0.069	<0.407	<1.05	0.46	0.08	normal
1 year and 6 months	15.4	<0.303	196	<0.069	<0.407	<1.05	0.63	0.13	K^+ 3.3
2 years and 2 months	44.2	<0.303	–	<0.69	–	–	0.69	0.14	normal
2 years and 7 months	142	–	–	1.07	–	–	0.62	0.13	normal
3 years and 2 months	<10	<0.303	–	<0.69	<0.407	<1.05	–	–	normal
3 years and 7 months	261	<0.303	32	<0.69	<0.407	<1.05	0.57	0.13	normal
4 years and 1 month	1067	3.96	–	<0.69	0.738	<1.05	2.09	0.15	normal
4 years and 6 months	447	5.04	23.6	<0.69	0.532	<1.05	7.6	<0.97	normal
5 years	1250	9.01	24.6	<0.69	3.61	2.58	14.5	<0.97	normal
5 years and 7 months	674	2.66	35	<0.69	0.54	<1.05	5.8	3.86	normal
6 years and 1 month	643	18.37	67.6	<0.69	5.84	5.18	170.2	3.33	normal
6 years and 5 months	268	<0.303	–	<0.69	<0.41	<1.05	15.7	1.28	normal
6 years and 8 months	<10	<0.303	118	<0.69	<0.41	<1.05	12.6	<0.97	normal
6 years and 11 months	117	3.54	<27.6	<0.69	0.456	<1.05	109.8	1.43	normal
7 years and 5 months	<10	<0.303	60.7	<0.69	<0.41	<1.05	8.1	<0.97	normal
8 years	55.2	0.48	<27.6	<0.69	<0.41	<1.05	61	<0.97	normal

Table 5. *HSD3B2* gene results of 3 cases

Cases	Mutation site		Mutation type	Exon	Father	Mother
	Nucleotide change	Amino acid change				
Case 1	c.154_162delinsTCCTGTT	p.Arg52Serfs*10	frameshift mutation	3	none	hybrid
	c.1003C>T	p.Arg335Ter	nonsense mutation	4	none	none
Case 2	c.424G>A	P.E142K	missense mutation	4	hybrid	none
	c.674T>A	P.V225D	missense mutation	4	none	hybrid
Case 3	c.776C>T	p.259, T>M	missense mutation	4	none	hybrid
	c.1003C>T	P.335, R>X(38)	nonsense mutation	4	hybrid	none

Fig. 1. Gene mutation sites

Adrenal cortical hormone replacement therapy

Case 1 was treated with hydrocortisone replacement therapy immediately after the initial diagnosis (Table 6). The highest dose of hydrocortisone was administered at the beginning during infancy but was gradually decreased with age. The dose at 2–5 years of age was 8–10 mg/m^2/day, and was slightly increased after 5 years of age. The dose of fludrocortisone was gradually increased within the first 3 months of life, but the maximum dose did not exceed 100 μg/day and was slowly decreased after 3 months of age. Adrenal insufficiency control was satisfactory during treatment as evidenced by lack of adrenal crisis, hypertension and normal electrolytes. Dehydroepiandrosterone sulfate (DHEAS) and other androgens were well-controlled. Bone age was not advanced and consistent with age. In infancy, the curve of children's height fluctuates greatly due to repeated pneumonia, diarrhea and other diseases. After 1 year and 8 months, the height of children grows along the P3 curve of children of the same age. At 4 years old and 4 months of age, the height curve significantly increased.

Case 2 was treated with hydrocortisone and fludrocortisone replacement therapy. The dose of the drug was adjusted after the initial diagnosis (Table 7). The dose of hydrocortisone fluctuated between 5 mg/m^2/day and 10 mg/m^2/day. The dose of fludrocortisone was gradually decreased with age. During treatment, adrenal insufficiency was controlled satisfactorily (no adrenal crisis, no hypertension, no bone advanced age and normal electrolytes), with normal physical development.

Case 3 was treated with hydrocortisone and fludrocortisone replacement therapy after the initial diagnosis (Table 8). The dose of hydrocortisone was highest at initial dose in infancy and gradually decreased with age. The dose at 3–6 years old was maintained at 10 mg/m^2/day, and the dose was slightly increased after reaching the age of 6. The dose of fludrocortisone was gradually reduced with age. During treatment, adrenal insufficiency was controlled satisfactorily. At 4 years and 1 month, there was an increase in blood pressure, which indicated that there may be mineralocorticoid overtreatment; after dose reduction, blood pressure returned to normal. Electrolytes were normal. At the age of 8, the age of the bones was 6 years and 9 months, slightly behind normal, suggesting that the treatment of sex hormone synthesis disorders may also be warranted.

Table 6. Physical examination and medication results of Case 1 during follow-up

Age	Height/weight [cm/kg]	Blood pressure [mm Hg)]	Penis length* circumference [cm]	Testis [mL]	Hydrocortisone [mg/m^2/day]	Fluorocortisone [μg/day]	Bone age [years]
1 month and 13 days	52/3.5	–	1.0*3.0	1.5	33.7	50	–
1 month and 27 days	58/4.0	–	1.0*3.0	1.5	31.25	75	–
3 months and 2 days	59/5.0	–	1.5*3.0	2	27.27	100	–
5 months and 12 days	65/7.0	–	2.0*3.0	2	21.74	75	–
7 months and 27 days	65/7.5	–	2.0*3.0	2	20.69	75	–
11 months and 3 days	67/8.0	–	2.0*3.0	2	15.79	75	–
1 year and 1 month	70/8.5	–	2.0*3.5	2	15.09	75	–
1 year and 4 months	70/8.5	–	2.0*3.5	2	12.58	60	–
1 year and 8 months	78/10	–	2.0*4.0	2	10.18	50	1.4
1 year and 11 months	80.5/11.5	96/56	3.5*4.0	2	12.12	50	–
2 years and 4 months	88/13	100/50	3.5*4.0	2	9.01	50	3.2
2 years and 11 months	91/13.5	98/53	4.0*4.5	2	8.73	50	–
3 years and 6 months	93/15	100/60	4.0*4.5	2	9.28	33.3	5.3
4 years	97/15	101/53	4.0*4.5	2	9.6	50	5.8
4 years and 7 months	101/17	129/96	4.0*4.5	2	8.63	40	–
4 years and 11 months	103.3/17	107/62	4.0*4.5	2	11.99	40	–
5 years and 2 months	104.5/18	105/65	4.0*4.5	2	11.41	40	6.5
5 years and 8 months	110.5/20	110/68	4.0*4.5	2	12.5	40	7.2

Table 7. Physical examination and medication results of Case 2 during follow-up

Age	Height/weight [cm/kg]	Blood pressure [mm Hg]	Penis length* circumference [cm]	Testis [mL]	Hydrocortisone [mg/m^2/day]	Fluorocortisone [μg/day]	Bone age [years]
2 months and 27 days	61/6	–	1.2*3.0	2.5	9.68	66.67	–
3 months and 26 days	64/7	–	1.5*3.0	2.5	8.7	75	–
5 months and 27 days	68/8.7	–	2.0*3.5	2.5	7.42	60	–
9 months and 15 days	74/11	–	3.5*4.5	3	6.19	50	–
1 year and 4 months	83/13	–	4.0*4.5	3	5.41	50	–
1 year and 8 months	88/13	102/73	4.0*4.5	3	9.01	50	2.5
2 years and 3 months	94.5/14	100/73	4.0*4.5	3	8.47	33.3	–
2 years and 8 months	99.5/15	–	4.0*4.5	3	9.33	40	–

Table 8. Physical examination and medication results of Case 3 during follow-up

Age	Height [cm]	Blood pressure [mm Hg]	Penis length* circumference [cm]	Testis [mL]	Hydrocortisone [mg/m^2/day]	Fluorocortisone [μg/day]
5 months and 8 days	59.8	4.8	–	37.31	50	–
6 months and 18 days	65	6.3	94/46	23.41	60	–
7 months and 15 days	66	9.2	71/41	17.77	60	–
10 months and 29 days	72	9	90/65	14.46	50	0.8
1 year and 2 months	72.3	9.2	72/42	14.22	50	–
1 year and 6 months	78	9.5	86/64	13.87	50	–
2 years and 4 months	83	11	86/55	12.37	50	1.7
2 years and 7 months	86	12	90/60	14.42	50	–
3 years and 2 months	88	14	90/62	10.17	50	–
3 years and 7 months	94.5	15	90/62	8.8	33.3	–
4 years and 1 month		15	140/106	9.6	33.3	3.9
4 years and 6 months	102.5	16.5	101/55	8.86	33.3	–
5 years		17.5	106/48	8.42	33.3	5.2
5 years and 7 months	109	19	104/54	9.8	16.7	–
6 years and 1 month	113.5	20	93/60	9.38	16.7	6.6
6 years and 5 months		21	–	13.96	16.7	–
6 years and 8 months	116	21.5	101/61	11.73	50	–
6 years and 8 months	117	23	96/55	14.73	33.3	6.8
7 years and 5 months	118.9	25	116/73	11.96	16.7	–
8 years	122.5	27	109/54	11.16	16.7	6.8

Masculine insufficiency treatment for 2 cases

Case 1

Figure 2A shows the abnormal external genital manifestations of the child at the time of initial diagnosis. The child was given long-acting testosterone intramuscular injections at the age of 1 year and 9 months at a dose of 100 mg/m^2 once every 15 days, 4 times in total over 2 months. The penis size increased significantly at 1 year and 11 months (Fig. 2B); namely, the length was about 3.5 cm and the circumference was 4.0 cm. After topical application of dihydrotestosterone cream for 1 month, the drug was discontinued for 3 months. At the age of 2 years and 3 months, the patient underwent hypospadias repair at the local hospital. The postoperative penis (Fig. 2C,D) was about 4.0 cm long and 4.5 cm in circumference.

Case 2

Figure 3A shows the external genital performance of the child at the time of initial diagnosis. At the age of 3 months, intramuscular injection of gonadotropin (1500 U) was administered once every 2 weeks for a total of 6 times over 3 months. The penis of the child was slightly enlarged (Fig. 3B) – about 2.0 cm long and 3.5 cm in circumference. At 6 months of age, long-acting testosterone began to be injected (intramuscularly) in a dose

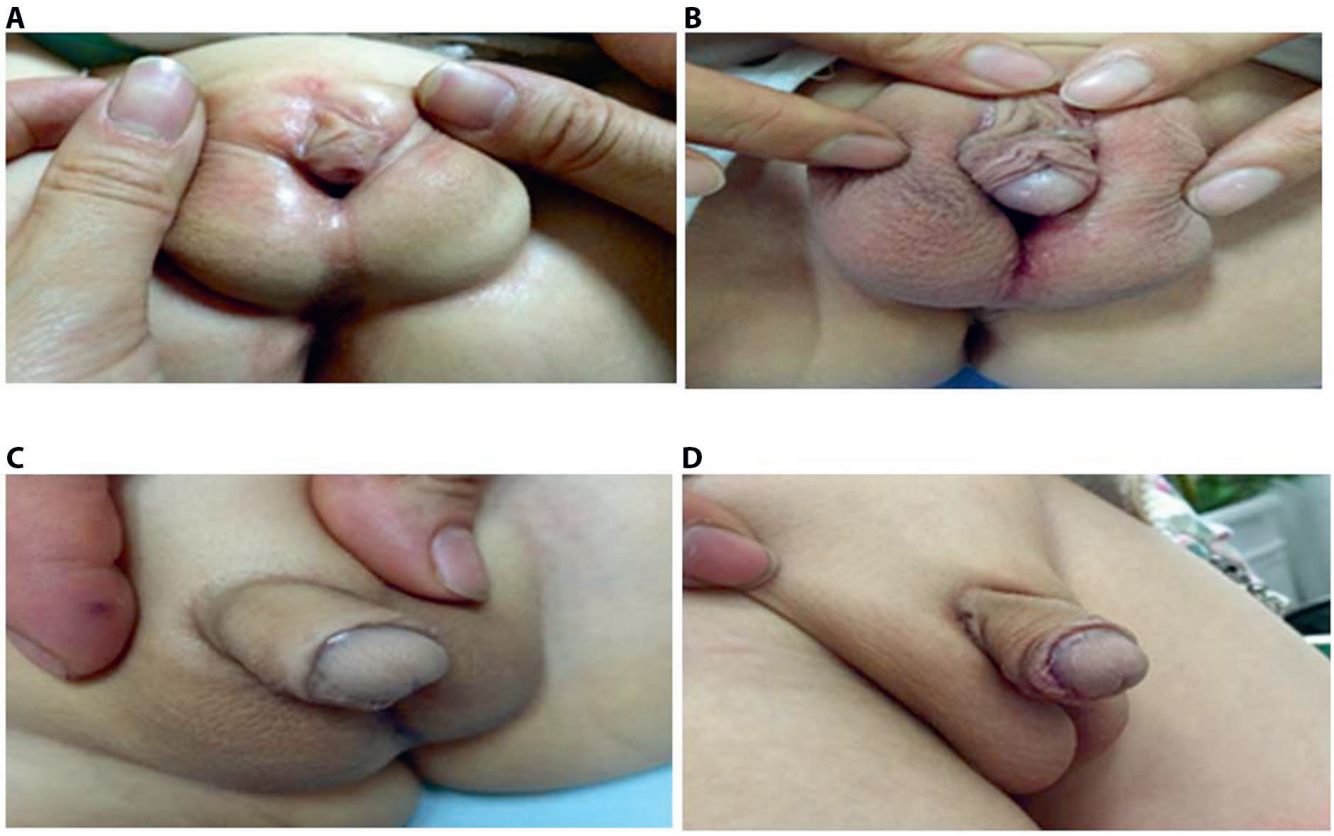

Fig. 2. External genitalia size of intramuscular long-acting testosterone (A), intramuscular long-acting testosterone 2 months later (B), 8 months after hypospadias repair (C) and 28 months after hypospadias repair (D) for Case 1

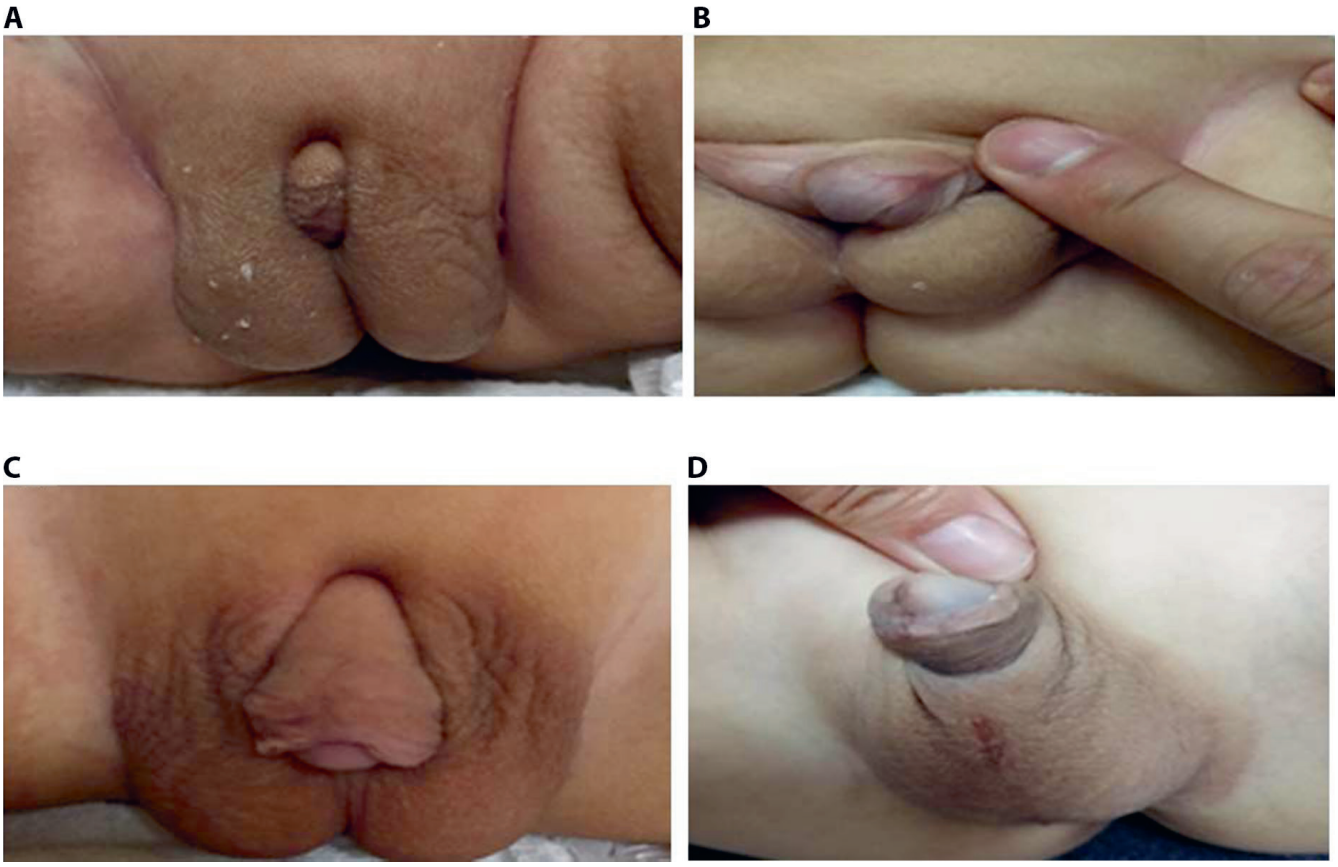

Fig. 3. External genitalia size of HCG and long-acting testosterone (A), intramuscular injection of HCG 6 times (B), intramuscular long-acting testosterone 3 months later (C) and 4 months after hypospadias repair (D) for Case 2

of 100 mg/m^2 once every 2 weeks. The course of treatment was 3 months and the size of the penis increased significantly (Fig. 3C) to a length of about 3.5 cm and circumference of 4.5 cm. At the age of 2 years and 10 months, the patient underwent hypospadias repair at the local hospital. After 4 months, the penis (Fig. 3D) was about 4.0 cm long and 4.5 cm in circumference.

Case 3

Female child had mild masculinization of the external genitalia (slightly hypertrophied clitoris). However, the pigmentation of the vulva was not aggravated and the clitoris size did not increase progressively. No surgical correction was needed.

Discussion

3β-HSD deficiency is mainly caused by mutations in the *HSD3B2* gene that cause adrenocortical hormone and sex hormone synthesis disorders.[11] Levels of pre-steroidal steroids, such as pregnenolone, 17-hydroxypregnenolone, dehydroepiandrosterone, and androstenediol, were observed to be increased, while progesterone, 17-OHP, androstenedione, testosterone, and other downstream products were decreased, resulting in adrenal insufficiency and external genital abnormalities as clinical manifestations. In this paper, we reported 3 3β-HSD deficiency cases, including 2 male children and 1 female child, with the age of onset in infancy, who suffered from loss of salts caused by decreased aldosterone synthesis with clinical consequences – namely, spitting milk, diarrhea, slow weight gain, and high potassium and low sodium levels. All cases had reduced cortisol levels, which is known to promote melanocytes to stimulate hormones that lead to increased melanin synthesis, causing pigmentation in skin folds, areola, vulva, and other parts of the body. All of the 3 children had abnormal genital function caused by sexual steroid synthesis disorder. Among them, 2 male patients showed serious insuffciency in masculine features and the female child showed mild masculinity with heavy salt loss. Usually, 3β-HSD deficiency can cause levels of 17-OHP and testosterone and other downstream products to decrease, but in all 3 children, we observed an elevation of 17-OHP and testosterone, which was mainly due to a lack of 3β-HSD2 and 3β-HSD1 expression; the latter is known to convert 17-hydroxypregnenol to 17-OHP in extra-adrenal tissue to cause an increase in its levels. An increase in testosterone may be due to the conversion of excess dehydroepiandrosterone to testosterone by 3β-HSD1 in the periphery, or further conversion of dehydroepiandrosterone to testosterone by elevated 17-OHP level under the action of an enzyme such as 17,20 carbon lyase. All 3 children suffered from severe salt loss in early infanthood, as shown with laboratory tests. Dehydroepiandrosterone increased in Case 1 and Case 3 at diagnosis. On the basis of the observed clinical manifestations and laboratory results, it can be established that the 3 children had the classic manifestations of 3β-HSD deficiency.

The results of *HSD3B2* gene sequencing in the 3 children are shown in Table 5. All of the children had compound heterozygous mutations and the mutation types were different, including 1 nonsense mutation, 1 frameshift mutation and 3 missense changes. The frameshift mutation was located at exon 3 while the remaining mutations were located at exon 4. After reviewing the OMIM (Online Mendelian Inheritance in Man; www.omim.org), ClinVar (https://www.ncbi.nlm.nih.gov/clinvar/) and NCBI (National Center for Biotechnology Information; www.ncbi.nlm.nih.gov) databases, it was found that the mutation sites c.1003C>T, c.424G>A and c.776C>T have been reported in the literature,[6,12,13] while c.154_162delinsTCCTGTT and c.674T>A are novel. According to a previous study, the c.424G>A and c.776C>T mutations result in undetectable enzyme activity in vitro, whereas the c.1003C>T mutation yielded an activity level of only 2% in vitro.[7] It has been demonstrated that more than 2% of residual enzyme activity may offer sufficient mineralocorticoid production to avoid severe salt loss.[8] Therefore, the genetic results of the 3 children explain the clinical manifestations as a classical type of 3β-HSD deficiency. Thus, there was a strong genotype–phenotype correlation in the 3 patients.

The gene sequencing results presented in Table 5 showed that the healthy father and healthy mother of Case 2 and Case 3 were carriers of these mutations of the *HSD3B2* gene. In addition, *HSD3B2* gene sequencing resulted in the identification of 2 compound heterozygous mutations consistent with an autosomal recessive form of 3β-HSD deficiency. Interestingly, the mutation was not detected in the father of Case 1 and was a de novo change. The c.154_162delinsTCCTGTT/p.Arg52Serfs*10 was a frameshift mutation that was predicted to end in an early termination of the peptide chain. Thus, this change is considered to be associated with a pathogenic variant. In Case 2, sequencing results suggested that there were 2 compound heterozygous mutations, c.424G>A (p.E142K) and c.674T>A (p.V225D). Segregation demonstrated that the 2 mutations were derived from each of the healthy parents, thus supporting an autosomal recessive mode of inheritance and providing more evidence for the pathogenicity of these 2 changes.

The standard treatment for 3β-HSD deficiency is hormone replacement therapy. The commonly used drugs in children are hydrocortisone and fludrocortisone. Garagorri et al.[14] showed that cortisol increased linearly with age beginning at 6 months of age, and that the concentration of basal cortisol in children did not change dramatically.[15] There were both similarities and differences in hydrocortisone treatment options for the 3 cases in this study. The similarities were that the dose of hydrocortisone in infancy decreased with age and was maintained

at 8–10 mg/m^2/day in early childhood, increased slightly before and after school age, and was maintained at about 10–12 mg/m^2/day thereafter. The differences included the initial doses in Case 1 and 3 being significantly higher than those in Case 2. Case 3 had significantly higher doses of hydrocortisone in infancy compared to Case 1, mainly due to the late treatment of Case 3.[16] The physiological secretion of endogenous cortisol in children is 6–8 mg/m^2/day, and pre-child cortisol levels fluctuate less. The dose of hydrocortisone in early childhood is maintained at slightly higher concentrations than physiological levels. A slight increase in levels before and after school age may be related to learning and environmental changes.

We gained important insight into disease treatment from the 3 cases studied here. Treatment is somewhat similar to the treatment for 21-hydroxylation deficiency. However, compared with 21-hydroxylation deficiency treatment, the hydrocortisone dosage for the 3 cases in our study was limited and androgen elevation was easier to control. It should be noted, though, that the patients could be prone to overtreatment. The dose of fludrocortisone is gradually decreased with age, and the maximum dosage should not exceed 100 μg/day. The dose should be adjusted according to blood pressure and electrolyte and renin activity during treatment to maintain plasma renin activity in the normal to medium range.[17]

Masculinization treatment is mainly aimed at treating male patients with a small penis and with hypospadias and other incomplete masculinization.[18] Genital abnormalities in 3β-HSD deficiency are caused by 3β-HSD2 activity being the highest during the critical period of external genital development before the 12th week of gestation during the fetal period.[19] Therefore, male children can be affected by impaired testosterone biosynthesis in the early fetal stage due to a lack of 3β-HSD2 in the testis, causing androgen deficiency leading to genital abnormalities, small penis, hypospadias, and severe external genitalia underdevelopment.[20] 3β-HSD1 activity is higher than 3β-HSD2, which is most active in the 3rd trimester of pregnancy, after genital development.[21] Although 3β-HSD1 mediates the conversion of excess dehydroepiandrosterone to testosterone, for a man with a 46 XY karyotype and 3β-HSD2 deficiency, androgen levels are not sufficient for the normal development of genitalia. For female children, the lack of testosterone in early pregnancy can degrade the Wolffian catheter, while the Müllerian catheter can develop into the fallopian tubes and uterus,[21] and 3β-HSD1 mediates the conversion of dehydroepiandrosterone to testosterone in the 3rd trimester. Elevated androgen levels can cause affected women to be mildly masculinized (with different degrees of clitoral enlargement, with or without labial fusion).[22] Treatment of hypospadias after the penis is enlarged is usually recommended for hypospadias from 6 months to 2 years of age, which is in the mini-puberty range. We reported Cases 1 and 2 at 1 year and 9 months and 6 months of age, respectively, treated with long-acting testosterone to increase penis size. Case 1 was treated with a combination of topical testosterone cream and penile lengthening, both of which resulted in satisfactory penis growth and excellent recovery after hypospadias repair. During follow-up for growth and development, 2 patients who were treated with long-acting testosterone had bone age consistent with their age, which indicates the safety of short-term testosterone therapy in patients younger than 2 years. The masculinization of Case 3 was mild, and there was no progress in masculinization with age, so no surgical intervention was needed.

Conclusions

This study reported on 3 children with classic 3β-HSD deficiency. All infants had typical adrenal insufficiency and abnormal genital manifestations, along with abnormal steroid hormone levels and with compound mutations in *HSD3B2*. Specifically, the mutations were diverse and located in exons 3 and 4, with a strong genotype–phenotype correlation. The c.154_162delinsTCCTGTT and c.674T>A (p.V225D) mutations were novel changes and were classified as pathogenic. The treatment of the disease was mainly corticosteroid replacement, after which adrenal function was observed to normalize. For male children with hypospadias and small penis, in order to obtain the best surgical effect of hypospadias repair, testosterone use was recommended instead of interventions to increase penis size at adolescence. In addition, the 3 probands reported in this study did not enter puberty and are still being followed to evaluate hormone levels and puberty development performance.

ORCID iDs

Lanni Chen https://orcid.org/ 0000-0003-3953-0941
Haihua Huang https://orcid.org/ 0000-0002-4555-8214
Huijiao Zhang https://orcid.org/ 0000-0001-9617-7721
Gaohui Zhu https://orcid.org/ 0000-0002-8811-6619
Min Zhu https://orcid.org/ 0000-0002-7794-1779

References

1. Gomez-Sanchez CE, Lewis M, Nanba K, Rainey WE, Kuppusamy M, Gomez-Sanchez EP. Development of monoclonal antibodies against the human 3β-hydroxysteroid dehydrogenase/isomerase isozymes. *Steroids*. 2017;127:56–61. doi:10.1016/j.steroids.2017.08.011
2. Pham JH, Will CM, Mack VL, et al. Structure–function relationships for the selective inhibition of human 3β-hydroxysteroid dehydrogenase type 1 by a novel androgen analog. *J Steroid Biochem Mol Biol*. 2017;174:257–264. doi:10.1016/j.jsbmb.2017.10.004
3. Thomas JL, Bose HS. Regulation of human 3-beta-hydroxysteroid dehydrogenase type-2 (3βHSD2) by molecular chaperones and the mitochondrial environment affects steroidogenesis. *J Steroid Biochem Mol Biol*. 2015;151:74–84. doi:10.1016/j.jsbmb.2014.11.018
4. Jeandron DD, Sahakitrungruang T. A novel homozygous Q334X mutation in the *HSD3B2* gene causing classic 3β-hydroxysteroid dehydrogenase deficiency: An unexpected diagnosis after a positive newborn screen for 21-hydroxylase deficiency. *Horm Res Paediatr*. 2012;77(5):334–338. doi:10.1159/000336004
5. Donadille B, Houang M, Netchine I, Siffroi JP, Christin-Maitre S. Human 3beta-hydroxysteroid dehydrogenase deficiency associated with normal spermatic numeration despite a severe enzyme deficit. *Endocr Connect*. 2018;7(3):395–402. doi:10.1530/EC-17-0306

6. Maik W, Nele W, Gunter SS, et al. Carboxyl-terminal mutations in 3beta-hydroxysteroid dehydrogenase type II cause severe salt-wasting congenital adrenal hyperplasia. *J Clin Endocrinol Metab.* 2008; 93(4):1418–1425. doi:10.1210/jc.2007-1874
7. Baquedano MS, Guercio G, Costanzo M, Marino R, Rivarola MA, Belgorosky A. Mutation of *HSD3B2* gene and fate of dehydroepiandrosterone. *Vitam Horm.* 2018;108:75–123. doi:10.1016/bs.vh.2018.05.002
8. Fujieda K, Nakae J, Mukai T. 3β-hydroxysteroid dehydrogenase deficiency, classical. *Genet Steroid Dis.* 2014:99–110.
9. Simard J, Ricketts MS, Soucy P, Feltus FA, Melner MH. Molecular biology of the 3beta-hydroxysteroid dehydrogenase/delta5-delta4 isomerase gene family. *Endocrine Rev.* 2005;26(4):525–582. doi:10.1210/er.2002-0050
10. Rabbani B, Mahdieh N, Ashtiani MTH, Setoodeh A, Rabbani A. In silico structural, functional and pathogenicity evaluation of a novel mutation: An overview of *HSD3B2* gene mutations. *Gene.* 2012;503(2):215–221. doi:10.1016/j.gene.2012.04.080
11. Podgórski R, Aebisher D, Stompor M, Podgórska D, Mazur A. Congenital adrenal hyperplasia: Clinical symptoms and diagnostic methods. *Acta Biochim Pol.* 2018;65(1):25–33. doi:10.18388/abp.2017_2343
12. Simard J, Rhéaume E, Sanchez R, et al. Molecular basis of congenital adrenal hyperplasia due to 3 beta-hydroxysteroid dehydrogenase deficiency. *Mol Endocrinol.* 1993;7(5):716–728. doi:10.1210/mend.7.5.8316254
13. Moisan AM, Ricketts ML, Tardy V, et al. New insight into the molecular basis of 3beta-hydroxysteroid dehydrogenase deficiency: Identification of eight mutations in the *HSD3B2* gene eleven patients from seven new families and comparison of the functional properties of twenty-five mutant enzymes. *J Clin Endocrinol Metabol.* 1999; 84(12):4410–4425. doi:10.1210/jcem.84.12.6288
14. Garagorri JM, Rodríguez G, Lario-Elboj AJ, Olivares JL, Lario-Muñoz A, Orden I. Reference levels for 17-hydroxyprogesterone, 11-desoxycortisol, cortisol, testosterone, dehydroepiandrosterone sulfate and androstenedione in infants from birth to six months of age. *Eur J Pediatr.* 2008;167(6):647–653. doi:10.1007/s00431-007-0565-1
15. Bailey D, Colantonio D, Kyriakopoulou L, et al. Marked biological variance in endocrine and biochemical markers in childhood: Establishment of pediatric reference intervals using healthy community children from the CALIPER cohort. *Clin Chem.* 2013;59(9):1393–1405. doi:10.1373/clinchem.2013.204222
16. Hahn-Holbrook J, Le TB, Chung A, Davis EP, Glynn LM. Cortisol in human milk predicts child BMI. *Obesity.* 2016;24(12):2471. doi:10.1002/oby.21682
17. Bornstein SR, Allolio B, Arlt W, et al. Diagnosis and treatment of primary adrenal insufficiency: An Endocrine Society clinical practice guideline. *J Clin Endocrinol Metab.* 2016;101(2):364–389. doi:10.1210/jc.2015-1710
18. Agarwal CA, Scheefer MF, Wright LN, Walzer NK, Rivera A. Quality of life improvement after chest wall masculinization in female-to-male transgender patients: A prospective study using the BREAST-Q and body uneasiness test. *J Plast Reconstr Aesthet Surg.* 2018;71(5):651–657. doi:10.1016/j.bjps.2018.01.003
19. Levy-Shraga Y, Pinhas-Hamiel O. High 17-hydroxyprogesterone level in newborn screening test for congenital adrenal hyperplasia. *BMJ Case Reports.* 2016;2016(41):bcr2015213939. doi:10.1136/bcr-2015-213939
20. Johannsen TH, Delphine M, Harriet DP, et al. Delayed diagnosis of congenital adrenal hyperplasia with salt wasting due to type II 3beta-hydroxysteroid dehydrogenase deficiency. *J Clin Endocrinol Metab.* 2005;90(4):2076–2080. doi:10.1210/jc.2004-1374
21. Park SY, Larry J. Minireview: Transcriptional regulation of gonadal development and differentiation. *Endocrinology.* 2005;146(3):1035–1042. doi:10.1210/en.2004-1454
22. Chantal L, Weihua W, Mason JI, et al. Newly proposed hormonal criteria via genotypic proof for type II 3beta-hydroxysteroid dehydrogenase deficiency. *J Clin Endocrinol Metab.* 2002;87(6):2611–2622. doi:10.1210/jcem.87.6.8615

Immunoexpression of RANK, RANKL and OPG in sporadic odontogenic keratocysts and their potential association with recurrence

Konrad Kisielowski[1,A–D,F], Bogna Drozdzowska[2,A,C,E,F], Rafał Koszowski[3,A–C,E,F], Magdalena Rynkiewicz[2,B,C,E], Mariusz Szuta[1,C–F], Mansur Rahnama[4,C,E,F], Karolina Babiuch[5,C,E], Michał Tyrakowski[1,C,E], Anna Bednarczyk[1,C,E], Tomasz Kaczmarzyk[1,A–D,F]

[1] Department of Oral Surgery, Jagiellonian University Medical College, Kraków, Poland
[2] Department of Pathomorphology, Faculty of Medical Sciences in Zabrze, Medical University of Silesia, Poland
[3] Academic Centre of Dentistry and Specialized Medicine in Bytom, Poland
[4] Department of Oral Surgery, Medical University of Lublin, Poland
[5] Chair of Periodontics and Oral Medicine, Jagiellonian University Medical College, Kraków, Poland

A – research concept and design; B – collection and/or assembly of data; C – data analysis and interpretation; D – writing the article; E – critical revision of the article; F – final approval of the article

Advances in Clinical and Experimental Medicine, ISSN 1899–5276 (print), ISSN 2451–2680 (online) *Adv Clin Exp Med*. 2021;30(3):301–307

Address for correspondence
Mariusz Szuta
E-mail: mariusz.szuta@uj.edu.pl

Funding sources
The study was supported by a grant from the Medical University of Silesia, Poland.

Conflict of interest
None declared

Received on October 22, 2020
Reviewed on November 17, 2020
Accepted on November 26, 2020

Published online on March 25, 2021

Abstract

Background. Odontogenic keratocysts (OKCs) are clinically aggressive lesions with relatively high recurrence rates. Dysregulation of functional equilibrium in the RANK/RANKL/OPG system is responsible for osteolysis associated with the development of OKCs. Previously published findings imply that immunoexpression of these 3 proteins may correlate with bone resorption activity in OKCs.

Objectives. The rationale behind this study was to assess the potential for receptor activator of nuclear factor kappa-B (RANK), receptor activator of nuclear factor kappa-B ligand (RANKL) and osteoprotegerin (OPG) expression, as well as RANKL/OPG expression ratio, to serve as prognostic indicators for OKC recurrence.

Materials and methods. We investigated the immunoexpression patterns of RANK, RANKL and OPG, and their correlation with recurrence rates, in 41 patients with OKCs treated with enucleation.

Results. We found no statistically significant differences between recurrent and non-recurrent cysts in terms of either: epithelial ($p = 0.404$) and stromal ($p = 0.469$) immunoreactivity of RANK; epithelial ($p = 0.649$) and stromal ($p = 0.198$) immunoreactivity of RANKL; or epithelial ($p = 1$) and stromal ($p = 0.604$) immunoreactivity of OPG. We also did not find significant differences in the distribution of cases with respect to ratios of RANKL/OPG immunostaining scores between recurrent and non-recurrent OKCs, both in the epithelium and in the connective tissue ($p = 1$ and $p = 0.237$, respectively).

Conclusions. Our results suggest that immunoexpression levels of RANK, RANKL and OPG at the time of pathological diagnosis, as well as the RANKL/OPG ratio, are not useful as prognostic markers for OKC recurrence.

Key words: OPG, RANK, RANKL, odontogenic keratocyst, keratocystic odontogenic tumor

Cite as
Kisielowski K, Drozdzowska B, Koszowski R, et al. Immunoexpression of RANK, RANKL and OPG in sporadic odontogenic keratocysts and their potential association with recurrence. *Adv Clin Exp Med*. 2021;30(3):301–307. doi:10.17219/acem/130907

DOI
10.17219/acem/130907

Background

Several histopathologically benign odontogenic tumors, including keratocystic odontogenic tumor (KCOT), ameloblastoma (AM), ameloblastic fibroma (AF), and odontogenic myxoma (OM), exhibit clinically aggressive progression with a tendency towards infiltrative growth. Recently, the World Health Organization (WHO) reclassified KCOT from the tumor category into the cyst category as odontogenic keratocyst (OKC).[1] However, published reports stress the significance of its aggressive growth and relatively high recurrence rate (approx. 25%).[2,3] Many attempts have been made to elucidate the biological mechanisms of OKC onset and development, and investigators have also evaluated various molecular markers as indicators of the potential for OKC to relapse. It has been suggested that expression of epithelial cell proliferation and apoptosis markers might be correlated with propensity for OKC recurrence, but these results are ambiguous. In our recent report, we demonstrated that expression levels of COX-2 (cyclooxygenase-2), BCL-2 (B-cell lymphoma 2), PCNA (proliferating cell nuclear antigen), and tumor protein p53 are not associated with OKC recurrence.[4] Thus, it is essential to continue to investigate other molecular factors in the search for prognostic candidates.

One key event responsible for the aggressiveness and progression of intraosseous lesions is bone resorption, which mainly depends on the formation and activation of osteoclasts.[5] Under physiological conditions, there is a delicate balance between the activities of osteoblasts and osteoclasts, through which the bone tissue is subjected to continuous remodeling.[6–8] Two members of the tumor necrosis factor (TNF) receptor superfamily, RANK (receptor activator of nuclear factor kappa-B) and RANKL (receptor activator of nuclear factor kappa-B ligand), are critical regulators of the bone remodeling process.[7,9,10] In vitro, the RANK/RANKL signaling pathway, together with macrophage colony-stimulation factor, promotes osteoclast differentiation from blood-born hemopoietic precursors, whereas the addition of the soluble receptor osteoprotegerin (OPG) into these culture systems prevents osteoclastogenesis.[11] Osteoprotegerin binds directly to RANKL and interrupts the activation of osteoclasts.[12] Hence, the balance between OPG and RANKL regulates bone resorption and formation.[3,8] The upregulation of RANKL and the downregulation of OPG are involved in various bone-associated diseases, including osteoporosis,[13] rheumatoid arthritis[14] and bone heredopathia.[15] This expression pattern also has a role in various bone tumors, including primary malignancies, such as multiple myeloma[16] and osteosarcoma,[17] as well as soft tissue malignant tumors with secondary bone invasion by metastasis[7] or direct infiltration.[11]

Several studies have demonstrated expression of RANK, RANKL and OPG in the epithelium and stroma of some odontogenic cysts and tumors, including OKC,[5,12] AM,[5,12,18] AF,[19] OM,[19] radicular cyst (RC),[5,20] and dentigerous cyst (DC).[5,12] In 2013, de Matos et al.[5] suggested that higher imumunodetection of RANKL and lower imumunodetection of OPG could indicate greater bone and tooth resorption activity in OKC and AM in comparison with RC and DC, which present indolent clinical behavior. Likewise, Tekkesin et al.[3] revealed a greater number of RANK-positive cells in the epithelial component of OKC and AM than in RC. This may indicate that greater bone/tooth resorption activity occurs in OKC and AM as compared to RC, which is consistent with the clinical presentation of these lesions. However, little is known about the prognostic value of RANK, RANKL and OPG expression (as measured with immunohistochemical staining) in aggressive odontogenic lesions. Therefore, the aim of this study was to investigate the potential for RANK, RANKL and OPG expression, as well as the balance between levels of RANKL and OPG, as prognostic markers in patients with OKC.

Materials and methods

Samples

Original hematoxylin-and-eosin (H&E)-stained slides and formalin-fixed, paraffin-embedded specimen blocks representing 41 cases of OKC were retrieved from the archives of the Chair of Pathomorphology at the Jagiellonian University Medical College, Kraków, Poland, and the Chair of Pathomorphology of the Medical University of Silesia, Zabrze, Poland. The OKCs had been surgically removed from 20 females and 21 males, with a mean age of 40.24 (±18.3) years at the time of surgery. All lesions were treated between 1997 and 2015 at the Department of Oral Surgery at the Jagiellonian University Medical College or at the Academic Center of Dentistry and Specialized Medicine in Bytom, Poland. In all cases, surgical enucleation of the lesion was conducted by careful removal of the cyst lining, followed by primary closure. No bone regeneration graft materials were applied. Surgical technique was standardized between surgeons performing enucleation. Subjects with nevoid basal cell carcinoma syndrome (NBCCS)-associated OKCs were not included in this analysis. The recurrence period was defined as the time between diagnosis of the primary lesion and the time of detection of any recurrent lesion in the same location that was subsequently histopathologically confirmed to meet the WHO (2017) microscopic criteria for OKC.

Immunohistochemistry

Formalin-fixed, paraffin-embedded archival blocks were sectioned and stained with H&E. Slides with 5-µm thick tissue sections were used to confirm a diagnosis of OKC using a light microscope.

For immunohistochemical analysis, paraffin-embedded, 3-µm thick tissue sections were placed on salinized slides.

Samples were deparaffinized with xylene, rehydrated in graded alcohol and washed in deionized water. Antigen retrieval was performed by heating slides in Heat-Induced Epitope Retrieval Buffer (Thermo Scientific, Fremont, USA), at pH 6 or pH 9, for 20 min at 95°C. Sections were then blocked by incubation with 3% H_2O_2 and protein block (Thermo Scientific), and then slides were incubated overnight in a humidified chamber at 4°C with one of the following antibodies:

– mouse monoclonal anti-RANK (ab13918; Abcam Inc., Cambridge, USA; diluted 1:200);
– rabbit polyclonal anti-RANKL (ab169966; Abcam; 1:400);
– rabbit polyclonal anti-OPG (ab183910; Abcam; 1:400).

After washing in Tris-buffered saline (TBS), sections were treated according to the manufacturer's instructions with the Primary Antibody Amplifier Quanto system, followed by the HRP Polymer Quanto system (both Thermo Scientific). Slides were stained using a 3-3'-diaminobenzidine (DAB) Quanto kit (Thermo Scientific). Finally, tissue sections were counterstained with hematoxylin, dehydrated, and covered with coverslips for further analysis. A case of central giant cell granuloma was used as the positive control for expression of RANK, RANKL and OPG. For the negative control, sections were treated as above, but without primary antibody exposure. Cellular staining patterns for RANK, RANKL and OPG in the epithelium and stroma of OKC were cytoplasmic.

Semiquantitative assessment was conducted using a four-point scoring system:

– grade 0 (no reaction): 0% of cells stained;
– grade 1 (weak reaction): 1–25% of cells stained;
– grade 2 (moderate reaction): 26–50% of cells stained;
– grade 3 (strong reaction): >50% of cells stained.

All histopathological and immunohistochemical evaluations were made by board-certified specialists in pathomorphology.

Results were reported either as mean (± standard deviation (SD)), or as number of cases plus percentages, as appropriate. Differences in immunohistochemical data between recurrent and non-recurrent OKCs were analyzed using Fisher's exact test. The Cox proportional hazard model for time-dependent variables was implemented to evaluate hazard ratio, and 95% confidence intervals (95% CI) were used as estimates of hazard risk for a recurrence potential. Probability values (p-values) less than 0.05 were considered significant. All analyses were performed using R statistical software (the R Project for Statistical Computing; http://www.R-project.org/).

Results

The number of cases included in the analysis totaled 41. The mean time until follow-up was 8.49 (±4.34) years. Recurrences were ascertained in 12 (29.27%) cases. The mean recurrence period was 3.92 (±2.61) years.

Positive immunohistochemical staining for RANK was identified in 15 (36.58%) cases in epithelium, and in 28 (68.29%) cases in stroma. In all but 1 positive case, only a weak reaction was observed. We did not find a single OKC case exhibiting a strong response for RANK within both epithelial and stromal components. There were no statistically significant differences between recurrent and non-recurrent cysts in terms of epithelial ($p = 0.404$) or stromal immunoreactivity to RANK ($p = 0.469$) (Table 1). Representative immunohistochemical images are shown in Fig. 1 and 2.

With respect to RANKL, all cases of OKCs were positive for expression within the epithelium, and all but 1 case also showed expression in the cystic connective tissue (Table 1). Epithelial samples exhibited moderate-to-strong reactions in 85.36% of cases, whereas stromal reactions were mostly weak (51.2% of cases) (Fig. 3). There were no statistically significant differences between recurrent and non-recurrent cysts in terms of epithelial ($p = 0.649$) or stromal immunoreactivity to RANKL ($p = 0.198$) (Table 1).

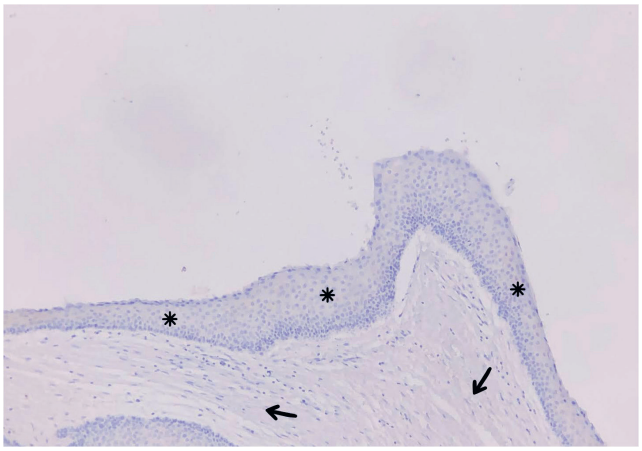

Fig. 1. Immunohistochemical reaction for RANK: no cytoplasmic staining in epithelium (* no reaction) or in stroma (–> no reaction) (×100 magnification)

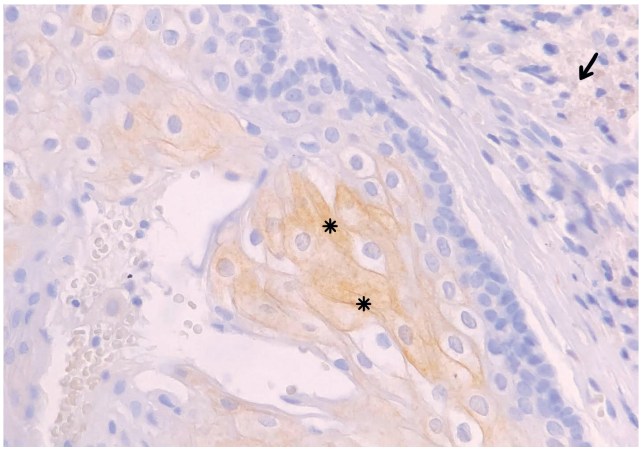

Fig. 2. Immunohistochemical reaction for RANK: cytoplasmic brown staining in epithelium (* weak reaction) and no staining in stroma (–> no reaction) (×200 magnification)

Table 1. Histopathological characteristics of cases, with hazard risks for recurrence of OKCs

Immuno-localization	Immunostain		Recurrent cysts (n = 12)		Non-recurrent cysts (n = 29)		p-value (Fisher's exact test)	Cox proportional hazard model	
	protein	type of reaction	n	%	n	%		HR (95% CI)	p-value
Epithelium	RANK	none	7	58.33%	19	65.52%	0.404	1.00	
		weak	4	33.33%	10	34.48%		0.917 [0.268–3.139]	0.891
		moderate	1	8.33%	0	0.00%		4.040 [0.488–33.435]	0.195
		strong	0	0.00%	0	0.00%		NA	
	RANKL	none	0	0.00%	0	0.00%	0.649	NA	
		weak	1	8.33%	5	17.24%		1.00	
		moderate	4	33.33%	12	41.38%		1.671 [0.187–14.963]	0.646
		strong	7	58.33%	12	41.38%		2.515 [0.309–20.451]	0.388
	OPG	none	1	8.33%	2	6.90%	1	1.00	
		weak	8	66.67%	19	65.52%		0.944 [0.118–7.559]	0.957
		moderate	1	8.33%	4	13.79%		0.606 [0.038–9.722]	0.724
		strong	2	16.67%	4	13.79%		0.856 [0.077–9.492]	0.899
Stroma	RANK	none	5	41.67%	8	27.59%	0.469	1.00	
		weak	7	58.33%	21	72.41%		0.633 [0.201–1.996]	0.435
		moderate	0	0.00%	0	0.00%		NA	
		strong	0	0.00%	0	0.00%		NA	
	RANKL	none	0	0.00%	1	3.45%	0.198	NR	
		weak	7	58.33%	14	48.28%		0.449 [0.116–1.743]	0.247
		moderate	2	16.67%	12	41.38%		0.169 [0.028–1.022]	0.053
		strong	3	25.00%	2	6.90%		1.00	
	OPG	none	1	8.33%	2	6.90%	0.604	1.00	
		weak	5	41.67%	18	62.07%		0.613 [0.071–5.252]	0.655
		moderate	4	33.33%	7	24.14%		1.140 [0.127–10.226]	0.907
		strong	2	16.67%	2	6.90%		1.356 [0.123–14.981]	0.804

OKCs – odontogenic keratocysts; RANK – receptor activator of nuclear factor kappa-B; RANKL – receptor activator of nuclear factor kappa-B ligand; OPG – osteoprotegerin; NR – no recurrence; NA – not applicable; HR – hazard ratio; 95% CI – 95% confidence interval.

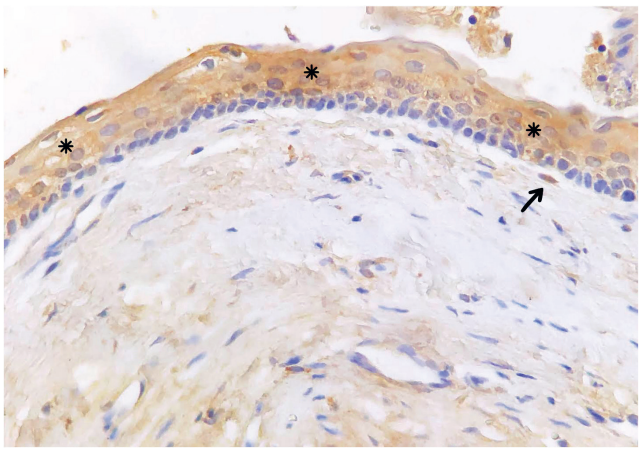

Fig. 3. Immunohistochemical reaction for RANKL: cytoplasmic brown staining in epithelium (* strong reaction) and in stroma (–> weak reaction) (×150 magnification)

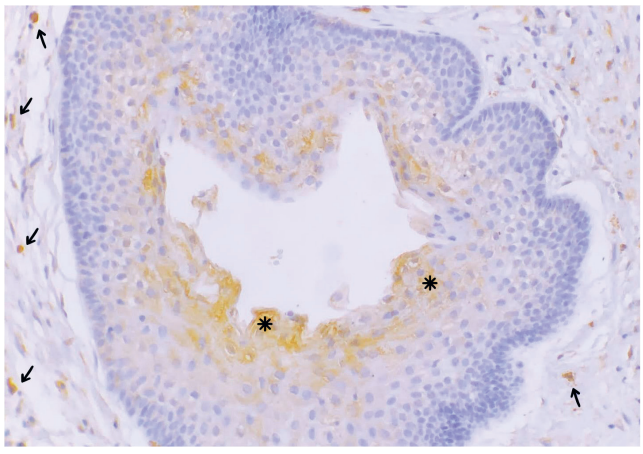

Fig. 4. Immunohistochemical reaction for OPG: cytoplasmic brown staining in epithelium (* weak reaction) and in stroma (–> moderate reaction) (×150 magnification)

Immunoreactivity to OPG was observed in 92.68% of OKCs both within the epithelium and within the stroma. Epithelial expression of OPG was mostly weak, as found in 27 cases (65.85%), as was stromal expression, which was weak in 23 cases (56.09%). There were no statistically significant differences between recurrent and non-recurrent

Table 2. RANKL/OPG ratio of immunostaining scores between recurrent and non-recurrent OKCs

Immuno-localization	RANKL/OPG ratio	Recurrent cysts (n = 12)	Non-recurrent cysts (n = 29)	Total (n = 41)	p-value (Fisher's exact test)	Cox proportional hazard model	
		n (%)	n (%)	n (%)		HR (95% CI)	p-value
Epithelium	RANKL > OPG	8 (66.67%)	19 (65.52%)	27 (65.86%)	1.00	1.00	
	RANKL = OPG	4 (33.33%)	8 (27.59%)	12 (29.27%)		0.997 [0.3–3.316]	0.997
	RANKL < OPG	0 (0.00%)	2 (6.90%)	2 (4.87%)		NR	
Stroma	RANKL > OPG	5 (41.67%)	10 (34.48%)	15 (36.59%)	0.237	1.00	
	RANKL = OPG	3 (25.00%)	15 (51.72%)	18 (43.90%)		0.435 [0.104–1.821]	0.254
	RANKL < OPG	4 (33.33%)	4 (13.79%)	8 (19.51%)		1.548 [0.415–5.772]	0.515

RANKL – receptor activator of nuclear factor kappa-B ligand; OPG – osteoprotegerin; NR – no recurrence; HR – hazard ratio; 95% CI – 95% confidence interval.

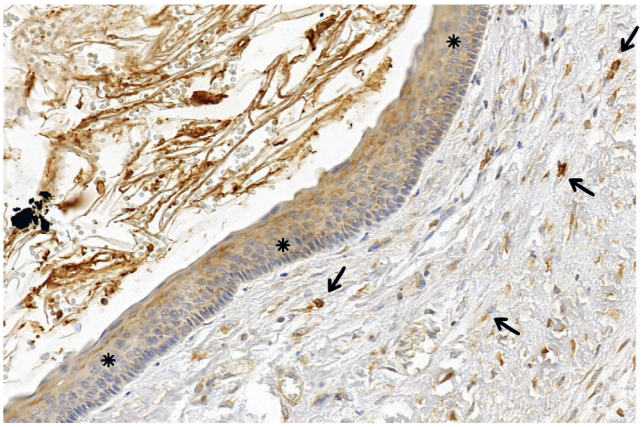

Fig. 5. Immunohistochemical reaction for OPG: cytoplasmic brown staining in epithelium (* moderate reaction) and in stroma (–> moderate reaction) (×150 magnification)

cysts in terms of epithelial (p = 1) or stromal immunoreactivity to OPG (p = 0.604) (Table 1). Representative immunohistochemical images are shown in Fig. 4 and 5.

We did not find any significant differences in the distribution of cases with respect to the ratio of RANKL/OPG immunostaining scores between recurrent and non-recurrent OKCs. This was true of both the epithelium and the connective tissue (p = 1 and p = 0.237, respectively) (Table 2). Within the epithelial subset, most cases (65.86%) demonstrated higher immunoreactivity to RANKL than OPG, whereas within the stromal component, most cases demonstrated uniform immunoreactivity to each marker (43.90%) (Table 2). We therefore did not identify any prognostic significance of the RANKL/OPG ratio in either cystic component (Table 2).

Discussion

Bone is a tissue that is continuously being rebuilt and remodeled.[7] Two types of cells are involved in this process: osteoblasts – bone building cells that deposit new bone tissue, and osteoclasts – bone-resorbing cells responsible for breaking tissue down. The RANK, RANKL and OPG proteins are critical for the control of osteoclastogenesis and pathophysiological bone remodeling. Osteoprotegerin is a decoy receptor for RANKL that blocks osteoclast formation by inhibiting RANKL from binding to RANK.[3,21]

The dysregulation of functional equilibrium in the RANK/RANKL/OPG system is responsible for osteolysis associated with the development of intraosseous odontogenic lesions, including AM, OKC, DC, and RC, to name but a few.[3,5,12] Various lesions exhibit different levels of aggressiveness and tendency towards infiltrative growth. Accordingly, we attempted to elucidate a relationship between level of clinical aggressiveness and modulated expression of RANK, RANKL and OPG in the epithelial and stromal components of lesions.

Most previous studies have compared the immunoexpression levels of these markers across various lesions exhibiting different levels of clinical aggressiveness. In particular, the results of disturbances in the RANK/RANKL/OPG triad were compared between AM, OKC, DC, and/or RC pathologies.[3,5,12] From a comparative point of view, AM represents a locally aggressive odontogenic neoplasm with a high tendency to infiltrative growth and recurrence, with OKC (previously also classified as neoplasm) representing a cystic lesion with a moderate potential for destructive growth and infiltrative growth, and both DC and RC as benign odontogenic cysts with relatively little tendency for local destruction. Tekkesin et al.[3] found a greater number of RANK-positive cells in OKCs than in AM or RC (in both epithelial and stromal lesion components) as well as a greater number of RANK-positive cells in AM than in RC (but only in epithelial tissue). The expression of RANKL was similar (strong) in both components of all 3 types of lesion. Moreover, all lesions showed very low expression of OPG.[3] The authors concluded that the variable most strongly determining osteoclastogenesis was RANK expression, since it was upregulated in lesions exhibiting aggressive behavior (AM and OKC) as compared with benign RC.[3]

Surprisingly, we did not find even 1 case of OKC exhibiting strong expression of RANK within either epithelial or stromal components. In fact, most cases presented with

a negative RANK-reaction in epithelial tissue, and merely weak reactions within stroma. The reasons for the discrepancy between our findings and those of Tekkesin et al.[3] are obscure. It is likely that the different antibodies and methods used for immunohistochemical analyses are a contributing factor. We also did not include syndromic cases, which may exhibit higher local aggressiveness,[22] in our investigation.

In this study, the majority of OKC cases exhibited positive immunoexpression of RANKL. Specifically, epithelial components showed moderate to strong reactions in as many as 85.4% cases. These findings are in line with those of de Matos et al.,[5] who revealed higher expression of RANKL in the epithelium of AM and OKC than in RC and DC, deducing that increased epithelial expression of RANKL would be related to elevated osteoclast activity, thus favoring bone resorption.[5] Moreover, in the present study, most cases exhibited merely weak immunohistoreactivity for OPG in both cystic components. The downregulation of OPG may also suggest elevated osteolytic activity, since lack of this molecule allows for interaction between RANK and RANKL, thereby promoting bone resorption. Accordingly, our findings suggest that it is strong expression of RANKL accompanied by weak expression of OPG that may facilitate the local aggressiveness of OKC.

Interestingly, elevated RANKL/OPG ratios were mostly found in the epithelial rather than the stromal components. This suggests that osteolytic activity of OKC may be related to the epithelium of the lesion rather than its capsule. Some previous studies hypothesized that the expansive potential of OKC is most likely explained by increased RANK and RANKL activity in the lesional connective tissue, as indicated by higher immunoreactivity levels. It was suggested that this might have indirectly indicated the presence in the lesion capsule of osteoclast precursors that are able to interact with the receptor, leading to osteoclast differentiation and maturation.[23,24] Our findings, however, do not corroborate this hypothesis, and are in line with results of the study by da Silva,[12] who also found that the stroma of OKCs contained a higher number of OPG-positive cells than RANKL-positive cells. Hence, it is likely that enhanced epithelial expression of RANKL and/or decreased levels of OPG play an important role in cyst-associated bone destruction (which was also suggested by da Silva[12]).

Limitations

To the best of our knowledge, the present study was the first to evaluate immunoexpression levels of RANK, RANKL and OPG in the epithelium and stroma of OKCs as potential prognostic markers for recurrence. We did not, however, demonstrate any significant association between cyst relapse and levels of these immunostains. Likewise, RANKL/OPG ratios in both histological components of OKC were not correlated with recurrence. Although RANK, RANKL and OPG are critical for osteoclastogenesis, and although levels of their immunoexpression may be associated with local aggressiveness of intraosseous lesions, our findings suggest that they would not serve as useful prognostic indicators of OKC relapse.

There are other markers of local OKC invasiveness involved in bone metabolism and cyst progression. Among them, podoplanin, osteopontin and its receptors CD44v6 and integrin α_v have recently generated much research interest[25]; however, their relevance in terms of OKC recurrence is still unknown. It is also possible that the immunoreactivity of the bone reabsorption regulators studied here (RANK/RANKL/OPG) should be measured along with that of proteins which participate in epithelial invasion into the cyst capsule and into adjacent structures (e.g., CD138).[26]

Conclusions

The results presented here suggest that immunoexpression levels of RANK, RANKL and OPG at the time of pathological diagnosis, as well as RANKL/OPG ratio, are not useful as prognostic indicators of OKC recurrence. The local aggressiveness of OKCs may be related to upregulation of RANKL and downregulation of OPG in the cystic epithelium. Further investigation is necessary to identify the precise molecular factors behind OKC relapse.

ORCID iDs

Konrad Kisielowski https://orcid.org/0000-0001-7894-0105
Bogna Drozdzowska https://orcid.org/0000-0002-2287-6842
Rafał Koszowski https://orcid.org/0000-0002-9533-549X
Magdalena Rynkiewicz https://orcid.org/0000-0001-8002-7366
Mariusz Szuta https://orcid.org/0000-0002-7182-4811
Mansur Rahnama https://orcid.org/0000-0002-5622-7330
Karolina Babiuch https://orcid.org/0000-0001-8899-9880
Michał Tyrakowski https://orcid.org/0000-0002-7669-9650
Anna Bednarczyk https://orcid.org/0000-0001-9891-0157
Tomasz Kaczmarzyk https://orcid.org/0000-0003-3024-9926

References

1. Wright JM, Vered M. Update from the 4th Edition of the World Health Organization Classification of Head and Neck tumours: Odontogenic and maxillofacial bone tumours. *Head Neck Pathol.* 2017;11(1):68–77. doi:10.1007/s12105-017-0794-1
2. Shear M, Speight PM. *Cysts of the Oral and Maxillofacial Regions*. 4th ed. Hoboken, NJ: Wiley-Blackwell; 2009:6–58.
3. Tekkesin MS, Mutlu S, Olgac V. The role of RANK/RANKL/OPG signaling pathways in osteoclastogenesis in odontogenic keratocysts, radicular cysts, and ameloblastomas. *Head Neck Pathol.* 2011;5(3): 248–253. doi:10.1007/s12105-011-0271-1
4. Kaczmarzyk T, Kisielowski K, Koszowski R, et al. Investigation of clinicopathological parameters and expression of COX-2, bcl-2, PCNA, and p53 in primary and recurrent odontogenic keratocysts. *Clin Oral Investig.* 2018;22(9):3097–3106. doi:10.1007/s00784-018-2400-7
5. de Matos FR, de Moraes M, das Neves Silva EB, Galvão HC, de Almeida Freitas R. Immunohistochemical detection of receptor activator nuclear κB ligand and osteoprotegerin in odontogenic cysts and tumors. *J Oral Maxillofac Surg.* 2013;71(11):1888–1892. doi:10.1016/j.joms.2013.05.023

6. Charles JF, Aliprantis AO. Osteoclasts: More than "bone eater". *Trends Mol Med*. 2014;20(8):449–459. doi:10.1016/j.molmed.2014.06.001
7. Sigl V, Jones LP, Penninger JM. RANKL/RANK: From bone loss to the prevention of breast cancer. *Open Biol*. 2016;6(11):160230. doi:10.1098/rsob.160230
8. Rahnama M, Jastrzebska-Jamrogiewicz I, Jamrogiewicz R, Nogalski A, Jagielak M. Influence of hormone replacement therapy on osteoprotegerin and receptor activator of nuclear factor kappa-B ligand concentrations in menopausal women. *J Interferon Cytokine Res*. 2013;33(9):485–492. doi:10.1089/jir.2012.0149
9. Dougall WC, Glaccum M, Charrier K, et al. RANK is essential for osteoclast and lymph node development. *Genes Dev*. 1999;13(18):2412–2424. doi:10.1101/gad.13.18.2412
10. Kong YY, Yoshida H, Sarosi I, et al. OPGL is a key regulator of osteoclastogenesis, lymphocyte development and lymph-node organogenesis. *Nature*. 1999;397(6717):315–323. doi:10.1038/16852
11. Jimi E, Shin M, Furuta H, Tada Y, Kusukawa J. The RANKL/RANK system as a therapeutic target for bone invasion by oral squamous cell carcinoma (review). *Int J Oncol*. 2013;42(3):803–809. doi:10.3892/ijo.2013.1794
12. da Silva TA, Batista AC, Mendonça EF, Leles CR, Fukada S, Cunha FQ. Comparative expression of RANK, RANKL, and OPG in keratocystic odontogenic tumors, ameloblastomas and dentigerous cysts. *Oral Surg Oral Med Oral Pathol Oral Radiol Endod*. 2008;105(3):333–341. doi:10.1016/j.tripleo.2007.06.009
13. Vega D, Maalouf NM, Sakhaee K. The role of receptor activator of nuclear factor-κB (RANK)/RANK ligand/osteoprotegerin: Clinical implications. *J Clin Endocrinol Metab*. 2007;92(12):4514–4521. doi:10.1210/jc.2007-0646
14. Pettit A, Walsh N, Manning C, Goldring S, Gravallese E. RANKL protein is expressed at the pannus–bone interface at sites of articular bone erosion in rheumatoid arthritis. *Rheumatol (Oxford)*. 2006;45(9):1068–1076. doi:10.1093/rheumatology/kel045
15. Sobacchi C, Frattini A, Guerrini MM, et al. Osteoclast-poor human osteopetrosis due to mutations in the gene encoding RANKL. *Nat Genet*. 2007;39(8):960–962. doi:10.1038/ng2076
16. Giuliani N, Colla S, Sala R, et al. Human myeloma cells stimulate the receptor activator of nuclear factor-κB ligand (RANKL) in T lymphocytes: A potential role in multiple myeloma bone disease. *Blood*. 2002;100(13):4615–4621. doi:10.1182/blood-2002-04-1121
17. Mori K, Le Goff B, Berreur M, et al. Human osteosarcoma cells express functional receptor activator of nuclear factor-kappa B. *J Pathol*. 2007;211(5):555–562. doi:10.1002/path.2140.
18. Kumamoto H, Ooya K. Expression of parathyroid hormone-related protein (PTHrP), osteoclast differentiation factor (ODF)/receptor activator of nuclear factor-kappaB ligand (RANKL) and osteoclastogenesis inhibitory factor (OCIF)/osteoprotegerin (OPG) in ameloblastomas. *J Oral Pathol Med*. 2004;33(1):46–52. doi:10.1111/j.1600-0714.2004.00204.x
19. Andrade FR, Sousa DP, Mendonça EF, da Silva TA, Lara VS, Batista AC. Expression of bone resorption regulators (RANK, RANKL, and OPG) in odontogenic tumors. *Oral Surg Oral Med Oral Pathol Oral Radiol Endod*. 2008;106(4):548–555. doi:10.1016/j.tripleo.2008.05.042
20. Menezes R, Bramante CM, da Silva Paiva KB, et al. Receptor activator NFkappaB-ligand and osteoprotegerin protein expression in human periapical cysts and granulomas. *Oral Surg Oral Med Oral Pathol Oral Radiol Endod*. 2006;102(3):404–409. doi:10.1016/j.tripleo.2005.10.054
21. Suda T, Takahashi N, Udagawa N, Jimi E, Gillespie MT, Martin TJ. Modulation of osteoclast differentiation and function by the new members of the tumor necrosis factor receptor and ligand families. *Endocr Rev*. 1999;20(3):345–357. doi:10.1210/edrv.20.3.0367
22. Kahraman D, Gunhan O, Celasun B. A series of 240 odontogenic keratocysts: Should we continue to use the terminology of "keratocystic odontogenic tumour" for the solid variant of odontogenic keratocyst? *J Craniomaxillofac Surg*. 2018;46(6):942–946. doi:10.1016/j.jcms.2018.04.007
23. de Moraes M, De Lucena HF, De Azevedo PR, Queiroz LM, Costa Ade L. Comparative immunohistochemical expression of RANK, RANKL and OPG in radicular and dentigerous cysts. *Arch Oral Biol*. 2011;56(11):1256–1263. doi:10.1016/j.archoralbio.2011.05.009
24. de Moraes M, de Matos FR, de Souza LB, de Almeida Freitas R, de Lisboa Lopes Costa A. Immunoexpression of RANK, RANKL, OPG, VEGF, and vWF in radicular and dentigerous cysts. *J Oral Pathol Med*. 2013;42(6):468–473. doi:10.1111/jop.12036
25. Kechik KA, Siar CH. Spatial distribution of osteopontin, CD44v6 and podoplanin in the lining epithelium of odontogenic keratocysts, and their biological relevance. *Ann Diagn Pathol*. 2018;32:17–22. doi:10.1016/j.anndiagpath.2017.08.002
26. Brito-Medoza L, Bologna-Molina R, Irigoyen-Camacho ME, Martinez G, Sanchez-Romero C, Mosqueda-Taylor A. A comparison of Ki67, Syndecan-1 (CD138), and molecular RANK, RANKL, and OPG triad expression in odontogenic keratocysts, unicystic ameloblastoma, and dentigerous cysts. *Dis Markers*. 2018;2018:7048531. doi:10.1155/2018/7048531

Intra-aneurysm sac pressure measurement using a thin pressure wire during endovascular aneurysm repair

Maciej Antkiewicz[1,A,C–F], Wiktor Kuliczkowski[2,A,C,E,F], Marcin Protasiewicz[2,A,C,E,F], Magdalena Kobielarz[3,C–F], Piotr Barć[1,B,E,F], Maciej Malinowski[1,B,E,F], Katarzyna Frączkowska[1,C,D,F], Katarzyna Kulikowska[1,B,E,F], Marcin Merenda[1,B,E,F], Krzysztof Jacyna[1,B,E,F], Tomasz Dawiskiba[1,A,E,F], Dariusz Janczak[1,A,C,E,F]

[1] Department and Clinic of Vascular, General and Transplantation Surgery, Wroclaw Medical University, Poland
[2] Department and Clinic of Cardiology, Wroclaw Medical University, Poland
[3] Department of Mechanics, Materials Science and Biomedical Engineering, Wrocław University of Science and Technology, Poland

A – research concept and design; B – collection and/or assembly of data; C – data analysis and interpretation; D – writing the article; E – critical revision of the article; F – final approval of the article

Advances in Clinical and Experimental Medicine, ISSN 1899–5276 (print), ISSN 2451–2680 (online) *Adv Clin Exp Med*. 2021;30(3):309–313

Address for correspondence
Marcin Protasiewicz
E-mail: mprot@poczta.onet.pl

Funding sources
Ministry of Health grants according to No. of SUB. C020.19.064 and STM.C021.20.036 from the IT Simple system of Wroclaw Medical University, Poland.

Conflict of interest
None declared

Received on December 10, 2020
Reviewed on December 31, 2020
Accepted on February 17, 2021

Published online on March 23, 2021

Abstract

Background. An endoleak is a typical complication of endovascular aneurysm repair (EVAR). It is characterized by persistent blood flow between a stent graft and the aneurysm sac. Usually, it can be visualized during primary EVAR, but in many cases, this remains impossible. Therefore, other methods of endoleak assessment are urgently needed. The measurement of aneurysm sac pressure (ASP) seems to be a promising direction of research in this area.

Objectives. We aimed to evaluate the safety and efficacy of a new method for invasive pressure measurement inside the abdominal aortic aneurysm (AAA) during EVAR. We also assessed a correlation between pressure values and early angiographic occurrence of an endoleak after the procedure.

Materials and methods. A total of 20 patients with AAA were included in this experimental prospective study. During EVAR, systolic, diastolic and mean pressure values were recorded both for ASP and aortic pressure (AP) before procedure, after stent graft opening and after final stent graft ballooning.

Results. The measurements were successfully obtained in all participants without any complications. There were no significant differences between all ASP and AP before procedure. After the procedure, blood pressure significantly decreased in the aneurysm sac but not in the aorta. Systolic ASP was significantly lower than systolic AP both after stent graft opening (80.4 ±20.9 mm Hg compared to 110.7 ±21.6 mm Hg, $p < 0.01$) and after its balloon post-dilatation (65.6 ±26.1 mm Hg compared to 107.4 ±22.1 mm Hg, $p < 0.001$). Diastolic ASP decreased significantly in comparison to diastolic AP only after stent graft ballooning (48.0 ±14.6 mm Hg compared to 56.4 ±13.6 mm Hg, $p < 0.05$).

Conclusions. Our study confirmed that the novel method for the measurement of ASP during EVAR, using a thin pressure wire, is feasible and safe.

Key words: endoleak, endovascular aneurysm repair, abdominal aortic aneurysm, aneurysm sac pressure

Cite as
Antkiewicz M, Kuliczkowski W, Protasiewicz M, et al. Intra-aneurysm sac pressure measurement using a thin pressure wire during endovascular aneurysm repair. *Adv Clin Exp Med*. 2021;30(3):309–313. doi:10.17219/acem/133425

DOI
10.17219/acem/133425

Background

One of the most serious conditions in current vascular surgery is abdominal aortic aneurysm (AAA), which is defined as an enlargement of the aortic diameter by at least 50%. The major complication of AAA is rupture, which is a life-threatening condition that requires emergency treatment. The risk of aneurysm rupture grows exponentially with an increase in aneurysm diameter. Therefore, aneurysms of 55 mm in diameter are an indication for surgical treatment, even if they are asymptomatic.

Currently, there are 2 methods of surgical treatment for AAA: a classic open surgery and endovascular aneurysm repair (EVAR). The latter is becoming increasingly popular and is gradually replacing classic open surgeries. Endovascular repair involves implantation of a stent graft, that is, endovascular prosthesis, using common femoral artery access. The stent graft, which is deployed in the aneurysm lumen, creates a new channel for blood flow and closes its way to the aneurysm sac, thereby protecting it from high pulsatile blood pressure. The advantages of this method include less extensive trauma, faster recovery and a lower risk of infection than with open aortic repair.

Despite its obvious benefits, EVAR is not without limitations. A typical complication of the procedure is the so-called endoleak, which involves the presence of blood flow between a stent graft and the aneurysm sac. It is estimated that endoleaks occur in 17–26% of patients after EVAR,[1–4] especially those who show aneurysm growth and rupture.[5]

Although endoleaks can typically be visualized during primary EVAR, in many cases, this remains impossible. Therefore, there is an urgent need to develop novel methods of endoleak assessment. The measurement of aneurysm sac pressure (ASP) seems to be a promising direction of research. We postulate that continuation of ASP and its systolic–diastolic amplitude after EVAR may suggest the presence of endoleak while the decrease of these parameters indicates a correct result of the procedure.

Objectives

In this study, we aimed to evaluate the efficacy and safety of a new method for the measurement of intra-aneurysm pressure during EVAR. We also assessed the correlation between ASP and early occurrence of an endoleak early after the procedure.

Materials and methods

Study design and population

This was a prospective study based on the analysis of invasive pressure measurements obtained during endovascular treatment of infrarenal AAAs. A total of 23 patients (18 men and 5 women) at a mean age of 71.8 ±6.6 years (range: 58–85 years) were enrolled. The inclusion criteria were as follows: 1) a referral for primary surgical treatment of an AAA using EVAR; 2) the presence of an asymptomatic AAA; and 3) the length of the aneurysm neck of at least 20 mm. The demographic and clinical data of patients is presented in Table 1.

Endovascular aneurysm repair

We performed a standard stent graft implantation in a hybrid operating room with a fixed C-arm system.[6] The procedure was carried out under local anesthesia of the inguinal region. Bilateral femoral artery access was used. The main body of the bifurcated stent graft was deployed, positioned and opened under angiographic guidance, just below the origin of the renal arteries. Then, the ipsilateral and contralateral arms of the stent graft were deployed. The EVAR outcome, including early endoleak, was monitored using angiography. Femoral punctures were sealed using an endovascular closure device. After the procedure, all patients received dual antiplatelet therapy (aspirin plus clopidogrel, both 75 mg daily) for 3 months, followed by lifelong 75 mg aspirin according to protocol.[7]

Pressure measurement

The pressure measurements were taken with a 0.014-inch wire (COMET II Pressure Guidewire; Boston Scientific, Marlborough, USA). A 6F Judkins right guiding catheter (Boston Scientifi) was inserted using percutaneous radial access and advanced proximally to the aneurysm. The guidewire was advanced through the catheter into the aneurysm sac before stent graft implantation to monitor the ASP (position of pressure guidewire is visible in Fig. 1). Aortic pressure (AP) was measured through the catheter. Pressure measurements were taken at each stage of the procedure – that is, before and after stent graft deployment – as well as after ballooning of the stent graft. Systolic, diastolic and mean pressure values were recorded both for ASP and AP. Once the stent graft implantation was completed, the guidewire and the catheter were removed.

Ethics

All patients gave their written informed consent to undergo treatment, and the study protocol was approved by the local ethics committee. The study was conducted in line with the principles of the Declaration of Helsinki.

Statistical analysis

The Shapiro–Wilk test for normality was performed, followed by the Student's t-test for comparison between the obtained coefficients (dependent samples).

Table 1. Patients enrolled in the study

Patient No.	Gender	Age [years]	BMI	Comorbidities	Model of implanted stent graft
1	F	71	25.3	HT, COPD	Gore Excluder
2	M	85	27.8	HT, CVD, DM	Gore Excluder
3	M	68	27.7	HT, NE	Terumo Aortic Treo
4	M	73	26.5	HT, KD, NE	Jotec E-tegra
5	M	69	21.8	HT	Terumo Aortic Treo
6	M	83	28.7	HT, CVD, NE	Terumo Aortic Treo
7	M	62	31.1	HT	Terumo Aortic Treo
8	F	72	31.1	HT	Terumo Aortic Treo
9	F	73	25.0	HT	Terumo Aortic Treo
10	M	66	38.1	HT	Terumo Aortic Treo
11	M	80	24.7	HT, CVD, COPD, DM	Jotec E-tegra
12	M	66	31.3	HT	Terumo Aortic Treo
13	M	80	29.4	HT, CVD	Gore Excluder
14	M	75	32.3	HT, CVD, DM	Gore Excluder
15	M	72	26.3	–	Cook Zenith Alpha
16	M	66	28.7	–	Gore Excluder
17	M	68	24.2	–	Gore Excluder
18	F	74	31.3	HT	Cook Zenith Alpha
19	M	58	34.7	HT	Medtronic Endurant
20	M	75	31.7	HT	Medtronic Endurant
21	F	72	23.5	HT, CVD	Cook Zenith Alpha
22	M	66	23.5	HT	Cook Zenith Alpha
23	M	78	30.9	HT, CVD	Cook Zenith Alpha

M – male; F – female; BMI – body mass index; COPD – chronic obstructive pulmonary disease; CVD – cardiovascular disease; DM – diabetes mellitus; HT – hypertension; KD – kidney disease; NE – neurologic events.

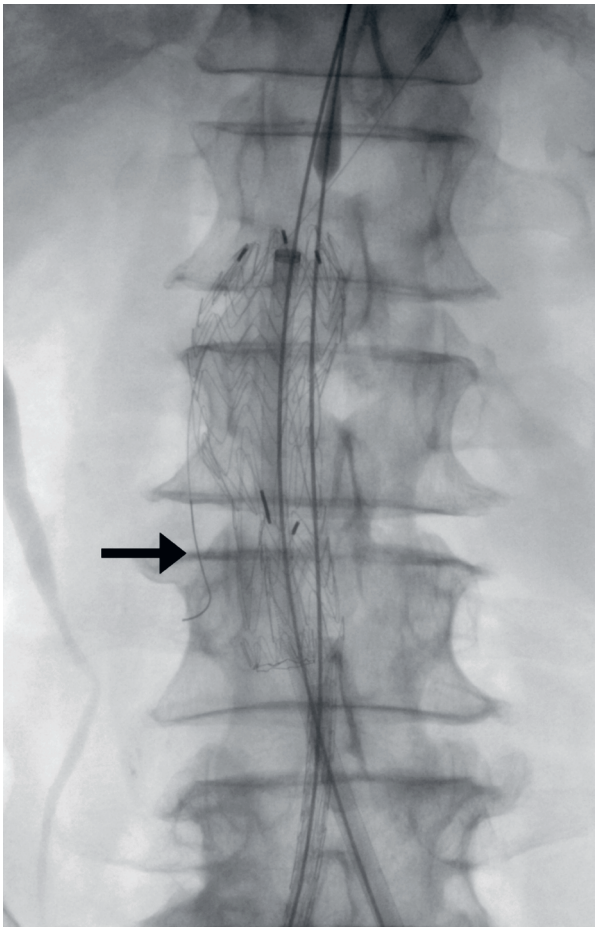

Fig. 1. Position of pressure guidewire during EVAR (black arrow)

The significance level was set at a p-value of less than 0.05. The analysis of correlation was performed using Pearson's correlation coefficient. STATISTICA v. 13.3 software (StatSoft Inc., Tulsa, USA) was used for analysis.

Results

The measurements were successfully obtained during EVAR in all patients without any complications.

Systolic, diastolic and mean pressure values for ASP and AP during the main stages of EVAR are shown in Fig. 2–4. Before stent graft deployment, all ASP and AP were almost equal. The systolic AP was maintained at the same level throughout the procedure (109.5 ±22.8 mm Hg before procedure compared to 110.7 ±21.6 mm Hg after opening compared to 107.4 ±22.1 mm Hg after ballooning, not significant (NS)). Similar observation was noted for diastolic AP (58.7 ±13.2 mm Hg compared to 55.2 ±13.5 mm Hg compared to 56.4 ±13.6 mm Hg, respectively, NS) and mean AP (74.2 ±14.8 mmHg compared to 74.8 ±14.1 mm Hg compared to 73.4 ±13.8 mm Hg, respectively, NS). However, after the main body and limbs

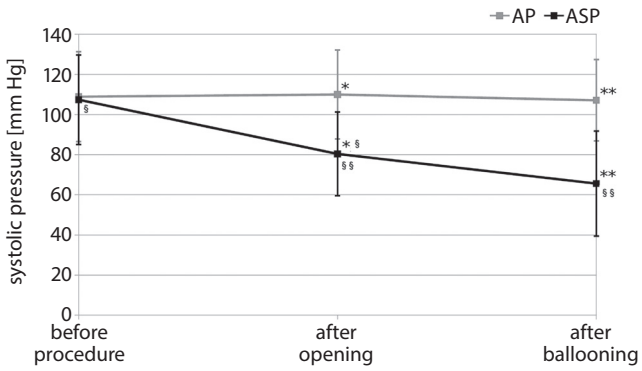

Fig. 2. ASP and AP values for systolic pressure on each stage of stent graft deployment. Data shown as means ± 95% confidence interval (95% CI); Student's t-test paired comparison

*ASP after opening compared to AP after opening, $p < 0.001$; **ASP after ballooning compared to AP after ballooning, $p < 0.001$; §ASP after opening compared to baseline ASP, $p < 0.001$; §§ASP after opening compared to ASP after ballooning, $p < 0.001$.

of the stent graft were opened, systolic ASP was reduced significantly from 107.4 ±22.3 mm Hg to 80.4 ±20.9 mm Hg ($p < 0.001$ compared to baseline systolic ASP and $p < 0.001$ compared to AP after opening) and after ballooning

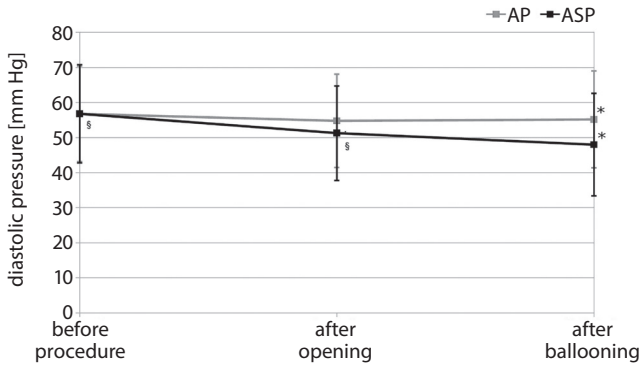

Fig. 3. ASP and AP values for diastolic pressure on each stage of stent graft deployment. Data shown as means ±95% CI; Student's t-test paired comparison

*ASP after ballooning compared to AP after ballooning, $p < 0.05$; §ASP after opening compared to baseline ASP, $p < 0.05$.

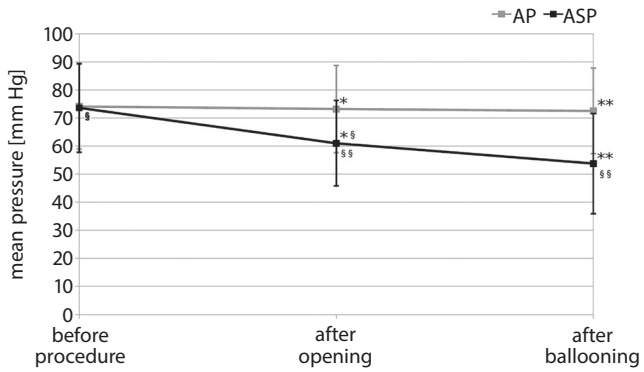

Fig. 4. ASP and AP values for mean pressure on each stage of stent graft deployment

Data shown as means ±95% CI; Student's t-test paired comparison *ASP after opening compared to AP after opening, $p < 0.001$; **ASP after ballooning compared to AP after ballooning, $p < 0.001$; §ASP after opening compared to baseline ASP, $p < 0.001$; §§ASP after opening compared to ASP after ballooning, $p < 0.01$.

to 65.6 ±26.1 mm Hg ($p < 0.001$ compared to ASP after opening and $p < 0.01$ compared to AP after ballooning) (Fig. 2). Diastolic ASP after opening dropped from 56.8 ±14.0 mm Hg to 51.3 ±13.5 mm Hg ($p < 0.05$ compared to baseline diastolic ASP) and after ballooning it decreased to 48.0 ±14.6 mm Hg ($p = 0.06$ compared to diastolic ASP after opening and $p < 0.05$ compared to AP after ballooning) (Fig. 3). Mean ASP after opening dropped from 73.6 ±15.8 mm Hg to 61.0 ±15.2 mm Hg ($p < 0.001$ compared to baseline mean ASP and $p < 0.001$ compared to AP after opening) and subsequently to 53.8 ±17.8 mm Hg ($p < 0.01$ compared to mean ASP after opening and $p < 0.001$ compared to AP after ballooning) (Fig. 4). The correlation results for AP and ASP are presented in Table 2.

Angiography performed after EVAR demonstrated the presence of an endoleak in 5 patients (1 endoleak type I and 4 endoleaks type II; please see the Discussion section for explanations of endoleak types). The ASP values for mean pressure in endoleak type II appeared to be

Table 2. Correlations between aneurysm sac pressure and aortic pressure

ASP and AP	r-value	p-value
Systolic baseline	0.98	<0.001
Systolic after stent graft opening	0.45	<0.05
Systolic after ballooning	0.47	<0.05
Diastolic baseline	0.99	<0.001
Diastolic after stent graft opening	0.74	<0.001
Diastolic after ballooning	0.64	<0.01

AP – aortic pressure; ASP – aneurysm sac pressure.

comparable with ASP mean pressure in group without endoleak (48.8 ±1.4 mm Hg compared to 54.1 ±19.7 mm Hg, respectively, $p = 0.06$). Mean ASP in 1 case of endoleak type I was higher (70.0 mm Hg) than in the other cases.

Discussion

Our study showed that pressure wire usage to measure ASP is feasible and safe. It was free of complications, including those associated with radial artery access. The presence of the pressure wire in the aneurysm lumen had no influence on the efficacy of the EVAR procedure. Moreover, the use of a 0.0014-inch pressure wire instead of a standard catheter allowed us to avoid leakage between the stent graft and the aneurysm neck. We observed a significant decrease in ASP during EVAR. The value of ASP diminished both after stent graft opening and its ballooning.

As the measurement of ASP is invasive and its clinical significance remains unclear, it is still rarely performed in the patients with AAA. When it is performed, it is usually done within 6 months from EVAR. Velazquez et al. performed ASP measurement in 76 patients, 17% of whom were shown to develop an endoleak (mostly associated with patent inferior mesenteric artery). Two-thirds of patients with endoleak had equal ASP and AP values.[2] A similar study was conducted by Baum et al. in 27 patients. Endoleak was present in 17 patients; ASP and AP values were comparable in 15 patients, while in 2 patients, ASP was half as low as AP.[8]

Depending on etiology, there are 5 types of endoleak: type I is caused by a leak at the end of prosthesis; type II is a leak from the branches of the aneurysm; type III is the leak connected with the defect of the stent graft; type IV is a leak through the fabric microporosity of stent graft; and type V is associated with so-called endotension, which means an enlargement of the aneurysmal sac with no visible endoleak.[9,10] Type I and III endoleaks are considered high-pressure endoleaks, with a high risk of aneurysm sac rupture because of direct exposure of the aneurysm wall to aortic pressure. Type II, IV and V endoleaks are considered lower risk and many of them may close spontaneously over time.[11,12]

A number of studies demonstrated a positive relationship between increased ASP and aneurysm growth or endoleak presence.[13,14] Using the experimental model of endotension, Shawn Skillern et al. concluded that high ASP after EVAR might be associated with a need for re-intervention in the future.[15] Chaudhuri et al. studied the impact of an endoleak on the experimental aneurysm model and revealed that only some types of endoleak were related to higher ASP.[16] A pending issue is ASP response to the different types of endoleak. Due to an insufficient sample size, this question could not be adjudicated in this study; however, it is of note that 1 case of endoleak type I presented high ASP values after the procedure, while cases with no endoleak or endoleak type II presented a decrease of ASP.

In contrast to the aforementioned studies, our measurements were performed during EVAR. Such a measurement is much less invasive and may be performed intraoperatively. Previous findings were long-term results that were frequently associated with EVAR-related changes inside the aneurysm sac, such as thrombus formation. This may suggest that the early outcome of EVAR may be less satisfactory than we expected.

We believe that potential clinical application of pressure measurements during the EVAR could be detection of early endoleaks that cannot be visualized by angiography, which may be very important in case of high-pressure endoleaks. These measurements may also facilitate the identification of patients at risk of endoleak and aneurysm growth, who thus require closer monitoring.

Limitations

Our study has several limitations. Most importantly, it was based on a small group of patients followed for a short time. However, we are planning to expand our study population and investigate the significance of correlations between the measured parameters and possible changes in aneurysm anatomy, the rate of re-interventions and the occurrence of endoleaks.

Conclusions

Our study proved that the novel method for the measurement of aneurysm sac pressure using a pressure wire during EVAR is safe and feasible. Our planned research will compare the current results with follow-up computed tomography angiography of our patients, which should provide further important insights, with possible implications for future research and clinical practice.

ORCID iDs

Maciej Antkiewicz https://orcid.org/ 0000-0003-1227-7720
Wiktor Kuliczkowski https://orcid.org/ 0000-0001-6284-0820
Marcin Protasiewicz https://orcid.org/ 0000-0003-0253-0585
Magdalena Kobielarz https://orcid.org/ 0000-0002-0191-6390
Piotr Barć https://orcid.org/ 0000-0003-1080-227X
Maciej Malinowski https://orcid.org/ 0000-0002-8443-0125
Katarzyna Frączkowska https://orcid.org/ 0000-0002-1395-348X
Katarzyna Kulikowska https://orcid.org/ 0000-0003-2427-4471
Marcin Merenda https://orcid.org/ 0000-0003-2282-6228
Krzysztof Jacyna https://orcid.org/ 0000-0001-6665-1402
Tomasz Dawiskiba https://orcid.org/ 0000-0003-2329-2918
Dariusz Janczak https://orcid.org/ 0000-0003-4671-9128

References

1. Frego M, Lumachi F, Bianchera G, et al. Risk factors of endoleak following endovascular repair of abdominal aortic aneurysm: A multicentric retrospective study. *In Vivo*. 2007;21(6):1099–1102. PMID:18210763
2. Velazquez OC, Baum RA, Carpenter JP, et al. Relationship between preoperative patency of the inferior mesenteric artery and subsequent occurrence of type II endoleak in patients undergoing endovascular repair of abdominal aortic aneurysms. *J Vasc Surg*. 2000; 32(4):777–788. doi:10.1067/mva.2000.108632
3. Chuter TA, Faruqi RM, Sawhney R, et al. Endoleak after endovascular repair of abdominal aortic aneurysm. *J Vasc Surg*. 2001;34(1):98–105. doi:10.1067/mva.2001.111487
4. Corriere MA, Feurer ID, Becker SY, et al. Endoleak following endovascular abdominal aortic aneurysm repair: Implications for duration of screening. *Ann Surg*. 2004;239(6):800–805, discussion 805–807. doi:10.1097/01.sla.0000128300.60156.ab
5. Koole D, Moll FL, Buth J, et al. Annual rupture risk of abdominal aortic aneurysm enlargement without detectable endoleak after endovascular abdominal aortic repair. *J Vasc Surg*. 2011;54(6):1614–1622. doi:10.1016/j.jvs.2011.06.095
6. Nishibe T, Iwahashi T, Kamiya K, et al. Two-year outcome of the Endurant stent graft for endovascular abdominal aortic repair in Japanese patients: Incidence of endoleak and aneurysm sac shrinkage. *Int Angiol*. 2017;36(3):237–242. doi:10.23736/S0392-9590.16.03726-3
7. Protasiewicz M, Szymkiewicz P, Kuliczkowski W, Mysiak A, Witkiewicz W. Modern antiplatelet therapy: Opportunities and risks. *Adv Clin Exp Med*. 2013;22(6):875–885. PMID:24431318
8. Baum RA, Carpenter JP, Cope C, et al. Aneurysm sac pressure measurements after endovascular repair of abdominal aortic aneurysms. *J Vasc Surg*. 2001;33(1):32–41. doi:10.1067/mva.2001.111807
9. Wacker FK, Valdeig S, Raatschen HJ, Meyer BC. C-arm CT: An adjunct to DSA for endoleak classification in patients with endovascular repair of abdominal aortic aneurysms. *Rofo*. 2014;186(3):247–252. doi:10.1055/s-0033-1350500
10. Phade SV, Garcia-Toca M, Kibbe MR. Techniques in endovascular aneurysm repair. *Int J Vasc Med*. 2011;2011:964250. doi:10.1155/2011/964250
11. Bashir MR, Ferral H, Jacobs C, McCarthy W, Goldin M. Endoleaks after endovascular abdominal aortic aneurysm repair: Management strategies according to CT findings. *AJR Am J Roentgenol*. 2009;192(4): W178–W186. doi:10.2214/AJR.08.1593
12. Stavropoulos SW, Charagundla SR. Imaging techniques for detection and management of endoleaks after endovascular aortic aneurysm repair. *Radiology*. 2007;243(3):641–655. doi:10.1148/radiol.2433051649
13. Dias NV, Ivancev K, Malina M, Resch T, Lindblad B, Sonesson B. Intra-aneurysm sac pressure measurements after endovascular aneurysm repair: Differences between shrinking, unchanged, and expanding aneurysms with and without endoleaks. *J Vasc Surg*. 2004;39(6):1229–1235. doi:10.1016/j.jvs.2004.02.041
14. Dias NV, Ivancev K, Resch TA, Malina M, Sonesson B. Endoleaks after endovascular aneurysm repair lead to nonuniform intra-aneurysm sac pressure. *J Vasc Surg*. 2007;46(2):197–203. doi:10.1016/j.jvs.2007.04.016
15. Shawn Skillern C, Stevens SL, Piercy KT, Donnell RL, Freeman MB, Goldman MH. Endotension in an experimental aneurysm model. *J Vasc Surg*. 2002;36(4):814–817. https://doi.org/10.1067/mva.2002.127520
16. Chaudhuri A, Ansdell LE, Grass AJ, Adiseshiah M. Intrasac pressure waveforms after endovascular aneurysm repair (EVAR) are a reliable marker of type I endoleaks, but not type II or combined types: An experimental study. *Eur J Vasc Endovasc Surg*. 2004;28(4):373–378. doi:10.1016/j.ejvs.2004.07.006

The protective effect of astaxanthin on cisplatin-induced ototoxicity

Suat Terzi[1,A,B,D], Abdulkadir Özgür[2,B,C], Metin Çeliker[1,B,C], Tolga Mercantepe[3,C,D], Adnan Yilmaz[4,B,C], Levent Tümkaya[3,B,C], Şeyma Kaya[1,C], Emine Demir[1,E,F], Engin Dursun[1,E,F]

[1] Department of Otorhinolaryngology, Faculty of Medicine, Recep Tayyip Erdogan University, Rize, Turkey
[2] Department of Otorhinolaryngology, Samsun Health Practices and Research Center, Ondokuz Mayıs University, Turkey
[3] Department of Histology and Embryology, Faculty of Medicine, Recep Tayyip Erdogan University, Rize, Turkey
[4] Department of Biochemistry, Faculty of Medicine, Recep Tayyip Erdogan University, Rize, Turkey

A – research concept and design; B – collection and/or assembly of data; C – data analysis and interpretation; D – writing the article; E – critical revision of the article; F – final approval of the article

Advances in Clinical and Experimental Medicine, ISSN 1899–5276 (print), ISSN 2451–2680 (online) *Adv Clin Exp Med*. 2021;30(3):315–321

Address for correspondence
Suat Terzi
E-mail: drsterzi@hotmail.com

Funding sources
This work was supported by Recep Tayyip Erdogan University Scientific Research Project Unit (RTEUBAP) under the project number of 2016/360. Compliance with ethical standards; the study was performed in accordance with the 2011 Guide for the Care and Use of Laboratory Animals

Conflict of interest
None declared

Received on August 23, 2020
Reviewed on September 18, 2020
Accepted on February 4, 2021

Published online on March 31, 2021

Abstract

Background. Promising studies have been conducted with many substances to reduce the ototoxic effects of cisplatin, but there is no treatment that completely eliminates the ototoxic effect.

Objectives. To determine the effectiveness of astaxanthin (ASX) as a protective agent against cisplatin-induced ototoxicity.

Materials and methods. Thirty-six rats were randomly divided into 6 groups. Group 1 received no drug injections except for anesthetics; group 2 received intraperitoneal (IP) olive oil only for 8 days; group 3 received only IP ASX 75 mg/kg dissolved in olive oil for 8 days; group 4 received a single dose of only IP 16 mg/kg cisplatin on the 5th day; group 5 received 25 mg/kg ASX IP daily for 8 days and a single 16 mg/kg dose of cisplatin on the 5th day; group 6 received 75 mg/kg ASX IP daily for 8 days and a single 16 mg/kg dose of cisplatin on the 5th day. The animals were tested for distortion product otoacoustic emissions (DPOAE) before and 3 days after cisplatin treatment. The animals in all groups were sacrificed under anesthesia on the 10th day. Before sacrifice, inferior vena cava blood samples were drawn into commercial tubes for biochemical analysis and their cochlea were prepared for histological analysis.

Results. The ASX+cisplatin groups demonstrated significantly higher DPOAE thresholds when compared to the cisplatin-only group ($p < 0.05$). The ASX 25 mg/kg/day+cisplatin group showed a significant increase in total antioxidant capacity compared to the cisplatin-only group, whereas the ASX 75 mg/kg/day+cisplatin group had significantly lower total oxidative stress and oxidative stress index. Histologic results showed that the cortical organ was better preserved in the ASX+cisplatin groups compared to the cisplatin-only group, and the degeneration in the spiral ganglion and inner and outer hair cells was less visible in the ASX groups.

Conclu-sions. Astaxanthin can protect hearing from cisplatin-induced ototoxicity, prevent cellular degeneration and significantly reduce oxidative stress.

Key words: cisplatin, astaxanthin, ototoxicity

Cite as
Terzi S, Özgür A, Çeliker M, et al. The protective effect of astaxanthin on cisplatin-induced ototoxicity. *Adv Clin Exp Med*. 2021;30(3):315–321. doi:10.17219/acem/133081

DOI
10.17219/acem/133081

Background

Cisplatin is an antineoplastic drug commonly used to treat various neoplasms, especially those in the head and neck. However, it has several side effects, including nephrotoxicity, marrow suppression, gastrointestinal disorders, and ototoxicity, which is observed in up to 36% of patients due to cisplatin use. Ototoxicity may occur within hours to days after treatment.[1–4] Hearing loss appears to be dose-related, cumulative, bilateral and usually permanent, and occurs at a higher frequency initially. Cisplatin has been assumed to have a destructive effect, particularly by increasing free oxygen radicals on the outer hair cells in the cochlea.[5,6] Its main cytotoxic effect is believed to be caused by its monohydrate complex reacting with nuclear DNA. Due to the close relationship between cytotoxicity and free oxygen radicals, antioxidants have been used for the prevention of ototoxicity.[7,8]

Astaxanthin (ASX) is a natural red carotenoid pigment mainly found in certain marine organisms such as microalgae, fish and shrimps.[9] It is a powerful extinguisher of reactive nitrogen and oxygen species (ROS), particularly monovalent oxygen.[10] Humans cannot produce carotenoids and must obtain them through diet. Many studies have demonstrated the strong antioxidant,[11–13] anti-apoptotic,[14,15] anti-inflammatory,[16] and anticancer[17] activities of ASX. Moreover, ASX offers a high degree of safety.[18]

Objectives

Although studies have explored many substances to reduce ototoxic effects of cisplatin with promising results,[1–4] there is no treatment that completely eliminates them. The purpose of this study was to investigate the potential protective effect of ASX against cisplatin ototoxicity.

Materials and methods

This study was approved by the Experimental Animals Ethics Committee of Recep Tayyip Erdogan University, Rize, Turkey (decision No. 2014/65). The rats used for the study were obtained from the Basic Medical Sciences Experimental Animals Application Unit of our university, and the entire study was conducted in our laboratory. The study was performed in accordance with the 2011 Guide for the Care and Use of Laboratory Animals.

Study protocol

For the purposes of this study, 36 male Wistar albino rats aged 3–3.5 months and weighing approx. 250–280 g were used. Their hearing was verified using a distortion product otoacoustic emissions (DPOAE) test. They were then randomly divided into 6 groups with 6 animals in each group. The groups and administered treatments are shown in Table 1.

All invasive procedures were performed under anesthesia. To induce anesthesia, 50 mg/kg ketamine hydrochloride (Ketalar; Eczacıbaşı, Istanbul, Turkey) and 10 mg/kg xylazine hydrochloride (Alfazyne; Alfasan International B.V., Woerden, the Netherlands) were administered intraperitoneally (ip.). The rats were kept in 12-hour light/dark cycles at a temperature of 22 ±3°C and 55–60% humidity.

Table 1. Groups and implemented treatments

Group	Treatment
Control (n = 6)	received no drug injections except for anesthetics
Olive oil (n = 6)	intraperitoneal (IP) olive oil only for 8 days
ASX 75 mg (n = 6)	received only IP ASX 75 mg/kg dissolved in olive oil
Cisplatin (n = 6)	received a single dose of only 16 mg/kg cisplatin IP on the 5th day
Cisplatin+ASX 25 mg (n = 6)	received 25 mg/kg ASX IP daily for 8 days and a single 16 mg/kg dose of cisplatin IP on the 5th day
Cisplatin+ASX 75 mg (n = 6)	received 75 mg/kg ASX IP daily for 8 days and a single 16 mg/kg dose of cisplatin IP on the 5th day

ASX – astaxanthin.

The doses and administration routes of ASX and cisplatin were selected based on previously published data.[1–4,11,12] On the 10th day, inferior vena cava blood samples were collected from the rats under anesthesia for biochemical analysis, and all the animals were sacrificed. Their cochleae were removed and dissected for histopathological and biochemical analyses.

Preparation of chemicals

Cisplatin (Cisplatinum Ebewe, 1 mg/mL) was obtained from Liba laboratories (Istanbul, Turkey), and 98% pure ASX (Chemical Abstracts Service No. 472-61-7) was purchased from Sigma-Aldrich (St. Louis, USA). Astaxanthin was dissolved in olive oil to produce a concentration of 50 mg/mL prior to administration.

DPOAE testing

The DPOAE test was performed using an Otodynamics Echoport USB cochlear emissions analyzer and Otodynamics ILO software v. 6.0 (Otodynamics, London, UK) in a quiet room. An infant hearing screening probe was attached to the external auditory canal. The stimulus consisted of 2 pure tones (f1 and f2; f1/f2 ratio = 1.22) at a sound pressure level (SPL) of 70 dB. The results were expressed as the geometric mean of the 2 primary tones. The DPOAEs were measured at the 2f1–f2 frequency, with the microphone on the outer ear canal. The resulting otoacoustic emissions were evaluated at 2 kHz, 3 kHz, 4 kHz, 6 kHz, and 8 kHz. The DPOAE test was considered positive for signal-to-noise ratios (SNR) of 6 dB SPL. The rats in all groups were

subjected to DPOAE before the start of the experiment, and the baseline SNR values at each frequency were calculated. The DPOAE test was repeated on the 8th day of the study, and the SNR values were calculated again for comparison.

Biochemical analysis

After centrifuging the collected inferior vena cava blood samples at 3500 rpm for 5 min, the total antioxidant status (TAS) and total oxidative stress (TOS) levels were measured using an autoanalyzer (Abbott C16000; Abbott Diagnostics, Abbott Park, USA) using TAS and TOS assay kits (Rel Assay Diagnostics, Gaziantep, Turkey) in the biochemistry laboratory of our institution. The measurements were expressed as micromole (μmol) Trolox equivalent per litre.[19,20] The oxidative stress index (OSI) was calculated using the following formula:

$$\text{OSI} = \text{TOS } (\mu\text{mol } H_2O_2 \text{ equivalent/L}) / \text{TAS } (\mu\text{mol Trolox equivalent/L})$$

Histopathological examination

The rats' temporal bones were dissected, and their auditory bullae were opened. The lateral wall of the cochlea was removed, 2.5% glutaraldehyde solution was slowly injected and fixation was performed. The temporal bones were kept in the same solution at 4°C overnight. After fixation, the temporal bones were kept in 10% EDTA solution for decalcification at 4°C for 10 days. The cochlea specimens were dehydrated with ethanol, embedded in paraffin blocks, prepared in 5-μm sections, and stained with hematoxylin and eosin (H&E). At least 15 sections were evaluated for each rat cochlea. Histological examination was performed under a light microscope. Five microscopic areas were randomly selected from each section. Images were obtained from the basal turn of the cochlea. Signs of degeneration, such as dilation, cell apoptosis, cell degeneration, nerve degeneration, and cytoplasmic vacuolization, were scored separately by a histopathologist blinded to the groups, on a scale of 0–4, where 0 meant normal, 1 mild, 2 moderate, 3 moderate-advanced, and 4 severe.

Statistical analysis

The data were processed using SPSS v. 15.0 for Windows (SPSS Inc., Chicago, USA). The biochemical data were calculated as the mean ± standard deviation (SD) based on the minimum and maximum values. Intergroup comparisons were made using one-way analysis of variance (ANOVA) and the Bonferroni post hoc test. The histopathological data were calculated as the median and 25–75% interquartile range (IQR) values. The Kruskal–Wallis and Tamhane T2 test was used in the comparison of histopathological data. Differences were considered significant at a value of $p < 0.05$ in all analyses.

Results

DPOAE results

The obtained SNR values were compared within and between groups. There was no significant difference in DPOAE values between the groups before the start of the experiment ($p > 0.05$). On the 8th day of the experiment, the SNR values in the cisplatin-only group were significantly decreased at all frequencies compared to baseline ($p < 0.01$). In addition, they were lower than those in the other groups at all frequencies ($p < 0.017$ for 2 kHz, 3 kHz and 4 kHz, $p < 0.001$ for 6 kHz and 8 kHz).

In the 2 ASX+cisplatin groups, there was no significant difference in SNR values on the 8th day of the experiment compared to baseline ($p > 0.05$). The ASX-only group also showed no significant difference in terms of hearing ($p > 0.05$).

Biochemical analysis results

The TAS, TOS and OSI values are summarized in Table 2. The TAS values in the 25 mg/kg ASX+cisplatin group were higher than those in the cisplatin-only group ($p = 0.036$). The TOS and OSI values in the 75 mg/kg ASX+cisplatin group were significantly lower than those in the cisplatin-only group ($p = 0.026$, $p = 0.01$, respectively).

Histopathological results

The histological morphology and cell structure in the control group was normal (Fig. 1). In the ASX and olive oil group, the histological structure of the cochlear tissue was normal. Astaxanthin and olive oil administration did not induce any pathological changes compared with the morphology and cell structure of the control group (Fig. 2,3).

Samples from the cisplatin-only group exhibited an edematous area, formed due to the loss of bipolar neurons of cochlear ganglion cells. Thickening of the acellular basilar and Reissner's membranes was observed. In the organ of Corti, degeneration of the extensions of the inner and outer hair cells and cell bodies was observed. Moreover, focal denudation of the superficial epithelium with strial edema was detected (Fig. 4).

In the 25 mg/kg ASX+cisplatin group, although the integrity of the organ of Corti had been protected, the extensions of the inner and outer hair cells and cell bodies had degenerated. However, although edema was observed in the stria vascularis area, its intensity was lower than in the cisplatin-only group. Spiral neurons showed a normal ganglion cell structure (Fig. 5).

In the 75 mg/kg ASX+cisplatin group, the general histological structure had a normal appearance. However, although the integrity of the organ of Corti had been protected, degeneration was observed in the extensions

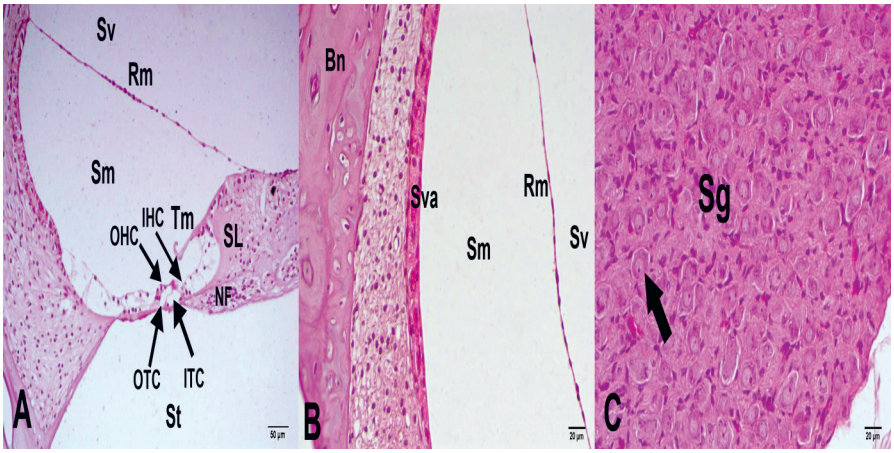

Fig. 1. Image of inner ear structures examined with light microscopy in control group (H&E staining). A. Cochlear structure, ×40 magnification; B. Stria vascularis, ×40 magnification; C. Spiral (cochlear) ganglion, ×40 magnification

Sva – stria vascularis; Rm – Reissner's membrane; Sm – scala media; Sv – scala vestibuli; St – scala tympani; Tm – tectorial membrane; SL – stira limbus; OHC – outer hair cell; IHC – inner hair cell: Sg – spiral (cochlear) ganglion; Bn – bone; arrow – cochlear neurons.

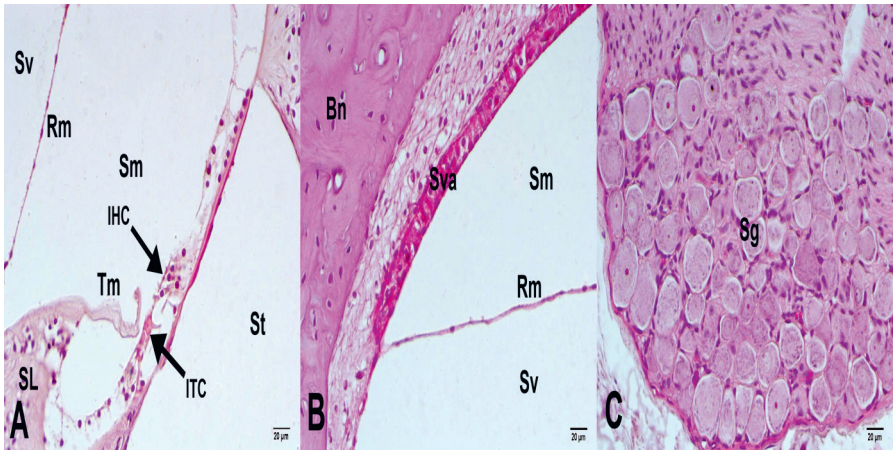

Fig. 2. Image of inner ear structures examined with light microscopy in olive oil group (H&E staining). A. Cochlear structure, ×40 magnification; B. Stria vascularis, ×40 magnification; C. Spiral (cochlear) ganglion, ×40 magnification

Sva – stria vascularis; Rm – Reissner's membrane; Sm – scala media; Sv – scala vestibuli; St – scala tympani; Tm – tectorial membrane; SL – stira limbus; OHC – outer hair cell; IHC – inner hair cell: Sg – spiral (cochlear) ganglion; Bn – bone; arrow – cochlear neurons.

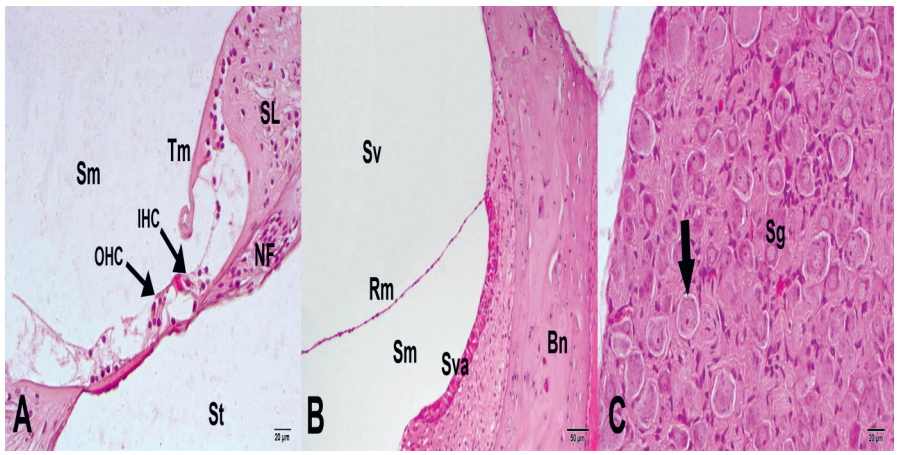

Fig. 3. Image of inner ear structures examined with light microscopy in ASX 75 mg group (H&E staining). A. Cochlear structure, ×40 magnification; B. Stria vascularis, ×20 magnification; C. Spiral (cochlear) ganglion, ×40 magnification

Sva – stria vascularis; Rm – Reissner's membrane; Sm – scala media; Sv – scala vestibuli; St – scala tympani; Tm – tectorial membrane; SL – stira limbus; OHC – outer hair cell; IHC – inner hair cell: Sg – spiral (cochlear) ganglion; Bn – bone; arrow – cochlear neurons.

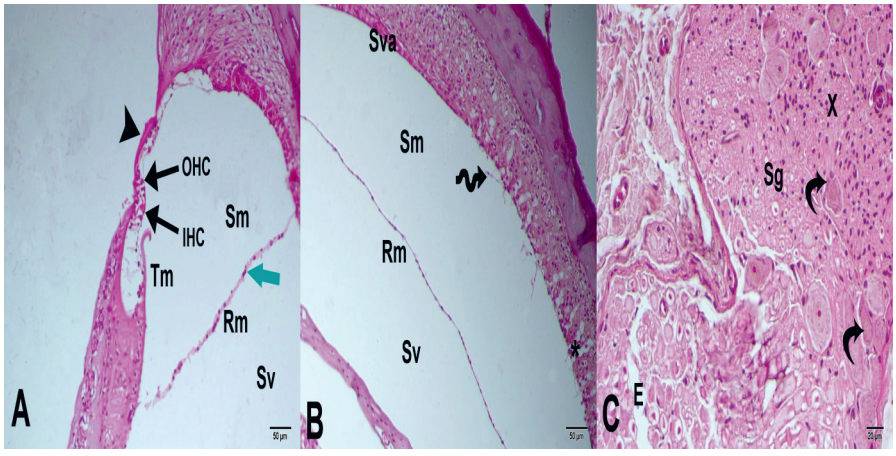

Fig. 4. Image of inner ear structures examined with light microscopy in cisplatin group (H&E staining). A. Cochlear structure; Acelular basilar membrane thickening (arrow head) and Reissner's membrane thickening (green arrow), ×20 magnification; B. Stria vascularis, ×20 magnification; C. Spiral (cochlear) ganglion, ×40 magnification

Sva – stria vascularis; Rm – Reissner's membrane; Sm – scala media; Sv – scala vestibuli; St – scala tympani; Tm – tectorial membrane; SL – stira limbus; OHC – outer hair cell; IHC – inner hair cell: Sg – spiral (cochlear) ganglion; Bn – bone; arrow – cochlear neurons; * strial edema; spiral arrow – focal denudation of superficial epithelium; curved arrow – loss of cochlear bipolar neurons.

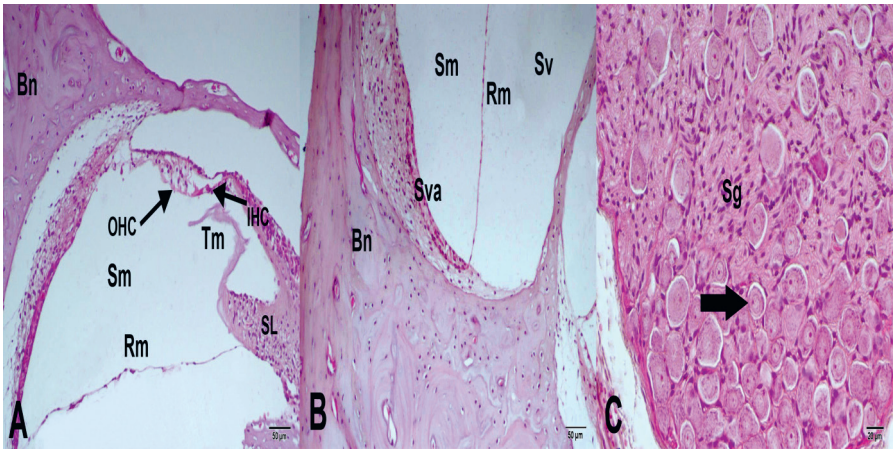

Fig. 5. Image of inner ear structures examined with light microscopy in cisplatin+ASX 25 mg group (H&E staining). A. Cochlear structure, ×20 magnification; B. Stria vascularis, ×20 magnification; C. Spiral (cochlear) ganglion, ×40 magnification

Sva – stria vascularis; Rm – Reissner's membrane; Sm – scala media; Sv – scala vestibuli; St – scala tympani; Tm – tectorial membrane; SL – stira limbus; OHC – outer hair cell; IHC – inner hair cell: Sg – spiral (cochlear) ganglion; Bn – bone; arrow – cochlear neurons.

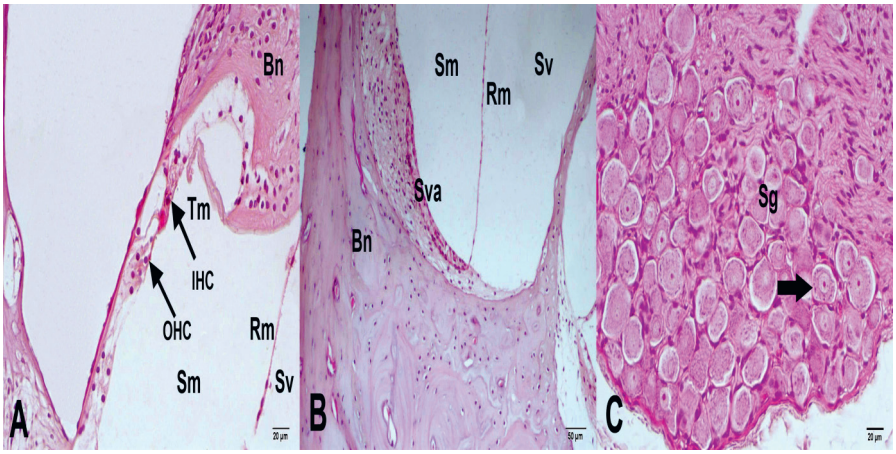

Fig. 6. Image of inner ear structures examined with light microscopy in cisplatin+ASX 75 mg group (H&E staining). A. Cochlear structure, ×40 magnification; B. Stria vascularis, ×20 magnification; C. Spiral (cochlear) ganglion, ×40 magnification

Sva – stria vascularis; Rm – Reissner's membrane; Sm – scala media; Sv – scala vestibuli; St – scala tympani; Tm – tectorial membrane; SL – stira limbus; OHC – outer hair cell; IHC – inner hair cell: Sg – spiral (cochlear) ganglion; Bn – bone; arrow – cochlear neurons.

Table 2. Blood oxidative stress parameters in the groups (mean ± standard deviation (SD))

Group	TOS (μmol H_2O_2 equivalent/L)	TAS (mmol trolox equivalent/L)	OSI
Control	7.65 ±1.22	1.28 ±0.11	5.97 ±1.42
Olive oil	15.04 ±1.10	1.13 ±0.11	13.31 ±2.88
ASX-only (75 mg/kg)	7.71 ±1.82	1.33 ±0.21	5.72 ±1.16
Cisplatin-only	18.72 ±7.35[a] (p = 0.005)	1.07 ±0.13[a] (p = 0.013)	17.43 7.32[a] (p = 0.004)
Cisplatin+ASX 25 mg/kg	15.55 ±6.55	1.44 ±0.35[b] (p = 0.036)	10.75 ±5.70
Cisplatin+ASX 75 mg/kg	10.18 ±3.19[b] (p = 0.026)	1.31 ±0.12[b] (p = 0.008)	7.74 ± 0.8[b] (p = 0.01)

[a]p < 0.05 compared to control group; [b]p < 0.05 compared to cisplatin group; one-way ANOVA/Bonferroni post hoc correction; TOS – total oxidative stress; TAS – total antioxidant capacity; OSI – oxidative stress index; ASX – astaxanthin.

of the inner and outer hair cells and cell bodies, and significant cell spillage was detected. In the organ of Corti, both Reissner's and the tectorial membrane exhibited normal morphology. The stria vascularis and spiral ligament-forming cells were normal in terms of arrangement and nucleus appearance. Spiral ganglion connective tissue cells and pseudounipolar neurons presented a normal ganglion cell structure (Fig. 6).

The median values of the histopathological blind grading of strial edema, inner and outer cell degeneration in the organ of Corti, and degenerative bipolar neuron density in the groups are summarized in Table 3. No significant difference was observed between the control, olive oil and ASX-only groups in terms of degeneration findings ($p > 0.05$). The ASX 25 mg/kg+cisplatin group ($p = 0.000$, $p = 0.000$, $p = 0.000$, for strial edema, inner and outer cell degeneration in the organ of Corti, and degenerative bipolar neuron, respectively) and ASX 75 mg/kg+cisplatin group ($p = 0.000$, $p = 0.001$, $p = 0.000$, for strial edema, inner and outer cell degeneration in the organ of Corti, and degenerative bipolar neuron, respectively) had significantly lower strial edema, inner and outer cell degeneration

Table 3. Histopathological grading of all groups (median (interquartile range))

Group	Strial edema	Corti degeneration	Bipolar neuron degeneration
Control	0.5 (0–1)	0.5 (0–1)	0 (0–0.5)
Olive oil	0.5 (0–1)	0 (0–0.5)	0 (0–1)
ASX-only (75 mg/kg)	0 (0–0.5)	0 (0–0.5)	0.5 (0–1)
Cisplatin-only	3 (2.5–3)[a] (p = 0.000)	3 (2–3)[a] (p = 0.000)	3 (2.5–3)[a] (p = 0.000)
Cisplatin+ASX 25 mg/kg	1 (1–1.5)[b] (p = 0.000)	1 (1–1)[b] (p = 0.000)	1 (0.5–1)[b] (p = 0.000)
Cisplatin+ASX 75 mg/kg	1 (1–1)[b] (p = 0.000)	1 (1–1)[b] (p = 0.001)	1 (0–1)[b] (p = 0.000)

[a]p < 0.05 compared to control group; [b]p < 0.05 compared to cisplatin group; Kruskal–Wallis/Tamhane T2 test; SD – standard deviation; ASX – astaxanthin.

in the organ of Corti, and degenerative bipolar neuron density values than the cisplatin-only group. Moreover, there was no significant difference between the 2 ASX+cisplatin groups in terms of strial edema, degeneration in the organ of Corti and degenerative bipolar neuron density.

Discussion

The prevention of side effects caused by cisplatin is very important for its safe use as an antineoplastic. Although many substances have been trialed to that end, none have been routinely applied in clinical practice.[1–4] This study evaluated the potential protective effect of ASX on cisplatin-induced ototoxicity. The histopathological findings and hearing test results show that ASX reduces cochlear damage caused by cisplatin. Moreover, the biochemical data show that ASX has antioxidant effects against oxidative stress in the blood, indirectly mitigating cisplatin-induced damages.

In cisplatin-induced ototoxicity, hearing loss is generally reported 3 days after the first cisplatin dose and is usually bilateral. Various cisplatin doses and routes of administration to produce ototoxicity have been examined in previous studies.[3,4,6] A single dose of 16 mg/kg is generally preferred. Accordingly, we administered cisplatin in a single dose of 16 mg/kg intraperitoneally on the 5th day of the experiment, which induced bilateral ototoxicity on the 8th day. This practice did not cause any deaths.

Several pharmacological agents, such as thymoquinone, curcumin, α-tocopherol, lycopene, α-lipoic acid, and erdosteine, have been used to prevent ototoxic effects of cisplatin.[1–4] Unfortunately, no agent has been widely accepted for use in clinical practice to date. Therefore, the search for an alternative effective protective treatment continues. Astaxanthin is a carotenoid pigment obtained from the microalga *Hematococcus pluvialis* and other biological sources.[9] As several studies have demonstrated its strong antioxidant, anti-inflammatory, anticancer, and anti-apoptotic activities,[10–16] we decided to investigate its potential protective effect on cisplatin-induced ototoxicity. Its safety and tolerability, even at high doses, have been well established in both animal and clinical studies.[9–17] In our study, we observed no side effects of ASX in doses of 25 mg/kg and 75 mg/kg.

The mechanism of cisplatin-induced cochlear damage is thought to result from increased amounts of toxic free radicals or cell membrane changes, which cause a decrease in intracellular calcium content.[5,6] Cisplatin ototoxicity is also believed to be related to a malfunction of the antioxidant system. Impaired antioxidant enzyme activity in the cochlea may result in an increase in reactive oxygen species (ROS), which induce lipid peroxidation, leading to apoptosis of hair cells, support cells, auditory nerves, and the stria vascularis.[21,22] The antioxidant activity of ASX is known to be 10 times more potent than that of zeaxanthin, lutein and other carotenoids, and 100 times more potent than that of α-tocopherol.[23]

Yeh et al.[14] reported that ASX reduced retinal oxidative stress in streptozocin-induced diabetic rats. Mosaad et al.[15] found that ASX protects the kidneys from gentamicin-induced nephrotoxicity. Mizuta et al.[16] demonstrated that it is a potent therapeutic agent for vocal cord scarring through oxidative stress regulation. Wolf et al.[13] showed that it reduces the production of reactive oxygen radicals by mitochondria and mitigates the loss of mitochondrial function under oxidative stress, concluding that it is a potential therapeutic agent for various diseases involving oxidative stress. We evaluated the antioxidant effect of ASX with TAS, TOS and OSI measurements. Our results show that a high dose of ASX is more effective in reducing oxidative stress caused by cisplatin, but even a lower dose is sufficient to reduce oxidative stress by increasing tissue antioxidant capacity.

The DPOAE tests are an objective and highly selective tool for evaluation of cochlea function. Authors of many studies on cisplatin-induced ototoxicity have used them to evaluate hearing.[1–4] Similarly, we used DPOAE to assess hearing in rats. In the cisplatin-only group, the DPOAE values at all frequencies were significantly decreased on the 8th day of the experiment compared to baseline, while they were preserved in both ASX+cisplatin groups. Astaxanthin significantly mitigated cisplatin-induced hearing damage, while it had no effect in the control group.

Our histopathological data show that strial edema, inner and outer cell degeneration in the organ of Corti, and degenerative bipolar neuron density in both ASX+cisplatin groups were significantly lower than in the cisplatin-only group. The ASX dose of 75 mg/kg did not cause any pathological changes in tissue morphology and cell structure compared with the control group. These results show that ASX has protective effects against cisplatin-induced ototoxicity and has no ototoxic effects itself. We believe that its protective role is due not only to its antioxidant activity, but also to its anti-inflammatory effect on cisplatin-induced ototoxicity.

Limitations

Certain limitations of this study should be mentioned. Firstly, we could not perform DPOAE measurements at frequencies higher than 8 kHz. Another important limitation is that we only applied H&E staining to the cochlea sections. We did not perform immunohistochemistry staining to demonstrate apoptosis in the cochleae. Finally, the small size of our animal sample constitutes another limitation.

Conclusions

Astaxanthin has protective biochemical, audiological and histopathological effects against cisplatin-induced ototoxicity in both low and high doses. We believe that it may reduce drug side effects in patients undergoing chemotherapy, especially those receiving cisplatin. However, further studies are needed to investigate the effects of ASX on different species, in different doses, and with different routes of administration and treatment durations.

ORCID iDs

Suat Terzi https://orcid.org/ 0000-0002-1131-3649
Abdulkadir Özgür https://orcid.org/ 0000-0002-6155-5988
Metin Çeliker https://orcid.org/ 0000-0002-9833-402X
Tolga Mercantepe https://orcid.org/ 0000-0002-8506-1755
Adnan Yilmaz https://orcid.org/ 0000-0003-4842-1173
Levent Tümkaya https://orcid.org/ 0000-0002-2814-5194
Şeyma Kaya https://orcid.org/ 0000-0002-1150-6467
Emine Demir https://orcid.org/ 0000-0003-4087-432X
Engin Dursun https://orcid.org/ 0000-0002-2070-8677

References

1. Yazici ZM, Meric A, Midi A, Arınc YV, Kahya V, Hafız G. Reduction of cisplatin ototoxicity in rats by oral administration of pomegranate extract. *Eur Arch Otorhinolaryngol*. 2012;269(1):45–52. doi:10.1007/s00405-011-1582-2
2. Kalcioglu MT, Kizilay A, Gulec M, et al. The protective effect of erdosteine against ototoxicity induced by cisplatin in rats. *Eur Arch Otorhinolaryngol*. 2005;262(10):856–863. doi:10.1007/s00405-004-0909-7
3. Ozkırış M, Kapusuz Z, Karaçavuş S, Saydam L. The effects of lycopene on cisplatin-induced ototoxicity. *Eur Arch Otorhinolaryngol*. 2013;270(12):3027–3033. doi:10.1007/s00405-013-2352-0
4. Özdemir D, Özgür A, Kalkan Y, et al. The protective effects of whortleberry extract against cisplatin-induced ototoxicity in rats. *Braz J Otorhinolaryngol*. 2019;85(1):55–62. doi:10.1016/j.bjorl.2017.10.009
5. Rabik CA, Dolan ME. Molecular mechanisms of resistance and toxicity associated with platinating agents. *Cancer Treat Rev*. 2007;33(1):9–23. doi:10.1016/j.ctrv.2006.09.006
6. Laurell G, Bagger-Sjöbäck D. Dose-dependent inner ear changes after i.v. administration of cisplatin. *J Otolaryngol*. 199;20(3):158–167. PMID:1870163
7. Sluyter S, Klis SF, de Groot JC, Smoorenburg GF. Alterations in the stria vascularis in relation to cisplatin ototoxicity and recovery. *Hear Res*. 2003;185(1–2):49–56. doi:10.1016/s0378-5955(03)00260-0
8. Giordano P, Lorito G, Ciorba A, Martini A, Hatzopoulos S. Protection against cisplatin ototoxicity in a Sprague-Dawley rat animal model. *Acta Otorhinolaryngol Ital*. 2006;26(4):198–207. PMID:18236636
9. Wu H, Niu H, Shao A, et al. Astaxanthin as a potential neuroprotective agent for neurological diseases. *Mar Drugs*. 2015;13(9):5750–5766. doi:10.3390/md13095750
10. Naguib YM. Antioxidant activities of astaxanthin and related carotenoids. *J Agric Food Chem*. 2000;48(4):1150–1154. doi:10.1021/jf991106k
11. Zheng D, Li Y, He L, et al. The protective effect of astaxanthin on fetal alcohol spectrum disorder in mice. *Neuropharmacology*. 2014;84:13–18. doi:10.1016/j.neuropharm.2014.04.013
12. Turkez H, Geyikoglu F, Yousef MI. Beneficial effect of astaxanthin on 2,3,7,8-tetrachlorodibenzo-p-dioxin-induced liver injury in rats. *Toxicol Ind Health*. 2013;29(7):591–599. doi:10.1177/0748233711434959
13. Wolf AM, Asoh S, Hiranuma H, et al. Astaxanthin protects mitochondrial redox state and functional integrity against oxidative stress. *J Nutr Biochem*. 2010;21(5):381–389. doi:10.1016/j.jnutbio.2009.01.011
14. Yeh PT, Huang HW, Yang CM, Yang WS, Yang CH. Astaxanthin inhibits expression of retinal oxidative stress and inflammatory mediators in streptozotocin-induced diabetic rats. *PLoS One*. 2016;11(1):e0146438. doi:10.1371/journal.pone.0146438
15. Mosaad YO, Gobba NA, Hussein MA. Astaxanthin: A promising protector against gentamicin-induced nephrotoxicity in rats. *Curr Pharm Biotechnol*. 2016;17(13):1189–1197. doi:10.2174/1389201017666160922110740
16. Mizuta M, Hirano S, Hiwatashi N, et al. Effect of astaxanthin on vocal fold wound healing. *Laryngoscope*. 2014;124(1):E1–E7. doi:10.1002/lary.24197
17. Chew BP, Park JS, Wong MW, Wong TS. A comparison of the anticancer activities of dietary beta-carotene, canthaxanthin and astaxanthin in mice in vivo. *Anticancer Res*. 1999;19(3A):1849–1853. PMID:10470126
18. Spiller GA, Dewell A. Safety of an astaxanthin-rich *Haematococcus pluvialis* algal extract: A randomized clinical trial. *J Med Food*. 2003;6(1):51–56. doi:10.1089/109662003765184741
19. Erel O. A novel automated method to measure total antioxidant response against potent free radical reactions. *Clin Biochem*. 2004;37(2):112–119. doi:10.1016/j.clinbiochem.2003.10.014
20. Erel O. A new automated colorimetric method for measuring total oxidant status. *Clin Biochem*. 2005;38(12):1103–1111. doi:10.1016/j.clinbiochem.2005.08.008
21. Rybak LP. Mechanisms of cisplatin ototoxicity and progress in otoprotection. *Curr Opin Otolaryngol Head Neck Surg*. 2007;15(5):364–369. doi:10.1097/MOO.0b013e3282eee452
22. Clerici WJ, DiMartino DL, Prasad MR. Direct effects of reactive oxygen species on cochlear outer hair cell shape in vitro. *Hear Res*. 1995;84(1–2):30–40. doi:10.1016/0378-5955(95)00010-2
23. Kim JH, Kim YS, Song GG, Park JJ, Chang HI. Protective effect of astaxanthin on naproxen-induced gastric antral ulceration in rats. *Eur J Pharmacol*. 2005;514(1):53–59. doi:10.1016/j.ejphar.2005.03.034

The effects of chicken egg white cystatin and proteinase inhibitor on cysteine peptidase-like activity in the sera of patients with breast cancer

Maciej Siewiński[1,A–F], Ewa Kilar[2,A–D], Lidia Hirnle[3,B,C,E,F], Teresa Skiba[4,B,C,E], Jakub Gburek[5,B,C,E], Krzysztof Gołąb[5,B,C,E], Marek Murawski[3,B,C,E], Anna Janocha[6,C–F]

[1] Department of Basic Sciences, Wroclaw Medical University, Poland
[2] Department of Oncology, Świdnica District Hospital, Poland
[3] 1st Department and Clinic of Gynecology and Obstetrics, Wroclaw Medical University, Poland
[4] Department of Animal Product Technology and Quality Management, Wroclaw University of Environmental and Life Sciences, Poland
[5] Department of Pharmaceutical Biochemistry, Wroclaw Medical University, Poland
[6] Department of Pathophysiology, Wroclaw Medical University, Poland

A – research concept and design; B – collection and/or assembly of data; C – data analysis and interpretation; D – writing the article; E – critical revision of the article; F – final approval of the article

Advances in Clinical and Experimental Medicine, ISSN 1899–5276 (print), ISSN 2451–2680 (online) *Adv Clin Exp Med*. 2021;30(3):323–330

Address for correspondence
Lidia Hirnle
E-mail: lidia.hirnle@umed.wroc.pl

Funding sources
None declared

Conflict of interest
None declared

Received on July 30, 2018
Reviewed on February 18, 2019
Accepted on August 11, 2020

Published online on March 30, 2021

Cite as
Siewiński M, Kilar E, Lidia Hirnle L, et al. The effects of chicken egg white cystatin and proteinase inhibitor on cysteine peptidase-like activity in the sera of patients with breast cancer. *Adv Clin Exp Med.* 2021;30(3):323–330. doi:10.17219/acem/126288

DOI
10.17219/acem/126288

Abstract

Background. The activity of autogenic proteolytic enzymes is regulated in vivo by autogenic inhibitors. They play important roles in maintaining a balance in many processes in the human body. In pathological conditions, enzymes are overexpressed and the balance is disturbed. Such uncontrolled changes may lead to the development of local or systemic cancer.

Objectives. To evaluate the effects of specific inhibitors, i.e., chicken egg white cystatin (CEWC) and proteinase inhibitor (E-64) on autogenic cysteine peptidases (CPs) in the sera of patients reporting for subsequent stages of treatment after being diagnosed with breast cancer. Cysteine peptidases play a vital role in the basic processes that are associated with cancer progression.

Materials and methods. We selected serum samples from 108 patients with a diagnosis of breast cancer (stages IIA–IIIA) who had received no previous treatment. The blood samples were centrifuged, and the resulting serum was placed in liquid nitrogen and stored at –80°C. The biochemical tests were performed at the laboratory of the Department of Physical Chemistry and Microbiology.

Results. For CEWC, we found an inhibitory effect in 37 out of 108 samples; for E-64, 14 out of 22 samples displayed an inhibitory effect. In the remaining blood samples, these inhibitors caused an increase in fluorescence. In a parallel test, we added pure cathepsin B to 9 serum samples, and then used CEWC to inhibit the activity of autogenic CPs. Chicken egg white cystatin completely inhibited the cathepsin B that was added to the serum without changing its effect on the autogenic CPs.

Conclusions. The results suggest that there may be a potential difference between the commercially available cathepsin B and its autogenic analogues found in the serum of cancer patients. The increase in fluorescence induced in the reaction between the inhibitors and autogenic CPs is still unexplained. There was no relationship between the observed inhibition/activation of CPs and any of the available indicators of the health of the patients examined.

Key words: breast cancer, serum cysteine peptidase-like activity, chicken egg white cystatin, E-64 proteinase inhibitor

Background

Autogenic proteolytic enzymes have various functions throughout the body and their activity is regulated in vivo by autogenic inhibitors. They play important roles in maintaining the balance in many processes in the human body. Under pathological conditions, enzymes are overexpressed, the balance is disturbed, and there can be either an excess of active enzymes or a lack of active inhibitors in vivo. Such uncontrolled changes in the body may lead to the development of local or systemic cancer or other diseases.

It was therefore proposed to inhibit the activity of these enzymes under pathological conditions. The inhibitory effect is achieved by supplying specific exogenous inhibitors. This represents a chance to develop a new type of treatment using specific non-toxic inhibitors to alter the in vivo activity of enzymes that catalyze pathogenic processes. Studies on experimental animal models have demonstrated that many autogenic inhibitors obtained through chemical synthesis or from biological sources prevent the neoplastic process both in vitro and in vivo, but their toxicity in humans is too high for them to be used as new drug components.[1–4] It has been suggested that cathepsin B plays a particularly significant role in certain individual biological processes associated with cancer progression. For this reason, cathepsin B has become potentially the most efficient new target for anticancer therapy employing specific inhibitors. So far, many molecules regulating the in vitro activity of cathepsin B have been identified, and studies are continually finding inhibitors able to produce inhibitory effects in vivo.[5,6] It was also found that cathepsin B attenuates the efficiency of conventional chemotherapy.[7] Research has confirmed that an overexpression of cysteine peptidases – with a simultaneous reduction in their activity achieved by reducing the number of their active inhibitors – decreases immune system function and facilitates the invasion of cancer cells and metastasis. Autogenic cystatins are specific inhibitors which are able to suppress this process.

Cystatins are involved in many physiological and pathological processes, and a deficiency of them can disturb key immunomodulatory functions. The overexpression of cysteine peptidases suppresses immunity, decreasing the control of the autogenic inhibition of neoplastic processes. This finding leads to the hypothesis that reduced activity of pathogenic cysteine cathepsins in vivo caused by autogenic or exogenous inhibitors can enhance the immune system, which can then be used as a defense against the progression of cancer.[8] Studies on cell lines of human breast cancer have confirmed the expression of cathepsin B on the surface of mutant cells in the form of an inactive precursor that was activated by enzymes in the next stage. It was found that the active enzyme is inhibited by specific inhibitors. Findings from in vitro studies were confirmed in vivo on transgenic mice who received a graft of breast cancer cells. In this experiment, the inhibitors of cysteine peptidases reduced the progression of breast cancer by inhibiting CPs, strongly limiting the progression of the disease.[9] Moreover, it was found that cathepsin D attenuates the anticancer immune response by degrading chemokines and limiting the activity of dendritic cells. On the other hand, cathepsins B, K and L play key roles in the degradation of the extracellular matrix during cancer invasion, acting directly or through the activation of precursors of proteolytic enzymes, such as metalloproteinases, collagenases, plasminogen activator, and others involved in this mechanism. It has been confirmed that specific inhibitors of cysteine peptidases successfully inhibit the cancer invasion and metastasis, and that cathepsin B and other cysteine cathepsins are important targets for anticancer therapy.[2,10]

The activity of CPs is regulated in vivo by their autogenic inhibitors – mainly from the cystatin family, including cystatins, stefins and kininogens – and a low level/activity of them in bodily fluids may be associated with a depleted ability of the body to regulate the overexpression of CPs. Therefore, some researchers have suggested that a deficiency of these autogenic inhibitors may be supplemented by their exogenous analogues, including chemically synthesized ones. A synthetic cathepsin B inhibitor, CA-074, as well as antibodies directed against cathepsin B, were able to exert a powerful anticancer activity without any further additional drugs, limiting metastasis and cancer invasion.

This information has inspired researchers to analyze a number of synthetic cysteine peptidase inhibitors as potential drugs for anticancer therapy.[11,12] In vitro studies have confirmed the ability of specific inhibitors to block active cysteine peptidases, but the toxicity of inhibitors was found to be too high to use them in vivo as potential drugs for anticancer therapy.[13] The proteolytic activity of CPs was also inhibited using the most efficient currently known inhibitors of these enzymes. Chicken egg white cystatin was found to be the most effective inhibitor of processes involved in the overexpression of cathepsins B and L (resulting in over 80% inhibition of cancer cell invasion and metastasis), and was more effective than the synthetic inhibitor, E-64. Other inhibitors derived from biological materials or through chemical synthesis also inhibited these processes, but not as effectively as CEWC. It was also confirmed that the efficient inhibition of these enzymes was associated with limited tumor aggressiveness in breast cancer.[14]

This paper presents the effects of CEWC on the activity of autogenic CPs in the sera of patients with breast cancer. To complement the results, the activity of CPs in selected serum samples was also inhibited using a specific inhibitor (E-64). We found that CEWC inhibited the autogenic CP-like activity in 37 out of 108 serum samples; in the remaining samples, fluorescence increased after this inhibitor was added, which may suggest the increased activity of these

enzymes in serum. To confirm this finding, the activity of CPs in selected blood samples was also inhibited using a synthetic inhibitor (E-64). We found that E-64 inhibited the activity of the same enzymes in 14 out of 22 serum samples, while in the remaining samples fluorescence increased, similar to the samples to which CEWC was added. We also found that the activity of pure cathepsin B added to the serum samples was completely inhibited by CEWC, without changing the previously observed effects of this inhibitor on the autogenic cysteine peptidases in the serum samples.

Objectives

The aim of our study was to determine changes in groups of patients at different stages of cancer or different phases of treatment. We present the effects of specific inhibitors on the serum of patients with breast cancer. Similar results were also found after the analysis of serum from patients with prostate cancer (unpublished data).

Materials and methods

Chemical reagents

We used Z-Phe-Arg-N-Mec (N-alpha-benzyloxycarbonyl-L-phenyl-alanyl-L-arginine-7-amido-4-methylcoumarin), Mec (7-amino-4-methylcoumarin), E-64 inhibitor L-epoxysuccinylleucyl-amido (4-guanidino) butane (Fluka BioChemika, Buchs, Switzerland), and the enzymes papain (3.4.22.1) and cathepsin B (3.4.22.2) (Sigma-Aldrich, St. Louis, USA). The other reagents were chemically pure. Chicken egg white cystatin was isolated using affinity chromatography on a carboxymethylpapain Sepharose 4B column.[15]

Clinical material (recruitment of human subjects)

Serum samples were taken from patients diagnosed with breast cancer. The patients had been referred for routine tests to the Department of Oncology of the Regional Hospital in Świdnica, Poland, between 2007 and 2009. Blood for the biochemical tests was taken in parallel with blood taken for routine follow-up tests. For the study, we recruited 108 patients with breast cancer (age: 56.36 ±9.90 years), and the decision of whether to include each patient was based on preliminary chest radiographs, mammography, ultrasonography, and blood tests – in which the levels of CEA and CA 15-3 markers were measured. The patients were diagnosed with cancer (stages IIA–IIIA of the TNM system), but had not undergone surgical treatment, radiotherapy or chemotherapy. The blood samples were centrifuged and the resulting serum was placed in liquid nitrogen and stored at –80°C. Biochemical tests were performed at the laboratory of the Department of Pharmaceutical Chemistry and Microbiology at the University of Wrocław.

Determination of cysteine peptidase-like activity in the serum

Each 100-µL serum sample was augmented with 700 µL of 0.4 M phosphate buffer (pH 6.0) – containing 4 mM EDTA and 2.5 mM DTT – and a 200-µL solution of diluted Z-Phe-Arg-N-Mec substrate in order to achieve a final substrate concentration of 40 µM. Enzymatic hydrolysis of the substrate in each sample was carried out for 60 min at 37°C. The hydrolysis was terminated by adding 2.0 mL of 1.0 mM iodoacetic acid. In a parallel experiment, a control solution was prepared for each sample by adding 2.0 mL of iodoacetic acid before adding the substrate. Apart from that, other reagents were the same. These samples were marked as controls. After the inhibition of substrate hydrolysis, we measured the fluorescence of the 7-amino-4-methylcoumarin (Mec) released at an excitation wavelength of 370 nm and an emission wavelength of 440 nm. The results are expressed in units of activity for cysteine endopeptidases after conversion into the amount of protein present in 1 mL of serum. One unit of enzymatic activity (U) was defined as the amount of enzyme able to catalyze the release of 1 nmol of Mec in 1 min under the conditions described above.[16]

Inhibition of cysteine peptidase-like activity in serum

One hundred microliters of the tested serum was added to 700 µL of 0.01 M phosphate buffer (pH 6.8) containing 2.0 mM EDTA and 2.0 mM glycine. Then, 100 µL of the inhibitor solution was added in relevant concentrations: 50.0 nM CEWC or 5.0 nM E-64. The sample was incubated at 37°C for 10 min; then, 100 µL of the Z-Arg-AMC substrate solution was added and the sample was incubated again for 30 min. After 30 min, the hydrolysis of the substrate was terminated by adding 2.0 mL of 1.0 mM iodoacetic acid to each sample. The amount of 7-AMC released was measured against a sample containing the same reagents, but the reaction was interrupted immediately after adding the substrate. In a parallel test, the enzyme activity was measured for samples that contained 0.01 M pH 6.8 phosphate buffer instead of the inhibitor. Inhibition or activation units were not converted. Instead, the observed changes in inhibition/activation were expressed as a percentage of change in autogenic CP-like activity in the serum samples.

Inhibition of pure cathepsin B in 9 serum samples with CEWC

Ten microliters of cathepsin B solution from Sigma-Aldrich, enzyme activity 6000 U/mL, was added to 690 µL

of 0.01 M phosphate buffer (pH 6.8); after 10 min, 100 mL of 100 nM CEWC was added. Nine serum samples were measured. The inhibition of autogenic CPs was found in 3 samples, and increased fluorescence was found in 6 samples.

Statistics

A standard statistical Student's t-test was conducted to compare the 2 variables. The values are presented as the means ± standard deviation (SD), and the level of statistical significance was set at $p < 0.05$. Statistical differences between the groups were assessed using one-way analysis of variance (ANOVA). Tukey's test was used for the post hoc analysis.

Results

In this paper, we tried to explain the effect of CEWC on the blood components of patients with breast cancer, focusing on autogenic CP-like activity in vitro. After adding CEWC to the samples of serum from patients with breast cancer, we found inhibition of CP-like activity in 36 out of 108 samples (Table 1a), and increased fluorescence in the remaining samples (Table 1b).

To confirm the results, we repeated the tests using a specific inhibitor of these enzymes (E-64). In the 2nd experiment we found inhibition of the activity of the same enzymes for 14 out of 22 serum samples; in the remaining samples, the fluorescence increased. Chicken egg white cystatin added to the same serum samples inhibited the enzyme activity in 8 samples, and in 14 caused an increase in the level of fluorescence. The purpose of the next stage of the study was to clarify the increase in fluorescence after the addition of CEWC. We used pure, commercially available cathepsin B in the tests to compare its reaction with CEWC and to obtain additional information on the similar reaction with autogenic CP-like activity in the serum of cancer patients (Table 2).

The same amount of pure cathepsin B was added to 9 randomly selected samples (Table 3). Chicken egg white cystatin inhibited CP-like activity in 3 of these samples, while in 6 samples, an increase in fluorescence was observed. We found that CEWC completely inhibited the activity of the commercially available cathepsin B, but there was no change in its effect on autogenic cysteine peptidases.

Table 1a. Effects of CEWC on CP-like activity in the sera of patients with breast cancer (samples with inhibited activity)

Sample No.	CP-like activity in serum [U/mL]	CP-like activity in serum + cystatin [U/mL]	Remaining activity + cystatin (%)
1	11.56	9.8	84.78
4	6.45	6.12	94.88
6	5.01	4.16	83.03
9	0.44	0.25	56.82
14	7.82	4.45	56.91
21	2.75	1.71	62.18
22	3.3	2.69	81.52
24	9.5	7.4	77.89
25	6.97	5.2	74.61
37	6.46	5.9	91.33
38	6.38	5.8	90.91
40	5.2	3.48	66.92
43	6.33	5.64	89.10
44	11.56	5.92	51.21
45	21.93	6.38	29.09
46	8.08	5.5	68.07
47	6.45	6.12	94.88
49	5.01	4.16	83.03
52	0.44	0.25	56.82
57	7.82	4.45	56.91
64	2.75	1.71	62.18
65	3.3	2.69	81.52
67	9.5	7.4	77.89
68	6.97	5.2	74.61
80	6.46	5.9	91.33
81	6.38	5.8	90.91
83	5.2	3.48	66.92
86	6.33	5.64	89.10
88	7.0	5.52	78.86
90	7.6	5.98	78.68
92	7.86	5.09	64.76
95	10.77	6.86	63.7
97	2.34	1.24	52.99
103	4.99	4.43	88.78
104	8.8	4.06	46.14
106	7.9	6.17	78.1

Discussion

The involvement of cysteine peptidases, including cathepsins B, L and K in cancer has inspired scientists to investigate changes in CP-like activity in the serum of patients with breast cancer in relation to changes in the activity of these enzymes. There are a number of papers presenting the inhibition of CPs using various substances, including CEWC. In our study, we decided to demonstrate the effects of CEWC on blood components, including autogenic CPs (Tables 1a,b). Findings on the efficiency of this inhibitor, E-64, and other synthetic inhibitors generated interest in them as potential components in next-generation anticancer drugs. They have been reported to be efficient inhibitors in some processes that play

Table 1b. Effects of CEWC on CP-like activity in the sera of patients with breast cancer (samples with increased fluorescence)

Sample No.	CP-like activity in serum [U/mL]	CP-like activity in serum + cystatin [U/mL]	Remaining activity + cystatin (%)
2	21.96	26.76	121.86
3	8.08	7.63	94.43
5	4.47	5.84	130.65
7	2.65	4.69	176.98
8	8.19	9.70	118.44
10	5.12	5.15	100.59
11	4.55	8.80	193.41
12	1.42	2.78	195.77
13	10.56	13.05	123.58
15	4.6	6.89	149.78
16	3.7	3.8	102.70
17	7.9	17.83	225.70
18	1.55	6.61	426.45
18	10.78	11.44	106.12
20	8.82	12.69	143.88
23	4.65	4.69	100.86
26	5.48	7.18	131.02
27	5.9	7.26	123.05
28	5.8	6.42	110.69
29	8.34	10.08	120.86
30	4.5	4.84	107.56
31	4.88	5.74	117.62
32	4.73	6.09	128.75
33	10.35	12.38	119.61
34	5.55	7.71	138.92
35	5.3	8.43	159.06
36	1.57	2.46	156.69
39	15.36	16.08	104.69
41	2.33	7.73	331.76
42	3.64	7.78	213.74
48	4.47	5.84	130.65
50	2.65	4.69	176.98
51	8.19	9.7	118.44
53	5.12	5.15	100.59
54	4.55	8.8	193.41
55	1.42	2.78	195.77
56	10.56	13.05	123.58
58	4.6	6.89	149.78
59	3.7	3.8	102.70
60	7.9	17.83	225.70
61	1.55	6.61	426.45
62	10.78	11.44	106.12
63	8.82	12.69	143.88
66	4.65	4.69	100.86
69	5.48	7.18	131.02
70	5.9	7.26	123.05
71	5.8	6.42	110.69
72	8.34	10.08	120.86
73	4.5	4.84	107.56
74	4.88	5.74	117.62
75	4.73	6.09	128.75
76	10.35	12.38	119.61
77	5.55	7.71	138.92
78	5.3	8.43	159.06
79	1.57	2.46	156.69
82	15.36	16.08	104.69
84	2.33	7.73	331.76
85	3.64	7.78	213.74
87	7.7	12.58	163.38
89	7.9	8.1	102.53
91	8.9	10.93	122.81
93	6.41	14.42	224.96
94	4.77	12.02	251.99
96	4.86	7.44	153.09
98	5.02	7.75	154.38
99	2.35	3.57	151.91
100	5.73	7.27	126.88
101	5.16	5.39	104.46
102	8.23	10.19	123.82
105	3.63	5.1	140.5
107	4.12	6.8	165.05
108	15.36	17.18	111.85

key roles in cancer development. Our research is focused on finding CP inhibitors that would be non-toxic and could replace or supplement the relevant autogenic analogues, including cystatins, in a patient's body.[2,17–19] A deficiency of autogenic cysteine peptidase inhibitors with simultaneous overexpression of these enzymes are key factors responsible for neoplastic processes. Because of this disturbed balance, researchers have suggested supplementing the level of active CP inhibitors in patients' bodies by using exogenous inhibitors that are able to block overexpression in vivo. So far, the efficiency of chemically synthesized inhibitors has been best investigated, particularly CA-074Me and E-64. However, they were found to be too toxic to humans to be used for scheduled anticancer therapy, and so far they have only been tested on cell lines and experimental animal models.[18–22]

Our choice of research topic was inspired by findings about the use of specific cysteine peptidase inhibitors for the in vitro regulation of neoplastic processes. Two of these inhibitors were found to be very effective. It was found that

Table 2. Changes in cysteine peptidase-like activity induced by CEWC and E-64 in selected serum samples from patients with breast cancer

Sample No.*	CP-like activity in serum [U/mL]	CP-like activity in serum M + E-64 [U/mL]	Remaining CP-like activity in serum + E-64 (%)	Remaining CP-like activity in serum + cystatin [U/mL]	Remaining CP-like activity in serum + cystatin (%)
87	7.7	6.8	**88.31**	12.58	163.38
88	**7.0**	**6.72**	**96**	**5.52**	**78.86**
89	7.9	9.12	115.44	8.1	102.53
90	**7.6**	**7.37**	**96.97**	**5.98**	**78.68**
91	8.9	11.51	129.33	10.93	122.81
92	**7.86**	**0.99**	**12.6**	**5.09**	**64.76**
93	**6.41**	**0.1**	**1.56**	14.42	224.96
94	4.77	5.17	108.39	12.02	251.99
95	**10.77**	**3.11**	**28.88**	**6.86**	**63.7**
96	4.86	10.5	216.05	7.44	153.09
97	**2.34**	**1.95**	**83.33**	**1.24**	**52.99**
98	**5.02**	**2.63**	**52.39**	7.75	154.38
99	2.35	3.06	130.21	3.57	151.91
100	**5.73**	**4.97**	**86.74**	7.27	126.88
101	**5.16**	**4.57**	**88.57**	5.39	104.46
102	8.23	10.15	123.33	10.19	123.82
103	4.99	5.15	103.21	**4.43**	**88.78**
104	**8.8**	**3.86**	**43.86**	**4.06**	**46.14**
105	**3.63**	**2.6**	**71.63**	5.1	140.5
106	**7.9**	**5.03**	**63.67**	**6.17**	**78.1**
107	**4.12**	**3.1**	**75.24**	6,8	165.05
108	15.36	15.5	100.91	17.18	111.85

* Sample numbers in bold font were previously depicted in Table 1a; samples in standard font were previously depicted in Table 1b.
Samples with inhibited activity are in bold font. Samples with increased fluorescence are in standard font.

the activity of cysteine peptidases associated with breast cancer cells was most effectively inhibited by CEWC and, to a lesser extent, by E-64 peptide (Table 2). This indicates that these inhibitors can be used as potential components of anticancer drugs targeting processes that regulate cancer progression.[14] Recent studies have also indicated that E-64 cannot be used in practice, not only because of its high price, but also its significant toxicity. The dose of E-64 used in vitro or in vivo in experimental studies on animals per kilogram of human body weight is highly toxic, and therefore cannot be used as a potential component of novel anticancer drugs.

The results of our study indicate that CEWC, or its derivatives obtained from other biological sources, may be a potential component of next-generation anticancer drugs. So far, numerous in vitro studies have also confirmed that this cystatin is highly efficient in inhibiting the activity of enzymes associated with major neoplastic processes. This suggests that inhibitors isolated from biological sources – chicken egg white protein, in particular – may be new targets for anticancer therapy. It is also known that CEWC shows more than 40% similarity to its autogenic analogues in the human body. This suggests that a new therapeutic target can be planned to employ this inhibitor as a potential component of next-generation anticancer drugs for "inhibitor therapy".[23,24] The results presented in this paper provide additional information suggesting the use of CEWC for the inhibition of CP overexpression in cancer patients (Table 1a). Surprisingly, CEWC caused an increase in fluorescence in about 60% of the serum samples from patients with breast cancer, which suggests the activation of autogenic cysteine peptidases (Table 1b).

This observation was confirmed by replacing CEWC with another inhibitor, E-64, which also inhibited the CP activity in some serum samples, and increased fluorescence in other samples (Table 2). Other results indicated differences in inhibiting CP-like activity and pure cathepsin B by CEWC. The findings from our study are insufficient to suggest the activation of autogenic CP or differences between CP-like activity and pure cathepsin B (Table 3). Nevertheless, it is important that the same incomplete inhibitory effect on CP-like activity was obtained in about 30% of the samples, and that fluorescence increased in the remaining samples, which was similar to serum samples from patients with prostate cancer (unpublished data). Similar results were reported 20 years ago in a paper on a peptide isolated from the urine of patients with colorectal cancer which was able to activate autogenic CP-like activity. This study from 20 years ago and the findings of our research

Table 3. Inhibitory effect of commercially available cathepsin B on autogenic CP-like activity in 9 serum samples from patients with breast cancer

Sample no.	CP-like activity in serum [U/mL]	CP-like activity in serum + 10 pl cathepsin B [U/mL]	CP-like activity in serum + cystatin [U/mL]	Remaining activity + cystatin (%)
2	21.96	**81.79**	28.13	128.10
13	10.56	**77.39**	13.11	124.15
33	10.35	**73.15**	11.97	115.65
42	3.64	**59.67**	8.18	224.73
51	8.19	**65.93**	10.23	124.91
76	10.35	**73.14**	11.97	115.65
64	**2.75**	**62.12**	**1.97**	**71.64**
81	**6.38**	**69.02**	**6.03**	**94.51**
86	**6.33**	**67.80**	**5.58**	**88.15**

Samples with inhibited activity are in bold font. Samples with increased fluorescence are in standard font.

seem to be complementary, but require additional studies to find a detailed explanation.[25]

The results presented herein provide important additional information, not only regarding CEWC tested in vitro on cell lines, but also about the use of CEWC for the inhibition of autogenic CP-like activity in the ascitic fluid of patients with pancreatic cancer, tumor tissue homogenates of the stomach, colon, and tongue, and ovarian cancer inhibited by a CP inhibitor isolated from human placenta. In these tests, CEWC showed an inhibitory effect on the activity of cysteine peptidases in almost 100% of samples. However, this experiment was not aimed at the complete inhibition of CPs; the target range was 50–80% in order to assess differences between the samples depending on the patients' cancer stage. The relevant results have been published.[26–31] Chicken egg white cystatin and its analogues isolated from placentas were also used in the experimental anticancer therapies, where they inhibited neoplastic processes in experimental animals with a grafted human inhibitor, or in combined inhibitor therapy, and photodynamic therapy.[32–35] Current research on the effects of CEWC on blood components in cancer patients have provided useful information for the assessment of this inhibitor as a potential component of new generation anticancer drugs for inhibitor therapy. The effects of CEWC on autogenic CP-like activity require additional studies in order to evaluate its suitability for intravenous administration.

Limitations

The limitations of this study were caused by the lack of some reagents and limited access to medical equipment.

Conclusions

The results suggest that there may be a potential difference between the commercially available cathepsin B and its autogenic analogues found in the serum of cancer patients. The increase in fluorescence induced in the reaction between the inhibitors and autogenic CPs is still unexplained. There was no relationship between the observed inhibition/activation of CPs and any of the available indicators of the health of the patients examined.

References

1. Weidle UH, Tiefenthaler G, Georges G. Proteases as activators for cytotoxic prodrugs in antitumor therapy. *Cancer Genom Proteom*. 2014;11(2):67–79. PMID:24709544
2. Turk V, Stoka V, Vasiljeva O, et al. Cysteine cathepsins: From structure, function and regulation to new frontiers. *Biochim Biophys Acta*. 2012;1824(1):68–88. doi:10.1016/j.bbapap.2011.10.002
3. Cudic M, Fields GB. Extracellular proteases as targets for drug development. *Curr Protein Pept Sci*. 2009;10(4):297–307. doi:10.2174/138920309788922207
4. Kos J, Lah TT. Cysteine proteinases and their endogenous inhibitors: Target proteins for prognosis, diagnosis and therapy in cancer. *Oncol Rep*. 1998;5(6):1349–1361. doi:10.3892/or.5.6.1349
5. Gondi CS, Rao JS. Cathepsin B as a cancer target. *Expert Opin Ther Targets*. 2013;17(3):281–291. doi:10.1517/14728222.2013.740461
6. Keppler D. Towards novel anti-cancer strategies based on cystatin function. *Cancer Lett*. 2006;235(2):159–176. doi:10.1016/j.canlet.2005.04.001
7. Zhong YJ, Shao LH, Li Y. Cathepsin B-cleavable doxorubicin prodrugs for targeted cancer therapy. *Int J Oncol*. 2013;42(2):373–383. doi:10.3892/ijo.2012.1754
8. Magister S, Kos J. Cystatins in immune system. *J Cancer*. 2013;4(1):45–56. doi:10.7150/jca.5044
9. Mullins SR, Sameni M, Blum G, Bogyo M, Sloane BF, Moin K. Three-dimensional cultures modeling premalignant progression of human breast epithelial cells: Role of cysteine cathepsins. *Biol Chem*. 2012;393(12):1405–1416. doi:10.1515/hsz-2012-0252
10. Nomura T, Katunuma N. Involvement of cathepsins in the invasion, metastasis and proliferation of cancer cells. *J Med Invest*. 2005;52(1–2):1–9. doi:10.2152/jmi.52.1
11. Szpaderska AM, Frankfater A. An intracellular form of cathepsin B contributes to invasiveness in cancer. *Cancer Res*. 2001;61(8):3493–3500. PMID:11309313
12. Frlan R, Gobec S. Inhibitors of cathepsin B. *Curr Med Chem*. 2006;13(19):2309–2327. doi:10.2174/092986706777935122
13. Tomoo K. Development of cathepsin inhibitors and structure-based design of cathepsin B-specific inhibitor. *Curr Top Med Chem*. 2010;10(7):696–707. doi:10.2174/156802610791113441
14. Premzl A, Puizdar V, Zavasnik-Bergant V, et al. Invasion of ras-transformed breast epithelial cells depends on the proteolytic activity of cysteine and aspartic proteinases. *Biol Chem*. 2001;382(5):853–857. doi:10.1515/BC.2001.104
15. Anastasi A, Brown MA, Kembhavi AA, et al. Cystatin, a protein inhibitor of cysteine proteinases. Improved purification from egg white, characterization, and detection in chicken serum. *Biochem J*. 1983;211(1):129–138. doi:10.1042/bj2110129

16. Barrett AJ, Kirschke H. Cathepsin B, cathepsin H, and cathepsin L. *Methods Enzymol.* 1981;80(Pt C):535–561. doi:10.1016s0076-6879(81)80043-2.
17. Saleem M, Qadir MI, Perveen N, et al. Inhibitors of apoptotic proteins: New targets for anticancer therapy. *Chem Biol Drug Des*. 2013;82(3):243–251. doi:10.1111/cbdd.12176
18. Lankelma JM, Voorend DM, Barwari T, et al. Cathepsin L, target in cancer treatment? *Life Sci*. 2010;86(7–8):225–233. doi:10.1016/j.lfs.2009.11.016
19. Palermo C, Joyce JA. Cysteine cathepsin proteases as pharmacological targets in cancer. *Trends Pharmacol Sci*. 2008;29(1):22–28. doi:10.1016/j.tips.2007.10.011
20. Katunuma N. Structure-based development of specific inhibitors for individual cathepsins and their medical applications. *Proc Jpn Acad Ser B Phys Biol Sci*. 2011;87(2):29–39. doi:10.2183/pjab.87.29
21. Montaser M, Lalmanach G, Mach L. CA-074, but not its methyl ester CA-074Me, is a selective inhibitor of cathepsin B within living cells. *Biol Chem*. 2002;383(7–8):1305–1308. doi:10.1515/BC.2002.147
22. Szpaderska AM, Frankfater A. An intracellular form of cathepsin B contributes to invasiveness in cancer. *Cancer Res*. 2001;61(8):3493–3500. PMID:11309313
23. Saitoh E, Isemura S, Sanada K. Cystatin superfamily. Evidence that family II cystatin genes are evolutionary related to family III cystatin genes. *Biol Chem Hoppe Seyler.* 1988;369(Suppl):191–197. PMID:3202964
24. Agrawal AK, Ekonjo GB, Teterycz E, et al. Cysteine peptidases and their inhibitors in breast and genital cancer. *Folia Histochem Cytobiol*. 2010;48(3):323–327. doi:10.2478/v10042-10-0067-2
25. Siewinski M, Gutowicz J, Kielan W, Bolanowski M. Cysteine peptidase inhibitors and activator(s) in urine of patients with colorectal cancer. *Oncology*. 1994;51(5):446–449. https://doi.org/10.1159/000227381
26. Agrawal AK, Kielan W, Katib A, et al. Inhibition of cysteine peptidase activity in ascitic fluid in pancreatic cancer patients. *Folia Histochem Cytobiol*. 2010;48(4):513–517. doi:10.2478/v10042-010-0057-4
27. Saleh Y, Siewinski M, Kielan W, Ziolkowski P, Grybos M, Rybka J. Regulation of cathepsin B, L expression in vitro in gastric cancer tissues by egg white cystatin. *J Exp Ther Oncol*. 2003;3(6):319–324. doi:10.1111/j.1533-869x.2003.01105.x
28. Hap A, Kielan W, Grzebieniak Z, et al. Control of active B and L cathepsins in tissues of colorectal cancer using cystatin isolated from chicken egg proteins: In vitro studies. *Folia Histochem Cytobiol*. 2011;49(4):670–676. doi:10.5603/FHC.2011.0075
29. Saleh Y, Wnukiewicz J, Trziszka T, Siewinski M, Ziolkowski P, Kopec W. Cathepsin B and cysteine protease inhibitors in human tongue cancer: Correlation with tumor staging and in vitro inhibition of cathepsin B by chicken cystatin. *J Cancer Molecules*. 2006;2:67–72.
30. Saleh Y, Siewinski M, Sebzda T, et al. Inhibition of cathepsin B activity in human breast cancer tissue by cysteine peptidase inhibitor isolated from human placenta – immunihistochemical and biochemical studies. *Folia Histochem Cytobiol*. 2003;41(3):161–167. PMID:13678335
31. Siewinski M, Saleh Y, Popiela A, Ziolkowski P, Jelen M, Grybos M. Expression of high molecular weight cysteine proteinase inhibitor in ovarian cancer tissues: Regulation of cathepsin B expression by placental CPI. *Biol Chem*. 2003;384(7):1103–1107. doi:10.1515/BC.2003.123
32. Saleh Y, Siewinski M, Sebzda T, Grybos M, Pawelec M, Janocha A. Effect of combined in vivo treatment of transplantable solid mammary carcinoma in Wistar rats using vitamin E and cysteine peptidase inhibitors from human placenta. *J Exp Ther Oncol*. 2003;3(2):95–102. doi:10.1046/j.1359-4117.2003.01077.x
33. Sebzda T, Saleh Y, Siewinski M, Rudnicki J, Ziolkowski P. The influence of vitamin E and human placenta cysteine peptidase inhibitor on the expression of cathepsin B and L implanted hepatoma Morris 5123 tumor model in the Wistar rats. *World J Gastroenterol*. 2005;11(4):587–592. doi:10.3748/wjg.v11.i4.587
34. Saleh Y, Ziolkowski P, Siewinski M, Milach J, Marszalik P, Rybka J. The combined treatment of transplantable solid mammary carcinona in wistar rats by use photodynamic therapy and cysteine proteinase inhibbitors. *In Vivo*. 2001;15(4):351–357. PMID:11695229
35. Zsebik B, Symonowicz K, Saleh J, Ziolkowski P, Bronowicz A, Verb G. Photodynamic therapy combined with a cysteine proteinase inhibitor synergistically decrease VEGF production and promotor tumor necrosis in a rat mammary carcinoma. *Cell Profil*. 2007;40(1):38–49. doi:10.1111/j.1365-2184.2007.00420.x

Does the choice of drug in pharmacologic cardioversion correlate with the guidelines? Systematic review

Janusz Springer[1,A–F], Tomasz Szmuda[2,B–F], Dariusz Kozłowski[3,A,E,F]

[1] Department of Emergency Medicine, Medical University of Gdańsk, Poland
[2] Department of Neurosurgery, Medical University of Gdańsk, Poland
[3] Department of Cardiology and Electrotherapy, Medical University of Gdańsk, Poland

A – research concept and design; B – collection and/or assembly of data; C – data analysis and interpretation;
D – writing the article; E – critical revision of the article; F – final approval of the article

Advances in Clinical and Experimental Medicine, ISSN 1899–5276 (print), ISSN 2451–2680 (online) *Adv Clin Exp Med*. 2021;30(3):331–348

Address for correspondence
Janusz Springer
E-mail: janusz.springer@gumed.edu.pl

Funding sources
None declared

Conflict of interest
D. Kozłowski reports grants and lecture fees from Polpharma and Sanofi-Aventis.

Acknowledgements
The authors thank Zuzanna Konieczna-Czerwińska for the illustration. In addition, we thank Alexandra Asanovna Elbakyan MSc for her immense help with the literature search.

Received on September 29, 2020
Reviewed on November 5, 2020
Accepted on November 18, 2020

Published online on March 23, 2021

Abstract

Background. Atrial fibrillation (AF) is the most common sustained arrhythmia, the most common cause of supraventricular tachycardia in the global population and the most common arrhythmia requiring treatment in an emergency department.

Objectives. To systematically review recent literature and quantify the correlation between the choice of pharmacological cardioversion (PCV) drug and the national or international guidelines.

Materials and methods. A systematic review was performed in accordance with the PRISMA statement methodology. The PubMed search engine was used to search for articles regardless of type or language and published in the last 6 years (May 2014–May 2020). In addition, we searched for AF guidelines and recommendations published online by cardiology and emergency medicine societies.

Results. The search strategy returned a total of 2615 abstracts. A total of 2598 full texts were screened; 2540 full texts were excluded with reasons and 58 articles from 32 countries were included in the analysis. In 17 of the 58 articles (29%), we noted discrepancies with the AF guidelines, specifically regarding the PCV drug used, the patients' comorbidities and the contraindications associated with the PCV drug. The most common clinical situation for the use of a contraindicated drug was when ibutilide was administered to patients with heart failure. The analysis did not reveal any statistically significant correlations, although the correlation between the sample size and guideline adherence was close to statistical significance ($p < 0.06$).

Conclusions. Our systematic analysis revealed substantial non-adherence to AF treatment guidelines.

Key words: atrial fibrillation, cardioversion, guideline adherence, antiarrhythmic

Cite as
Springer J, Szmuda T, Kozłowski D. Does the choice of drug in pharmacologic cardioversion correlate with the guidelines? Systematic review. *Adv Clin Exp Med*. 2021;30(3):331–348. doi:10.17219/acem/130592

DOI
10.17219/acem/130592

Background

Atrial fibrillation (AF) is the most common sustained arrhythmia and the most common cause of supraventricular tachycardia in the world.[1,2] Furthermore, acute AF is a common complaint among emergency department (ED) patients and is the most common arrhythmia requiring treatment in the ED.[3] It commonly occurs because AF is often caused by common diseases (see Table 1). However, ongoing academic discussions seek to answer whether a patient with AF who does not have any cardio-pulmonary disease should be diagnosed with "lone AF".[4] According to the latest AF guidelines published by the European Society of Cardiology (ESC), the term/diagnosis of "lone AF" should not be used because AF always has an underlying cause.[5]

Table 1. Etiology of atrial fibrillation (AF) (according to Benjamin et al. and Kirchhof et al.)

Ageing
Cardiomyopathies
Chronic obstructive pulmonary disease
Coronary artery disease
Diabetes
Heart failure
Heart valve disease
Hypertension
Obesity
Post-operative
Thyroid disease
Unknown (not yet diagnosed, formerly "lone AF")

There are 2 widely accepted and separate goals of AF treatment: rate control and rhythm control. In the case of paroxysmal AF, a clinician has a choice of 2 methods to restore sinus rhythm (SR): pharmacological (chemical) cardioversion (PCV) or electric cardioversion (ECV). According to a large international emergency physician survey, PCV is the first line of treatment for recent-onset AF.[6] The efficacy of PCV in restoring sinus rhythm varies among published studies and is subject to ongoing debate.

When deciding to perform PCV, clinicians have several antiarrhythmic drugs to choose from, which are listed in national and international guidelines (Table 2). Little is known about adherence to AF guidelines when it comes to PCV, particularly in the ED.

Objectives

The aim of this study was to systematically review the most recent literature in an attempt to answer the following clinical question: Do recently published articles about PCV reveal any correlation between the choice of PCV drug and national or international guidelines?

Materials and methods

A systematic review was performed in accordance with the Preferred Reporting Items for Systematic Reviews and Meta-Analyses (PRISMA) statement methodology.[7] The PubMed search engine was used to find articles regardless of type or language and published in the last 6 years (May 2014–May 2020). The unusual six-year timespan was purposefully chosen because the American Heart Association (AHA)/American College of Cardiology (ACC)/Heart Rhythm Society (HRS) and National Institute for Health and Care Excellence (NICE) guidelines were published in December and August of 2014, respectively.[6,7] The following search terms were applied: atrial fibrillation AND pharmacological cardioversion AND antazoline OR amiodarone OR dronedarone OR flecainide OR ibutilide OR procainamide OR propafenone OR vernakalant.

(((((((("atrial fibrillation"[MeSH Terms] OR ("atrial"[All Fields] AND "fibrillation"[All Fields]) OR "atrial fibrillation"[All Fields]) AND (("pharmacology"[MeSH Terms] OR "pharmacology"[All Fields] OR "pharmacological"[All Fields]) AND ("electric countershock"[MeSH Terms] OR ("electric"[All Fields] AND "countershock"[All Fields]) OR "electric countershock"[All Fields] OR "cardioversion"[All Fields]))) AND ("antazoline"[MeSH Terms] OR "antazoline"[All Fields])) OR ("amiodarone"[MeSH Terms] OR "amiodarone"[All Fields])) OR ("dronedarone"[MeSH Terms] OR "dronedarone"[All Fields])) OR ("flecainide"[MeSH Terms] OR "flecainide"[All Fields])) OR ("ibutilide"[Supplementary Concept] OR "ibutilide"[All Fields])) OR ("propafenone"[MeSH Terms] OR "propafenone"[All Fields])) OR ("procainamide"[MeSH Terms] OR " procainamide"[All Fields])) OR ("vernakalant"[Supplementary Concept] OR "vernakalant"[All Fields]) AND ("2014/05/01"[PDAT] : "2020/05/01"[PDAT])

The search strategy yielded a total of 2615 abstracts. A total of 2598 (full texts) were screened, of which 2540 were excluded with reasons (Fig. 1). Although they included large patient samples, meta-analyses were excluded due to an insufficient amount of detail about PCV and the patients' comorbidities. Articles describing the use of antiarrhythmic drugs as prophylaxis of AF prior to surgery were also excluded. So-called "pre-treatment" studies with an antiarrhythmic drug immediately prior to electric cardioversion did not meet the criteria of PCV and were also excluded. The following data was extracted from the 58 eligible full-text articles: number of patients (n), patient age (or average age), patient sex, etiology of AF (or significant comorbidities), antiarrhythmic drug chosen for PCV, dose, bolus or infusion, success of PCV, time to SR, management after PCV attempt (e.g., Was the dose of PCV drug repeated? Was another antiarrhythmic drug administered? Was ECV performed instead?), and country where the patients were treated.

Data were extracted from the articles and entered into Excel spreadsheets (Microsoft Office 2007; Microsoft Corp., Redmond, USA) and subsequently exported to STATISTICA v. 12.0 (StatSoft Inc., Tulsa, USA) for analysis.

Table 2. Pharmacological cardioversion recommendations published in national and international guidelines

Drug	Route	Dose								Indications (class, source)	Contraindications (class, source)
		ACEP	AHA/ACC/HRS 2014 + 2019 update	CAEP 2018	CCS 2018	ERC 2015	ESC 2016	NHFA/ CSANZ 2018	NICE 2014		
Amiodarone	iv*	not stated	150 mg over 10 min, then 1 mg/min for 6 h, then 0.5 mg/min for 18 h or change to oral dosing	not recommended	150 mg bolus, then 60 mg/h for 6 h, then 30 mg/h for 18 h	300 mg over 20–60 min followed by 900 mg over 24 h. Less effective than flecainide, ibutilide, and propafenone	5–7 mg/kg over 1–2 h; follow-up dose: 50 mg/h to a maximum of 1.0 g over 24 h	recommended	recommended for patients with structural heart disease	newly detected HF in the presence of AF with a rapid ventricular response (AHA), hypertrophic cardiomyopathy + AF (AHA Class IIa), ACS + AF associated with severe LV dysfunction and HF or hemodynamic instability (AHA Class IIb), severely impaired heart function (ERC), HF + AF (ESC), IHD + AF (ESC), structural heart disease (CCS)	hyperthyroidism + AF ("Antiarrhythmic drugs and cardioversion often fail to achieve sustained sinus rhythm while thyrotoxicosis persists; therefore, efforts to restore normal sinus rhythm may be deferred until the patient is euthyroid." – AHA)
Antazoline	iv	not stated	not stated	not stated	not stated	not stated	not stated	not stated	not stated	paroxysmal atrial arrhythmias including tachycardia/ AF, nor reacting to standard treatment	avoid in patients with history of seizures, concurently using MAO inhibitors, anticholinergic drugs, CNS depressants, or alcohol); use carefully in patients with HTN, DM, hyperthyroidism, and prostatic hyperplasia
Flecainide	po	300 mg PO ×1 if ≥70 kg or 200 mg PO ×1 if <70 kg	200–300 mg ×1**	not stated	300 mg (>70 kg), 200 mg (≤70 kg)	recommended; more effective than amiodarone	200–300 mg; iv: 1.5–2 mg/kg over 10 min	recommended; more effective than amiodarone	recommended for patients without ischemic or structural heart disease	no evidence of structural or ischemic heart disease + AF (ACEP, NICE)	known ischemic or structural heart disease + AF (ESC, NICE), LV systolic dysfunction, moderate LV hypertrophy or coronary artery disease (GRADE: Strong, Evidence: Moderate, NHFA)
Ibutilide	iv	1 mg iv over 10 min; may repeat same dose 10 min after first infusion if still in AF; if still in AF at 60 min after last infusion consider electrical cardioversion	1 mg over 10 min; may repeat 1 mg once if necessary (if weight <60 kg, use 0.01 mg/kg)	not stated	1 mg iv over 10 min, may repeat once	recommended; more effective than amiodarone	1 mg over 10 min; follow-up dose: 1 mg over 10 min after waiting for 10 min	not stated	not stated	post-cardiac and thoracic surgery + AF (AHA Class IIa), hemodynamically stable WPW and pre-excitation syndromes + AF (AHA Class IIa), "no need to confirm lack of structural heart disease or occlusive coronary disease" (ACEP)	long QTc, hypokalemia, HF (ACEP, CAEP, ESC), severe LVH (ESC), hypomagnesemia (CCS)

Table 2. Pharmacological cardioversion recommendations published in national and international guidelines – cont.

Drug	Route	Dose								Indications (class, source)	Contraindications (class, source)
		ACEP	AHA/ACC/HRS 2014 + 2019 update	CAEP 2018	CCS 2018	ERC 2015	ESC 2016	NHFA/CSANZ 2018	NICE 2014		
Procainamide	iv	not stated	not stated	15 mg/kg in 500 mL NS over 30–60 min	15–18 mg/kg over 30–60 min	not stated	not stated	not stated	not stated	hemodynamically stable WPW and pre-excitation syndromes + AF (AHA Class I), (CAEP)	Brugada syndrome (CCS), hypotension (SBP < 100 mm Hg) or long QT (QTc > 500 ms) (CAEP)
Propafenone	po	not stated	450–600 mg ×1**	not stated	600 mg (>70 kg), 450 mg (≤70 kg)	recommended; more effective than amiodarone	450–600 mg; iv: 1.5–2 mg/kg over 10 min	not stated	not stated	COPD + AF ("may be considered in patients with obstructive lung disease who develop AF and do not have bronchospasm" – AHA)	COPD + AF ("contraindicated in patients with bronchospasm" – AHA), known ischemic or structural heart disease + AF (ESC, NICE)
Vernakalant	iv	not stated	not stated	not stated	3 mg/kg over 10 min, followed by 2 mg/kg if no conversion	not stated	3 mg/kg over 10 min/follow-up dose: 2 mg/kg over 10 min after waiting for 15 min	not stated	not stated	mild HF (NYHA Class I–II) + AF, IHD + AF (ESC)	avoid in patients with hypotension (SBP < 100 mm Hg), recent (<30 days) ACS, HF (NYHA Class III–IV), QT long QT (uncorrected >440 ms) and severe aortic stenosis (CCS, ESC)

* Use a large peripheral vessel and change to oral amiodarone within 24 h of IV (central line) administration.
** It is recommended to pre-treat with a β-blocker or nondihydropyridine calcium channel antagonist ≥30 min before administering this drug.
ACEP – American College of Emergency Physicians; ACS – acute coronary syndrome; AF – atrial fibrillation; AHA/ACC/HRS – American Heart Association/American College of Cardiology/Heart Rhythm Society; AV – atrio-ventricular; CAD – coronary artery disease; CAEP – Canadian Association of Emergency Physicians; CCS – Canadian Cardiovascular Society; COPD – chronic obstructive pulmonary disease; ERC – European Resuscitation Council; ESC – European Society of Cardiology; GI – gastrointestinal; IHD – ischemic heart disease; iv – intravenous; LV – left ventricular; MAO – monoamine oxidase; NICE – National Institute for Health and Care Excellence; NHFA/CSANZ – National Heart Foundation of Australia/Cardiac Society of Australia and New Zealand; NYHA – New York Heart Association; po – per os (orally); SBP – systolic blood pressure WPW – Wolff–Parkinson–White syndrome.

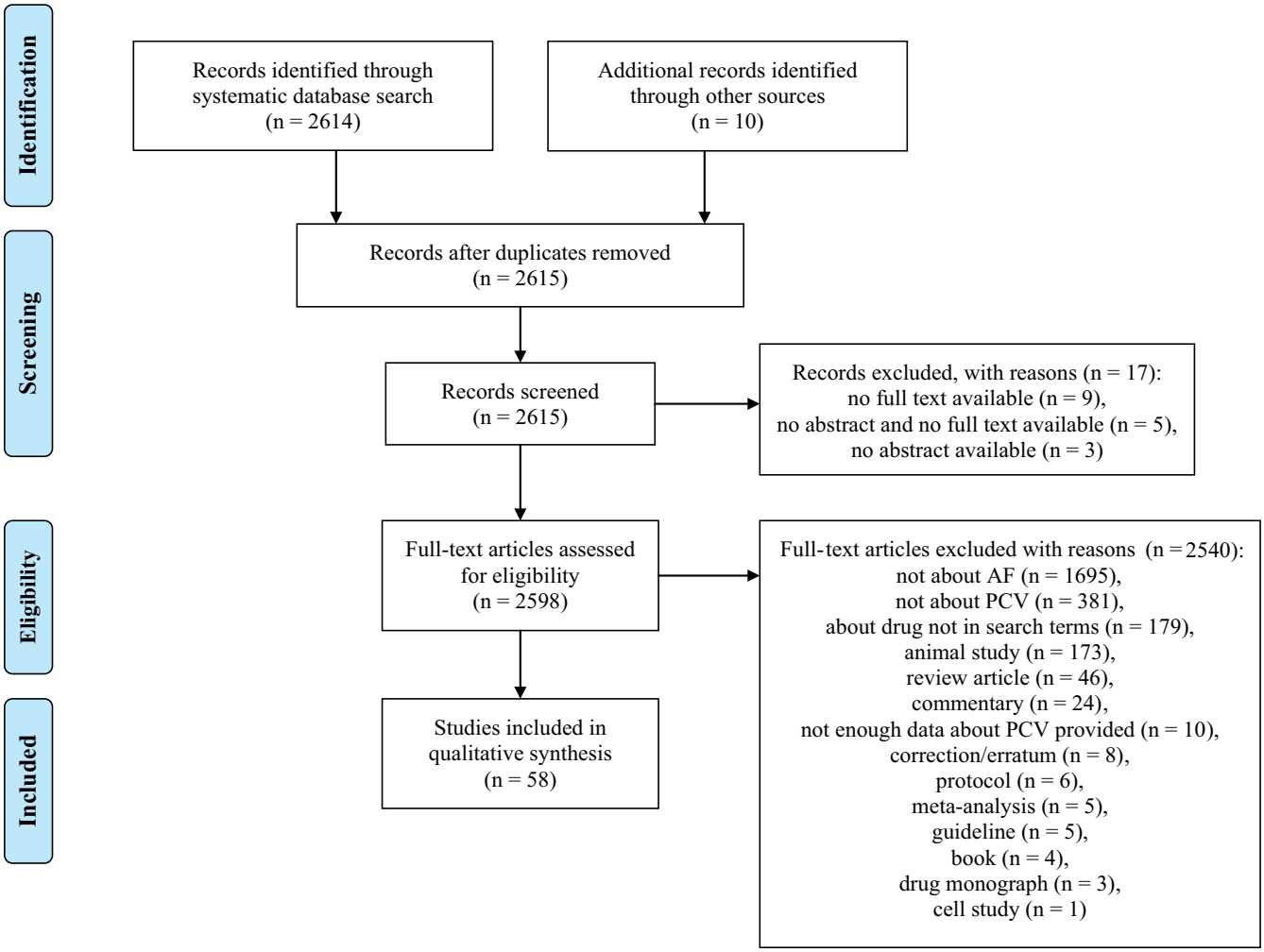

Fig. 1. Flowchart of the literature search strategy

The following statistical tests were performed: Mann–Whitney U test (for continuous variables) and Fisher's two-tailed test (for categorical variables). Values of $p < 0.05$ were considered statistically significant.

In addition, we searched for AF guidelines and recommendations published online by cardiology and emergency medicine societies. Our search returned guidelines from Australia (National Heart Foundation of Australia (NHFA)/Cardiac Society of Australia and New Zealand (CSANZ)),[8] Canada (Canadian Association of Emergency Physicians (CAEP), Canadian Cardiovascular Society (CCS)),[9,10] Europe (European Resuscitation Council (ERC), ESC)[5,11] UK (NICE),[12] and USA (American College of Emergency Physicians (ACEP), AHA/ACC/HRS) (Table 2).[13,14] We used these recommendations as a reference point to answer the research question described earlier.

Results

Our search returned 58 articles from 32 countries; most articles were published in 2017–2018 (Fig. 2,3).[15–71] Unfortunately, not all relevant data was provided by the authors, thus making it impossible to perform a full meta-analysis. Detailed results of the systematic review are summarized in Table 3 (Fig. 2,3).

Despite the incomplete data, the analyzed articles revealed a surprising trend of non-adherence to AF treatment guidelines. In 17 of the 58 articles (29%), we noted discrepancies with AF guidelines, specifically regarding the PCV drug used, the patients' comorbidities and the PCV contraindications (Table 4).[16,18,20–22,26–28,31,32,36,39,41,49,55,60,63] According to the data presented in the articles, it appeared that a total of 239 patients underwent PCV using a drug that was contraindicated given their specific comorbidities. In the described cases, the most common culprit PCV drug was ibutilide, followed by vernakalant, amiodarone, propafenone, and flecainide. The most commonly described clinical situation for the use of contraindicated drug was ibutilide when administered to a patient with HF, which is contraindicated according to the ACEP, CAEP and ESC guidelines (Table 2).[10,12,13,31,39,55,63] In 9 of the 17 articles, using a contraindicated drug during PVC was performed in the ED (Table 4).[21,22,26,27,32,36,39,55,63] Due to incomplete data, it was impossible to assess whether an additional 338 patients were administered a PCV drug that was contraindicated or not.[21,36] (Table 4).

Fig. 2. Number of analyzed articles describing pharmacological cardioversion in the particular country's patient population (illustration by Zu).

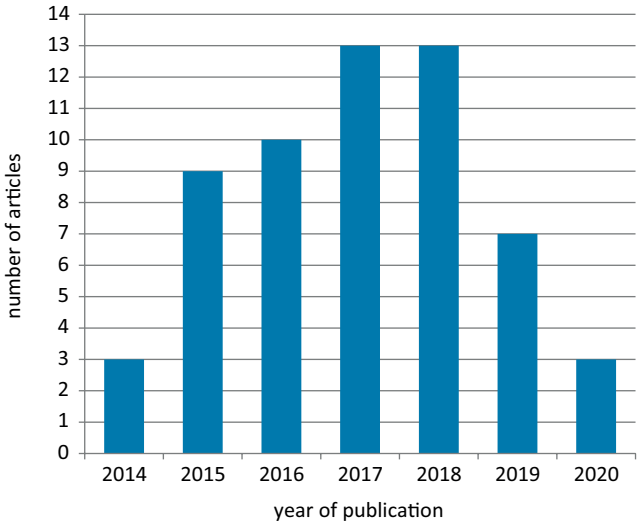

Fig. 3. Number of analyzed articles published in a given year

Analysis using the Mann–Whitney U test and Fisher's test did not reveal any statistically significant correlations between adherence to AF guidelines and demographic variables such as sample size, patient age, and male sex (Table 5). However, it is noteworthy that the correlation between the sample size and guideline adherence was close to statistical significance ($p < 0.059$). It appears that the larger the sample size, the less adherence was observed. The analysis using Fisher's two-tailed tests did not reveal any statistically significant correlations between adherence to AF guidelines and the type of study/article, region/country or department where the PCV was performed (Table 5).

It is noteworthy that our search retrieved a total of 6 articles (in 1612 patients) that included PCV using antazoline mesilate.[19,32–34,42,66] This is an old antihistaminic drug, which, despite its proven antiarrhythmic efficacy, is not currently mentioned in any AF guidelines.[72–74] According to publicly available data, it appears that the intravenous form of antazoline is registered and sold in Poland only; therefore, it is not surprising that majority of the research on antazoline was conducted and published by Polish physicians.[74–78]

Discussion

Although we found articles describing PCV performed on all of the inhabited continents of the world, we are aware that they do not necessarily reflect daily clinical practice. The articles we analyzed did not contain enough data to answer the question why the AF guidelines were not followed. We do not want to speculate about the particular authors' intent or the circumstances during the described PCV. However, given our institutional experience with PCV, we can think of several possible reasons, most of which are rather mundane or perhaps even temporary, e.g., the availability of antiarrhythmic drugs, institutional/personal experience with particular drug(s), and interest in comparing the efficacy of a new drug (e.g., vernakalant) compared to a "tried and tested" drug.

The very same issue of non-adherence with AF guidelines was addressed in the literature, although the answers

Table 3. Detailed results of the systematic review

Author(s)	Date of publication	Study type	Country	Number of patients	Age of patients [years]	Sex of patients	PCV setting	PCV drug	PCV drug dose and route	PCV successful, n	Time to SR [min]	Management after failed PCV attempt	Comorbidities	AF guideline adherence
Albakri et al.	VII 2017	case report	Germany	1	60	M	IMD	flecainide	1 mg/kg	1	30	after 25 min → 2nd infusion of flecainide 0.3 mg/kg	borderline hypertension without LV hypertrophy, obstructive bronchitis, episodic orthostatic intolerance (most probably vasovagal)	Y
Amin et al.	III 2015	prospective single-center observational	Netherlands	112	63 ±1	52 F, 60 M	CER	flecainide	2 mg/kg (maximum dose of 150 mg) iv infusion over 10 min	97	not stated	if AF 6 h after infusion → ECV	CAD 11, HTN 52, DM 8, THY 5	N
Andrade et al.	I 2018	prospective single-center observational	Canada	80	53.0 ±12.6	27 F, 53 M	AF clinic	immediate release AV nodal blocker + AAD Class Ic	diltiazem 30–60 mg po, verapamil 30–60 mg po or metoprolol 25–50 mg po + if <70kg → F: 200 mg po or PROP: 450 mg po; if ≥70kg → F: 300 mg po or P 600 mg po	in 30/43	<6 h	if AF 6 h after infusion → ECV	HVD 2, CAD 4, DM 8, HTN 16	Y
Balik et al.	X 2017	retrospective	Czech Republic	197	67.8 ±11.4 (amiodarone), 66.8 ±11.3 (propafenone)	not stated	ICU	amiodarone; propafenone	AMIO: 1.8–4.6 g iv infusion over 2–6 days; PROP: 460–700 mg/day iv infusion*	amiodarone in 114/197;	not stated	switch drugs, ECV	hyperthyroidism (5 A)	N
Balsam et al.	IX 2015	retrospective, non-randomized, no placebo-controlled observational study	Poland	141 (74 persistent AF, 67 paroxysmal AF)	57 (49–63)	38 F, 103 M	EPL	antazoline	maximum 500 mg iv 30–50 mg/min	in 79/141 (31% of persistent AF patients, 83% of paroxysmal AF patients)	≤20	not stated	HTN 69.3%, lone AF 22.7%, THY 18.4%, DM 12.1%, HVD 2.8%	Y
Beatch et al.	V 2016	RCT	Canada, Chile, Israel, Mexico, Peru, South Africa, USA	129	63.7 (SD 12.7)	53 F, 76 M	not stated	vernakalant	3 mg/kg iv infusion over 10 min	59	25% converted in ≤11; endpoint at 90	if AF 15 min after 1st infusion → vernakalant 2 mg/kg iv over 10 min; if AF 2 h after 1st infusion → ECV	HTN 89, HVD 27, CAD 18, DM 18	Y

Table 3. Detailed results of the systematic review – cont.

Author(s)	Date of publication	Study type	Country	Number of patients	Age of patients [years]	Sex of patients	PCV setting	PCV drug	PCV drug dose and route	PCV successful, n	Time to SR [min]	Management after failed PCV attempt	Comorbidities	AF guideline adherence
Beatch et al.	II 2017	RCT	China, Hong-Kong, India, Korea, Taiwan	55	60.7 ±13.7	18 F, 37 M	not stated	vernakalant	3 mg/kg iv infusion over 10 min	29	median 17, endpoint at 90	if AF 15 min after 1st infusion → 2 mg/kg iv over 10 min; if AF 2 h after 1st infusion → ECV	HF 5, IHD 4, VHD 2	N
Bonora et al.	IX 2017	retrospective propensity matching	Italy	179 (amiodarone), 179 (flecainide, propafenone)	66.2 ±12.8 (amio), 66.4 ±11.6 (flec or prop)	not stated	ED	amiodarone, flecainide, propafenone	AMIO: 5 mg/kg in a 20 min infusion; FLEC or PROP: 2 mg/kg in 15 min rapid infusion	after 12 h → A 95/179 and F or P 130/179; after 48 h → A 139/179 and F or P 154/179	A 420 (331.6–508.3); F or P 55 (44.8–65.1)	a 15 mg/kg dose in 24 h slow maintenance infusion)	IHD 76 (A), 18 (F or P); HTN 290 (A), 223 (F or P); VHD 48 (A), 53 (F or P); THY 23 (A), 67 (F or P)	N
Carbajosa et al.	X 2017	prospective multi-center observational	Spain	165	68 (56–77)	76 F, 89 M	ED	vernakalant	3 mg/kg iv infusion over 10 min	in 128/165	8 (6–12); after 2nd dose → 34 (22–62)	if AF 15 min after 1st infusion → vernakalant 2 mg/kg iv over 10 min	HTN 99, DM 16, HF 15	N
Champion et al.	VI 2018	prospective single-center observational	France	75	not stated	not stated	ICU	amiodarone	median dose of 300 mg (150–600 mg)	51	NS	ECV	not stated	Y
Chauveau et al.	VI 2019	case series	France	1	32	F	ICU	flecainide	100 mg iv	yes	NS	NA	speculation (thyroiditis? left-sided accessory pathway?)	Y
Comelli et al.	XI 2018	case report	Italy	1	56	M	ED	flecainide	100 mg iv infusion over 20 min	yes, spontaneous	~30	not stated	none	Y
Cosin-Sales et al.	VI 2016	prospective single-center observational	Spain	47	66 (24–89)	24 F, 23 M	ED	vernakalant	not stated	45	12.5 (1–115, median 8)	NS	HTN 28, DM 3, IHD 3, HF 1, CMP 1	N
Costabel et al.	II 2015	single-center, retrospective	Brazil	121	58.1 ±13.9	39 F, 82 M	ED	vernakalant	initial dose 3.0 mg/kg iv over 10 min	102	10	2nd dose 2 mg/kg iv	56 HTN, 16 structural heart disease, 6 HF (EF < 55%), 2 COPD, 2 DM	N
Dalyanoglu et al.	V 2018	single-center, retrospective	Germany	129	70.2 ±9.1	39 F, 90 M	CSD	vernakalant	3 mg/kg iv over 10 min	57	13.7 ±14.1	2nd dose 2 mg/kg iv over 10 min	124 CAD, 16 CAD + HVD, 37 DM, 70 hyperlipidemia, 109 HTN, 20 HVD, 21 LVEF < 50%	N

Table 3. Detailed results of the systematic review – cont.

Author(s)	Date of publication	Study type	Country	Number of patients	Age of patients [years]	Sex of patients	PCV setting	PCV drug	PCV drug dose and route	PCV successful, n	Time to SR [min]	Management after failed PCV attempt	Comorbidities	AF guideline adherence
Dasgupta et al.	III 2020	retrospective, single-center	USA	14	15 (14–17)	not stated	PED	ibutilide	if >60 kg: 1 mg iv over 10 min, if <60 kg 0.01 mg/kg iv over 10 min	9	not stated	a 2nd dose of equal amount, at the physician's discretion	not stated	Y
Dilber et al.	XI 2015	case report	Croatia	1	75	M	ED	amiodarone, propafenone	AMIO: 300 mg in 250 mL 5% dextrose solution iv infusion; PROP: 150 mg in 250 mL 5% dextrose solution iv infusion	0	NA	transesophageal echocardiography + ECV	HTN	Y
Dong et al.	VI 2017	prospective single-center observational	China	79	64.6 ±11.2 (40–80)	31 F, 48 M	not stated	ibutilide (39), ibutilide ± amiodarone (40)	AMIO 300 mg + I 1 mg iv; I 1 mg iv	I = 51.3% (20/39), A + I = 71.8% (28/39)	I 75–120; A+I 60–120	additional ibutilide 1 mg	CAD 51.31% (I), 47.11% (A+I); HTN 56.41%, 61.12%; DM 5.11%, 6.24%; HF 29.71%, 28.35%	N
Farkowski et al.	VI 2016	retrospective case-control	Poland	432	68.9 ±9.8	152 F, 280 M	ED	antazoline 334, propafenone 98	ANT: 50 mg every 3–5 min up to max 250–300 mg or SR; PROP: max 2 mg/kg iv slow bolus	A 239, P 54	not stated	other drug, ECV or discharge	CAD (A 138, P 28), DM (A 58, P 15), IHD (A 66, P 14), HTN (A 202, P 55), HVD (A 3, P 2), non-ischemic structural heart disease (A 3, P 0), THY (A 29, P 15)	N
Farkowski et al.	XII 2018	retrospective case-control	Poland	548	CAD(–) 66.9 ±9.9, CAD(+) 71.3 ±9.1	CAD(–) F 84, 112 M; CAD(+) F 27, 111 M	ED	antazoline	50 mg every 3–5 min up to max 250–300 mg or SR	CAD(–) 125, CAD(+) 114	not stated	not stated	HTN 95, 107; DM 10, 48; THY 23, 6; CAD(+): post-PCI 47, post-CABG 53, post-MI 65	Y
Farkowski et al.	V 2019	experimental prospective, control group	Poland	5	63.4 (59.9–66.8)	not stated	EPL	antazoline	257.1 (246.7–267.6) mg	5	8.4 ±6.2	not stated	not stated	Y
Gillinov et al.	IV 2016	multi-center RTC	Canada + USA	261	68.4 ±8.4	62 F, 199 M	CSD	amiodarone	3 g po before hospital discharge, with a maintenance dose of 200 mg/day or less for 60 days if direct-current cardioversion was successful	244 at hospital discharge, 227 from discharge to 60 days	not stated	ECV	all post-cardiac surgery (CABG 100, HVD 43, CABG + HVD 7), DM 79, HF 33, HTN 198, HVD 148, post-MI 48, post-stroke 15	Y

Table 3. Detailed results of the systematic review – cont.

Author(s)	Date of publication	Study type	Country	Number of patients	Age of patients [years]	Sex of patients	PCV setting	PCV drug	PCV drug dose and route	PCV successful, n	Time to SR [min]	Management after failed PCV attempt	Comorbidities	AF guideline adherence
Hamilton et al.	VI 2015	retrospective	UK	564	68 (mean)	257 F, 307 M	ED	flecainide (n = 85), amiodarone (n = 32)	NS	F 69, A 26, F + A 19	not stated	21 received PCV + ECV	COPD 40, DM 51, HF 29, HTN 249, HVD 52, IHD 162, previous congenital heart disease 5, stroke/TIA 37, THY 48	N
Kapelios	VII 2019	case report	Greece	1	55	M	not stated	amiodarone	300 mg in 60 min iv	1	not stated	NA	ibrutinib	Y
Karavelioglu et al.	I 2015	retrospective	Turkey	218	64.1 ±14.6	126 F, 92 M	ED	amiodarone	300 mg in 100 mL 5% dextrose solution (over 1 h) iv + 900 mg AMIO in 500 mL 5% dextrose (over 23 h) iv	not stated	not stated	not stated	CAD 27, DM 37, HF 20, HTN 125	Y
Kriz et al.	VIII 2016	prospective observational, single-centre	Austria	236	66.8 ±1.8	133 F, 103 M	ED	ibutilide 107, vernakalant 68, flecainide 59, amiodarone 2	I: 0.87 mg iv for 10 min; V: 3 mg/kg iv for 10 min; FLEC: 2 mg/kg (max 200 mg) iv for 10–20 min; AMIO: 150 mg iv for a 10 min	I 73, V 54, F 42, A 2	not stated	I: 2nd dose after 10 min, V: 2nd dose 2 mg/kg (max 340 mg) after 15 min	DM (I 17, V 0, F 6, A 1), HF/LV dysfunction (I 3, V 4, F 1, A 0), HTN (I 89, V 46, F 47, A 2), stroke/TIA/TE (I 7, V 7, F 1, A 0), vascular disease* (I 19, V 10, F 8, A 0)	N
Lewis et al.	XII 2015	case report	UK	1	38	M	not stated	flecainide	1.5 mg/kg (120 mg)	1	90	not stated	none	Y
Liberman et al.	VI 2018	retrospective, single-center	USA	13	16 (4.6–20.3)	not stated	PED	flecainide	<40 kg: 4–6 mg/kg, 40–70 kg: 200 mg, >70 kg: 300 mg	13	60 (30–120)	NA	CMP 6, HVD 3, post-heart transplantation 1	N
Maciag et al.	X 2017	single-center, randomized, double-blind, placebo-controlled, superiority clinical trial	Poland	36	68 ±12 (31–90)	35 F, 39 M	"ED or clinical ward"	antazoline	50 mg diluted to 10 cm^3 every 5 min iv (total dose 250 mg/50 cm^3)	26	16 (9–35)	not stated	HTN 52; CAD 13; THY 4	Y
Maimone et al.	IX 2015	case report	Italy	1	73	F	not stated	amiodarone	5 mg/kg (1st h), 50 mg/h (maintenance)	1	not stated	not stated	iodine contrast	Y
Manolis et al.	II 2018	retrospective single-center observational	Greece	23	63 ±12	10 F, 13 M	CD	vernakalant	3 mg/kg over 10 min, and after 15 min	15 (65%)	25 ±31 min (median ¼ 12 min)	2nd infusion of 2 mg/kg over 10 min	HTN 4, "mild CAD" 3, post-AVR normal EF 1, CMP 1, idiopathic 9	Y

Table 3. Detailed results of the systematic review – cont.

Author(s)	Date of publication	Study type	Country	Number of patients	Age of patients [years]	Sex of patients	PCV setting	PCV drug	PCV drug dose and route	PCV successful, n	Time to SR [min]	Management after failed PCV attempt	Comorbidities	AF guideline adherence
Mansoor et al.	XI 2014	retrospective, single-center	South Africa	59	16–82 (mean: 51.9)	26 F, 33 M	CSD	amiodarone	300 mg in 200 mL of 5% dextrose water over 45 min iv, followed by 900 mg in 1 L of 5% dextrose water over 24 h	7 (PCV only), 35 (ECV + PCV), 9 (ECV only), 5 (ECV + other PCV drug), 2 (other PCV drug), 1 spontaneous cardioversion	not stated	PCV was performed after failed ECV	all were immediately post-cardiac surgery (CABG or HVD); 24 DM, 33 CAD, 6 CAD + HVD, 35 HTN, 20 DM + HTN	Y
Milojevic et al.	I 2019	retrospective, single-center	France	200	65.9 ±16	58 F, 142 M	MICU	amiodarone	300 mg iv for 30 min (10 mg/min), if <40 kg: consider 150 mg for 30 min iv (5 mg/min), if >90 kg: consider 450 mg for 30 min iv (15 mg/min)	66	2% @ 20, 18% @ 40, 22% @ 60, 24% @ 90	not stated	not stated	Y
Mitrić et al.	IV 2016	retrospective, single-center	Australia	177	69 (60–75)	64 F, 113 M	ICU	amiodarone	median (IQR) total dose 905 mg (488–1651) (includes boluses and infusions)	86 (91 had recurrence of AF)	not stated (median treatment with amiodarone 24 h (16–40 h))	not stated	COPD 58, DM 25, HF 22, HTN 106, IHD 58, MI 43, HVD 9, PVD 40	Y
Mochalina et al.	III 2015	retrospective	Sweden	113	63 (23–87)	44 F, 69 M	not stated	vernakalant	3 mg/kg over 10 min	75	10 (4–90)	2nd infusion of 2 mg/kg over 10 min	HTN 57, IHD 18, DM 8, CHF 3	Y
Nemati et al.	VI 2016	RCT (2 centers)	Iran	122	A: 68.1 ±9.9, P: 66.7 ±8.7	not stated	ICU	amiodarone 67, propafenone 55	AMIO: 300 mg iv, followed by 600 mg iv over 12–24 h after the occurrence of AF; PROP: 600 mg po and 150 mg every 8 h for 10 days after the onset of AF	A 44, P 38	A 384.1 ±428.4, P 262.5 ±321.5	repeat dose, switch drugs, ECV	all after CABG, HTN P 39 A 52; hyperlipidemia P 38 A 45; DM P 28 A 33; CHF P 0 A 2; COPD P 9 A 21; right atrium enlargement P 0 A 1, intra-aortic balloon pump P 5 A 6; previously diagnosed AF P 5 A 2	N
Pluymaekers et al.	III 2019	multicenter, randomized, open-label, non-inferiority trial	Netherlands	219	65 ±11	89 F, 130 M	CD	not stated ("preferably with flecainide")	not stated	83	not stated	not stated	HTN 133, DM 25, MI 13	Y

Table 3. Detailed results of the systematic review – cont.

Author(s)	Date of publication	Study type	Country	Number of patients	Age of patients [years]	Sex of patients	PCV setting	PCV drug	PCV drug dose and route	PCV successful, n	Time to SR [min]	Management after failed PCV attempt	Comorbidities	AF guideline adherence
Pohjantahti-Maaroos et al.	III 2019	single-center non-randomized retrospective	Finland	200	F 55.3 ±13.0; V 59.3 ±12.5	F 65, V 66	ED	flecainide 100, vernakalant 100	F: 2.0 mg/kg (max 150 mg) during 30 min; V: 3.0 mg/kg (max 339 mg) during 10 min	F 46%, V 67%	120	AF after 15 min → 2nd dose of V 2.0 mg/kg (max 226 mg) during 10 min	DM F 9, V 9; HTN F 37, V 46; Prior AMI F 0, V 3	Y
Rudiger et al.	V 2014	retrospective single-center	Switzerland	32	74 (36–86)	10 F, 22 M	ICU	vernakalant	3 mg/kg over 10 min iv	17	30 (4–355)	2 mg/kg	all post-CS: 13 CABG, 18 HVD, 9 "major vascular", LV EF 35–80%	Y
Schnaubelt et al.	IV 2020	single-center trial	Austria	10	76 (63–79)	4 F, 6 M	ICU	vernakalant	3 mg/kg in 100 mL of normal saline iv	7	8.0 (6.0–9.0)	2 mg/kg in 100 mL of normal saline iv	all after elective cardiac surgery: 7 HVD, 3 HVD + CABG	Y
Shibata et al.	IV 2016	retrospective single-center	Japan	23	68 (60, 76)*	7 F, 16 M	ICU	amiodarone	150 mg over 30 min, followed by 20–50 mg/h	10	150	administration of a 2nd drug (not defined which), ECV	all post-surgery: CABG 8, CABG + HVD 4, HVD 9, vascular 2	Y
Simon et al.	III 2016	RCT	Austria	100	56.5 (SD 15.00)	32 F, 68 M	ED	vernakalant 49, ibutilide 51	V: 3 mg/kg in 100 mL normal saline iv infusion over 10 min; I: 1 mg in 100 mL normal saline iv infusion over 10 min	vernakalant: 34/49 (29 converted after 1st infusion); ibutilide: 22/51 (14 converted after 1st infusion)	V 10, I 26	if AF 15 min after vernakalant infusion → 2nd infusion (10 min) of vernakalant (2 mg/kg); if AF 10 min after ibutilide infusion → 2nd infusion of ibutilide (10 min, 1 mg); if AF 2 h after 1st infusion → ECV	HF (48 V, 51 I); HTN (30 V, 36 I); DM (5 V, 6 I); THY (7 V, 7 I); CAD (3 V, 4 I)	N
Simopoulos et al.	IX 2018	prospective, randomized, allocation-concealed, single-blind, single-site clinical trial	Greece	511	A: 65.5 ±9.6, A+R: 65.3 ±9.5	A: 31 F, 224 M; A+R: 35 F, 221 M	CSD	amiodarone 255; amiodarone + ranolazine 256	AMIO: 300 mg in 30 min + 750 mg in 24 h iv; AMIO + R: 500 mg po + 375 mg after 6 h and 375 mg twice daily thereafter	511	≤24 h: 37 A, 235 A+R > 24 h: 218 A, 21 A+R	A: 375 mg in 12 h	all after CABG surgery, DM (152 A, 146 A+R), HTN (140 in both groups), MI (139 A, 154 A+R)	Y
Stefatos et al.	VI 2018	case report	Canada	1	45	M	not stated	amiodarone	2 × 150 mg iv + 3 × 400 mg po	1	not stated ("by the next day")	not stated	bipolar-type schizoaffective disorder, apiprazole in depot	Y

Table 3. Detailed results of the systematic review – cont.

Author(s)	Date of publication	Study type	Country	Number of patients	Age of patients [years]	Sex of patients	PCV setting	PCV drug	PCV drug dose and route	PCV successful, n	Time to SR [min]	Management after failed PCV attempt	Comorbidities	AF guideline adherence
Stiell et al.	II 2020	multi-center partial factorial trial of 2 protocols (blinded, placebo-controlled RCT + nested, open-label trial)	Canada	204	60 (22–92)	70 F, 134 M	ED	procainamide	15 mg/kg in 500 mL of normal saline solution, over 30 min (max dose 1500 mg)	106	23 (14–35)**	ECV	age ≥75 years 29, CAD 16, CHF 6, COPD or asthma 19, DM type I 18, HVD 17, HTN 75, pacemaker or ICD 3, stroke or TIA 15	Y
Stoneman et al.	XI 2017	prospective, single-center	Ireland	42	57.7 (32–82)	10 F, 32 M	ED	vernakalant	3 mg/kg (max 113 kg) 10 min iv infusion	83%	8.8 (2–30), 9 required 2nd infusion	2nd iv infusion 2 mg/kg (max 113 kg), 10 min	HTN 20	Y
Su et al.	V 2017	retrospective	USA	48	68.9 ±14.0	12 F, 36 M	ICU	amiodarone	150 mg bolus iv followed by 1 mg/min for 6 h, then 0.5 mg/min for 18 h for a total of 1050 mg	not stated	not stated	not stated	AGE 33, reduced LV EF 6, LV hypertrophy 20, pulmonary HTN 14, prior MI 6, DM 13, OBE 11, THY 1	N
Tsanaxidis et al.	IV 2017	RCT	Greece	173	68 ±10	80 F, 93 M	not stated	amiodarone 81 ± ranolazine 92	AMIO: 5 mg/kg in 1 h followed by 50 mg/h; R: 1 g po	90%	10–15 h	not stated	HTN: A 53, A+R 65; IHD: A 13, A+R 29; OBE: A 32, A+R 27; DM: A 9, A+R 7	Y
Urtubia et al.	II 2016	retrospective single-center	Spain	12	56	1 F, 11 M	ED	vernakalant	3 mg/kg in 10 min	10	not stated (8 cardioverted with single dose)	2 mg/kg in 10 min, ECV	DM 2, HTN 6, stroke 2	Y
Vinson et al.	I 2018	retrospective cohort	USA	361	60.9 (14.8)	142 F, 219 M	ED	ibutilide	1 mg iv over 10 min	204	at 90 min was 44% (95% CI 38.9% to 49.3%), at 4 h it was 54.8% (95% CI 49.6% to 60.1%), and at ED discharge it was 56.5% (95% CI 51.2% to 61.7%)	2nd dose or ECV	HTN 202, DM 39, HF 18	N
Vogiatzis et al.	IV 2017	single-center RCT + cost-effectiveness analysis	Greece	78	63.72 ±6.67	22 F, 56 M	CD	vernakalant, ibutilide	V: 3 mg/kg iv over 10 min; I: 1 mg iv over 10 min	V 19, I 22	V 11.8 ±4.3, I 33.9 ±20.25 min	V 2 mg/kg, I 1 mg	HTN: V 27, I 23; CAD: V 18, I 13; HVD: V 5, V 6; lone AF: V 7, I 7	Y

Table 3. Detailed results of the systematic review – cont.

Author(s)	Date of publication	Study type	Country	Number of patients	Age of patients [years]	Sex of patients	PCV setting	PCV drug	PCV drug dose and route	PCV successful, n	Time to SR [min]	Management after failed PCV attempt	Comorbidities	AF guideline adherence
Wu et al.	II 2019	retrospective, single-center	China	181	60.1±8.5	22 F, 159 M	ICU	amiodarone	2 mg/kg in 10 min at 1 mg/kg/h until AF remission or 24 h	42	1584 (1.1 days)	ECV if hemodynamically unstable	all after esophageal or lung surgery, CAD 36, DM 39, HTN 71, OBE 51	Y
Wybraniec et al.	X 2018	retrospective, single-center, observational	Poland	450	65.5 ±11.9	238 F, 212 M	ED	antazoline, amiodarone, propafenone	AMIO: infusion in 5% glucose ± bolus 150 mg iv; PROP: 150 mg po or 70 mg in 100 mL 0.9% NaCl iv over 3 min; ANT: 100–200 mg iv bolus over 3 min or in 100 mL 0.9% NaCl iv over 5–15 min	314/450	not stated	not stated	HTN 328, DM 79), CAD/PAD 144	Y
Yarlagadda et al.	XII 2017	single-center retrospective study of consecutive patients	USA	378	64 ±11	dofetilide (205 M, 93 F), sotalol (46 M, 34 F)	not stated	D (n = 298), S (n = 80)	dofetilide, sotalol	D (125/215, 58%), S (30/48, 62.5%)	not stated	ECV	HTN (D: 252, 84.5%) (S: 67, 83.7%); DM (D: 63, 21.1%) (S: 20, 25%); CAD (D: 93, 31.2%) (S: 41, 51.2%)	Y
Zeemering et al.	VII 2018	retrospective	Netherlands	221	succ 61 ±13; fail 57 ±15	succ (93 M, 64 F); fail (52 M, 12 F)	not stated	flecainide	2 mg/kg (max 150 mg) iv infusion	157/221 (71%)	not stated	not stated	COPD 10, DM 15, HTN 95,	Y
Zeriouh et al.	V 2014	observational	Germany	24	69.6 ±6.3	F 26.1%	not stated	vernakalant ± flecainide	3 mg/kg/min iv infusion over 10 min	14	15–375	V: 2 mg/kg/min over 10 min; F: 300 mg po	DM 17.4%; HTN 78.3%	Y
Zhang et al.	XII 2018	single-center, open-label RCT	China	41	A: 72 ±13, A+W: 71 ±12	A: 11 F, 10 M; A+W: 12 F, 8 M	not stated	amiodarone 21, amiodarone + Wenxin Keli 20	5 mg/kg in 1 h iv followed by 50 mg/h iv ± Wenxin Keli 18 g thrice daily for 24 h	A 17, A+W 14	A 291 ±235, A+W 725 ±475	ECV or radiofrequency ablation	DM (A: 3, A+W: 9), HTN: (A: 14, A+W: 15)	Y
Zheng et al.	VII 2017	retrospective	China	48	63 ±12	A: 27 M	not stated	amiodarone	0.6 g/day (0.2 g tid) in the 1st week and then 0.4 g/day (0.2 g bid) in the 2nd week followed by 0.2 g/day (0.2 g qd) in the 3rd week and lasted for 11.5 months	A 43	A 211 ±126	not stated	CAD (A 36); CMP (A 7); HTN (A 40); HF (A 3)	Y

Table 4. Articles describing PCV performed using a contraidicated drug

Author(s)	Year of publication	Country	PCV setting	PCV drug	AF guideline adherence issue
Amin et al.	2015	Netherlands	CER	flecainide	11 patients had CAD
Balik et al.	2017	Czech Republic	ICU	amiodarone	5 patients had hyperthyroidism
Beatch et al.	2017	China, Hong-Kong, India, Korea, Taiwan	not stated	vernakalant	5 patients had HF (2 had NYHA III), 2 patients had HVD (not specified if aortic stenosis or not)
Bonora et al.	2017	Italy	ED	flecainide or propafenone, amiodarone	18 patients with IHD received flecainide or propafenone, 53 patients with HVD received flecainide or propafenone, 23 patients with THY received amiodarone
Carbajosa et al.	2017	Spain	ED	vernakalant	15 patients had HF (patients with NYHA II–IV HF were excluded)
Cosin-Sales et al.	2016	Spain	ED	vernakalant	1 patient had HF (NYHA not specified)
Costabel et al.	2015	Brazil	ED	vernakalant	"Patients with severe valvular heart disease, restrictive cardiomyopathy, hypertrophic cardiomyopathy, and those with known ejection fraction (EF) <35% were excluded" and yet 5.3% of 121 patients had EF < 55%
Dalyanoglu et al.	2018	Germany	CSD	vernakalant	21 patients had LVEF < 50%
Dong et al.	2017	China	not stated	ibutilide, amiodarone	29.71% of the patients had HF and received ibutilide, 28.35% had HF and received ibutilide + amiodarone (patients with LVEF < 35% were excluded)
Farkowski et al.	2016	Poland	ED	propafenone	14 patients had IHD, 2 patients had HVD
Hamilton et al.	2015	UK	ED	flecainide, amiodarone	52 patients had HVD, 5 had previous congenital heart disease, 162 had IHD (not stated how many of them received flecainide); 48 patients had unspecified THY (not stated how many received amiodarone)
Kriz et al.	2016	Austria	ED	ibutilide, flecainide, vernakalant	1 patient with HF/LV dysfunction received flecainide; 3 patients with HF/LV dysfunction received ibutilide, 4 patients with HF/LV dysfunction received vernakalant (elsewhere in the article it is stated that patients with HF and "severely reduced left ventricular ejection fraction" were excluded)
Lieberman et al.	2018	USA	PED	flecainide	6 patients had CMP + 3 patients had HVD
Nemati et al.	2016	Iran	not stated	propafenone	9 patients had COPD (not stated if patients had bronchospasm or dyspnea at the time of PCV)
Simon et al.	2016	Austria	ED	ibutilide	49 patients had HF (NYHA I) and 2 patients had NYHA II (patients with NYHA III and IV were excluded)
Su et al.	2017	USA	ICU	amiodarone	1 patient had hyperthyroidism
Vinson et al.	2018	USA	ED	ibutilide	18 patients had HF (3 of which had EF < 40%)

CAD – coronary artery disease; CER – cardiac emergency room; CMP – cardiomyopathy; ED – emergency department; EF – ejection fraction; HF – heart failure; HVD – heart valve disease; ICU – intensive care unit; LV – left ventricular; NYHA – New York Heart Association; PED – pediatrics department; THY – thyroid disease.

were not definitive. Authors suggested reasons such as lack of quality evidence (see Table 2 for information about the level of evidence in the analyzed AF guidelines), impossibility to establish AF onset, concerns about thromboembolic events, concerns about negative inotropic or proarrhythmic effect of PCV drugs, time constrains (excluding secondary causes of AF is time-consuming and adds more complexity to decision-making), and the fact that a significant number of ED patients with AF spontaneously revert to SR.[35,45,49,78–81] Finally, patient preference, or perhaps the physician's attitude, towards a given therapeutic option may influence the decisions about adopting a wait and observe approach or rhythm control or rate control, as well as electrical or pharmacological cardioversion.[46]

In a survey of 561 physicians, Heidbuchel et al. found 8 major barriers to AF guidelines implementation that were knowledge-related (e.g., diagnosing AF based on duration instead of etiology, uncertainty during decision-making, use and interpretation of risk assessment scores, difficulties in choosing stroke prevention treatment), skill-related (e.g., difficulties in EKG interpretation/detection of AF, difficulties in discussing with patients their treatment strategy) and systemic (e.g., poor cooperation between specialists and general practitioners, local regulations regarding the use of novel anticoagulants).[82]

Table 5. Correlation of several factors with the adherence to the PCV recommendations as described in AF treatment guidelines

Factor	AF guideline adherence		p-value
	PCV protocol adhered to the guidelines	PCV protocol did not adhere to the guidelines	
Overall guideline adherence (n, %)	47/64, 70.7%	17/64, 29.3%	–
Sample/number of patients in the study (mean ±SD)	124.0 ±147.8	184.6 ±155.7	p = 0.059
Age [years] (mean ±SD)	60.7 ±11.8	62.1 ±12.5	p = 0.345
Sex (n, % of males)	30/43, 66.1%	13/43, 60.7%	p = 0.284
Type of study/article			
RCT (n, %)	5/41, 12.2%	3/17, 17.7%	p = 0.680
case report (n, %)	7/41, 17.1%	0/17, 0%	p = 0.093
other than RCT or case report (n, %)	29/41, 70.7%	14/17, 82.4%	p = 0.514
Region/country where the PCV was performed			
Europe (n, %)	25/41, 61.0%	10/17, 58.8%	p = 1.000
USA (n, %)	3/41, 7.32%	3/17, 17.7%	p = 0.344
Department where PCV was performed			
ICU (n, %)	7/30, 23.3%	3/16, 18.8%	p = 1.000
ED (n, %)	9/30, 30.0%	9/16, 56.3%	p = 0.115
other than ICU or ED (n, %)	14/31, 45.2%	4/16, 25.0%	p = 0.218

AF – atrial fibrillation; ED – emergency department; ICU – intensive care unit; PCV – pharmacological cardioversion; RCT – randomized controlled trial; SD – standard deviation.

Limitations

Our systematic review had several limitations, most notably, the high heterogeneity and incompleteness of the obtained data which did not allow us to perform a meta-analysis. Specifically, we were unable to extract enough data about the patients (e.g., patient age is provided only as an average value, comorbidities listed as totals without mention if any patients had more than 1 comorbidity). Therefore, it was not possible to assess if AF guidelines were followed during PCV of those patients. Furthermore, although reports of single cases are universally defined as weak evidence, we had little data to choose from and decided to include them in the analysis. Had there been more data from large trials available, we would have chosen them over case reports, thus making our statistical analysis and conclusions more robust. Finally, we are aware that there might be national AF guidelines which we were unable to find.

Conclusions

Our review of the published clinical literature about PCV reveals significant non-adherence to AF treatment guidelines. Specifically, the drugs used for PCV in patients with AF and comorbidities such as heart failure and thyroid disease are inconsistent with the guidelines.

ORCID iDs

Janusz Springer https://orcid.org/0000-0002-4232-6557
Tomasz Szmuda https://orcid.org/0000-0003-1904-6773
Dariusz Kozłowski https://orcid.org/0000-0003-2089-0656

References

1. Chung MK, Eckhardt LL, Chen LY, et al. Lifestyle and risk factor modification for reduction of atrial fibrillation: A scientific statement from the American Heart Association. *Circulation*. 2020;141(16):e750–e772. https://doi.org/10.1161/CIR.0000000000000748
2. Kozłowski D. Method in the chaos: A step-by-step approach to ECG interpretation. *Eur J Transl Clin Med*. 2018;1(1):76–92. doi:10.31373/ejtcm/92255
3. Stiell IG, Sivilotti ML, Taljaard M, et al. Electrical versus pharmacological cardioversion for emergency department patients with acute atrial fibrillation (RAFF2): A partial factorial randomised trial. *Lancet*. 2020;395(10221):339–349. doi:10.1016/S0140-6736(19)32994-0
4. Kozlowski D, Budrejko S, Lip GY, et al. Lone atrial fibrillation: What do we know? *Heart*. 2010;96(7):498–503. doi:10.1136/hrt.2009.176321
5. Hindricks G, Potpara T, Dagres N, et al; ESC Scientific Document Group. 2020 ESC Guidelines for the diagnosis and management of atrial fibrillation developed in collaboration with the European Association of Cardio-Thoracic Surgery (EACTS). *Eur Heart J*. 2021;42(5):373–498. doi:10.1093/eurheartj/ehaa612
6. Rogenstein C, Kelly AM, Mason S, et al. An international view of how recent-onset atrial fibrillation is treated in the emergency department. *Acad Emerg Med*. 2012;19(11):1255–1260. doi:10.1111/acem.12016
7. Moher D, Liberati A, Tetzlaff J, Altman DG; PRISMA Group. Preferred reporting items for systematic reviews and meta-analyses: The PRISMA statement. *PLoS Med*. 2009;6(7):e1000097. doi:10.1371/journal.pmed.1000097
8. Brieger D, Amerena J, Attia JR, et al. National Heart Foundation of Australia and Cardiac Society of Australia and New Zealand: Australian clinical guidelines for the diagnosis and management of atrial fibrillation 2018. *Med J Aust*. 2018;209(8):356–362. https://doi.org/10.5694/mja18.00646.
9. Stiell IG, Scheuermeyer FX, Vadeboncoeur A, et al. CAEP acute atrial fibrillation/flutter best practices checklist. *Can J Emerg Med*. 2018;20(3):334–342. https://doi.org/10.1017/cem.2018.26
10. Andrade JG, Verma A, Mitchell LB, et al. 2018 focused update of the Canadian Cardiovascular Society guidelines for the management of atrial fibrillation. *Can J Cardiol*. 2018;34(11):1371–1392. doi:10.1016/j.cjca.2018.08.026
11. Soar J, Nolan JP, Böttiger BW, et al. European Resuscitation Council Guidelines for Resuscitation 2015: Section 3. Adult advanced life support. *Resuscitation*. 2015;95:100–147. doi:10.1016/j.resuscitation.2015.07.016

12. National Institute for Health and Care Excellence (NICE). Atrial fibrillation: Management. Clinical guideline. London, UK: NICE; 2014. https://www.nice.org.uk/guidance/cg180/resources/atrial-fibrillation-management-pdf-35109805981381. Accessed June 5, 2020.
13. Baugh C, Pate K, Brooks JA, et al. An evidence-driven tool to guide the selection and management of emergency department patients with atrial fibrillation and atrial flutter. Irving, USA: American College of Emergency Physicians. 2018. https://www.acep.org/patient-care/afib/. Accessed June 5, 2020.
14. January CT, Wann LS, Alpert JS, et al; ACC/AHA Task Force Members. 2014 AHA/ACC/HRS guideline for the management of patients with atrial fibrillation: Executive summary. A report of the American College of Cardiology/American Heart Association Task Force on practice guidelines and the Heart Rhythm Society. *Circulation*. 2014;130(23):2071–2104. doi:10.1161/CIR.0000000000000040
15. Albakri A, Klingenheben T. Unusual severe hemodynamic failure associated with standard dose of intravenous flecainide for pharmacological cardioversion of atrial fibrillation. *HeartRhythm Case Rep*. 2017;3(9):440–442. doi:10.1016/j.hrcr.2017.07.003
16. Amin AS, Peters RH, Verstraaten M, Wilde AA, Buijs EM. Baseline NT-ProBNP level predicts success of cardioversion of atrial fibrillation with flecainide. *Netherlands Heart J*. 2015;23(3):182–189. doi:10.1007/s12471-015-0659-8
17. Andrade JG, MacGillivray J, Macle L, et al. Clinical effectiveness of a systematic "pill-in-the-pocket" approach for the management of paroxysmal atrial fibrillation. *Heart Rhythm*. 2018;15(1):9–16. doi:10.1016/j.hrthm.2017.10.002
18. Balik M, Kolnikova I, Maly M, Waldauf P, Tavazzi G, Kristof J. Propafenone for supraventricular arrhythmias in septic shock: Comparison to amiodarone and metoprolol. *J Crit Care*. 2017;41:16–23. doi:10.1016/j.jcrc.2017.04.027
19. Balsam P, Koźluk E, Peller M, et al. Antazoline for termination of atrial fibrillation during the procedure of pulmonary veins isolation. *Adv Med Sci*. 2015;60(2):231–235. doi:10.1016/j.advms.2015.03.002
20. Beatch GN, Bhirangi K, Juul-Moller S, Rustige J. Efficacy and safety of vernakalant for cardioversion of recent-onset atrial fibrillation in the Asia-Pacific region: A phase 3 randomized controlled trial. *J Cardiovasc Pharmacol*. 2017;69(2):86–92. doi:10.1097/FJC.0000000000000445
21. Bonora A, Turcato G, Franchi E, et al. Efficacy and safety in pharmacological cardioversion of recent-onset atrial fibrillation: A propensity score matching to compare amiodarone vs class IC antiarrhythmic drugs. *Intern Emerg Med*. 2017;12(6):853–859. doi:10.1097/FJC.0000000000000445
22. Carbajosa DJ, Cosin-Sales J, Pérez-Durá MJ, et al. Vernakalant in hospital emergency practice: Safety and effectiveness [in Spanish]. *Emergencias*. 2017;29(6):397. PMID:29188914
23. Champion S, Gaüzère BA, Vandroux D, Lefort Y. Is it worth delivering direct-current counter shock to critically ill patients with supraventricular tachyarrhythmia? [in French]. *Ann Cardiol Angeiol (Paris)*. 2018;67(4):260–263. doi:10.1016/j.ancard.2018.04.003
24. Chauveau S, Le Vavasseur O, Morel E, Dulac A, Chevalier P. Flecainide is a safe and effective treatment for pre-excited atrial fibrillation rapidly conducted to the ventricle in pregnant women: A case series. *Eur Heart J Case Rep*. 2019;3(2):ytz066. doi:10.1093/ehjcr/ytz066
25. Comelli I, Pigna F, Cervellin G. 1:1 atrial flutter induced by flecainide, whilst the patient was at rest. *Am J Emerg Med*. 2018;36(11):2131.e3–2131.e5. doi:10.1016/j.ajem.2018.07.040
26. Cosin-Sales J, Loscos A, Peiró A, Sorando MR, Buendía F, Ruescas L. Real-world data on the efficacy of vernakalant for pharmacological cardioversion in patients with recent-onset atrial fibrillation. *Rev Esp Cardiol (Engl Ed)*. 2016;69(6):619–620. doi:10.1016/j.rec.2016.02.020
27. Costabel JP, Lambardi F, Aragon M, et al. Predictors of conversion of recent-onset atrial fibrillation treated with vernakalant. *Pacing Clin Electrophysiol*. 2015;38(2):196–200. doi:10.1111/pace.12548
28. Dalyanoglu H, Mehdiani A, Minol JP, et al. Conversion of atrial fibrillation after cardiosurgical procedures by Vernakalant® as an atrial repolarization delaying agent (ARDA). *Heart Surg Forum*. 2018;21(3):E201–E208. doi:10.1532/hsf.1970
29. Dasgupta S, Dave I, Whitehill R, Fischbach P. Chemical cardioversion of atrial flutter and fibrillation in the pediatric population with ibutilide. *Pacing Clin Electrophysiol*. 2020;43(3):322–326. doi:10.1111/pace.13890
30. Dilber D, Čerkez-Habek J, Barić H, Gradišer M. Atrial fibrillation cardioversion following acupuncture. *Saudi Med J*. 2015;36(11):1351–1353. doi:10.15537/smj.2015.11.12891
31. Dong Z, Yao H, Miao Z, et al. Pretreatment with intravenous amiodarone improves the efficacy of ibutilide treatment on cardioversion rate and maintenance time of sinus rhythm in patients with persistent atrial fibrillation. *Biomed Rep*. 2017;6(6):686–690. doi:10.3892/br.2017.896
32. Farkowski MM, Maciąg A, Żurawska M, et al. Comparative effectiveness and safety of antazoline-based and propafenone-based strategies for pharmacological cardioversion of short-duration atrial fibrillation in the emergency department. *Pol Arch Med Wewn*. 2016;126(6):381–387. doi:10.20452/pamw.3452
33. Farkowski MM, Maciag A, Zurawska M, Kowalik I, Szwed H, Pytkowski M. Clinical effectiveness and safety of antazoline-based therapy in patients with stable coronary artery disease undergoing pharmacological cardioversion of short-duration atrial fibrillation in the emergency department. *Cardiovasc Ther*. 2018;36(6):e12469. doi:10.1111/1755-5922.12469
34. Farkowski MM, Maciag A, Kowalik I, Konka M, Szwed H, Pytkowski M. Intravenous antazoline, a first-generation antihistaminic drug with antiarrhythmic properties, is a suitable agent for pharmacological cardioversion of atrial fibrillation induced during pulmonary vein isolation due to the lack of influence on atrio-venous conduction and high clinical effectiveness (AntaEP Study). *Brit J Clin Pharmacol*. 2019;85(7):1552–1558. doi:10.1111/bcp.13940
35. Gillinov AM, Bagiella E, Moskowitz AJ, et al. Rate control versus rhythm control for atrial fibrillation after cardiac surgery. *N Engl J Med*. 2016;374(20):1911–1921. doi:10.1056/NEJMoa1602002
36. Hamilton A, Clark D, Gray A, Cragg A, Grubb N. The epidemiology and management of recent-onset atrial fibrillation and flutter presenting to the emergency department. *Eur J Emerg Med*. 2015;22(3):155–161. doi:10.1097/MEJ.0000000000000198
37. Kapelios CJ, Bonou MS, Diamantopoulos P, et al. Ibrutinib-related atrial fibrillation: Therapeutic challenges. *J Oncol Pharm Pract*. 2019;25(5):1258–1260. doi:10.1177/1078155218785983
38. Karavelioğlu Y, Karapınar H, Yüksel M, et al. Neutrophil to lymphocyte ratio is predictor of atrial fibrillation recurrence after cardioversion with amiodarone. *Clin Appl Thromb Hemost*. 2015;21(1):5–9. doi:10.1177/1076029613518368
39. Kriz R, Freynhofer MK, Weiss TW, et al. Safety and efficacy of pharmacological cardioversion of recent-onset atrial fibrillation: A single-center experience. *Am J Emerg Med*. 2016;34(8):1486–1490. doi:10.1016/j.ajem.2016.05.012
40. Lewis G, Currie P. Atrial fibrillation during pregnancy: Cardioversion with flecainide. *Brit J Hosp Med (Lond)*. 2015;76(12):720–721. doi:10.12968/hmed.2015.76.12.720
41. Liberman L, Starc TJ, Silver ES. Usefulness of high-dose oral flecainide for termination of recent-onset atrial fibrillation in children. *Am J Cardiol*. 2018;121(12):1530–1533. doi:10.1016/j.amjcard.2018.03.001
42. Maciag A, Farkowski MM, Chwyczko T, et al. Efficacy and safety of antazoline in the rapid cardioversion of paroxysmal atrial fibrillation (the AnPAF Study). *Europace*. 2017;19(10):1637–1642. doi:10.1093/europace/euw384
43. Maimone S, Filomia R, Saitta C, Raimondo G, Squadrito G. Case report: Atrial fibrillation after intravenous administration of iodinated contrast medium in a patient with hepatocellular carcinoma. *Medicine (Baltimore)*. 2015;94(35):e1406. doi:10.1097/MD.0000000000001406
44. Manolis AS, Bethanis S, Metaxa S, Polytarchou K, Sakellaris N, Pyrros I. Use of intravenous vernakalant for atrial fibrillation conversion in the regular ward under only bedside monitoring. *Hellenic J Cardiol*. 2019;60(1):54–56. doi:10.1016/j.hjc.2018.02.003
45. Mansoor E. De novo atrial fibrillation post cardiac surgery: The Durban experience. *Cardiovasc J Afr*. 2014;25(6):282. doi:10.5830/CVJA-2014-067
46. Milojevic K, Beltramini A, Nagash M, Muret A, Richard O, Lambert Y. Esmolol compared with amiodarone in the treatment of recent-onset atrial fibrillation (RAF): An emergency medicine external validity study. *J Emerg Med*. 2019;56(3):308–318. doi:10.1016/j.jemermed.2018.12.010
47. Mitrić G, Udy A, Bandeshe H, Clement P, Boots R. Variable use of amiodarone is associated with a greater risk of recurrence of atrial fibrillation in the critically ill. *Crit Care*. 2016;20(1):1–9. doi:10.1186/s13054-016-1252-2

48. Mochalina N, Juhlin T, Öhlin B, Carlson J, Holmqvist F, Platonov PG. Predictors of successful cardioversion with vernakalant in patients with recent-onset atrial fibrillation. *Ann Noninvasive Electrocardiol*. 2015;20(2):140–147. doi:10.1111/anec.12178
49. Nemati MH, Astaneh B. Amiodarone versus propafenone to treat atrial fibrillation after coronary artery bypass grafting: A randomized double blind controlled trial. *Korean J Thorac Cardiovasc Surg*. 2016;49(3):177–184. doi:10.5090/kjtcs.2016.49.3.177
50. Pluymaekers NA, Dudink EA, Luermans JG, et al. Early or delayed cardioversion in recent-onset atrial fibrillation. *N Engl J Med*. 2019; 380(16):1499–1508. doi:10.1056/NEJMoa1900353
51. Pohjantähti-Maaroos H, Hyppölä H, Lekkala M, Sinisalo E, Heikkola A, Hartikainen J. Intravenous vernakalant in comparison with intravenous flecainide in the cardioversion of recent-onset atrial fibrillation. *Eur Heart J Acute Cardiovasc Care*. 2019;8(2):114–120. doi:10.1177/2048872617728558
52. Rudiger A, Breitenstein A, Arrigo M, Salzberg SP, Bettex D. Suitability, efficacy, and safety of vernakalant for new onset atrial fibrillation in critically ill patients. *Crit Care Res Pract*. 2014;2014:826286. doi:10.1155/2014/826286
53. Schnaubelt S, Niederdöckl J, Simon A, et al. Hemodynamic effects of vernakalant in cardio-surgical ICU-patients treated for recent-onset postoperative atrial fibrillation. *Sci Rep*. 2020;10(1):1–7. doi:10.1038/s41598-020-64001-8
54. Shibata SC, Uchiyama A, Ohta N, Fujino Y. Efficacy and safety of landiolol compared to amiodarone for the management of postoperative atrial fibrillation in intensive care patients. *J Cardiothorac Vasc Anesth*. 2016;30(2):418–422. doi:10.1053/j.jvca.2015.09.007
55. Simon A, Niederdoeckl J, Skyllouriotis E, et al. Vernakalant is superior to ibutilide for achieving sinus rhythm in patients with recent-onset atrial fibrillation: A randomized controlled trial at the emergency department. *Europace*. 2017;19(2):233–240. doi:10.1093/europace/euw052
56. Simopoulos V, Hevas A, Hatziefthimiou A, et al. Amiodarone plus ranolazine for conversion of post-cardiac surgery atrial fibrillation: Enhanced effectiveness in reduced versus preserved ejection fraction patients. *Cardiovasc Drugs Ther*. 2018;32(6):559–565. doi:10.1007/s10557-018-6832-8
57. Stefatos A, Ha JN, Baranchuk A, Baldessarini RJ, Vázquez GH. Atrial fibrillation and injected aripiprazole: A case report. *Innov Clin Neurosci*. 2018;15(5–6):43–45.
58. Stiell IG, Sivilotti ML, Taljaard M, et al. Electrical versus pharmacological cardioversion for emergency department patients with acute atrial fibrillation (RAFF2): A partial factorial randomised trial. *Lancet*. 2020;395(10221):339–349. doi:10.1016/S0140-6736(19)32994-0
59. Stoneman P, Gilligan P, Mahon P, Sheahan R. Chemical cardioversion of recent-onset atrial fibrillation in the emergency department using vernakalant hydrochloride achieves safe and rapid restoration of sinus rhythm and facilitates same day discharge. *Irish J Med Sci (1971–)*. 2017;186(4):903–908. doi:10.1007/s11845-017-1576-1
60. Su M, Seki D, Moheet AM. Pharmacologic cardioversion with intravenous amiodarone is likely safe in neurocritically Ill patients. *J Clin Neurosci*. 2017;39:59–61. doi:10.1016/j.jocn.2017.01.014
61. Tsanaxidis N, Aidonidis I, Hatziefthimiou A, et al. Ranolazine added to amiodarone facilitates earlier conversion of atrial fibrillation compared to amiodarone-only therapy. *Pacing Clin Electrophysiol*. 2017;40(4):372–378. doi:10.1111/pace.13048
62. Urtubia PA, Carbonell TM. Vernakalant for atrial fibrilation in an emergency department [in Spanish]. *Emergencias*. 2016;28(1):69. PMID: 29094833
63. Vinson DR, Lugovskaya N, Warton EM, et al. Ibutilide effectiveness and safety in the cardioversion of atrial fibrillation and flutter in the community emergency department. *Ann Emerg Med*. 2018; 71(1):96–108. doi:10.1016/j.annemergmed.2017.07.481
64. Vogiatzis I, Papavasiliou E, Dapcevitch I, Pittas S, Koulouris E. Vernakalant versus ibutilide for immediate conversion of recent-onset atrial fibrillation. *Hippokratia*. 2017;21(2):67–73. PMID:30455558
65. Wu D, Wu J, Chen M, Ji C, Xu M. Transient new-onset atrial fibrillation during general thoracic operations and its treatment with amiodarone: A retrospective analysis in a single centre. *Interact Cardiovasc Thorac Surg*. 2019;28(2):227–234. doi:10.1093/icvts/ivy214
66. Wybraniec MT, Wrobel W, Wilkosz K, Wrona K, Bula K, Mizia-Stec K. Pharmacological cardioversion with antazoline in atrial fibrillation: The results of the CANT study. *J Am Heart Assoc*. 2018;7(20):e010153. doi:10.1161/JAHA.118.010153
67. Yarlagadda B, Vuddanda V, Dar T, et al. Safety and efficacy of inpatient initiation of dofetilide versus sotalol for atrial fibrillation. *J Atr Fibrillation*. 2017;10(4):1805. doi:10.4022/jafib.1805
68. Zeemering S, Lankveld TA, Bonizzi P, et al. The electrocardiogram as a predictor of successful pharmacological cardioversion and progression of atrial fibrillation. *Europace*. 2018;20(7):e96–e104. doi:10.1093/europace/eux234
69. Zeriouh M, Sabashnikov A, Choi YH, et al. A novel treatment strategy of new onset atrial fibrillation after cardiac surgery: An observational prospective study. *J Cardiothorac Surg*. 2014;9(1):83. doi:10.1186/1749-8090-9-83
70. Zhang N, Tse G, Dahal S, et al. Efficacy of Wenxin Keli plus amiodarone versus amiodarone monotherapy in treating recent-onset atrial fibrillation. *Cardiol Res Pract*. 2018;2018:6047271. doi:10.1155/2018/6047271
71. Zheng H, Zhu F, Miao P, Mao Z, Redfearn DP, Cao RY. Antimicrobial natural product berberine is efficacious for the treatment of atrial fibrillation. *Biomed Res Int*. 2017;2017:3146791. doi:10.1155/2017/3146791
72. Kline SR, Dreifus LS, Watanabe Y, McGarry TF, Likoff W. Evaluation of the antiarrhythmic properties of antazoline: A preliminary study. *Am J Cardiol*. 1962;9(4):564–567. doi:10.1016/0002-9149(62)90075-9
73. Kehler JG, Gehring DA. Conversion of atrial fibrillation with antazoline hydrochloride (arithmin). *Angiology*. 1970;21(1):11–17. doi:10.1177/000331977002100104
74. Srzednicki M, Sadowski Z, Kulikowski A. Evaluation of the antiarrhythmia effectiveness of Phenazolinum Polfa in paroxysmal atrial fibrillation [in Polish]. *Pol Tyg Lek*. 1990;45(45–46):924–927.
75. Kuch M, Janiszewski M, Dluzniewski M. Antazoline: Ineffective or misprized in the treatment of paroxysmal atrial fibrillation. *Pol J Cardiol*. 2000;3:247–251.
76. Pejska M, Kozłowski D, Homenda W, Drapella A. The assessment of the antazoline in conversion atrial fibrillation for the patients over sixty. *Geriatr Pol*. 2005;1(4):7–11.
77. Piotrowski R, Kryński T, Baran J, Futyma P, Stec S, Kułakowski P. Antazoline for rapid termination of atrial fibrillation during ablation of accessory pathways. *Cardiol J*. 2014;21(3):299–303. doi:10.5603/CJ.a2013.0121
78. Drugs.com. Antazoline. https://www.drugs.com/international/antazoline.html. Accessed September 22, 2020.
79. Abadie BQ, Hansen B, Walker J, et al. Likelihood of spontaneous cardioversion of atrial fibrillation using a conservative management strategy among patients presenting to the emergency department. *Am J Cardiol*. 2019;124(10):1534–1539. doi:10.1016/j.amjcard.2019.08.017
80. Vinson DR, Hoehn T, Graber DJ, Williams TM. Managing emergency department patients with recent-onset atrial fibrillation. *J Emerg Med*. 2012;42(2):139–148. doi:10.1016/j.jemermed.2010.05.017
81. Weigner MJ, Caulfield TA, Danias PG, Silverman DI, Manning WJ. Risk for clinical thromboembolism associated with conversion to sinus rhythm in patients with atrial fibrillation lasting less than 48 hours. *Ann Intern Med*. 1997;126(8):615–620. doi:10.7326/0003-4819-126-8-199704150-00005
82. Heidbuchel H, Dagres N, Antz M, et al. Major knowledge gaps and system barriers to guideline implementation among European physicians treating patients with atrial fibrillation: A European Society of Cardiology international educational needs assessment. *Europace*. 2018;20(12):1919–1928. doi:10.1093/europace/euy039

Cerebral small vessel disease: A review

Justyna Chojdak-Łukasiewicz[1,A,D], Edyta Dziadkowiak[1,B], Anna Zimny[2,B], Bogusław Paradowski[1,E,F]

[1] Department of Neurology, Wroclaw Medical University, Poland
[2] Department of General Radiology, Interventional Radiology and Neuroradiology, Wroclaw Medical University, Poland

A – research concept and design; B – collection and/or assembly of data; C – data analysis and interpretation;
D – writing the article; E – critical revision of the article; F – final approval of the article

Advances in Clinical and Experimental Medicine, ISSN 1899–5276 (print), ISSN 2451–2680 (online) *Adv Clin Exp Med*. 2021;30(3):349–356

Address for correspondence
Justyna Chojdak-Łukasiewicz
E-mail: justyna.ch.lukasiewicz@gmail.com

Funding sources
None declared

Conflict of interest
None declared

Received on July 26, 2020
Reviewed on October 31, 2020
Accepted on December 6, 2020

Published online on March 25, 2021

Abstract

Cerebral small vessel disease (CSVD) is the most common, chronic and progressive vascular disease. The changes affect arterioles, capillaries and small veins supplying the white matter and deep structures of the brain. It is the most common incidental finding on brain scans, especially in people over 80 years of age. Magnetic resonance imaging (MRI) plays a key role in the diagnosis of CSVD. The nomenclature and radiological phenotypes of CSVD were published in 2013 based on the unified position of the so-called Centres of Excellence in Neurodegeneration. The disease is characterized by a diverse clinical and radiological picture. It is primarily responsible for stroke incidents, gait disturbances, depression, cognitive impairment, and dementia in the elderly. The CSVD contributes to about 20% of strokes, including 25% of ischemic strokes and 45% of dementias. Common causes of CSVD include arteriosclerosis, cerebral amyloid angiopathy (CAA), genetic small vessel angiopathy, inflammation and immune-mediated small vessel diseases, and venous collagenosis. There is no causal treatment and management is mainly based on combating known risk factors for cardiovascular disease (CVD).

Key words: amyloidosis, cerebral small vessel disease, white matter hyperintensities, lacunar infarcts, microbleeds

Cite as
Chojdak-Łukasiewicz J, Dziadkowiak E, Zimny A, Paradowski B. Cerebral small vessel disease: A review. *Adv Clin Exp Med*. 2021;30(3):349–356. doi:10.17219/acem/131216

DOI
10.17219/acem/131216

Introduction

Cerebral small vessel disease (CSVD) is a chronic, progressive disorder of arterioles, capillaries and small veins supplying the white matter and deep structures of gray matter; it is characterized by a diverse clinical picture and specific changes in neuroimaging and neuropathological investigations of the brain.[1,2] The changes affect small vessels, 50–400 um in diameter, and lead to damage of the white matter in subcortical brain structures. The CSVD is a dynamic disease process not limited to cerebral vessels but affecting the whole body. It is clinically heterogeneous and constitutes the most common cerebrovascular disease (CVD).[1] The CSVD is responsible for about 20% of all strokes, including 25% of ischemic strokes and 45% of vascular dementias.[2,3]

The nomenclature and radiological phenotypes of CSVD were published in 2013 based on the unified position of the so-called Centres of Excellence in Neurodegeneration.[4] The STRIVE protocol (STandards for ReportIng Vascular changes on nEuroimaging) sets diagnostic standards and assesses individual radiological phenotypes of CSVD and their clinical consequences (Table 1).[4] The CSVD is typically recognized on both brain magnetic resonance imaging (MRI) and computed tomography (CT) scans, but MRI has greater sensitivity and specificity. A reliable radiological assessment is only possible with at least 1.5 T MRI including the following sequences: FLAIR (fluid-attenuated inversion recovery), T2* (gradient recalled echo T2*-weighted images) or SWI (susceptibility-weighted imaging), T1, and DWI (diffusion-weighted imaging). Figures 1–5 present MRI findings of CSVD.

Epidemiology

The CSVD occurs 6–10 times more often than stroke.[5] Silent brain infarcts are the most frequently identified incidental findings on brain scans, especially in older people. As many as 25% of people over 80 years of age have had ≥1 silent stroke.[6,7] It has been estimated that for every symptomatic stroke, there are about 10 silent brain changes.[8] The prevalence of CSVD increases with age, with no significant sex differences.[9] Prevalence of white matter

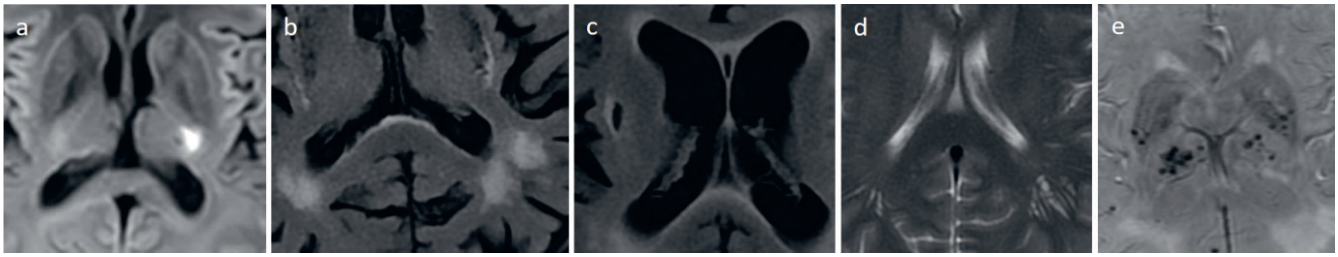

Fig. 1. A. Acute lacunar infarction on DWI; B. White matter hyperintensities (WMHs) on the FLAIR image; C. Old lacunar infarction seen on the FLAIR image as a dark fluid-filled cavity surrounded by a hyperintense rim; D. Enlarged perivascular spaces on a T2-weighted image; E. Multiple microbleeds bilaterally within basal ganglia and thalami

Table 1. Types of cerebral small vessel disease (CSVD) according to STRIVE after Wardlaw et al.[4]

Type of CSVD	Description
Recent subcortical infarcts	fresh, small (less than 20 mm in axial section) ischemic lesions with respect to perforating arteries, whose radiological features or clinical signs and symptoms indicate their formation in the few weeks before the test; best seen in the DWI sequence; these changes are hypointense in the T1 sequence, hyperintense in the T2 and FLAIR sequences, and isointense in the GRE-T2 sequence
Lacunae of presumed vascular origin	round or oval subcortical lesions 3–15 mm in diameter, filled with fluid, with cerebrospinal fluid-like signal; these lacunae correspond to history of acute cerebral infarction or bleeding from the area of vascularization of the perforating artery; the lesions are characterized by a distinctive image in the FLAIR examination; each lesion is a cavity filled with cerebrospinal fluid and surrounded by a hyperintense rim; they are isointense in the DWI sequence, hypointense in the FLAIR and T1 sequences, and hyperintense in the T2 sequence
White matter hyperintensities	symmetric regardless of size; hyperintense in the T2, FLAIR and GRE-T2 (gradient-echo T2) sequences; isointense in DWI; and hypointense in T1
Widened perivascular spaces (Virchow–Robin perivascular spaces)	mostly seen in basal ganglia <2 mm in size; they usually accompany hyperintense lesions of the white matter and lacunar condition but not brain atrophy; the lesions are hyperintense in T2 sequences, hypointense in FLAIR and T1 sequences, and isointense in the GRE-T2 sequence
Cerebral microbleeds (CMBs)	small, homogeneous lesions <10 mm in diameter, characterized by the 'blooming effect'; the lesions are best seen in the gradient-echo T2 sequence (hypointense lesions); in the T2, T1 and FLAIR sequences, they are isointense; microbleeds correspond to hemosiderin-loaded macrophages that are present in the perivascular space
Brain atrophy	brain atrophy in the context of CSVD is considered only when the patient has not suffered a stroke or head injury

DWI – diffuse-weighted imaging; FLAIR – fluid-attenuated inversion recovery.

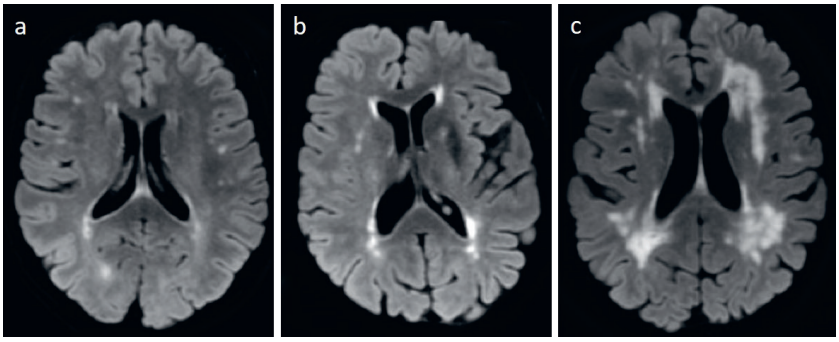

Fig. 2. Grading of white matter hyperintensities (WMHs) on the Fazekas scale

A. Grade 1, punctate foci; B. Grade 2, early confluent lesions; C. Grade 3, large confluent areas.

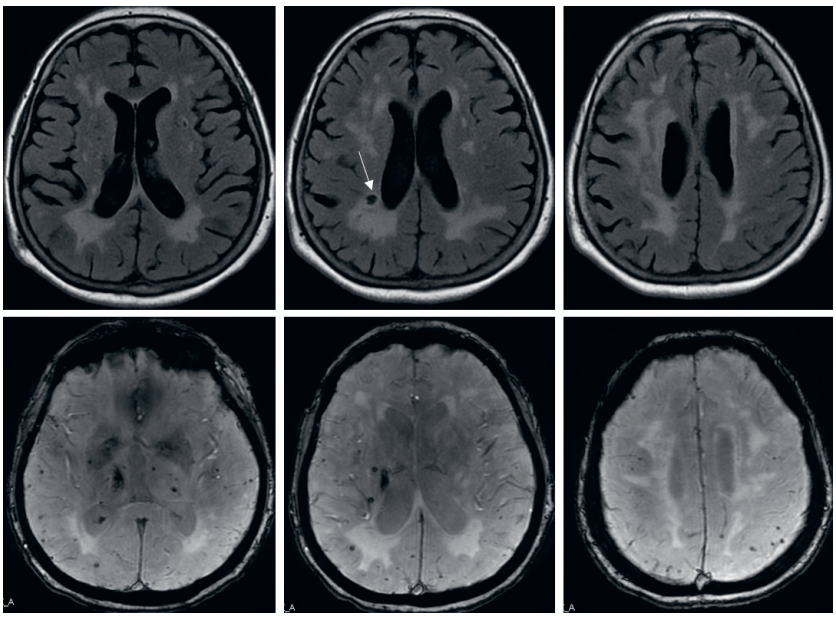

Fig. 3. Hypertensive encephalopathy

FLAIR images (upper row) show diffuse white matter hyperintensities in both hemispheres with old lacunar infarction (arrow). Multiple foci of microbleeds within cortex and deep brain structures on SWI (lower row).

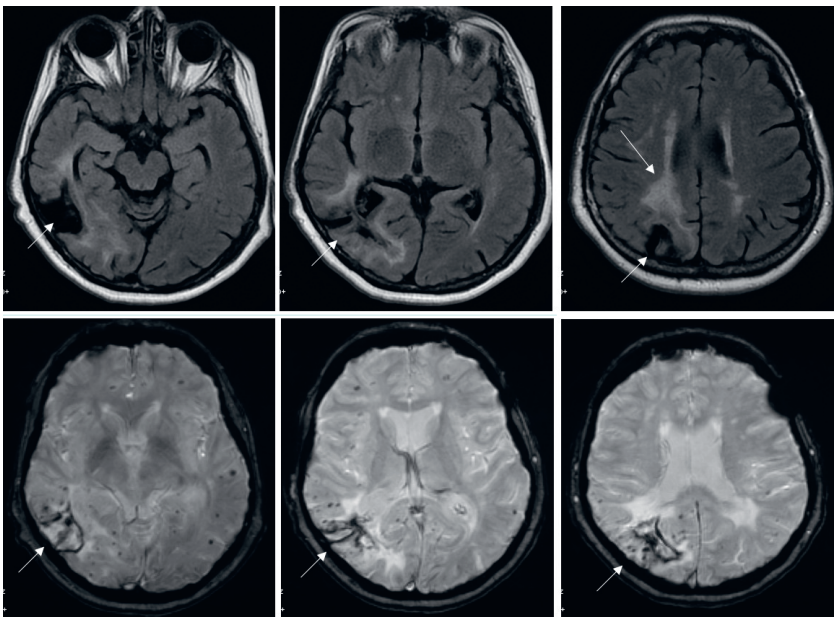

Fig. 4. Cerebral amyloid angiopathy (CAA)

FLAIR images (upper row) show diffuse white matter hyperintensities (long arrow) and focus of brain malacia due to cortical hematoma (short arrows). Multiple foci of microbleeds with cortical distribution and hemosiderin deposits within old cortical hematoma on SWI (lower row, short arrows).

hyperintensities increases from about 5% for people aged 50 years to nearly 100% for people aged 90 years.[10] Also, the prevalence of cerebral microbleeds increases from 6.5% for people aged 45–50 years to about 36% for people aged 80–89 years.[11] There is a noticeable population variability: CSVD lesions are more common in the Chinese population, where lacunar strokes account for 46% of ischemic episodes.[12]

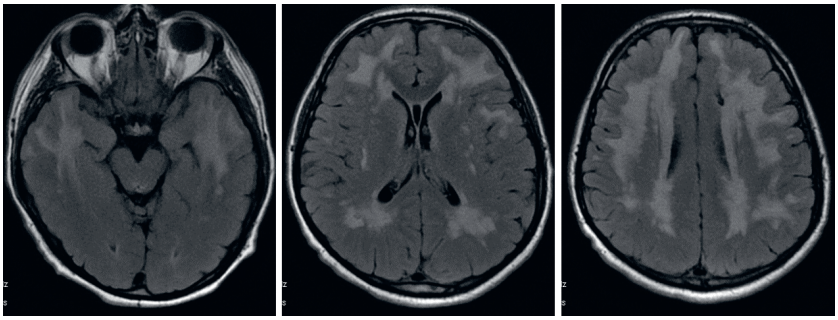

Fig. 5. CADASIL. A 38-year-old patient with cognitive impairment. Diffuse white matter hyperintensities in both hemispheres localized typically also within temporal lobes and external capsules

Clinical picture

The CSVD may be asymptomatic for many years, manifesting with accidentally detected changes in radiological examinations.[13–15] In its acute form, CSVD progresses as lacunar stroke or a focus of intracerebral hemorrhage.[16] According to the anatomopathological definition by Donnan, lacunar stroke covers a small area of ischemia formed as a result of microemboli of perforating arterioles in their proximal sections. In most cases, the changes concern lenticulostriate branches extending from the middle and anterior cerebral arteries, thalamoperforating branches extending from the posterior cerebral artery, and paramedian branches extending from the basilar artery and affect the basal ganglia, thalamus, pons, or white matter.[17] According to the classification of the Oxfordshire Community Stroke Project, lacunar stroke proceeds in the form of 1 of 5 syndromes.[18] In most cases (approx. 50–70%), it begins as pure motor stroke (PMS) – isolated, purely motor paresis or paralysis. Other clinical manifestations of this stroke include pure sensory stroke (PSS), sensorimotor stroke (SMS), ataxic hemiparesis (AH), and dysarthria-clumsy hand syndrome (DCHS).[18–20] Cerebral hemorrhage in the course of CSVD is located in deep brain structures and its signs and symptoms depend on the location.

Chronic CSVD is mainly associated with progressive cognitive impairment (from mild cognitive impairment to subcortical dementia).[21–24] Damage to the white matter of the brain leads to extrapyramidal syndrome with dominant posture and gait disorders, early and symmetrical involvement of the lower extremities, slight tremor of the limbs, pseudobulbar syndrome, and sphincter dysfunctions (mainly urgent tenesmus and urinary incontinence), as well as symptoms of depression.[21,25,26] The symptoms progress gradually, leading to loss of independence; the patient withdraws from social life. The risk of death increases, mainly due to falls and accompanying injuries.[27]

Etiology

In most cases, CSVD is sporadic; its occurrence is associated mainly with age and commonly known risk factors for vascular diseases, mainly hypertension and diabetes mellitus.[28] Other risk factors include current and former smoking, obstructive sleep apnea, chronic kidney disease, and branch atheromatous disease.[29]

Cerebral amyloid angiopathy (CAA), a form of CSVD, is the 2nd most common cause of cerebral hemorrhage, after hypertension.[30,31] It is associated with recurrent cerebral hemorrhage, coexisting ischemic strokes and cognitive impairments. The CAA may be sporadic or genetically conditioned; it involves build-up of β-amyloid deposits in the media and adventitia of small- and medium-caliber cerebral arterial vessels and in the venous vessels of the cerebral cortex and pia mater. The familial form of CAA occurs less frequently and involves mutations in different genes on autosomal dominant chromosome 20. The CAA lesions account for about 30% of spontaneous hemorrhages and 5–20% of all hemorrhages in the elderly. The occurrence of CAA type lesions increases with age; they affect 10–40% of older people and 80% of patients with Alzheimer's disease.[32,33] Radiologically, CAA leads to various types of abnormal findings, including microbleed, subarachnoid hemorrhage, superficial siderosis, microinfarction, reversible edema, and irreversible leukoaraiosis (Fig. 4).

In young people, changes in cerebral vessels are determined by genetic factors, with several single-gene disorders causing CSVD. Most often, these are systemic diseases associated with various neurological abnormalities, mainly ischemic or hemorrhagic stroke.[34,35] Uncommon and rare forms of CSVD are presented in Table 2.[2,3]

The most common genetically determined disease characterized by involvement of small vessels is cerebral autosomal-dominant arteriopathy with stroke and ischemic leukoencephalopathy (CADASIL), described for the first time by Van Bogaert in 1955 as a familial form of Binswanger's disease. The CADASIL affects young people and is autosomal dominant due to mutations in the *NOTCH* gene on chromosome 19. It is characterized by systemic signs and symptoms with accompanying neurological abnormalities, most often recurrent ischemic stroke, epilepsy, dementia, and psychiatric disorders.[36–39] Neuroimaging shows 3 types of lesions in patients with CADASIL: white matter hyperintensities; lacunar infarcts in the semioval center, thalamus, basal ganglia, and pons; and cerebral microbleeds (Fig. 5).

Table 2. Uncommon and rare forms of cerebral small vessel disease (CSVD)

Genetic conditions causing CSVD: – cerebral autosomal dominant arteriopathy with subcortical infarcts and leukoencephalopathy (CADASIL); – CARASIL: cerebral autosomal recessive arteriopathy subcortical infarcts and leukoencephalopathy (CARASIL); – mitochondrial encephalomyopathy lactic acidosis and stroke-like episodes (MELAS); – Fabry disease; – Type IV collagen mutation-related CSVD (COL4A1/COLA2); – frameshift mutations in *TREX1* gene: retinal vasculopathy with cerebral leukoencephalopathy; – hereditary cerebral hemorrhage with amyloidosis (HCHWA) (Dutch-, Italian-, and Flemish-APP mutations; Icelandic-like mutation of cystatin C).
Immune-mediated CSVD: – primary vasculitis; – secondary central nervous system (CNS) vasculitis; – systemic lupus erythematosus; – Sjögren's syndrome-associated vasculitis; – Behçet's vasculitis.
Infection-mediated CSVD: – meningovascular neurosyphilis; – viral: varicella-zoster virus, cytomegalovirus, hepatitis B and C, human immunodeficiency virus (HIV); – fungi; – schistosomiasis; – cerebral malaria.

A similar condition is cerebral autosomal recessive arteriopathy with subcortical infarcts and leukoencephalopathy (CARASIL), more common in Asian regions. It is inherited in an autosomal recessive manner and is associated with mutation in the *HTRA1* gene, located on chromosome 10q26. Abnormalities in the form of recurrent lacunar strokes appear at the age of 20–30 years. In addition, cognitive impairment, gait disturbances, degenerative spinal pain syndrome, and premature baldness are observed.[39]

Changes with respect to *COL4A1* and *COL4A2* genes responsible for the synthesis of type IV collagen alpha chains and associated with microangiopathies may be sporadic or genetically determined.[40] Type IV collagen acts as a scaffold for the cell; it is a component of the basement membrane and extracellular matrix. Abnormal collagen IV structure is associated with fragility of blood vessels and a diverse clinical picture. The spectrum of type IV collagen disorders includes autosomal dominant type I porencephaly; CSVD with hemorrhage; cerebral microangiopathy with Axenfeld–Rieger anomaly; and hereditary angiopathy with nephropathy, aneurysms and muscle cramps (HANAC).[41,42]

Mutations in the *TREX-1* gene may result in Aicardi–Goutières syndrome, systemic and cutaneous lupus erythematosus, and retinal vasculopathy with cerebral leukodystrophy (RVCL). The latter manifests around the age of 40 years and is associated with ischemic strokes, transient cerebral ischemia and psychiatric symptoms. It shows characteristic ocular signs: retinal hemorrhages, macular atrophy and capillary microaneurysms. Additional signs and symptoms may involve other organs (liver, kidneys).[43]

One of the most common mitochondrial diseases – mitochondrial encephalopathy with lactic acidosis and stroke-like episodes (MELAS) – is also associated with involvement of small vessels. About 80% of all cases occur in childhood; the clinical picture is dominated by stroke-like signs and symptoms, increasing dementia, migraine headaches, myopathy, and lactic acidosis.[44] In the case of Fabry disease, which is an X-linked inherited disorder of glycosphingolipid metabolism, strokes are observed. The disease is associated with mutation of the *GLA* gene, which is responsible for the activity of lysosomal α-galactosidase A. As a result, trihexosylceramide deposits accumulate in endothelial and smooth muscle cells, ganglion cells, kidneys, eyes, and other tissues. This involves a number of cardiovascular and renal complications at an early age. Patients have symptoms of painful peripheral neuropathy, dysfunction of the autonomic nervous system, and corneal disorders. The disease is associated with frequent strokes and myocardial infarctions. Fabry disease is responsible for 0.5% of vascular events at a young age. Ischemic strokes occur in 76%, transient ischemic attacks in 16% and hemorrhagic strokes in 8% of the cases. Involvement of cerebral small vessels occurs even in asymptomatic individuals; there are characteristic lesions of the pulvinar and frontal and parietal lobes.[45–47]

Pathomechanism

The etiopathogenesis of CSVD takes into account several mechanisms. Pathological processes associated mainly with hypertension in the vascular wall lead to development of lipohyalinosis and fibrohyalinosis; there is a proliferation of connective tissue fibers and dilatation of perivascular space, which causes loss of contractibility and thus vascular sclerosis. In addition, vascular endothelial dysfunction occurs due to blood–brain barrier impairment. The 2nd most common cause of damage to small perforating vessels is CAA. The changes lead to hypoperfusion or vascular flow disorders associated with abnormal self-regulation and impaired vascular wall permeability, and result in multifocal stroke lesions. An important role in the pathogenesis is also played by inflammatory

processes due to the presence of increased inflammatory parameters (interleukin 6, C-reactive protein (CRP)) in cerebrospinal fluid and blood.[2,15]

Prognosis

The CSVD remains clinically silent for a long time and does not affect the condition of the patients. Screening the asymptomatic general population with MRI to detect silent CVD is not recommended. However, changes in the vessels are adverse in long-term evaluation. Asymptomatic, radiologically enhanced small vessel disease diagnosed in the acute period of stroke is associated with a worse prognosis.[48] It was found that the presence of silent cerebral ischemic lesions causes a threefold increase of future stroke, regardless of other risk factors; the risk increases in the case of a larger number of lesions.[49,50] Most incident strokes are ischemic (81–89%), not hemorrhagic (11–19%). In a study by Poggesi et al., CSVD was associated with a worse prognosis. The 12-year prognosis after lacunar stroke is significantly worse than in strokes with different etiologies (7.9 years compared to 4.3 years).[51]

The presence of lesions in the white matter is associated with the risk of stroke, dementia or death, which increased during the five-year follow-up in the Framingham Heart Study. There is a known correlation between the occurrence of clinically silent lesions and cognitive impairment. tHE CSVD on its own or with Alzheimer's disease is the most common cause of cognitive dysfunction and dementia.[52] The risk of dementia increases twofold in patients with silent brain infarction.[49] The patients perform worse in neuropsychological tests if the lesions are located in the thalamus. Lesions outside the thalamus are related to deterioration of psychomotor functions.[22,53] In post-stroke epilepsy, about 11% of patients had lacunar infarcts. Studies suggest involvement of small vessel pathology in epileptogenesis and a higher incidence of temporal lobe epilepsy in the case of comorbid CSVD lesions.[54–56] Intensified retinal vascular remodeling also correlates with a higher incidence of lacunar stroke.[57]

A decrease in the glomerular filtration rate is associated with more frequent presence of silent ischemic lesions regardless of hypertension.[58] At the same time, Oksala et al. showed that a reduction of the estimated glomerular filtration rate (eGFR) below 60 mL/min/1.73 m^2 is an independent risk factor for increased damage to the white matter of the brain.[59]

Treatment

At the moment, there is no specific treatment available for genetic forms of CSVD. Only for Fabry disease is there a replacement therapy based on intravenously administered α-galactosidase A, which is taken up by cells and tissues by the mannose-6-phosphate receptor pathway and delivered to lysosomes.[3] There are no established therapeutic strategies for either preventing or treating sporadic CSVD. Potential prophylactic and treatment strategies might include those that target brain microvascular endothelium and the blood–brain barrier, microvascular function, and neuroinflammation. Because CSVD and ischemic stroke are presumed to share the same pathology, the diagnostic and therapeutic approaches should be the same. For all patients with CSVD, we should assess common vascular risk factors such as hypertension, diabetes mellitus, hyperlipidemia, and smoking.[60] The treatment is based primarily on the fight against vascular risk factors and primary and secondary prevention of vascular events. One of the most important modifiable risk factors is hypertension. Non-pharmacological treatment is also important and includes diet, sodium restriction, increased physical activity, and abstaining from smoking. Genetic testing should be considered in young people with extensive CSVD in the absence of sufficient conventional vascular risk factors. A closer understanding of the mechanisms leading to damage of small blood vessels may be associated with new therapeutic approaches.

Conclusions

The CSVD is a very common problem in older people. It is an important clinical problem due to its frequent occurrence and serious clinical consequences. The underlying mechanisms of CSVD are not known in detail. Blood pressure is the most important modifiable risk factor. The presence of genetic CSVD should be considered in young people without typical risk factors for vascular disease.

ORCID iDs

Justyna Chojdak-Łukasiewicz https://orcid.org/0000-0002-0777-4565
Edyta Dziadkowiak https://orcid.org/0000-0002-9618-9308
Anna Zimny https://orcid.org/0000-0001-6214-0322
Bogusław Paradowski https://orcid.org/0000-0003-2940-380X

References

1. Cuadrado-Godia E, Dwivedi P, Sharma S, et al. Cerebral small vessel disease: A review focusing on pathophysiology, biomarkers, and machine learning strategies. *J Stroke*. 2018;20(3):302–320. doi:10.5853/jos.2017.02922
2. Li Q, Yang Y, Reis C, et al. Cerebral small vessel disease. *Cell Transplant*. 2018;27(12):1711–1722. doi:10.1177/0963689718795148
3. Wardlaw JM, Smith C, Dichgans M. Small vessel disease: Mechanisms and clinical implications. *Lancet Neurol*. 2019;18(7):684–696. doi:10.1016/S1474-4422(19)30079-1
4. Wardlaw JM, Smith EE, Biessels GJ, et al. Neuroimaging standards for research into small vessel disease and its contribution to ageing and neurodegeneration. *Lancet Neurol*. 2013;12(8):822–838. doi:10.1016/S1474-4422(13)70124-8
5. Leary MC, Saver JL. Annual incidence of first silent stroke in the United States: A preliminary estimate. *Cerebrovasc Dis*. 2003;16(3):280–285. doi:10.1159/000071128
6. Caruso P, Signori R, Moretti R. Small vessel disease to subcortical dementia: A dynamic model, which interfaces aging, cholinergic dysregulation and the neurovascular unit. *Vasc Health Risk Manag*. 2019;15:259–281. doi:10.2147/VHRM.S190470

7. Yousufuddin M, Young N. Aging and ischemic stroke. *Aging (Albany NY).* 2019;11(9):2542–2544. doi:10.18632/aging.101931
8. Smith E, Saposnik G, Biessels GJ, et al; American Heart Association Stroke Council; Council on Cardiovascular Radiology and Intervention; Council on Functional Genomics and Translational Biology; and Council on Hypertension. Prevention of stroke in patients with silent cerebrovascular disease: A scientific statement for healthcare professionals from the American Heart Association/American Stroke Association. *Stroke.* 2017;48(2):e44–e71. doi:10.1161/STR.0000000000000116
9. Hilal S, Mok V, Youn YC, Wong A, Ikram MK, Chen CL. Prevalence, risk factors and consequences of cerebral small vessel diseases: Data from three Asian countries. *J Neurol Neurosurg Psychiatry.* 2017;88: 669–674. doi:10.1136/jnnp-2016-315324
10. de Leeuw FE, de Groot JC, Achten E, et al. Prevalence of cerebral white matter lesions in elderly people: A population based magnetic resonance imaging study. The Rotterdam Scan Study. *J Neurol Neurosurg Psychiatry.* 2001;70(1):9–14. doi:10.1136/jnnp.70.1.9
11. Poels MM, Vernooij MW, Ikram MA, et al. Prevalence and risk factors of cerebral microbleeds: An update of the Rotterdam scan study. *Stroke.* 2010;41(10 Suppl):S103–S106. doi:10.1161/STROKEAHA.110.595181
12. Tsai CF, Thomas B, Sudlow CL. Epidemiology of stroke and its subtypes in Chinese vs white populations: A systematic review. *Neurology.* 2013;81(3):264–272. doi:10.1212/WNL.0b013e31829bfde3
13. Wardlaw JM, Smith C, Dichgans M. Mechanisms of sporadic cerebral small vessel disease: Insights from neuroimaging. *Lancet Neurol.* 2013;12(5):483–497. doi:10.1016/S1474-4422(13)70060-7
14. Saini M, Ikram K, Hilal S, Qiu A, Venketasubramanian N, Chen C. Silent stroke: Not listened to rather than silent. *Stroke.* 2012;43(11):3102–3104. doi:10.1161/STROKEAHA.112.666461
15. Shi Y, Wardlaw JM. Update on cerebral small vessel disease: A dynamic whole-brain disease. *Stroke Vasc Neurol.* 2016;1(3):83–92. doi:10.1136/svn-2016-000035
16. Park YS, Chung MS, Choi BS. MRI assessment of cerebral small vessel disease in patients with spontaneous intracerebral hemorrhage. *Yonsei Med J.* 2019;60(8):774–781. doi:10.3349/ymj.2019.60.8.774
17. Donnan GA, Norrving B, Bamford JM, Bogousslavsky J. Classification of subcortical infarcts. In: Donnan GA, Norrving B, Bamford JM, Bogousslavsky J, eds. *Subcortical Stroke*. 2nd ed. Oxford, UK: Oxford Medical Publications; 2002:27–34.
18. Asdaghi N, Jeerakathil T, Hameed B, et al. Oxfordshire Community Stroke Project classification poorly differentiates small cortical and subcortical infarcts. *Stroke.* 2011;42(8):2143–2148. doi:10.1161/STROKEAHA.111.613752
19. Wardlaw JM. What is a lacune? *Stroke*. 2008;39(11):2921–2922. https://doi.org/10.1161/STROKEAHA.108.523795
20. Loos CM, Staals J, Wardlaw JM, van Oostenbrugge RJ. Cavitation of deep lacunar infarcts in patients with first-ever lacunar stroke: A 2-year follow-up study with MR. *Stroke.* 2012;43(8):2245–2247. doi:10.1161/STROKEAHA.112.660076
21. Rensma SP, van Sloten TT, Launer LJ, Stehouwer CD. Cerebral small vessel disease and risk of incident stroke, dementia and depression, and all-cause mortality: A systematic review and meta-analysis. *Neurosci Biobehav Rev.* 2018;90:164–173. doi:10.1016/j.neubiorev.2018.04.003
22. Das AS, Regenhardt RW, Vernooij MW, Blacker D, Charidimou A, Viswanathan A. Asymptomatic cerebral small vessel disease: Insights from population-based studies. *J Stroke*. 2019;21(2):121–138. doi:10.5853/jos.2018.03608
23. Levit A, Hachinski V, Whitehead SN. Neurovascular unit dysregulation, white matter disease, and executive dysfunction: The shared triad of vascular cognitive impairment and Alzheimer disease. *GeroScience.* 2020;42(2):445–465. doi:10.1007/s11357-020-00164-6
24. Carey CL, Kramer JH, Josephson SA, et al. Subcortical lacunes are associated with executive dysfunction in cognitively normal elderly. *Stroke*. 2008;39(2):397–402. doi:10.1161/STROKEAHA.107.491795
25. van der Holst HM, van Uden IW, Tuladhar AM, et al. Cerebral small vessel disease and incident parkinsonism: The RUN DMC study. *Neurology.* 2015;85(18):1569–1577. doi:10.1212/WNL.0000000000002082
26. Hatate J, Miwa K, Matsumoto M, et al. Association between cerebral small vessel diseases and mild parkinsonian signs in the elderly with vascular risk factors. *Parkinsonism Relat Disord*. 2016;26:29–34. doi:10.1016/j.parkreldis.2016.02.011
27. Direk N, Perez HS, Akoudad S, et al. Markers of cerebral small vessel disease and severity of depression in the general population. *Psychiatry Res Neuroimaging*. 2016;253:1–6. doi:10.1016/j.pscychresns.2016.05.002
28. van Norden AG, de Laat KF, Gons RA, et al. Causes and consequences of cerebral small vessel disease. The RUN DMC study: A prospective cohort study. Study rationale and protocol. *BMC Neurol.* 2011;11:29. doi:10.1186/1471-2377-11-29
29. Khan U, Porteous L, Hassan A, Markus HS. Risk factor profile of cerebral small vessel disease and its subtypes. *J Neurol Neurosurg Psychiatry.* 2007;78:702–706. doi:10.1136/jnnp.2006.103549
30. Yilmaz P, Ikram MA, Ikram MK, et al. Application of an imaging-based sum score for cerebral amyloid angiopathy to the general population: Risk of major neurological diseases and mortality. *Front Neurol.* 2019;10:1276. doi:10.3389/fneur.2019.01276
31. Pontes-Neto OM, Auriel E, Greeberg SM. Advances in our understanding of the pathophysiology, detection and management of cerebral amyloid angiopathy. *Eur Neurol Review* 2012;7(2):134–139. doi:10.17925/enr.2012.07.02.134
32. Greenberg SM, Charidimou A. Diagnosis of cerebral amyloid angiopathy: Evolution of the Boston Criteria. *Stroke.* 2018;49(2):491–497. doi:10.1161/STROKEAHA.117.016990
33. Gahr M, Nowak DA, Connemann BJ. Cerebral amyloid angiopathy: A disease with implications for neurology and psychiatry. *Brain Res*. 2013;1519:19–30. doi:10.1016/j.brainres.2013.04.052
34. Yamamoto Y, Craggs L, Baumann M, Kalimo H, Kalaria RN. Review: Molecular genetics and pathology of hereditary small vessel diseases of the brain. *Neuropathol Appl Neurobiol*. 2011;37(1):94–113. doi:10.1111/j.1365-2990.2010.01147.x
35. Federico A, Di Donato I, Bianchi S, Di Palma C, Taglia I, Dotti MT. Hereditary cerebral small vessel diseases: A review. *J Neurol Sci*. 2012; 322(1–2):25–30. doi:10.1016/j.jns.2012.07.041
36. Kim H, Lim YM, Lee EJ, Oh YJ, Kim KK. Clinical and imaging features of patients with cerebral autosomal dominant arteriopathy with subcortical infarcts and leukoencephalopathy and cysteine-sparing NOTCH3 mutations. *PLoS One.* 2020;15(6):e0234797. doi:10.1371/journal.pone.0234797
37. Chabriat H, Joutel A, Dichgans M, Tournier-Lasserve E, Bousser MG. Cadasil. *Lancet Neurol*. 2009;8(7):643–653. doi:10.1016/S1474-4422(09)70127-9
38. Guidetti D, Casali B, Mazzei RL, Dotti MT. Cerebral autosomal dominant arteriopathy with subcortical infarcts and leukoencephalopathy. *Clin Exp Hypertens*. 2006;28(3–4):271–277. doi:10.1080/10641960600549223
39. Haffner C, Vinters HV. CADASIL, CARASIL, CARASAL: The linguistic subtleties of cerebral small vessel disease. *Neurology*. 2016;87(17): 1752–1753. doi:10.1212/WNL.0000000000003271
40. Vahedi K, Alamowitch S. Clinical spectrum of type IV collagen (COL4A1) mutations: A novel genetic multisystem disease. *Curr Opin Neurol*. 2011;24(1):63–68. doi:10.1097/WCO.0b013e32834232c6
41. Giau VV, Bagyinszky E, Youn YC, An SA, Kim SY. Genetic factors of cerebral small vessel disease and their potential clinical outcome. *Int J Mol Sci.* 2019;20(17):4298. doi:10.3390/ijms20174298
42. Joutel A, Faraci FM. Cerebral small vessel disease: Insights and opportunities from mouse models of collagen IV-related small vessel disease and cerebral autosomal dominant arteriopathy with subcortical infarcts and leukoencephalopathy. *Stroke*. 2014;45(4):1215–1221. doi:10.1161/STROKEAHA.113.002878
43. Rice GI, Rodero MP, Crow YJ. Human disease phenotypes associated with mutations in TREX1. *J Clin Immunol*. 2015;35(3):235–243. doi:10.1007/s10875-015-0147-3.
44. DiMauro S. Mitochondrial encephalomyopathies: Fifty years on. The Robert Wartenberg Lecture. *Neurology.* 2013;81(3):281–291. doi:10.1212/WNL.0b013e31829bfe89
45. Testai FD, Gorelick PB. Inherited metabolic disorders and stroke part 1: Fabry disease and mitochondrial myopathy, encephalopathy, lactic acidosis, and stroke like episodes. *Arch Neurol.* 2010;67(1):19–24. doi:10.1001/archneurol.2009.309
46. Burlina A, Politei J. The central nervous system involvement in Fabry disease: A review. *J Inborn Errors Metab Screen.* 2016;4:1–7. https://doi.org/10.1177/2326409816661361
47. Rolfs A, Böttcher T, Zschiesche M, et al. Prevalence of Fabry disease in patients with cryptogenic stroke: A prospective study. *Lancet*. 2005;366(9499):1794–1796. doi:10.1016/S0140-6736(05)67635-0

48. Norrving B. Long-term prognosis after lacunar infarction. *Lancet Neurol*. 2003;2(4):238–245. doi:10.1016/s1474-4422(03)00352-1
49. Vermeer SE, Longstreth WT Jr, Koudstaal PJ. Silent brain infarcts: A systematic review. *Lancet Neurol*. 2007;6(7):611–619. doi:10.1016/S1474-4422(07)70170-9
50. Melkas S, Putaala J, Oksala NK, et al. Small-vessel disease relates to poor poststroke survival in a 12-year follow-up. *Neurology*. 2011;76(8):734–739. doi:10.1212/WNL.0b013e31820db666
51. Poggesi A, Pasi M, Pescini F, Pantoni L, Inzitari D. Circulating biologic markers of endothelial dysfunction in cerebral small vessel disease: A review. *J Cereb Blood Flow Metab*. 2016;36(1):72–94. doi:10.1038/jcbfm.2015.116
52. Aguero-Torres H, Kivipelto M, von Strauss E. Rethinking the dementia diagnoses in a population-based study: What is Alzheimer's disease and what is vascular dementia? A study from the Kungsholmen Project. *Dement Geriatr Cogn Disord*. 2006;22(3):244–249. doi:10.1159/000094973
53. Chen X, Wang J, Shan Y, et al. Cerebral small vessel disease: Neuroimaging markers and clinical implication. *J Neurol*. 2019;266(10):2347–2362. doi:10.1007/s00415-018-9077-3
54. Maxwell H, Hanby M, Parkes LM, Gibson LM, Coutinho C, Emsley HC. Prevalence and subtypes of radiological cerebrovascular disease in late-onset isolated seizures and epilepsy. *Clin Neurol Neurosurg*. 2013;115(5):591–596. doi:10.1016/j.clineuro.2012.07.009
55. Gasparini S, Ferlazzo E, Beghi E, et al. Epilepsy associated with leukoaraiosis mainly affects temporal lobe: A casual or causal relationship? *Epilepsy Res*. 2015;109:1–8. doi:10.1016/j.eplepsyres.2014.10.012
56. Russo E, Leo A, Scicchitano F, et al. Cerebral small vessel disease predisposes to temporal lobe epilepsy in spontaneously hypertensive rats. *Brain Res Bull*. 2017;130:245–250. doi:10.1016/j.brainresbull.2017.02.003
57. Cheung N, Liew G, Lindley RI, et al. Retinal fractals and acute lacunar stroke. *Ann Neurol*. 2010;68(1):107–111. doi:10.1002/ana.22011
58. Takahashi W, Tsukamoto Y, Takizawa S, Kawada S, Takagi S. Relationship between chronic kidney disease and white matter hyperintensities on magnetic resonance imaging. *J Stroke Cerebrovasc Dis*. 2012;21(1):18–23. doi:10.1016/j.jstrokecerebrovasdis.2010.03.015
59. Oksala NK, Salonen T, Strandberg T, et al. Cerebral small vessel disease and kidney function predict long-term survival in patients with acute stroke. *Stroke*. 2010;41(9):1914–1920. doi:10.1161/STROKEAHA.110.587352
60. Szcześniak D, Rymaszewska J, Zimny A, et al. Cerebral small vessel disease and other influential factors of cognitive impairment in the middle-aged: A long-term observational cohort PURE-MIND study in Poland. *Geroscience*. 2020. doi:10.1007/s11357-020-00271-4. Online ahead of print.